The Synthesis, Spectroscopic and Electrochemical Characterisation of Ru(II) Polypyridyl Complexes Containing Hydroquinone / Quinone Moieties

by

Fiona Catherine Lynch (B Sc)

A Thesis presented to Dublin City University for the degree of Doctor of Philosophy

Supervisor Prof J G Vos

School of Chemical Sciences

Dublin City University

December 2005

To my parents & husband.

I hereby certify that this material which I now submit for assessment on the programme of Study leading to award of Doctor of Philosophy by research and thesis is entirely my own work and has not been taken from the work of others save and to the extent that such work has been cited and acknowledged within the text of my work.

Signed: Fiona Catherine Lynch

Fiona Catherine Lynch

I.D. No. : 96604145

Date: 06/02/06

"Diligentia maximum etiam
mediocris ingeni subsidium"

"Diligence is a very great help even
to a mediocre intelligence "

Lucius Annaeus Seneca

Acknowledgements

This has been a long journey and there are so many people I wish to thank for their input over the past number of years First of all I would like to offer my gratitude to my supervisor Prof Han Vos for all his help and support over the past few years I would also like to acknowledge Dr Mary Pryce who inspired me to do a Ph D as an undergraduate student I would also like to show my appreciation to all in X246 (both sides!), past and present, to a great group of technicians who put up admirably with annoying postgrads, to the Prof Malcolm Smyth research group for their electrochemical expertise and equipment, to the Dr Tia Keyes research group for their extensive laser assistance and to all my other colleagues in the School of Chemical Sciences for their friendship and advice over the last few years Special thanks must go to my mum and dad, whose assistance & guidance have led me where I am today (and without whom I would actually have had to get a proper job!), to my sisters Caroline and Siobhan, my niece Caoimhe and to all the Killard family My final thanks are reserved for my incredible husband - for all his inspiration, dedication, and words of encouragement, for his unfaltering patience and most of all for his unwavering belief in me Thank you Tony

Abstract

A range of mononuclear and dinuclear $[Ru(bpy)_2L]^+$ and $[Ru(bpy)_2(L)Ru(bpy)_2]^{2+}$ complexes where L is 3(2',5'-dimethoxyphenyl)-5-(pyridin-2"-yl)-1H-1',2',4'-triazole, 3(2',5'-dimethoxyphenyl)-5-(pyrazin-2"-yl)-1H-1',2',4'-triazole, 1,4-bis(5'-(pyridin-2"-yl)-1H-1',2',4',-triazol-3'-yl)-2,5-dimethoxyphenyl, 1,4-bis(5'-(pyrazin-2"-yl)-1H-1',2',4',-triazol-3'-yl)-2,5-dimethoxyphenyl and their hydroquinone and quinone analogues are reported in this thesis Chapter one is an introductory chapter, which provides relevant background information and assists in placing the ideas and data contained in the main body of this thesis in context, while chapter two denotes the methods and procedures employed during the synthesis and characterisation of the complexes presented in the subsequent chapters In chapter three the first group of ruthenium (II) polypyridyl complexes are described These complexes are characterised by the presence of triazole moieties and a dimethoxyphenyl group These dimethoxyphenyl compounds represent model complexes for examination of the ensuing hydroquinone and quinone complexes Synthesis of the hydroquinone and quinone complexes was also achieved via these dimethoxyphenyl counterparts Chapter four pertains to the synthesis and characterisation of the mononuclear and dinuclear hydroquinone complexes, which differ only from the dimethoxyphenyl complexes by the presence of a dihydroxyphenyl group These complexes exhibit behaviour comparable in a number of ways to their dimethoxy analogues except for additional redox processes in the anodic region of their cyclic voltammograms These dihydroxyphenyl complexes also display interesting spectroelectrochemical behaviour, which was not noted in the spectra of the protected analogues, and that hence may be indicative of proton transfer between the hydroquinone and triazole moieties The synthesis and characterisation of the quinone complexes, which contain qumone moieties in place of the dihydroxy groups, is described in chapter five There is no quenching of the excited state noted for these complexes All of the compounds obtained have been characterised using ^{1}H-NMR, IR, UV/Vis and emission spectroscopies both at room and low temperatures and in neutral and acidic media The acid-base properties of each of the complexes have also been investigated in aqueous solutions The electronic structures of the mononuclear pyridine containing quinone and hydroquinone complexes have been examined using Gausssum and DOS spectra have hence been generated in order to ascertain the nature of the HOMO and LUMO levels In the final chapter, chapter six, a comprehensive examination of the behaviour of the range of complexes is provided and a number of observations and conclusions are proffered along with suggestions for future work Generally, the behaviour of each of the complexes was found to differ depending both on whether the complex contained a pyrazyl or a pyridyl group and on the nature of the pendant phenyl moiety Emission, lifetime, electrochemical and spectroelectrochemical analyses of the pyrazine containing complexes suggest that switching of the excited states of these complexes from the bipyridyl moiety to the ligand occurs upon protonation of the complex Three appendices are also provided the first of which, appendix I, contains additional NMR data Appendix II contains in-depth electrochemical studies exploring solvent conditions and identifying the optimum working-electrode Finally, appendix III comprises of additional syntheses undertaken during these studies, which have not been included in the main body of the thesis

Table of Contents

Chapter One

Introduction

The principles and processes involved in the photosynthetic system are described in this chapter and hence, place the proceeding chapters in context The growth and importance of artificial mimetic systems both of a biomimetic nature as well as the abiotic variety and the subsequent hyphenation of both styles are also discussed Finally, the importance of $[Ru(bpy)_3)]^{2+}$ *as a potential dye complex in these systems and the family of complexes it has spurred over the past few decades are also outlined*

1.1 Introduction

1.1.1 Photosynthesis: Joules from the sky

For millennia the sun has exerted a dominating influence on many aspects of human life. It was this heavenly potentate that archaic man worshiped and on which they depended as a means of unravelling the unpredictable nature of their day-to-day lives. When it is considered that the process of photosynthesis captures more than a hundred times the food requirement of mankind and is the origin of fossil fuels, perhaps early man's quixotic faith in this energy-giving doyen was not misplaced. [1]

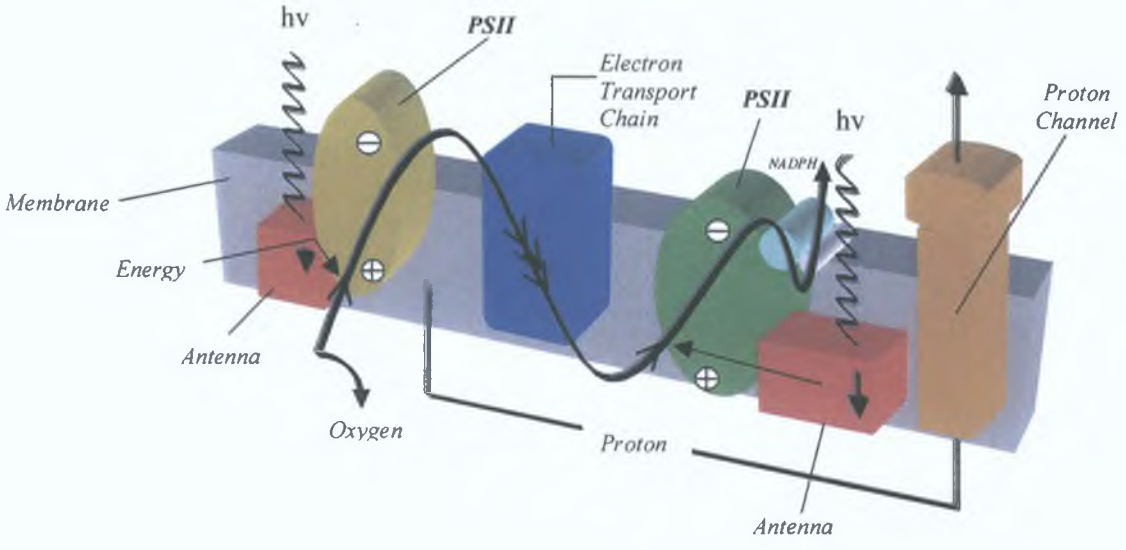

Figure 1.1 Schematic representation of the natural photosynthetic process in green plants [2]

The process by which this radiative energy is captured is known as photosynthesis, and describes the basic method by which, under the action of solar light, living organisms convert abundant low-energy substrates into valuable chemicals of high energy content (biological fuels). [2] A schematic representation of this system is given in *figure 1.1*. In green plant photosynthesis, this reaction is the conversion of water and carbon dioxide into oxygen and carbohydrates as given by the following equation (*Eqn. 1*).

$$H_2O + CO_2 + hv \longrightarrow O_2 + 1/6\ (C_6H_{12}O_6) \qquad (Eqn.\ 1)$$

In recent years there has been much experimental and theoretical interest in photosynthetic light-harvesting systems and X-ray crystallographic data have supplied much detailed information on the structural features of these systems [3] For example, in 2001, a high-resolution X-ray crystal structure was reported for *Thermosynechococcus elongatus* and *Thermosynechococcus vulcanus* [4][5] Late 2003 saw two new structures for the cytochrome *b6f* complex from *Mastigocladus laminosus* and *Chlamydomonas reinhardtn* and in the most recent report, Jones *et al* describe the structure of Photosystem II from *T elongatus*, at a resolution of 3 5 Å [5] These investigations deepen our understanding of the photosynthetic process and the chain of electron transfer reactions that follow the initial excitation in the photosynthetic reaction centres [6] The initial steps involve the absorption of light by different antenna pigments and the funneling of the excitation energy to the photosynthetic reaction center chlorophylls Hence, a chain of electron transfer reactions between the reaction center cofactors begins [7]

In plants and algae, the electrons needed for this process are generated in the reaction where water is oxidised to molecular oxygen Water oxidation occurs in the photosystem II (PSII) reaction centre (*figure 1 1*), which consists of a large membrane-spanning heterodinuclear protein (denoted D1 and D2) and binds most of the redox components including the primary photoelectron donor, a chlorophyll dimer P_{680} [7][8] This dimer is surrounded by approximately 30 protein subunits including some chlorophyll binding proteins that absorb light After absorption of one quantum of light, P_{680} is excited and a very rapid "down hill" electron transfer (ET) chain starts [8][9] An electron is then transferred from $*P_{680}$ to the acceptor pheophytin and further to two quinones, Q_A and Q_B For these steps to be repeatable, the highly oxidising form of P_{680}^+ (E^0 = 1 12V vs NHE) has to be reduced [7] An electron is transferred to P_{680}^+ from the donor side through the oxidation of a tetranuclear manganese complex in PSII [10] The transfer of electrons is mediated to P_{680}^+ via the electron donor tyrosine$_Z$, which interfaces the manganese cluster and P_{680}^+ Four electron abstractions to P_{680}^+ lead to oxidation of two water molecules releasing one molecule of oxygen The manganese cluster has an important role in this process, coordinating water and storing four oxidising equivalents [9][7]

1 1 2 Artificial Photosynthesis A leaf by any other name

The elucidation of the processes and structures involved in photosynthesis to date means that these photochemical processes are no longer the closely guarded secrets of the plant Hence, for almost three decades, a concerted effort has been made by members of the scientific community to mimic the process of clean energy production that is so expertly demonstrated by nature The motivation for artificially photosynthesis is twofold Firstly, this biommetic chemistry might lead to a better understanding of the natural system Secondly, it is a long-standing challenge to be able to master these intricate and very important reactions to produce energy-rich compounds (fuels) using solar energy in the hope that this will lead to a new form of renewable energy for the future [7][8][11]

Examination of the process of photosynthesis outlined in *section 1 1 1*, reveals the dichotomous nature of this system The initial focus has been on the antenna system where the primary functions of light gathering occur, at present there is a shift of focus to the process of charge separation, which ends in the splitting water Over the last few decades' research into designing artificial systems has proceeded along these lines and two central approaches have been taken in an attempt to achieve these goals The first mvolves the creation of 'biomimetic' species, highly organised molecular assemblies reminiscent of those found in nature, while the second utilises totally "abiotic" components, particularly complexes of the second row transition metals and small organic molecules [12]

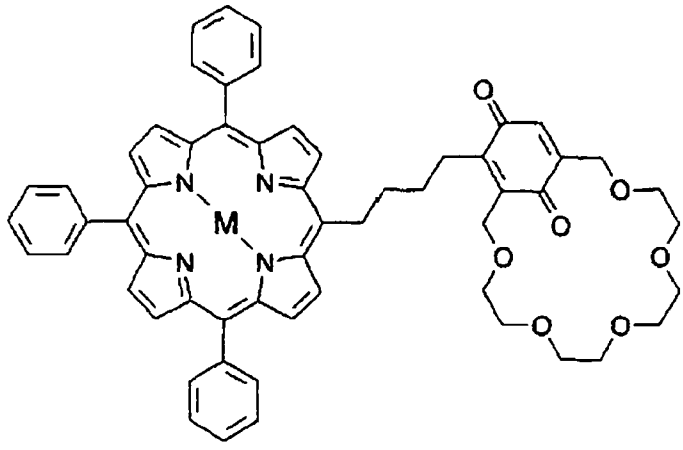

Figure 1.2 Porphyrin–quinone linked dyad (M = Zn) [13]

For example, with regard to biomimetic systems, over the past twenty years much effort has been devoted to studies of photoinduced electron transfer (ET) reactions from chlorophyll and analogues to acceptors in an attempt to mimic the acceptor side of PSII [11][9] Much of this work has focused on the use of porphyrins, cartenoid and quinones or assemblies of each creating dyads, triads, tetrads, pentads, or even hexads [14][2] Because of their widespread occurrence in biological electron-transfer systems such as photosynthetic reaction centers, porphyrin-type chromophores have played a central role in the design of covalently linked donor-acceptor systems for the study of photomduced intramolecular electron transfer [14] *Figure 1 2* shows a porphyrin covalently linked to a redox-active crown ether quinone (electron acceptor) [13] Sakata and co-workers also reported the synthesis and photophysical properties of a porphyrin tethered to two quinones acceptors as an example of a system mimicking the electron transfer properties of natural photosynthesis [15] Similar systems composed of a porphyrin-caretenoid-quinone format have also been reported by Moore *et al*, [16] while porphyrin dyes as models for the antenna system in natural photosynthesis have been investigated by Officer *et al* [17] Several reviews can be found, which elaborate further on these systems [2][14]

Although systems mimicking the photomduced electron-transfer reactions of photosynthesis have dominated research in the area of biomimetic chemistry, synthetic manganese complexes have been made, motivated by the manganese cluster of PSII For example, Hammarstrom and co-workers have developed biomimetic systems containing manganese and tyrosine moieties [18][6] However, while these biomimetic systems and approaches to photosynthetic mimetic chemistry remain exciting areas of research in the new millennium, the dawn of the abiotic system has arrived and hence systems, with clear advantages over their biomimetic kin, have been developed [12] This approach unifies the inspirational model that nature bestows in 'green-leaf' photosynthesis with more stable, flexible synthetic analogues as replacements for these naturally occurring compounds This is a more rational approach to artificial photosynthesis for a number of reasons not least of which is that nature was not in a hurry to develop her systems while mankind is [19][20]

For example, light-absorbing pigments, which in nature are not composed of particularly robust substances, may be replaced by artificial dyes. More convenient synthetic routes may also be formulated which achieve the same outcome as natural photosynthesis and furthermore, these abiotic systems could function at higher temperatures than natural systems and hence achieve higher efficiencies. [2] Finally, advancements in the area of photophysics and photochemistry over the last two decades means that the feasibility of constructing tailor-made ("fine-tuning") complexes with desired excited-state properties is now achievable. [21]

This abiotic route therefore is very alluring and has been the 'siren on the rock' for inorganic chemists for a number of years now. In the 1970's this path lead scientists to the door of ruthenium(II) and osmium(II) polypyridine complexes whose properties and reversible redox behaviour had been know for some time previously. [22] Their reputation as possible reactants and/or mediators in light induced and light generating electron transfer processes spurred by the energy crisis of the 70's, when interest in photosensitised water splitting was at its peak, launched $[Ru(bpy)_3]^{2+}$ and related complexes into the limelight.[23][24][25] This complex, with its outstanding spectroscopic, excited-state and redox properties, became highly popular as a potential photocatalyst for this purpose. [2][19] (A more detailed examination of these properties is provided in the following sections (*vide infra*).) Indeed, it was this interest in the potential application of $[Ru(bpy)_3]^{2+}$ as a photocatalyst for the photo-dissociation of water into hydrogen and oxygen that was, at first, the driving force behind much of the study of $[Ru(bpy)_3]^{2+}$.

Initially, many of these studies lay in the realm of intramolecular photochemistry with studies, such as Gafney and Adamson reporting on the photoredox properties of $[Ru(bpy)_3]^{2+}$, illustrating the use of this compound as a photosensitiser for the reduction of Co^{III} ammines.[26] Eventually, elucidation of this photoredox chemistry coupled with the knowledge that Ru(II) complexes exhibit sufficiently long excited-state lifetimes in fluid solution to be able to intervene as a reactant in bimolecular processes led to its use as a photosensitiser in electron transfer processes and hence a movement towards the study of intramolecular photochemistry began.[19][27]

$$2H_2O + 2e^- \rightarrow H_2 + 2OH^- \qquad (Eqn.\ 2)$$

$$2H_2O \rightarrow O_2 + 4H^+ + 4e^- \qquad (Eqn.\ 3)$$

Creutz and Sutin were among the first to recognise the possibilities of using $[Ru(bpy)_3]^{2+}$ as a photosensitiser for the splitting of water with visible light.[28] This process of photodecomposition of water by irradiation with solar light can be regarded in terms of the two half-cell reactions, which are shown in *Eqn. 2 & 3.* [27][29] *Figure 1.3* shows an idealised schematic for the photocatalytic splitting of water. [30] The prototype H_2-evolving system, developed by Lehn and Sauvage, demonstrated the possibility of producing hydrogen from water utilising $[Ru(bpy)_3]^{2+}$ as photosensitiser, $[Rh(bpy)_2Cl_2]Cl$ as an electron relay, colloidal Pt as reduction catalyst, and triethanolamine as a sacrificial electron donor.[31]

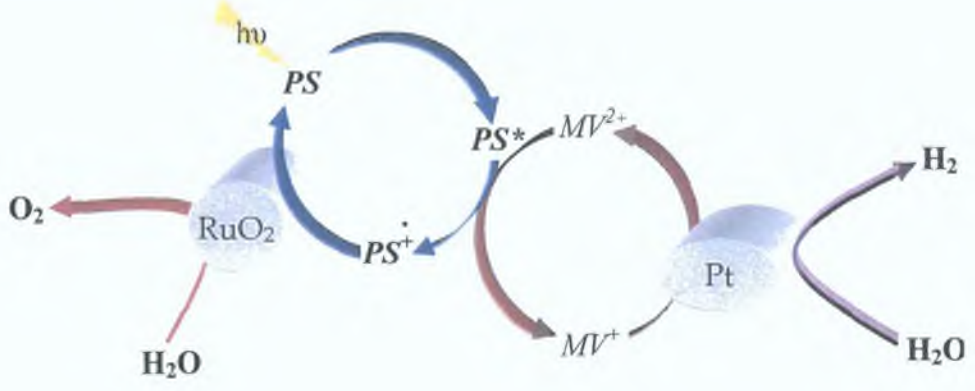

Figure 1.3 Idealised scheme for the photocatalytic splitting of water in which the photosensitiser (PS) is $[Ru(bpy)_3]^{2+}$, MV^{2+} is methylviologen, Pt is a colloidal catalyst of water reduction and RuO_2 is a colloidal catalyst of water oxidation.[30]

For a number of years this observation stimulated wide interest both for reduction and oxidation of water. However, it soon became clear that a major disadvantage, which lead to a disappointing performance of this water-splitting system, is that $[Ru(bpy)_3]^{2+}$ is not photochemically inert towards ligand substitution.[32][33] Alternative ways to prevent ligand dissociation such as linking the ligands together so as to make a cage structure around the metal have been proposed. [34]

However, inefficient electron-transfer processes, problems with the platinum catalyst, and separation of the evolving dihydrogen and dioxygen gasses also emerged The over-riding limitation of these systems however, was the use of sacrificial electron donors [35][30] Gratzel *at al* were the first to propose a solution to this problem by constructing a system containing $[Ru(bpy)_3]^{2+}$, [methylviologen]$^{2+}$, and TiO_2 particles loaded with RuO_2 and Pt as catalysts, which succeeded in evolving H_2 and O_2 simultaneously (*Eqn 4*) [36]

$$[Ru(bpy)_3]^{2+*} + MV^{2+} \longleftrightarrow [Ru(bpy)_3]^{3+} + MV^{+} \qquad (Eqn\ 4)$$

However, this system did not represent a perfect outcome as the subsequent back-reaction of $[Ru(bpy)_3]^{3+}$ and MV^+ limited the length of time during which charge separation and thus energy storage could be maintained Incorporating a sacrificial repair agent, which could suppress this energy wasting back reaction, solved this problem EDTA (ethylenediaminetetraacetate) is an example of such an agent which has the ability to donate an electron to $[Ru(bpy)_3]^{3+}$ to produce $[Ru(bpy)_3]^{2+}$ and the net reaction is electron transfer from EDTA to MV^{2+} [34] However, a different approach to this problem is to mechanically restrict the motion of $*[Ru(bpy)_3]^{2+}$, MV^{2+}, $[Ru(bpy)_3]^{3+}$, and MV^+ in rigid medium, which promotes the electron transfer to give $[Ru(bpy)_3]^{3+}$ and MV^+, but inhibits the probability of the back-reaction Cellulose provides such a medium, and it has been shown that MV^+ is formed upon excitation of $[Ru(bpy)_3]^{2+}$ [38] Similar systems involving micelles and layered zirconium phosphate systems were also investigated to this end [39][40]

Self-assembled arrays have also been constructed in media in which one or more of the components is confined within a fixed matrix, either sol-gel or zeolite [41] In functionalised zeolites, for example, Mallouk *et al* [42] have shown that a substantially extended charge separation lifetime of 37 μs can lead to quantum efficiency for charge separation of about 17% from flash photolysis measurements, although Dutta and co-workers [43], for a similarly constructed array, have reported quantum efficiency for hydrogen evolution of only 0 05%.

Another option to a self-assembling, multi-component, micro-heterogeneous array is using a covalent supramolecular assembly to accomplish long-term electron-hole pair separation. [44]

1.1.3 Supramolecular Chemistry: Chemistry beyond the molecule

As scientists continued to search for the "Übermoleküle", a shift in interest developed over the last decade, from intramolecular photochemical processes towards processes occurring in supramolecular systems. [45][46] Supramolecular chemistry is generally defined as "chemistry beyond the molecule, bearing on the organised entities of higher complexity that result from the association of two or more chemical species held together by intermolecular forces" and describes a field of study concerned with the chemistry of molecular assemblies and of the intermolecular bond. [2][47] According to Sauvage *et al*, from a photochemical and electrochemical viewpoint, the distinction between a large molecule and a supramolecular species can be based on the degree on interaction between the electronic subsystems of the component units. When the interaction energy between subunits is small compared to other relevant parameters, the system can be considered a supramolecular species. [12]

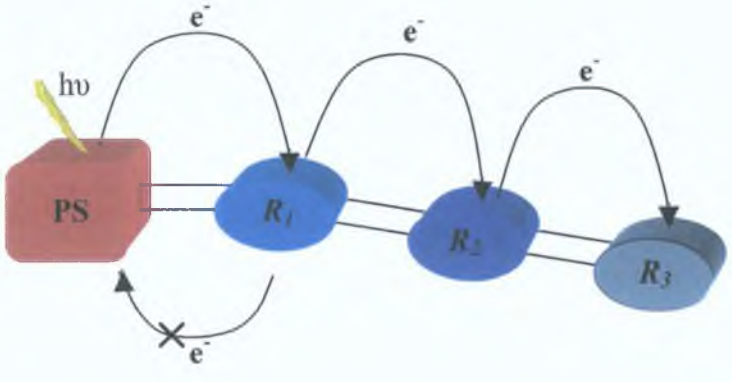

Figure 1.4 Schematic representation of the components involved in the design of a successful photochemical molecular device for light energy conversion

Structurally organised and functionally integrated systems for light energy conversion purposes are known as photochemical molecular devices (PMDs) and echo the themes presented by nature in photosynthesis. [12] For example *figure 1.1* may be regarded as nature's photochemical molecular device, which carries out the processes of photosynthesis within its highly organised confines.

Borrowing their blueprint from nature and utilising their knowledge of intra- and intermolecular processes, which they have accrued, chemists have been able to design and construct chemically stable and geometrically well-controlled supramolecular structures by linking molecular building blocks via covalent bonds [2][12][48] In designing an artificial photochemical molecular device to carry out useful functions such as solar energy conversion, two compulsory steps are involved (*Figure 1 4*) The first process is light capture by a photosensitising component (**PS**) and the second is the conversion of the collected excitation energy into chemical energy e g via a charge separation process ($\mathbf{R_1}$-$\mathbf{R_2}$-$\mathbf{R_3}$) This charge separation process can then be used to do 'work', for example to obtain electricity or simple fuels like hydrogen [2][46]

An excellent example of such a system, shown in *figure 1 5*, is Gratzel's photoelectrochemical solar cell This nanoporous, nanocrystalline semiconductor based, dye-sensitised solar cell (DSSC) represents the present generation of dyè-sensitised solar devices and has demonstrated laboratory conversion efficiencies of up to 10 4% [17][49][50] In the dye-sensitised solar cell illustrated in *figure 1 5*, sensitiser dyes are adsorbed on the surface of a porous film of TiO_2 particles Excitation of the dye with visible light leads to an electronically excited-state that injects electrons into the conduction band of the semiconductor on a femtosecond timescale

The electron donor, present m the electrolyte filling the pores, then reduces the oxidised dye back to the ground state Reduction of the oxidised dye occurs via the sacrificial donor (I), which is regenerated at the Pt counter electrode The net effect of visible light irradiation is regeneration of the dye, the redox mediator and the driving of electrons through the external circuit The process thus leads to the direct conversion of sunlight to electricity The photocurrent that is achievable is dependant upon the spectral and redox properties of the dye, effiency of charge injection and the structural properties of the semiconductor electrode to collect and channel the electrons through the external circuit [49][50]

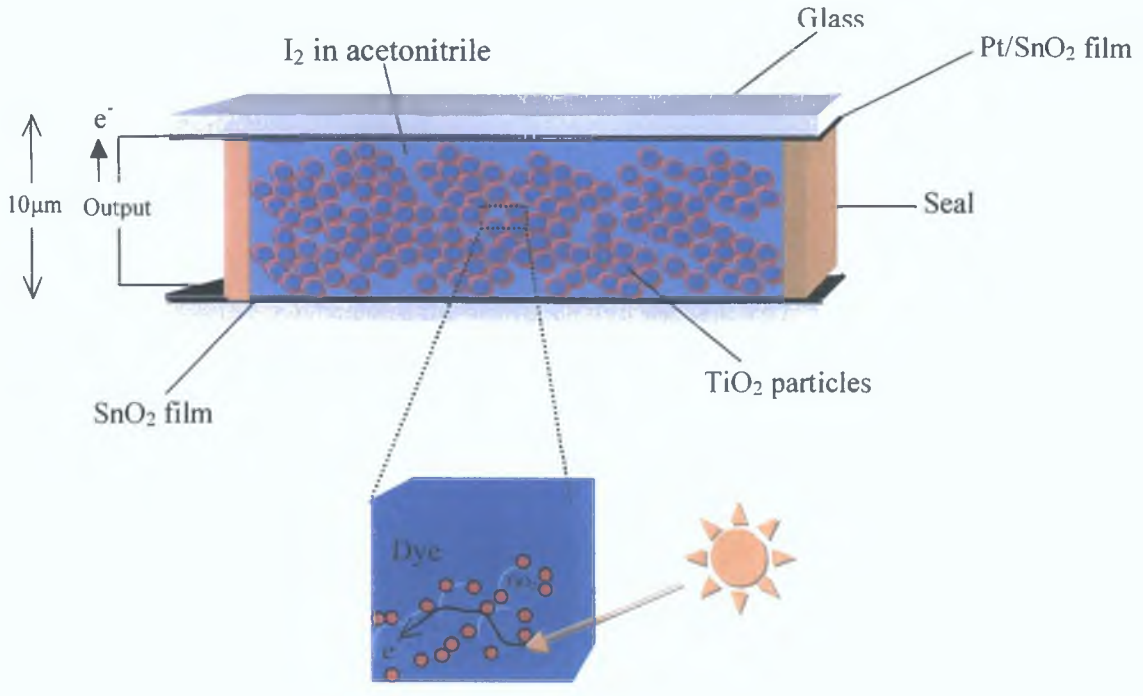

Figure 1.5 Diagrammatic representation of the components of the present generation of dye-sensitised photoelectrochemical cell [50]

Therefore, in order to achieve a successful PMD such as Gratzel's, two separate aspects of this system must be reconciled - that of the photosensitising component and that of the charge separation process. A number of studies, have focused on the photosensitising aspect of these systems with the ultimate aim of producing efficient antenna type systems, while many have concentrated on photoinduced energy and electron transfer processes within the supramolecular framework. [45][51] A number of factors must be addressed when designing useful supramolecular species. The first is the issue of obtaining "building blocks" that exhibit suitable ground and excited-state properties. Secondly, these building blocks need to then be linked by appropriate spacer groups to form supramolecular arrays while at the same time providing the electronic coupling necessary to permit the occurrence of intercomponent energy and electron transfer. [52]

(i) *Building blocks*

Ru(II) polypyridine complexes and their ilk, with low lying excited-state metal-to-ligand charge transfer (MLCT) and ligand centred (π-π^*) excited-states, are fairly long-lived to participate in electron transfer processes.

Furthermore, with their redox reactivity and the ease of tunability of their redox properties, they are excellent building blocks for supramolecular structures. These complexes have been investigated for use in the development of molecular-scale electronic devices in which they could function as molecular wires, insulators and chromophoric antennas. [51][53][30]

Ru(II) polypyridyl complexes as photoactive molecular wires and chromophoric antennas have been incorporated into DSSCs and to date they have proved to be the most efficient transition metal complexes employed in these solar cells.[50][54] A more detailed exegesis on the properties of ruthenium polypyridyl complexes is provided in the following section, however, it is important to mention their significance within these systems.

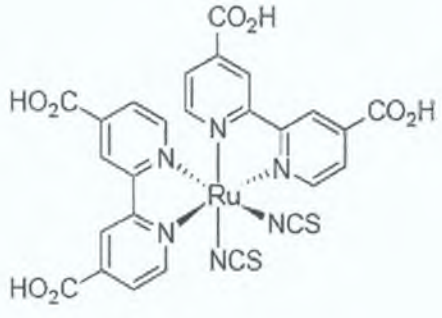

Figure 1.6 Ruthenium polypyridine photosensitiser complex $[Ru(dc\text{-}bpyH_2)_2(NCS)_2]$ used by Gratzel.[50]

For example, in Gratzel's cell (*figure 1.5*) a number of ruthenium polypyridyl complexes have been used as photosensitising compounds. The most effective sensitiser for nanostructured photoelectrochemical solar cells $[Ru(dc\text{-}bpyH_2)_2(NCS)_2]$ is shown in *figure 1.6*. The carboxyl functions (O-C=O) are anchoring groups which ensure uniform distribution of the dyes on the oxide surface and promote electronic coupling of the donor levels of the dye with the acceptor levels of the semiconductor. [50]

(ii) *Spacer Groups*

Once suitable Ru(II) polypyridyl complexes have been established as suitable building blocks for supramolecular arrays they then need to be tethered by a suitable group.

The importance of the spacer groups is crucial if the desired spatial organisation is to be achieved These groups may be simple CN^- bridges, simple rigid ligands like 4,4'-bipyridme, or more complex such as novel large aromatic bridging ligands (*figure 1 7*) [55][56][57] Furthermore, for covalently linked systems the electronic coupling between the donor and the acceptor chromophoric units arises from their mutual interaction through the orbitals of the intervening medium, i e the bridging ligand Therefore, the electronic nature of the bridging ligand, its length and configuration, provide not only the spatial organisation of the active components but are responsible for the electronic interaction between them [55] Indeed, the intervalence transfer (IT) bands of mixed-valence compounds have been studied extensively as its position, shape and intensity yield information about the interaction between metal centres Various bridged dinuclear systems, such as polyyne-, pyridyltriazole- and cyano-bridged polypyridyl complexes, have been employed in the investigations [58][59][60] For example, Kalyanasundaram and co-workers have observed an intervalence transition attributed to the mixed-valence species of a cyano-bridged complex [61] The electronic interaction was calculated to be 0 15 μm^{-1}, which is an indication that this complex is a class II, mixed-valence type complex [61] Dinuclear complexes containing alkyne spacers have been investigated by Ziessel and co-workers [53][62] The interaction between the metal centres is strong and hence they may be described as class III mixed-valence species and can therefore be considered to be molecular wires due their extremely efficient electronic transmission [53][62] A more in-depth examination of these phenomena is provided to *section 1 3*

The subunits of these bridging ligands may also behave as individual components affecting the photophysical properties of the Ru-based chromophores as a whole For example, $[(phen)_2Ru(tatpp)Ru(phen)_2]^{4+}$ where phen = 1,10-phenanthroline and the ligand *tatpp* is shown in *figure 1 7*, was found to undergo intramolecular electron transfer to specific subunits of the bridge [56] The spectral and redox properties of ruthenium polypyridyl complexes can also be 'tuned' via the bridging ligand either by introducing a ligand with a low-lying π^* molecular orbital or by destabilisation of the metal t_{2g} orbital through the introduction of a strong donor ligand [63] This phenomenon will be explored further in *section 1 2 2*

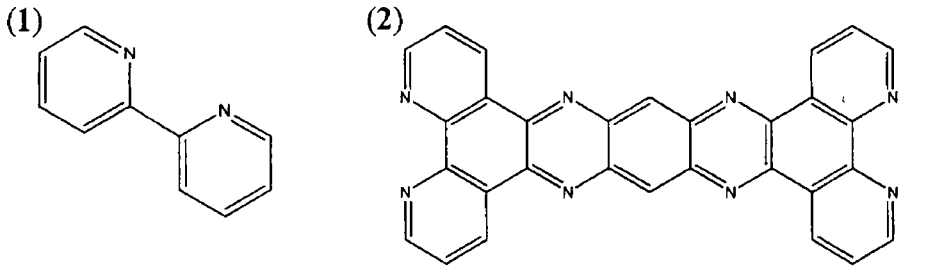

Figure 1 7 2,2'-bipyridine (**1**) & *tatpp* (**2**) [56]

Tailoring of the properties of the Ru(II) polypyridyl units within these systems is hence paramount when designing these supramolecular arrays and $[Ru(bpy)_3]^{2+}$ may be considered the archetypal complex

1 2 Ruthenium: Properties, Occurrence and Applications

Ruthenium, with a greyish white appearance and a hard, brittle character, was first discovered in 1844 and named after the Latin word Ruthenia, meaning "Russia" It has the atomic number 44, a mass of 101 07 amu and is a second row transition metal positioned under iron and above osmium in group VIIIA of the periodic table It has several stable isotopes and the electronic configuration [Kr] $(4d)^7(5s)^1$ [64][65] As one of the six platinum group metals, it is a member of a family of rare elements with an abundance of approximately 10^{-4} ppm in the earth's crustal rocks One of the interesting features of ruthenium chemistry is that as many as nine oxidation states exist, which makes its chemistry very diverse [66][67]

1 2.1 Polypyridyl Complexes

Since that first serendipitous day in the 1930's when the luminescence of $[Ru(bpy)_3]^{2+}$, whose structure is shown in *figure 1 8*, was first recognised, scientists have been investigating the latent qualities of this complex and today the photophysical, photochemical and electrochemical properties of this unique compound are well recognised by the scientific community

Paris & Brandt's pioneering work in their 1959 treatise on the observed luminescence of $[Ru(bpy)_3]^{2+}$ resulted in a boom of studies on ruthenium coordination compounds [22]

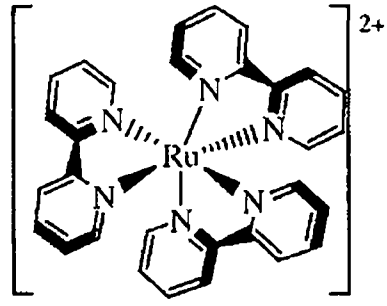

Figure 1 8 The Structure of $[Ru(bpy)_3]^{2+}$ [41]

The polypyridyl ligands are usually colourless molecules possessing σ-donor orbitals localised on the nitrogen atoms and π-donor and π*-acceptor orbitals more or less delocalised on aromatic rings The X-ray crystal structure for $[Ru(bpy)_3]^{2+}$ shows that the metal to ligand (Ru-N) bond lengths are short, indicating significant back-bonding between Ru(II) and the π* orbitals of bpy As previously discussed, these compounds form the foundation of photochemical molecular devices capable of performing complex functions such as light harvesting, charge separation, conversion of light into electrical energy, data process and storage as well as sensing systems and logic devices But, perhaps more importantly, they consequently help to extend and refine current theories of chemical reactivity and spectroscopy [2] Indeed, $[Ru(bpy)_3]^{2+}$ serves as a structural model system for a variety of distorted octahedral complexes whose properties (photophysical, electrochemical) may be tuned using different ligands [24][68] The ground state properties of this complex and the formation of its electronic structure, based on its constituents, may be understood from the energy level diagram in *figure 1 9*, which shows the ligand field splitting of the (t_{2g}, e_g) manifold in the complex and the interaction with the σ and π orbitals of the ligands [69] An additional advantage of this complex is the presence of two distinct redox sites, which means it can be oxidised (removal of a *metal* localised electron) or reduced (addition of an electron in a *ligand* π* orbital) (*figure 1 9*) Indeed, much of the photochemical interest in $[Ru(bpy)_3]^{2+}$ stems from its photoredox properties, which are closely interrelated to redox properties in the ground state

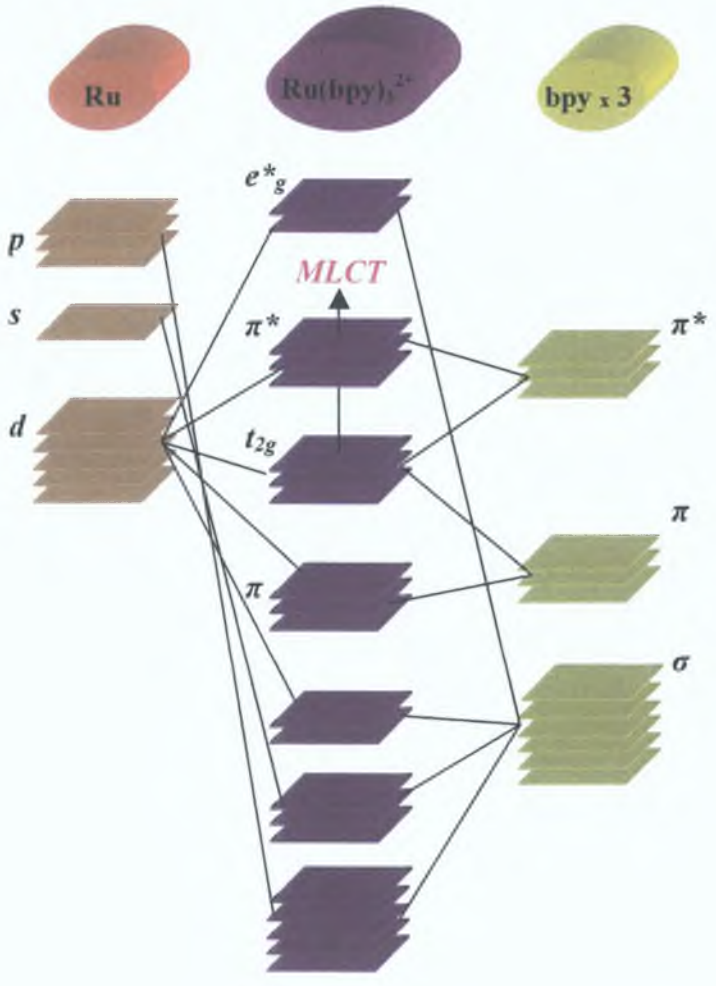

Figure 1.9 Molecular Orbital Diagram for the Interaction Between the Metal & Ligand Orbitals in $[Ru(bpy)_3]^{2+}$ [68]

The standard redox potentials of $[Ru(bpy)_3]^{2+}$, which are useful in establishing excited-state redox potentials, are shown in the following equations:

$$[Ru(bpy)_3]^{2+} + e^- \rightarrow [Ru(bpy)_3]^{+} \quad E^o = -1.28V \qquad (Eqn.\ 5)$$

$$[Ru(bpy)_3]^{3+} + e^- \rightarrow [Ru(bpy)_3]^{2+} \quad E^o = +1.26V \qquad (Eqn.\ 6)$$

Furthermore, the mono-, di- and trivalent cations are noted for their thermal inertness towards labilisation of bpy. Hence, they have the potential to participate in a variety of reversible electron transfer processes. [29] The absorption spectra of ruthenium polypyridyl complexes are dominated in the visible region (452 nm) by a metal-to-ligand charge transfer band (MLCT), with an extinction coefficient of ~14600 $M^{-1}cm^{-1}$. [21][70]

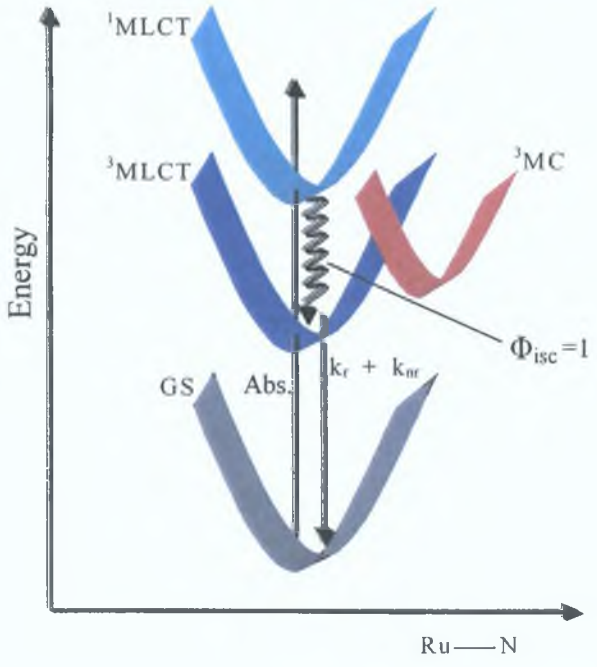

Figure 1.10 Schematic representation of the photophysical processes of $[Ru(bpy)_3]^{2+}$ [75]

Figure 1.9 shows that this MLCT arises when an electron is promoted from the t_{2g} orbital of the metal to the π^* orbital of the ligand. This transition is of great importance and many studies have reported on the MLCT excited-states as they dominate the spectroscopy, photochemistry and photophysics of polypyridyl complexes of Ru(II).[71][72] The most important photophysical properties of $[Ru(bpy)_3]^{2+}$ are depicted in *figure 1.10*. From an examination of *figure 1.10*, it can be seen that rapid intersystem crossing (ISC) occurs from the singlet to four closely spaced ^{3}MLCT triplet states (amalgamated in diagram), after which emission from the triplet state to the ground state (k_r) or non-radiative deactivation to the ground state (k_{nr}) may take place. The efficiency with which the lower ^{3}MLCT states are populated following direct absorption into the higher singlet state is known to be approximately 1. Deactivation may also occur via population of the metal centred (^{3}MC) excited-state, giving rise to either radiationless deactivation (k_{nr}') or to photodecomposition of the complex. [72][73]

There are two factors which limit the popularity of $[Ru(bpy)_3]^{2+}$ as a photocatalyst; first, the fact that the population of the ^{3}MC state leads to photodecomposition of the $[Ru(bpy)_3]^{2+}$ dication and also, due to the rather narrow adsorption band at 452 nm for $[Ru(bpy)_3]^{2+}$, only a small part of the solar energy spectrum can be used.

However, it has been shown that by changing the ligand systems around the Ru(II) centre it is hoped that the ground state and excited-state properties of the complexes can be improved By changing the nature of the ligands the redox potentials are altered along with the energies of the absorption and emission bands [74] Indeed, research has accumulated large amounts of data on the changes incurred on the electrochemical and chemical properties of these complexes, brought about by replacement of one or more of the bipyridyl rings by another bidentate chelating ligand, particularly by nitrogen-containing hetrocycles such as 2,2'-bipyridine, 1,10-phenanthroline, 2,2'-bipyrazine, 2,2'-bipyrimidine, bis(quinoline) and bis(imidazole) [75][76] Indeed, the value of these complexes lie in the fact that by judicious choice of ligand system, bespoke complexes may be created with tailored properties to suit their requirements

1 2 2 Emending the Excited-State

The spectral and redox properties of ruthenium polypyridyl complexes can be tuned in two ways First, by the introduction of a ligand with a low-lying π^* molecular orbital and second, by destabilisation of the metal t_{2g} orbital through the introduction of a strong donor ligand [50][63] For example, the introduction of a substituent on to the bpy moiety can cause either an increase in the electron density at the metal centre and thereby decrease the energy associated with the MLCT transition or the reverse may occur and the electron density at the metal centre can be decreased [77][63]

This phenomena was explored by Hou and co-workers [77] who adjusted the excited- state by varying the substituents on the bpy moiety of $[Ru(bpy)_2(bpy\text{-}X)]^{2+}$, where X = H, CO_2H, CO_2Et, NO_2, OCH_3, NH_2 As the properties of the substituents were varied from electron-donating (OCH_3, NH_2) to electron-withdrawing (CO_2Et, COOH, NO_2) both the absorption maximum in the MLCT band and the emission energy shift to lower energy compared to the prototype $[Ru(bpy)_3]^{2+}$ [77] At room temperature the complexes bearing electron-withdrawing substituents had higher luminescence quantum yield and longer excited-state lifetimes than that of the compounds bearing electron donating ones

This occurs because when the substituents are electron accepting groups the π^* ligand centred orbital is more stabilised than the $\pi(t_{2g})$ metal-centred orbital However, when the substituents are electron donating groups the MLCT excited-state energy decreases as a consequence of the larger destabilisation of the metal-centred $\pi(t_{2g})$ orbital compared with the ligand centred π^* orbital [77] This method of tuning has particular relevance in relation to tuning the properties of photosensitising dyes for solar cells For example, Huang *et al*, tailored the properties of a ruthenium polypyridyl complex by introducing the electron donor group $-CH_2N(CH_3)(C_6H_5)$ in place of the non-anchoring –COOH in order to achieve their required properties [63]

However, this 'tunability' of $[Ru(bpy)_3]^{2+}$ may also be achieved by replacing one of the bpy units by another aromatic ligand This gives rise to two classes of compound (*class a* and *class b*) The ligand (L) acts as a spectator ligand but does not become directly involved in the emission processes [78] Hence, through variation of L, the relative position of the d-d state can be significantly affected The affect that the L induces is an increase in the energy gap between the ^{3}MLCT and the ^{3}MC states, thereby preventing population of the deactivating state [79]

(i) Class a Type Ligand

A class **a** type ligand is one in which the ligand (L) is a weaker σ-donor but a better π-acceptor than bipyridine This type of ligand has the ability to participate directly in the excited-state reactions In doing so it alters the excited-state properties by decreasing the t_{2g} -^{3}MLCT energy gap, since the lowest π^* unoccupied molecular orbital (LUMO) will reside on this ligand The main aim of this process is to isolate the ^{3}MC state from the ^{3}MLCT state, but the weak σ-donor properties of class **a** ligands results in a reduced ligand field splitting and after excitation of the complex the ^{3}MC state may still be populated Examples of class **a** ligands include 2,2'-bipyrazine (bpz), 2-2'-bipyrimidine (bpm) and 2-2'-biquinolme (biq) [55][67][78]

(ii) Class b Type Ligand.

A class **b** type ligand is one in which L is a stronger σ-donor and a weaker π-acceptor than bipyridine Due to their strong σ-donor ability, this class of ligand possesses π* levels of much higher energy than bpy As a result, in mixed chelate complexes containing, both bpy and class **b** ligands, the excited-state is always bpy based However, the t_{2g} level is destabilised and this may lead to a reduction in the ^{3}MC - ^{3}MLCT energy gap [55][67][78] In these compounds L has only a minor effect on the excited-state and redox properties of the building blocks and it may allow the occurrence of vectorial energy or electron transfer along a suitable organised sequence of components [78]

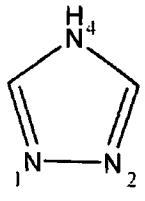

Figure 1.11 Structure of 1,2,4-triazole [80]

In the last decade there has been an increased interest in systems containing at least one class **b** ligand, such as pyrazoles [81] or triazoles (*figure 1 11*) [82] The measure of σ and π donating abilities of these ligands may be modified by introduction of substituents onto the ligand [82] In particular, the triazoles have been an important contribution to the class **b** ligands Vos *et al* first reported 1,2,4-triazole ligands and their ruthenium complexes in 1983 [80] They have the ability to form isomers based on whether the metal is N2 or N4 bound Triazole containing complexes also feature an interesting pH dependant photochemistry [83] These complexes show interesting properties as a result of the electronic properties of the triazole ring [79] The availability of different coordination sites on the triazole leads to variations of the magnitude of the σ-donation felt by the metal Another important feature of the triazole ring is that it can be deprotonated, leading to an extensive ground state and excited-state acid-base chemistry [82]

1.2.3 Pyridyl- and Pyrazyltriazole Moieties as Ligands in Ruthenium(II) Polypyridyl Complexes

Since the need to tune the excited-state properties was realised, there has been an interest in incorporating a coordinating ligand into ruthenium complexes that differs from bpy. [84] Following the pioneering work of Vos and co-workers in which two 1,2,4- triazoles were coordinated to the $[Ru(bpy)_2]^{2+}$ unit in a monodentate fashion a number of mixed ligand Ru(II) complexes with electron rich 1,2,4-triazole containing bridging ligands have been investigated in considerable detail by Vos and co-workers. [80] Two such ligands are the anions of 3,5-bis(pyridin-2-yl)-1,2,4-triazole (Hbpt) and 3,5-bis(pyrazine-2-yl)-1,2,4-triazole (Hbpzt) shown in *figure 1.12*.[85]

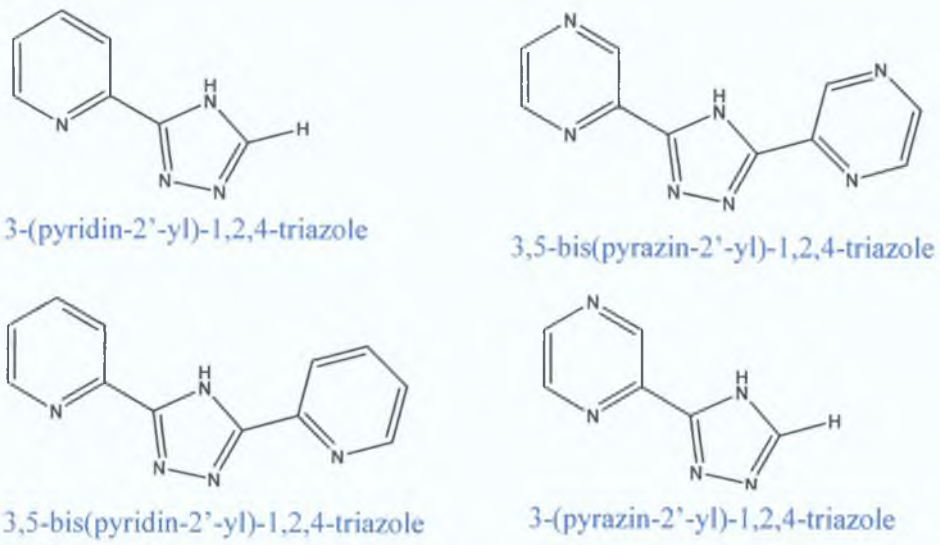

Figure 1.12 Bidentate chelating ligands. [75]

Vos and co-workers have also investigated the effect that the introduction of such asymmetric bidentate ligands has on the physical properties of ruthenium complexes. [86][87] These properties arise as it is known that five-membered rings, such as 1,2,4-triazole, pyrazoles and imidazoles, are strong σ-donor ligands and weak π-acceptor ligands compared to 2,2'-bipyridine. Asymmetric bidentate ligands of this kind therefore produce ruthenium compounds with unusual excited-state properties. [86][87] Furthermore, triazoles contain an acidic N–H group, which imparts unusual properties.

In the deprotonated state the ligand is a strong σ-donor while the second, pyridine or pyrazine, arm of the chelating ligand has well defined π-acceptor properties The two coordinating arms of the ligand therefore possess quite different electronic properties Furthermore, two binding positions are available on the triazole ring, namely N2 and N4, these sites are not equivalent and therefore introduce further asymmetry into the metal complex [84] The preparation of novel pyrazinyltriazole ligands and the physical properties of a series of ruthenium polypyridyl complexes containing these ligands have also been investigated It is known that bipyrazine has weaker σ-donor capacities and stronger π-acceptor properties than bipyridine [86] It is therefore expected that there will be substantial differences between the photophysical properties of the compounds containing pyridyltriazole and pyrazyltriazoles

Of particular interest is the nature of the lowest unoccupied molecular orbital (LUMO) in these compounds It has been found that by using ligands such as 3,5-bis(pyridin-2'-yl)-1,2,4-triazole the lowest energy excited-state is located on the polypyridyl ligands (i e bpy) whilst with the ligand 3,5-bis(pyrazine-2'-yl)-1,2,4-triazole the emitting state is located on the pyrazine bridging ligand [88] An additional feature of pyrazine-containing ligands is the possibility of protonation of the non-coordinating pyrazine atom m strong acidic media [89] Furthermore it has been shown that in dinuclear complexes based on pyridine and pyrazine triazole ligands the negative charge on the triazole ring greatly affects the interaction between the metal centers [59] For instance, it has been shown that in ruthenium polypyridyl complexes incorporating the ligands 3,5-bis(pyridin-2-yl)-1,2,4-triazole or 3,5-bis(pyrazine-2-yl)-1,2,4-triazole relatively strong interactions can be obtained between metal centres, so that both electron transfer and energy transfer processes can occur efficiently [85][74] For example, Hage *et al* have shown that in the dinuclear ruthenium polypyridyl complex contaimng 3,5-bis(pyridin-2-yl)-1,2,4-triazole a strong metal-metal interaction was observed and the species was classified as a class II material, indicated by a large value for the electron delocalisation ($\alpha^2 = 9\ 4 \times 10^{-3}$) [59]

1.3 Electronic coupling between metal centres

1 3 1 Optical Electron Transfer

Photomduced energy and electron transfer processes lie at the heart of fundamental natural phenomena, such as photosynthesis, as well as of a variety of applications In the last few years, research in this field has progressively moved from molecular to supramolecular systems [45] If these supramolecular species are composed of a photosensitiser (*S*) and a quencher (*Q*) covalently linked by a component (L) so that they are of the type *S*-L-*Q*, light excitation of the photosensitiser (*Eqn 7*) can be followed by energy (*Eqn 8*) or electron (*Eqn 9*) transfer processes [12]

$$S\text{-L-}Q + h\upsilon \rightarrow {}^{*}S\text{-L-}Q \qquad (Eqn\ 7)$$

$$^{*}S\text{-L-}Q \rightarrow S\text{-L-}^{*}Q \qquad (Eqn\ 8)$$

$$^{*}S\text{-L-}Q \rightarrow S^{+}\text{-L-}Q^{-} \qquad (Eqn\ 9)$$

Within these systems electron transfer from one metal centre to the other may also occur not only thermally, but also optically (*Eqn 10*)

$$S\text{-L-}Q + h\upsilon \rightarrow S^{+}\text{-L-}Q^{-} \qquad (Eqn\ 10)$$

Therefore, optical transitions such as charge transfer (CT) or intervalence transfer (IT) transitions can arise Typically, these are mixed-valence compounds of the type $[M_1L_n\text{-bridge-}M_2L'_n]^{m+}$ [12][21]

1 3 2 Spectroelectrochemistry

Dinuclear ruthenium compounds have attracted much attention, not only because of their ability to transfer two electrons but also because of the present interest in mixed-valence compounds The physical properties of these compounds have been discussed in light of models published by Hush [90] In particular, the intervalence transition (IT) of the mixed-valence compounds has been studied extensively as its position, shape and intensity yield information about the interaction between the metal centres [59] The most direct measure of the metal-metal electronic coupling in a mixed-valence system, $Ru^{II}Ru^{III}$, can therefore be obtained from intervalence transitions (IT) [90][91][92]

In situ electrochemical generation of stable species, united with spectroscopic characterisation by luminescence and absorption methods, broadens the possibilities for the investigation of the properties of novel excited-state species and their reactivity In many cases electrochemistry yields synthetically inaccessible oxidation states and therefore spectroelectrochemistry offers new windows for exploring novel chemical pathways [93] Other advantages of this method include (i) the species are studied near their ground state, avoiding large perturbations as in photochemically triggered reactions, (ii) the measurement, being static, is relatively simple and easy to perform, and (iii) interferences from intermolecular effects are absent/negligible [94] For this reason many spectroelectrochemical studies of ruthenium dinuclear complexes containing various bridging ligands have been undertaken and it has been noted that the oxidative spectroelectrochemistry of ruthenium dinuclear complexes exhibits rich near-infrared spectra (7000-10000 cm^{-1}) [95]

For example, Hage and co-workers have spectroelectrochemically investigated dinuclear ruthenium complexes containing 3,5-bis(pyridin-2'-yl)-1,2,4-triazole (*figure 1 12*) They found that in its deprotonated state this bridging ligand mediates a rather strong interaction between the ruthenium centres and classified it as a class II material with strong interaction between the metal sites [59] Conversely, Haga and co-workers [95] studied dinuclear complexes with benzimidazole groups in a similar manner They found that the metal-metal interaction increased when the complex was deprotonated [95] Vos and co-workers have also undertaken numerous spectroelectrochemical analyses of dinuclear ruthenium polypyridyl complexes containing various bridging moieties, including thiophene- and phenylene-bridged complexes, in order to determine the degree of metal-metal interaction These mixed-valence compounds were found to be class II type complexes (or valence trapped) dinuclear species [96][97][98]

However, although intervalence transitions in mixed-valence compounds have been studied more intensely, spectroelectrochemistry has also been used to probe ligand to metal charge transfer (LMCT) states These transitions arise due to the removal of an electron from the HOMO of the donor ligand to one of the partially filled t_{2g} orbitals of the metal ion

Generally, these transitions tend to display relatively weak intensities ($\varepsilon < 500$ cm ^{1}), as is the case for the archetypal complex $[Ru(bpy)_3]^{3+}$, or indeed are non-emissive in nature In certain ruthenium compounds, which contain electron rich donor ligands, LMCT bands have however, been noted For example, Haga *et al* observed an LMCT band in both the mononuclear (14,400 cm ^{1}) and dinuclear (8600 cm ^{1} and 12,400 cm^{-1}) ruthenium complexes containing 2,2'-bis(2-pyridyl)bibenzimidazole [95] Vos and co-workers have also reported LMCT bands for a range of triazole bridged Ru(III) complexes while Hage *et al* have observed these bands in the spectrum of Ru(III) complex containing the electron rich ligand 3,5-di(2-pyridyl)-1H-1,2,4-triazole [98][99] Hence, the energy and intensity of the LMCT band increases with increasing electron-donating capacity of the donor ligand Nazeeruddin and co-workers further verified this fact by notmg the effect that various ligands (OMe, Me, NH_2) in ruthenium polypyridyl complexes had on the LMCT transition [100]

1 3 3 Intervalence Charge Transfer Transitions

In ligand-bridged, mixed-valance complexes, low energy electronic transitions are often observed which have been assigned to intervalence transfer (IT) transitions [101] For mixed-valence species such bands are expected and are assigned to IT transitions between metal ions of different valencies (localised situation) or different combinations of metal-centred MOs (delocalised situation) [102] In multinuclear complexes, therefore, it is possible to determine the degree of metal-metal interaction by examination of the intervalence transition band In a valence localised description the overall charge corresponds to a Ru(II)-Ru(III) complex In a fully delocalised description an Ru(II½)-Ru(II½) complex would result In principle, the degree of intercomponent interaction may be determined from electrochemical measurements (K_c), however this is a somewhat limited approach to identify the true strength of the electron delocalisation [98] Hence, the factors determining the localised or delocalised nature of the complex can be more easily determined following the approach originally developed by Hush [14][90]

Hush related the energy, intensity and half-width at maximum intensity of the intervalence charge transfer transition to the degree of electronic coupling (H_{AB}) in a symmetrical system via the following equations [90][91][103]

$$\bar{\upsilon}_{max} = (\bar{\upsilon}_{½})^2 / 2\,31 \qquad (Eqn\ 11)$$

A measure of delocalisation in both the ground and excited-states is α^2, which can be calculated as follows

$$\alpha^2 = \frac{(4.2 \times 10^{-4})\, \varepsilon_{max}\, \bar{\upsilon}_{½}}{\bar{\upsilon}_{max}\, d^2} \qquad (Eqn\ 12)$$

$$H_{AB} = (\alpha^2\ E_{op}^2)^{½} \qquad (Eqn\ 13)$$

where $\bar{\upsilon}_{max}$ is the IT band maximum in $c\bar{m}^{-1}$, $\upsilon_{½}$ is the bandwidth at half height (cm^{-1}), d is the internuclear separation between the metal ions (in Å), ε_{max} is the molar extinction coefficient at $\bar{\upsilon}_{max}$ and E_{op} is the energy of the IT band (cm^{-1}) The calculated bandwidth can then be compared to the experimentally observed bandwidth If the two bandwidths are in agreement then the system may be deemed as valence-trapped (localised), while if the band is too narrow the system is more likely to be considered as delocalised ($M^{II½}$ - $M^{II½}$) [103] This degree of metal-metal interaction is dependant on a number of factors, for example, (i) the distance between the metal centres, (ii) the ability of the bridging ligand to delocalise the electronic charge and (iii) the coordination environments of the metal ions [104] If, for example, the two valence-localised "electronic isomers" Ru^{II}-Ru^{III} and Ru^{III}-Ru^{II} are considered then two different coupling strengths may arise Either the metal centres interact weakly or not at all This situation is presented visually in the following diagram (*figure 1 13*) Specific equilibrium geometries correspond to each of these species, in terms of both "inner" (bond lengths and angles within the two reaction partners (λ_i)) and "outer" (solvent reorientation around the reacting pair (λ_o)) nuclear degrees of freedom In *figure 1 13* (A) it may be seen that at the equilibrium geometry of each electronic isomer the other isomer can be considered as an electronically excited-state

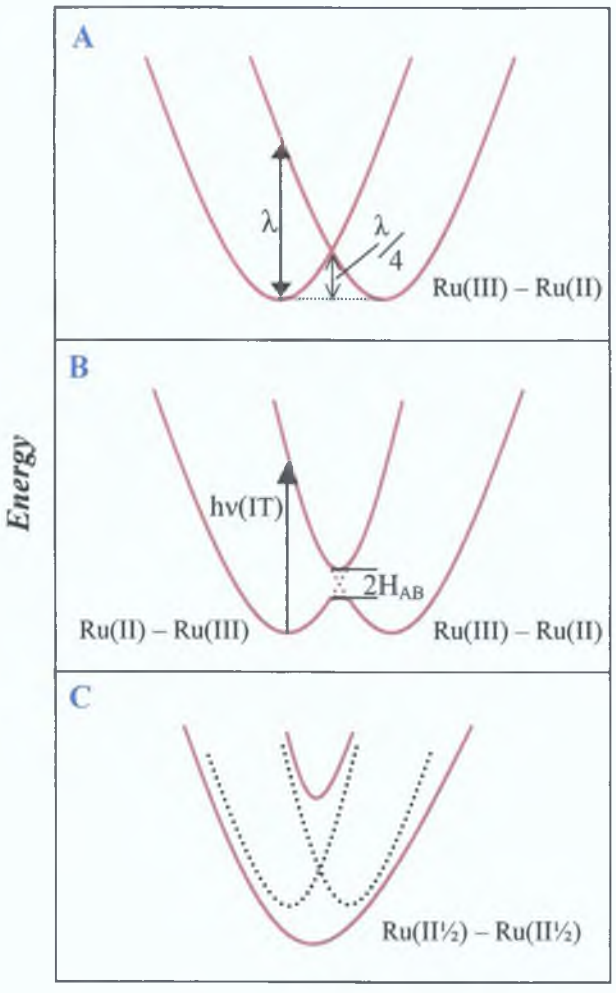

Figure 1.13 Potential energy curves of mixed valence compounds with negligible (A), weak (B), and strong (C) electronic coupling. In (B) and (C), the dashed curves represent zero-order states.

The energy separation between these two states at the equilibrium geometry is therefore the reorganisation energy (λ):

$$\lambda = \lambda_i + \lambda_o \qquad (Eqn.\ 14)$$

At the crossing point both isomers have the same energy and geometry and there are no Franck-Condon restrictions to electron exchange between the two centres. Hence, H_{AB} is negligible and the probability of electron exchange is negligible. [12][13]

However, generally, some electronic interaction is present between the Ru^{II} and Ru^{III} centres. This interaction arises due to either direct overlapping of the orbitals or across the bridge. This situation is represented in *figure 1.13* (B). Here, although there is little effect on the zero-order curves in the region of the equilibrium geometries, there is mixing of the zero-order states at the crossing points (*figure 1.13*). Therefore, although the system is still valence localised and both metal centres still behave as separate components, new properties do now arise due to the interaction of the metal centres and hence the IT band appears. [12][14] However, it may be the case that the interaction between the two metal centres is appreciably strong enough so that the zero-order levels are substantially perturbed in the region of their equilibrium geometries. This situation is represented in *figure 1.13* (C). In this case the complex is considered a fully delocalised species as represented by $M^{II½}$ - $M^{II½}$. [12][14]

1.3.4 Robin - Day Classification

For mixed-valence, bimetallic systems three classes may be delineated depending on the amount of metal-to-metal interaction. Robin and Day developed a system in order to distinguish these three separate classes. [105] Based on the above explanations these classes are as follows:

Class I: A bimetallic compound may be said to be class I if the interaction between the two metal centres is negligible. Within complexes of this type the properties are composed of the discreet properties of each independent metal component. In this type of complex no intervalence transition (IT) band is present in the spectrum. This type of bimetallic complex generally contains long chain bridging ligands or are systems in which the two metal units are separated by a saturated group. For example, 1,2-bis(4-pyridyl)ethane which was investigated by Meyer and co-workers [106] and was found to exhibit no appreciable metal-metal interaction due to the fact that the two π systems are separated by a saturated group (*figure 1.14*).[106] Vos and co-workers also noted the lack of an IT band in a class I, dinuclear ruthenium complex bridged by 1,3-bis(pyridin-2-yl-1,2,4-triazol-3-yl)benzene due to reduced electronic coupling (*figure 1.14*).[98]

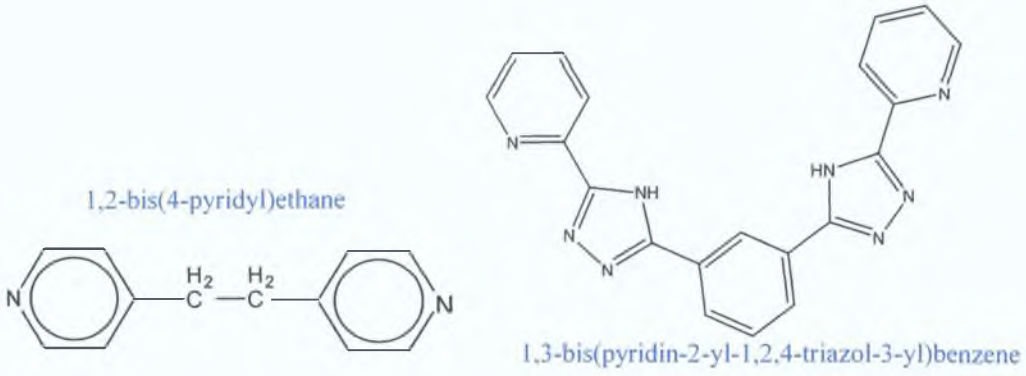

Figure 1.14 The bridging ligands contained in some class I dinuclear Ru(II) complexes.[98][106]

Class II: Bimetallic mixed-valence compounds are said to be class II if there is some degree of interaction between the metal centers albeit weak. This is evident by the presence of IT bands, which can be characterized by Hush. Furthermore, these systems have localised valencies however, they also have new properties due to the mixed-valence species. Some examples of this class of complex include the dinuclear ruthenium polypyridyl complexes bridged by 1,4-bis(pyridin-2-yl-1,2,4-triazol-3-yl)benzene and 1,4-bis(5-(pyridin-2-yl)-1,2,4-triazol-3-yl)-benzene as studied by Vos and co-workers and dinuclear ruthenium complexes containing back-to-back bis(terpyridine) ligands linked by phenylene spacers studied by Collin *et al.* (*figure 1.15*).[98][107]

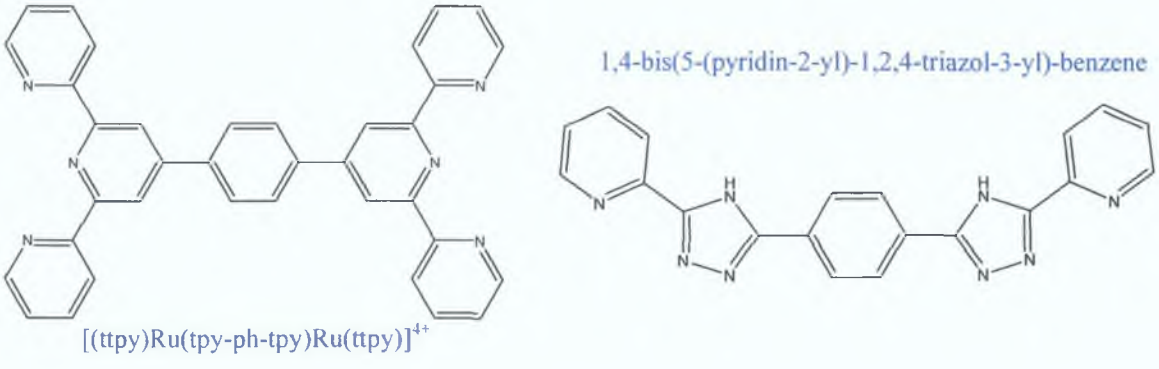

Figure 1.15 The bridging ligands contained in some class II dinuclear Ru(II) complexes.[98][107]

Class III: The metal centres within class III type complexes exhibit strong electronic communication such that they are considered as delocalised systems. The properties that arise within these systems are attributed neither to the M^{II} or the M^{III} centre and the system is best viewed as $M^{II½}$ - $M^{II½}$. Mixed-valence compounds that are deemed to be class I or class II lie in the realm of the supermolecule, while class III complexes approach the large molecule limit. [12] Some examples of class III compounds include the dinuclear ruthenium complexes studied by Creutz [108] which were bridged by (N≡C-C≡N) and the bis-cyclometalating, 3,3',5,5'-tetrapyridylbiphenyl bridged mixed-valence dinuclear ruthenium terpyridine complexes studied by Sauvage and co-workers (*figure 1.16*).[108][109]

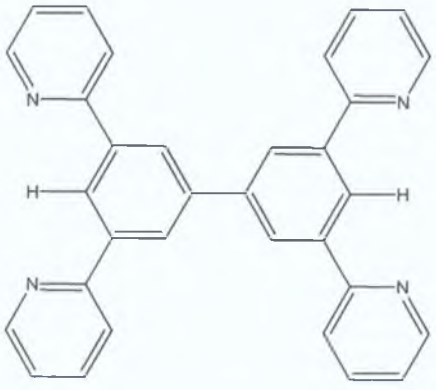

3,3',5,5'-tetrapyridylbiphenyl

Figure 1.16 The bridging ligand contained in the class III dinuclear Ru(II) complex studied by Sauvage and co-workers.[109]

1.4 Scope of Thesis

The focus of this thesis is based on a range of mononuclear and dinuclear ruthenium(II) polypyridyl complexes containing dimethoxyphenyl moieties and their hydroquinone and quinone analogues. Each of the complexes examined within this thesis will contain 1,2,3-triazole moieties which play a crucial role in the overall behaviour of these complexes as well as either pyridyl or pyrazyl groups which are known to exhibit different photophysical characteristics in acidic media. Chapter one provides a background to the nature and characteristics of such complexes with particular emphasis on the archetypal $[Ru(bpy)_3]^{2+}$ compound and its analogues.

In chapter two the procedures and experimental methodology employed during these investigations will be outlined The provenance of the starting materials and solvents as well as the technical details involved in the computational data will also detailed in this chapter The subsequent chapter three will present the synthesis and characterisation of the first group of complexes examined in this thesis These complexes are characterised by the presence of 1,2,4-triazole moieties and dimethoxyphenyl groups They are euphemistically referred to as 'protected' complexes and act as model complexes for the hydroquinone and quinone compounds contained in the subsequent chapters as well as being the synthetic precursors for the subsequent complexes The differences that arise between the pyridyltriazole and pyrazyltriazole complexes will also be examined in this chapter as the excited-state of pyrazine complexes are known to switch upon protonation

Chapters three and four will contain the hydroquinone and quinone analogues of the dimethoxyphenyl complexes These compounds form the nucleus of this thesis and the role of proton transfer within the hydroquinone complexes, which has been mooted in previous publications, is explored in depth in these two chapters Furthermore, the novel synthesis for the preparation of the quinone complexes will also be detailed in chapter five Each of the chapters, three, four and five, contain dinuclear complexes in which the level of intermetallic communication between the metal centres and its variation with changes in the nature of the ligand will also be explored The final chapter, chapter six, will provide on overall examination of the behaviour displayed by the range of complexes as well as suggestions for future work

Finally, three appendices will be provided which will contain additional NMR data, in-depth electrochemical studies aimed at elucidating the optimal solvent conditions and working electrode for these systems and supplementary synthetic data not contained in the main body of the thesis

1.5 Bibliography

1 J Barber, B Andersson, *Nature*, **1994,** 370, 31

2 V Balzani, F Scandola, *Comprehensive Supramolecular Chemistry, Supramolecular Technology,* **1996,**10, 687

3 P Reineker, C Suprıtz, C Warns, I Barvik, *J Luminescence*, **2004,** 108,149

4 S Iwata, J Barber, Current Opinion in Structural Biology, **2004,** 14, 447

5 M R Jones, P K Fyfe, *Current Bio* , **2004,** 14, 320

6 L Hammarstrom, L Sun, B Åkermark, S Styring, *Spectrochim Acta, Part A,* **2001,** 37, 2145

7 L Hammarstrom, *Curr Op Chem Bio* , **2003,** 7, 666

8 L Sun, H Berglund, R Davydov, T Norrby, L Hammarstrom, P Korall, A Borje, C Philouze, K Berg, A Tran, M Andersson, G Stenhagen, J Mårtensson, M Almgren, S Styring, B Åkermark, *J Am Chem Soc* , **1997,** 119, 6996

9 H Berglund-Baudin, L Sun, R Davidov, M Sundahl, S Styring, B Åkermark, M Almgren, L Hammarstrom, *J Phys Chem A* , **1998,** 102, 2512

10 L Hammarstrom, L Sun, B Åkermark, S Styring, *Catalysis Today*, **2000, 58,** 57

11 L Sun, L Hammarstrom, B Åkermark, S Styring, *Chem Soc Rev* , **2001,** 30, 36

12 J P Sauvage, J P Collin, J C Chambron, S Guillerez, C Coudret, V Balzani, F Barigelletti, L De Cola, L Flamigni, *Chem Rev* , **1994,** 94, 993

13 L Sun, J von Gersdorff, J Sobek, H Kurreck, *Tetrahedron,* **1995,** 51, 3535

14 V Balzani, F Scandola, *Supramolecular Photochemistry*, **1991,** Ellis Horwood Ltd

15 S Nishitani, N Kurata, Y Sakata, S Misumi, A Karen, T Okada, N Mataga, *J Am Chem Soc* , **1983,** 105, 7771

16 T A Moore, D Gust, P Mathis, J C Mialocq, C Chachaty, R V Bensasson, E J Land, D Doizi, P A Liddell, G A Nemeth, A L Moore, *Nature*, **1984,** 307, 630

17 W M Campbell, A K Burrell, D L Officer, K W Jolley, *Coord Chem Rev* , **2004,** 248, 1363

18 A Magnuson, Y Frapart, M Abrahamsson, O Horner, B Åkermark, L Sun, J J Girerd, L Hammarstrom, S Styring, *J Am Chem Soc*, **1999**, 121, 89

19 V Balzani, L Moggi, *Coord Chem Rev*, **1990**, 97, 313

20 J H Fendler, *J Chem Ed*, **1983**, 60, 872

21 K Kalyanasundaram, *Photochemistry of Polypyridine and Porphyrin Complexes*, **1992**, Academic Press

22 J P Paris, W W Brandt, *J Am Chem Soc*, **1959**, 81, 5001

23 K Kalyanasundaram, *Coord Chem Rev*, **1982**, 46, 159

24 A Juris, V Balzani, F Barigelletti, S Campagna, P Belser, A Von Zelewsky, *Coord Chem Rev*, **1988**, *84*, 85

25 K R Seddon, *Coord Chem Rev*, **1982**, *41*, 79

26 H D Gafney, A W Adamson, *J Am Chem Soc*, **1972**, 94, 8238

27 C Kutal, *J Chem Ed*, **1983**, 60, 885

28 N Sutin, C Creutz, *Pure Appl Chem*, **1980**, 52, 2717

29 R J Watts, *J Chem Ed*, **1983**, 60, 834

30 A Vlcek Jr, *Coord Chem Rev*, **2000**, 200, 933

31 J M Lehn, J P Sauvage, *Nouv J Chim*, **1977**, *1*, 449

32 F Barigelletti, L De Cola, V Balzani, P Belser, A von Zelewsky, F Vogtle, F Edmeyer, S Grammenudi, *J Am Chem Soc*, **1989**, 111, 4662

33 V Balzani, *J Photochem Photobio, A Chem*, **1990**, 51, 55

34 A Moradpour, E Amouyal, P Keller, H Kagan, *Nouv J Chim*, **1978**, 2, 547

35 S Boyde, G F Strouse, W E Jones Jr, T J Meyer, *J Am Chem Soc*, **1989**, 111, 7448

36 K Kalyanasundaram, M Gratzel, *Angew Chem Int Ed Engl*, **1979**, 18, 781

37 F M el Torki, R H Schmehl, W F Reed, *J Chem Soc, Faraday Trans*, **1989**, 1, 349

38 B H Milosavljevic, J K Thomas, *J Phys Chem*, **1983**, 87, 616

39 I Willner, W E Ford, J W Otvos, M Calvin, *Nature*, **1979**, 280, 823

40 J L Colon, C Y Yang, A Clearfield, C R Martin, *J Phys Chem*, **1990**, 94, 874

41 M H V Huynh, D M Dattelbaum, T J Meyer, *Coord Chem Rev*, **2004**, 249, 457

42 J S Krueger, J E Mayer, T E Mallouk, *J Am Chem Soc*, **1988**, 110, 8232

43 M Borja, P K Dutta, *Nature*, **1993**, 362, 43

44 A J Bard, M A Fox, *Acc Chem Res*, **1995**, 28,141

45 L De Cola, V Balzani, F Barigelletti, L Flamigni, P Belser, A von Zelewsky, M Frank, F Vogtle, *Inorg Chem* ,**1993**, 32, 5228

46 J M Lehn, *Angew Chem Int Ed Engl*, **1988**, 27, 89

47 J M Lehn, *Science*, **1993**, 260, 1762

48 T Klumpp, M Linsenmann, S L Larson, B R Limoges, D Burssner, E B Krissinel, C M Elliott, U E Steiner, *J Am Chem Soc*, **1999**, 121, 1076

49 B O'Regan, M Gratzel, *Nature*, **1991**, 353, 737

50 K Kalyanasundaram, M Gratzel, *Coord Chem Rev*, **1998**, 177, 347

51 V Balzani, *New Scientist*, **1994**, 372, 133

52 G Giuffrida, G Calogero, G Guglielmo, V Ricevuto, M Ciano, S Campagna, *Inorg Chem*, **1993**, 32, 1179

53 R F Ziessel, *J Chem Ed*, **1997**, 74, 673

54 A Islam, H Sugihara, H Arakawa, *J Photochem Photobio A Chem*, **2003**, 158, 131

55 L De Cola, P Belser, *Coord Chem Rev*, **1998**, 177, 301

56 M J Kim, R Konduri, H Ye, F M MacDonnell, F Puntoriero, S Serroni, S Campagna, T Holder, G Kinsel, K Rajeshwar, *Inorg Chem*, **2002**, 41, 2471

57 R Amadelli, R Argazzi, C A Bignozzi, F Scandola, *J Am Chem Soc*, **1990**, 112, 7099

58 A Harriman, R Ziessel, *J Chem Soc, Chem Comm*, **1996**, 1707

59 R Hage, A H J Dijkhuis, J G Haasnoot, R Prins, J Reedijk, B E Buchanan, J G Vos, *Inorg Chem*, **1988**, 27, 2185

60 A C Bennıston, V Goulle, A Harriman, J M Lehn, *J Phys Chem*, **1994**, 98, 7798

61 K Matsui, M K Nazeeruddin, R Humphry-Baker, M Gratzel, K Kalyanasundaram, *J Phys Chem*, **1992**, 96, 10587

62 A C Bennıston, V Grosshenny, A Harriman, R F Ziessel, *Angew Chem Int Edn Engl*, **1994**, 33, 1884

63 Q H Yao, Y Y Huang, L Q Song, B W Zhang, C H Huang, Z S Wang, F Y Li, X S Zhao, *Solar En Mat Solar Cells*, **2003**, 77, 319

64 F E Lytle, D M Hercules, *J Am Chem Soc*, **1969**, 91, 253

65 F E Lytle, D M Hercules, *J Am Chem Soc*, **1969**, 98, 58

66 F A Cotton, G Wilkinson, *Advanced Inorg Chem*, **1988,** Wiley, 5th Edn, New York

67 R Hage, *Ph D Thesis*, **1991,** Leiden University, The Netherlands

68 T E Keyes, J G Vos, J A Kolnaar, J G Haasnoot, J Reedijk, R Hage, *Inorg Chim Acta*, **1996**, 245, 237

69 K Westermark, H Rensmo, J Schnadt, P Persson, S Sodergren, P A Bruhwiler, S Lunell, H Siegbahn, *Chem Phys*, **2002**, 285, 167

70 P S Braterman, A Harriman, G A Heath, L J Yellowlees, *J Chem Soc Dalton Trans*, **1983**,1801

71 B Z Shan, Q Zhao, N Goswami, D M Eichhorn, D P Rillema, *Coord Chem Rev*, **2001**, 211, 117

72 V Balzani, A Juris, *Coord Chem Rev*, **2001**, 211, 97

73 B Durham, J V Caspar, J K Nagle, T J Meyer, *J Am Chem Soc*, **1982**, 104, 4803

74 J G Vos, *Polyhedron*, **1992,** 11, *18*, 2285

75 W R Browne, C M O'Connor, H P Hughes, R Hage, O Walter, M Doering, J F Gallagher, J G Vos, J *Chem Soc, Dalton Trans*, **2002**, 4048

76 R Hage, J G Haasnoot, H A Nieuwenhuis, J Reedijk, R Wang, J G Vos, *J Chem Soc, Dalton Trans*, **1991**, 3271

77 Y Hou, P Xie, K Wu, J Wang, B Zhang, Y Cao, *Solar En Mat Solar Cells*, **2001**, 70, 131

78 F Barigelletti, L De Cola, V Balzani, R Haga, J G Haasnoot, J Reedijk, J G Vos, *Inorg Chem*, **1989**, 28, 4344

79 B P Sullivan, H D Abruna, H O Finklea, D J Salmon, J K Nagle, T J Meyer, H Sprintschnick, *Chem Phys Lett*, **1978**, 58, 389

80 J G Vos, J G Haasnoot, G Vos, *Inorg Chim Acta*, **1983**, 162, 155

81 E V Dose, L J Wilson, *Inorg Chem*, **1978,** 17, 2660

82 P J Steel, E C Constable, *J Chem Soc, Dalton Trans*, **1990**, 1389

83 R Wang, J G Vos, R H Schmehl, R Hage, *J Am Chem Soc*, **1992**, 114, 1964

84 S Fanni, T E Keyes, C M O'Connor, H Hughes, R Wang, J G Vos, *Coord Chem Rev*, **2000**, 208, 77

85 C G Coates, T E Keyes, H P Hughes, P M Jayaweera, J J McGarvey, J G Vos, *J Phys Chem A*, **1998**, 102, 5013

86 C Long, J G Vos, *Inorg Chim Acta*, **1984**, 89, 125

87 R Hage, R Prins, J G Haasnoot, J Reedijk, J G Vos, *J Chem Soc , Dalton Trans* , **1987**, 1389

88 W R Browne, C M O'Connor, H P Hughes, R Hage, O Walter, M Doering, J F Gallagher, J G Vos, *J Chem Soc , Dalton Trans* , **2002**, 4048

89 H A Nieuwenhuis, J G Haasnoot R Hage, J Reedijk, T L Snoeck, D J Stufkens, J G Vos, *Inorg Chem* , **1991**, 30, 48

90 N S Hush, *Prog Inorg Chem* , **1967**, 8, 391

91 N S Hush, *Electrochim Acta*, **1968**, 13, 1005

92 C Creutz, O N Marshall, N Sutin, *J Photochem Photobiol , A Chem* , **1994**, 82, 47

93 J R Kirchhoff, *Current Sep* , **1997**, 16, 1

94 F Weldon, *Ph D Thesis*, **1998**, Dublin City University

95 M Haga, T Ano, K Kano, S Yamabe, *Inorg Chem* , **1991**, 30, 3843

96 P Passaniti, W R Browne, F C Lynch, D Hughes, M Nieuwenhuyzen, P James, M Maestri, J G Vos, *J Chem Soc , Dalton Trans* , **2002**, 1740

97 W R Browne, N O'Boyle, W Henry, A L Guckian, S Horn, T Fett, C M O'Connor, M Duati, L De Cola, C G Coates, K L Ronayne, J J McGarvey, J G Vos, *J Am Chem Soc* , **2005**, 127, 1229

98 W R Browne, F Weldon, A Guckian, J G Vos, *Collect Czech Chem Commun* , **2003**, 1467

99 R Hage, J G Haasnoot, H A Nieuwenhuis, J Reedijk, D J A De Rider, J G Vos, *New J Chem* , **1991**, 15, 501

100 K Kalyanasundaram, S M Zakeeruddin, M K Nazeeruddin, *Coord Chem Rev* , **1994**, 132, 259

101 R W Callahan, T J Meyer, *Chem Phys Letts* , **1976**, 39, 82

102 V Kasack, W Kaim, H Binder, J Jordanov, E Roth, *Inorg Chem* , **1995**, 34, 1924

103 R W Callaghan, F R Keene, T J Meyer, D J Salmon, *J Am Chem Soc* , **1977**, 99, 1064

104 C A Bignozzi, C Paradisi, S Roffia, F Scandola, *Inorg Chem* , **1988**, 27, 408

105 M B Robin, P Day, *Adv Inorg Chem Radiochem* , **1967**, 10, 247

106 R W Callaghan, G M Browne, T J Meyer, *Inorg Chem* , **1975**, 14, 1443

104 C A Bignozzi, C Paradisi, S Roffia, F Scandola, *Inorg Chem*, **1988**, 27, 408

105 M B Robin, P Day, *Adv Inorg Chem Radiochem*, **1967**, 10, 247

106 R W Callaghan, G M Browne, T J Meyer, *Inorg Chem*, **1975**, 14, 1443

107 J P Collin, P Laine, J P Launay, J P Sauvage, A Sour, *J Chem Soc, Chem Commun*, **1993**, 434

108 C Creutz, *Prog Inorg Chem*, **1980**, 30, 1

109 M Beley, J P Collin, R Louis, B Metz, J P Sauvage, *J Amer Chem Soc* **1991**, 113, 8521

Chapter Two

Experimental Methods and Procedures

This chapter details the experimental methods and procedures utilised in the ensuing chapters A brief description of the instrumentation involved in the measurements detailed in the ensuing chapters is also provided along with an explanation of the source and nature of the chemical materials used during these studies

2.1 Materials and Reagents

The synthetic reagents employed during the course of these studies were purchased from Sigma-Aldrich and were of the highest grades available and no further purification was undertaken Any solvents used during spectroscopic measurements were of HPLC grade For luminescence measurements UVASOL (Merck) grade solvents were used The solvents utilised for spectroscopic and electrochemical measurements were all of spectrophotometric grade D_2O (99 9%) and starting materials for the syntheses described were used as obtained from Sigma-Aldrich *Cis*-$Ru(bpy)_2Cl_2\ 2H_2O$ and its deuterated analogue were synthesised via literature methods and obtained in a pure form from *Complex Solutions* (DCU) [1][2] The ligand HL1 (*chapter three*) was supplied and synthesised by Claire Brennan (DCU) using previously reported procedures [3]

2.2 NMR Spectroscopy

The ^{1}H-NMR spectra were obtained on a Bruker AC400 instrument Deuterated solvents were employed for these measurements and generally either d_6-DMSO or d_3-acetonitrile were utilised unless otherwise stated The chemical shifts were recorded relative to TMS and spectra were converted from their free induction decay (FID) profiles using XWIN-NMR software

2.3 Column Chromatography

Column chromatography purification was performed on neutral alumina (Al_2O_3, 150 mesh) Generally, an 80/20 (*v/v*) solution of CH_3CN/H_2O was used as the mobile phase However, occasionally 5-10% MeOH was added in order to aid elution

2.4 Absorption Spectroscopy

The UV/Vis spectra presented in the following chapters were carried out on a Shimadzu *UV3100* UV-Vis-NIR spectrophotometer, which was interfaced to an Elonex *PC575* desktop computer The spectra were obtained in the ultraviolet to near infrared region in the wavelength range 200 to 2500 nm The data obtained were initially acquired on a UVPC graphics program before being converted to an ASCII format and processed using Microcal Origin *6 0* software

All samples were measured in acetonitrile in 0 1 or 1 cm path-length quartz cuvettes The pH of the complexes was adjusted to 8 0 via the addition of trifluoroacetic acid in order to obtain the protonated data The UV data obtain is accurate to within $^{+}$/- 2 nm Extinction coefficients are accurate up to 5%

2.5 Emission Spectroscopy

The Emission spectra presented in this study were obtained on a Perkin-Elmer *LS50B* luminescence spectrometer which was linked to a Dell *PC166* desktop computer Low temperature measurements were taken at 77K by encasing the samples in liquid nitrogen in a vacuumed cryostat environment Excitation and emission slit widths of 10 nm were used for all measurements except at low temperature, where an emission slit width of 2 5 nm was used All of the spectra were generated initially on Perkin-Elmer FL Winlab custom built software and were processed further using Microcal Origin *6 0* software Acetomtrile was used as the solvent for all room temperature measurements while 77K measurement were performed in EtOH / MeOH (4 1) as this provides a good glass Once again, the pH of the complexes was adjusted to 8 0 via the addition of trifluoroacetic acid in order to generate the protonated data The emission data obtained was found to be accurate to within $^{+}$/- 2 nm

2.6 Fluorescence Quantum Yield Determination

Relative fluorescence quantum yield measurements were carried out in accordance with Parker and Rees' methodology [4] $[Ru(bpy)_3]^{2+}$ was used as the reference and hence the reference and the sample were excited at a wavelength at which the absorption of $[Ru(bpy)_3]^{2+}$ and that of the sample coincided The samples were all prepared with an optical density circa 0 40 as concentrated samples can cause errors in these calculations and it is therefore necessary to examine the emissions in the linear region where the concentration is proportional to the luminescence The area under the emission spectrum of each sample was calculated using Microcal Origin 6 0 software and the relative quantum yield was hence calculated from the following equation

$$\Phi_s = \frac{A_r F_s n_s^2}{A_r F_r n_r^2} \Phi_r \qquad (Eqn\ 2\ 1)$$

where $[Ru(bpy)_3]^{2+}$ has an established quantum yield of 0 028 in aqueous, air equilibrated solution *r* and *s* indicate reference and sample, *F* is the integrated area of the emission spectrum with the wavelength in cm^{-1}, A is the absorbance at the excitation wavelength, *n* is the refractive index of the solvent and Φ is the quantum yield of emission These measurements were carried out in acetonitrile and therefore it was not necessary to correct for the refractive index of the solvent [5][6]

2 7 Acid-Base Measurements

All ground state and excited state pKa measurements reported in this thesis were carried out in the aqueous Britton-Robinson buffer Occasionally it was necessary to dissolve the samples in a small amount (circa 0 5 ml) of an organic solvent prior to dilution in the buffer solution The pH was adjusted by the careful addition of NaOH or H_2SO_4 via micropipette to a large volume (circa 100 ml) of the dissolved complex The pH of the solution was monitored using a Corning 240 digital pH meter Absorption and emission spectra were accordingly obtained over a range of pH values The pKa was determined from the changes in the absorption spectra of the complexes examined using the Henderson-Hasslebach equation (Eqn 2 2) at the point at which the concentration of the protonated and deprotonated analyte is equal [7] This is equivalent to the inflection point of the sigmoidal curve The inflection points of the subsequent graphs were estimated by differentiating the best-fit sigmoidal curve calculated using Microcal Origin *6 0* software

$$pH = pK_a + \log_{10}([HA]/[A^-]) \qquad (Eqn\ 2\ 2)$$

Isobestic points from the absorption spectra indicated a wavelength value at which the protonated and deprotonated species demonstrated corresponding absorption coefficients

These values were subsequently used as the excitation wavelengths during the fluorescence measurements in order to ensure that the results obtained were accurate

The excited state pKa (pKa*) data were obtained by manipulation of the observed intensity of each complex as a function of pH The inflection points of the subsequent graphs were estimated by differentiating the best-fit sigmoidal curve calculated using Microcal Origin *6 0* software Two methods were then employed from which the excited state values were calculated (*chapter three*) [8][9]

2.8 Single Photon Counter

The lifetimes of samples (< 20 ns) were determined using an Edinburgh Instruments nf900 ns flashlamp interfaced to a CD900 TAC photon counter in DCU by Dr Andrea McNally (DCU) Additional lifetime data were also provided by Bill Henry (DCU)

2.9 Electrochemical Measurements

An extensive electrochemical analysis was performed prior to this study in order to ascertain the most appropiate electrochemical conditions This data is presented in *appendix B* however, the technique that proved most suitable for the complexes presented in this study is recorded here

Electrochemical measurements were performed in anhydrous acetonitrile (circa 1 mM concentrations) with 0 1 M tetraethylammoniumperchlorate (TEAP) as electrolyte under a steady flow of N_2 to prevent absorption of atmospheric oxygen The TEAP electrolyte was synthesised by preparing a 1 M solution of tetraethylammonium bromide in distilled water Precipitation was then achieved via the addition of 1 mole equivalent of perchloric acid (70 % w/v) The precipitate was collected by vacuum filtration, redissolved in hot water and then neutralised with conc NaOH Upon cooling the product recrystallised and was collected under vacuum and washed with water (25 cm^3), followed by triple recrystallisation from hot water

A 3 mm glassy carbon electrode encased in Teflon was used as the working electrode, a platinum wire as the counter electrode and either a saturated calomel electrode (SCE) or a glass shrouded Ag/AgCl electrode was utilised as the reference electrode A platinum wire was used as the auxiliary electrode In order to negate the effects of hydrogen evolution, which occurs at approximately –0 8 V and causes graphical anomalies, each sample was deaerated prior to scanning at negative potentials

Extensive pre-treatment of the working electrodes were preformed prior to each electrochemical session and between scans Pre-treatment generally consisted of polishing of the electrode surface with decreasing grades of alumina polish (1 μm, 0 5 μm) in distilled water with finely graded polishing pads in a figure of eight motion Excess alumina particles on the surface of the electrodes were removed by sonication in distilled water for 10 min periods The electrodes were then allowed to air dry A CV of the solvent was obtained prior to each electrochemical measurement in order to ensure that all the peaks noted in the CVs were due to the sample being examined The electrodes utilised for the hydroquinone measurements were anodised prior to obtaining the CVs The electrodes were activated oxidatively in non-degassed 0 1 M H_2SO_4 for 180 seconds at an applied potential of 1 80 V after which time the electrodes were removed and washed with distilled water and allowed to air dry [10] Gold and platinum electrodes were cleaned when necessary with nitric acid Protonation of the complexes was achieved via the addition of either 0 1 M $HClO_4$ or 0 1 M CF_3CO_2H to the solution

Scan rates varied from 0 05 V/s to 1 V/s The values used during a particular experiment are quoted below the figures in each chapter All cyclic voltammetric measurements were carried out using either a CH Instruments Memphis 660 potentiostat interfaced to a Dell Inspiron 5100 laptop and interfaced with CHI 1000 software or an Autolab Instrument utilising Eco Chemie (2001) Autolab 4 8 software [11][12] Errors of < 20 mV was calculated for these measurements

2.10 Spectroelectrochemistry

Spectroelectrochemical measurements [13] were carried out using an OTTLE cell arrangement with an optically transparent platinum gauze as a working electrode, a platinum wire as a counter electrode and a glass shrouded Ag/AgCl electrode as a reference electrode Experimental conditions observed during the electrochemical measurements were also utilised during the course of the spectroelectrochemical analyses All samples were prepared as dilute solutions in order to ensure that comprehensive oxidation could occur over time The potential required for the working electrode was obtained using an EG&G PAR Model 362 scanning potentiostat and the resulting absorption spectra of the species generated in the OTTLE cell were recorded on a Shimadzu 3100 UV-Vis/NIR spectrophotometer interfaced with an Elonex PC-433

In the case of the fluorescence spectroelectrochemistry measurements, the cell was positioned at a 45° angle to the incident light The samples were excited at a wavelength which was obtained from the isobestic point of the absorption spectra [14] Repeat scans were then obtained as the potential was applied on a Perkin-Elmer *LS50B* luminescence spectrometer which was linked to a Dell *PC166* desktop computer and the data generated was processed using Microcal Origin 8 0

2.11 Emission Lifetimes

Transient emission data were generated using a Q-switched Nd-YAG spectrum laser system The data were plotted and analysed with the aid of Sigma Plot 8 0 software All measurements were obtained in acetomtrile at room temperature and EtOH / MeOH 4 1 (v/v) at 77 K Samples were prepared with an optical density of 0 4 absorption units in order to negate the consequences of the inner filter effect and the lifetimes were calculated at the maxima of the emission The pH was controlled via the addition of either triethylamine (TEA) or trifluoroacetic acid (TFA) Samples also underwent three freeze-pump-thaw cycles prior to carrying out the room temperature measurements The error in the lifetimes was calculated to be < 8%

2.12 IR Spectroscopy

Infra red spectra were measured using oven dried KBr or in dry chloroform on a Perkin Elmer 2000 FTIR spectrometer

2.13 Elemental Analysis

C, H, N elemental analysis was carried out at the Microanalytical Laboratory of University College Dublin These analyses were obtained using an Exador analytical CE440 instrument

2.14 Bibliography

1 B P Sullivan, D J Salmon and T J Meyer, *Inorg Chem* , **1978**, 17, 3334

2 W R Browne, C M O'Connor, J S Killeen, A L Guckian, M Burke, P James, M Burke, J G Vos, *Inorg Chem* , **2002**, 41, 4245

3 R Hage, *Ph D Thesis*, **1991**, Leiden University, The Netherlands

4 C A Parker and W T Rees , *Analyst*, **1960**, 85, 587

5 K Nakamura, *Bull Chem Soc Jap* , **1982**, 55, 2697

6 B Valeur, *Molecular Fluorescence, Principles and Applications*, **2002**, Wiley-VCH, New York

7 P W Atkins, *General Chemistry, International Student Edition*, **1989**, Scientific American Books, New York

8 J F Ireland and P A H Wyatt, *Adv Phys Org Chem* , **1976**, 12, 131

9 J G Vos, *Polyhedron* , **1992**, 11, 2285

10 G E Cabaniss, A A Diamantis, W R Murphy, R W Linton, T J Meyer *J Am Chem Soc* , **1985**, 107, 1845

11 G A Mabbott, *J Chem Ed* , **1983**, 60, 697

12 D H Evans, K M O'Connell, R A Peterson and M J Kelly, *J Chem Ed* , **1983**, 60, 290

13 W R Heineman, *J Chem Ed* , **1983**, 60, 4

14 J R Kirchhoff, *Current Sep* , **1997**, 16, 11

Chapter Three

Mono- and Dinuclear Ruthenium(II) Complexes Containing Dimethoxy-phenyl Moieties

This chapter details the synthesis, photophysical and photochemical characterisation of a group of mononuclear and dinuclear ruthenium(II) complexes These complexes are characterised by the presence of pyridyl- or pyrazyl-1,2,4-triazole unit(s) coupled with dimethoxy-phenyl moieties These complexes are the primary compounds in a series of related complexes They function as model systems and precursor molecules for the continuing series of complexes in the ensuing chapters

3.1 Introduction

Since that first serendipitous day in the 1930's when the luminescence of $[Ru(bpy)_3]^{2+}$ was first recognised, scientists have been investigating the latent qualities of this complex Recently, research in the area of Ru(II) polypyridyl complexes has entered the realm of supramolecular chemistry This exciting new sphere of research has focused on the development and study of dinuclear and polynuclear ruthenium complexes with the ultimate aim of creating photochemical molecular devices [1] As highly luminescent species, ruthenium (II) polypyridyl complexes are capable of sensitising a wide variety of photo-redox reactions and hence have potential as sensitiser components in artificial photosynthetic systems or even as catalysts for the photochemical splitting of water [2][3][4]

Extensive research is now available in which these complexes have been incorporated into the design and construction of multinuclear structures, in which they are capable of directing and modulating electron and energy transfer processes [5] Although the approaches within these studies are varied, generally, this research has focused on the design of ruthenium polypyridyl complexes in which donor-acceptor molecules such as hydroquinones and quinones are covalently attached to the metal centre [6]

The importance of the hydroquinone / quinone redox couple in natural systems is well established [7] Hydroqumones themselves are capable of acting as electron-donating moieties within these systems, while quinones are known to be moderate electron acceptors [8] It is therefore understandable that these properties have led to the utilisation of these ligands in studies of photo-induced electron transfer, particularly in systems incorporating porphyrin centres as models for artificial photosynthesis [2] Within these studies it has been shown that the quinone / hydroquinone redox couple displays reversible electrochemical inter-conversion in protic media by exchange of two protons and two electrons and the quinone unit has been shown to quench the luminescence of numerous photosensitive transition metal complexes [9][10] These studies have also investigated catechol and its oxidation products (semiquinone and quinone) as ligands [11]

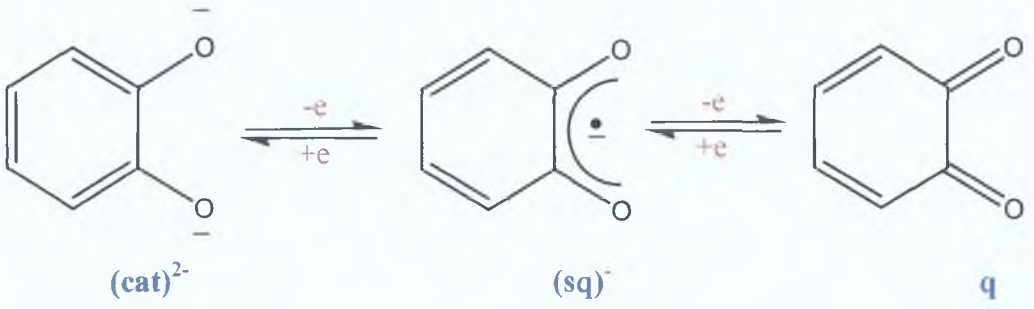

Figure 3.1 The dioxolene redox series [12]

The so-called 'dioxolene redox' series (*figure 3.1*), catecholate (cat), semiquinonate (sq) and quinone (q), when coordinated to metal centres has been studied in depth by Lever and Pierpont.[12] The metal complexes containing catechol moieties have been shown to exhibit mutable electronic effects associated with variable metal and ligand charge distribution, due to the delicate balance in energy between the frontier quinone and metal orbitals.[13] These ligands are "non-innocent" and can coordinate in three different formal oxidation states (q, sq, cat)[11] and studies by Lever and co-workers on the properties of the complex $[Ru(bpy)_2(cat)]$, where H_2cat = catechol, have shown that the complex can undergo two reversible one-electron oxidations, to give the species $[Ru^{II}(bpy)_2(sq)]^+$ and $[Ru^{II}(bpy)_2(q)]^{2+}$.[13]

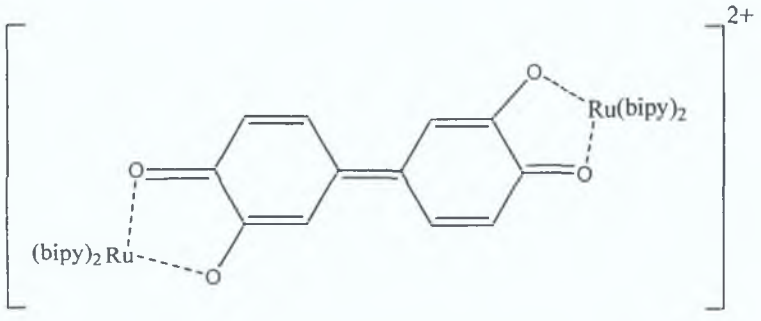

[(Ru(bpy)$_2$)$_2$(3,4,3`,4`-tetrahydroxybiphenyl)]

Figure 3.2 Dinuclear $Ru(bpy)_2$ O,O coordinated complex.[14]

Most metal-catechol compounds reported are based upon 1,2-dihydroxy-type ligands where the hydroquinone moiety acts as a 1,2 chelate through two metal-oxygen bonds. *Figure 3.2* depicts a typical metal catechol complex of this type.

Within these studies it has been shown that ruthenium dioxolene complexes have unusually large degrees of orbital mixing between the metal and the ligand and this gives rise to the possibility of electron delocalisation between the metal and the ligand [15 19] For example, Ward and co-workers have investigated ruthenium dioxolene complexes in which several $Ru(bpy)_2$ units were linked together by use of bridging ligands containing two or more dioxolene binding sites as depicted in *figure 3 3* This resulted in a series of polynuclear complexes displaying exceptionally rich electrochemical and spectroscopic behaviour [20][21]

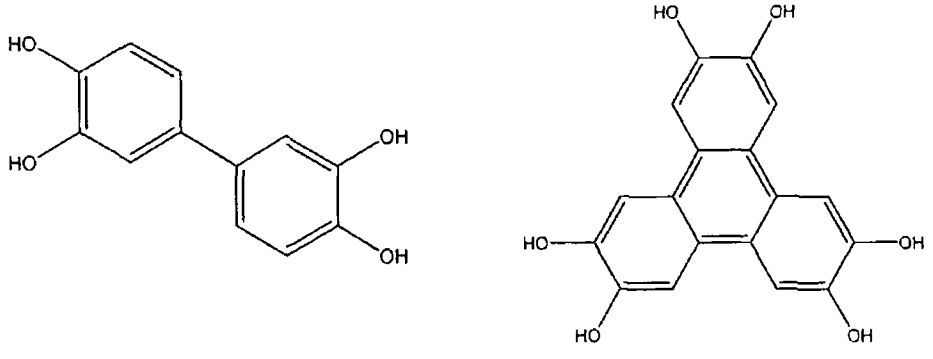

Figure 3 3 Multiple dioxolene binding site ligands prepared by Shukla *et al* [27]

Indeed, binuclear ruthenium complexes in which the metal centres are directly linked by a bridging ligand have attracted much attention due to the possibility of studying electron transfer and delocalisation in mixed valence $Ru^{II}Ru^{III}$ species and Ward and co-workers have also prepared $[(Ru(bpy)_2)_2(OMe)_2](PF_6)_2$, members of a new class of binuclear ruthemum(II) complexes with two alkoxide bridges [21][22] However, coordination via O,O leads to considerable orbital mixing and complicates the properties of the compounds Hence, Vos and co-workers prepared complexes in which the $Ru(bpy)_2$ centres were coordinated via a pyridyl nitrogen and a phenolic OH (*figure 3 4*) [23] The aim of their studies was to further investigate the electronic interaction between the hydroquinone and the Ru-polypyridyl units [23]

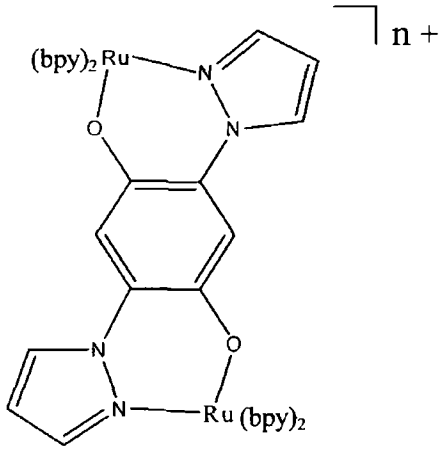

Figure 3 4 A dinuclear $Ru(bpy)_2$ N,O complex [23]

Another approach taken in preparing ruthenium-catechol complexes has been to attach the donating/accepting group to the ruthenium polypyridyl centre via the polypyridyl ligands [24] For example, Lehn and co-workers[25] reported luminescence quenching of the $[Ru(bpy)_3]^{2+}$ chromophore by the covalently connected quinone / hydroquinone grouping More complex forms of this approach were developed by Schanze and Sauer[26] and Shukla *et al* [27] as illustrated in *figure 3 5*

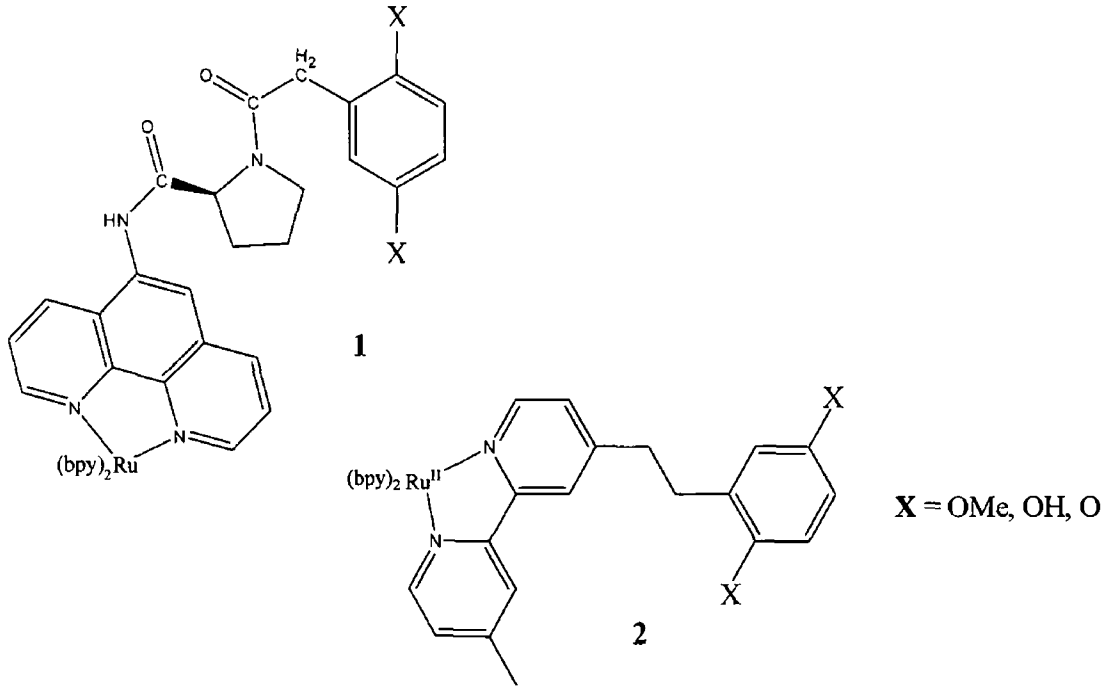

Figure 3.5 Dimethoxy / hydroquinone and quinone containing complexes linked to the metal via the polypyridyl moieties synthesised by Schanze and Sauer[26] (1) and Shukla *et al* (2)[27]

The main disadvantage associated with this approach however, is that the excited state is generally based on the polypyridyl ligands and hence strong coupling between the metal centre and the donor / acceptor moiety occurs and this precludes long-lived charge separation Hence, Vos and co-workers began an investigation into dyad chromophore – quencher systems in which the donor group was linked to a bridging ligand, which was not involved in the luminescent ^{3}MLCT state and furthermore was negatively charged Not only could this approach facilitate longer-lived charge separation but also the presence of the negative bridge is known to facilitate metal-metal communication [28]

Hence, a series of complexes were prepared in which hydroquinone / quinone redox electron donors / acceptors were also linked to a ligand, which is not involved in the luminescent ^{3}MLCT state and was negatively charged 5-(Pyridin-2-yl)-1,2,4-triazole and 5-(pyrazin-2-yl)-1,2,4-triazole are suitable building blocks for this purpose [28] It has been demonstrated that when these ligands are coordinated to Ru(II), the triazole moiety is easily deprotonated leading to a negatively charged triazolate which results in their potential as molecular switches [28] Furthermore, the inclusion of a pyrazyltriazole ligand is expected to produce complexes with interesting properties based on the phenomena of 'switching' of the excited state upon protonation of the triazole ring Finally, it must be noted that homo-dinuclear complexes have also be synthesised containing pyridyltriazole and pyrazyltriazole bridging ligands This is as a consequence of the fact that previous studies have indicated that these bridging ligands can support interaction between metal centres and they therefore also have the potential to form dinuclear complexes in which photomduced electron or energy transfer may occur [29]

Mono- and di-nuclear compounds based on this blueprint were synthesised by Weldon and Keyes,[29][30] however, direct preparation of the hydroquinone-containing complex resulted in low yields For this reason a new synthetic method for the preparation of these complexes from the protected dimethoxy containing analogues was developed [31][32] This approach is reminiscent of those undertaken by Ward and co-workers and other groups in their preparation of qumone containing complexes (*figure 3 5*) [26][27]

Based on these premises a series of complexes has been synthesised. In this chapter the first group of compounds of this series is presented. These complexes consist of dimethoxy spectator groups attached to the ruthenium centre(s) via a negatively charged pyrazyltriazole / pyridyltriazole bridge (*figure 3.6*).

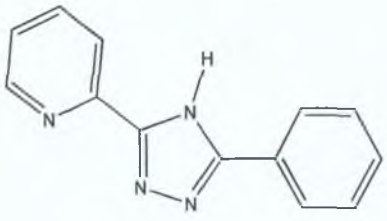

3-phenyl-5- (pyridin-2``-yl)-1H-1`, 2`,4`-triazole **(HL1)**

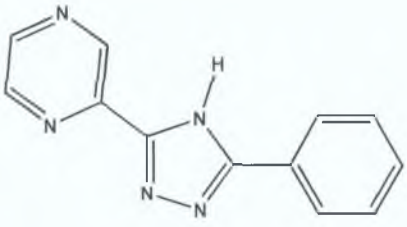

3-phenyl-5- (pyrazin-2``-yl)-1H-1`, 2`,4`-triazole **(HL2)**

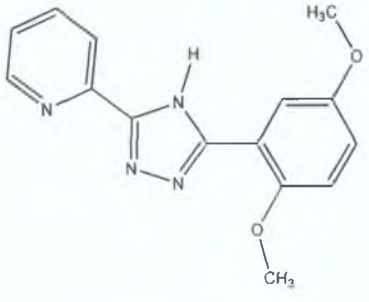

3-(2`, 5`-dimethoxyphenyl)-5-(pyridin-2``-yl)-1H-1`, 2`,4`-triazole **(HL3)**

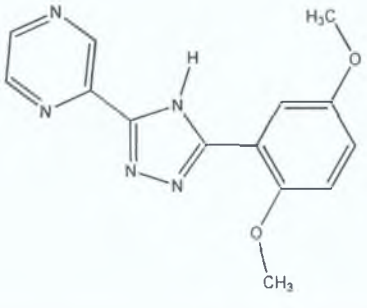

3-(2`, 5`-dimethoxyphenyl)-5-(pyrazin-2``-yl)-1H-1`, 2`,4`-triazole **(HL4)**

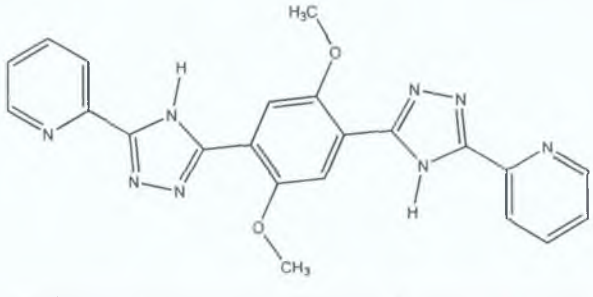

1,4-bis (5`-(pyridin-2``-yl)-1`H-1`, 2`, 4`-triazol-3`-yl)-2,5-dimethoxyphenyl **(H_2L5)**

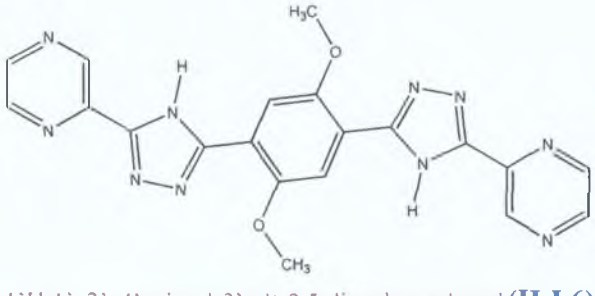

1,4-bis (5`-(pyrazin-2``-yl)-1`H-1`, 2`, 4`-triazol-3`-yl)-2,5-dimethoxyphenyl **(H_2L6)**

Figure 3.6 Structures and nomenclature of ligands cited in this chapter.

The metal complexes synthesised utilising these ligands are coordinated to the metal centre(s) via a triazolic nitrogen and the nitrogen of the pyridine or pyrazine group as shown in the following diagram (*figure 3 7*) of the proposed structure of $[Ru(bpy)_2(L5)Ru(bpy)_2]^{2+}$ which contains the ligand H_2L5 (*figure 3 6*)

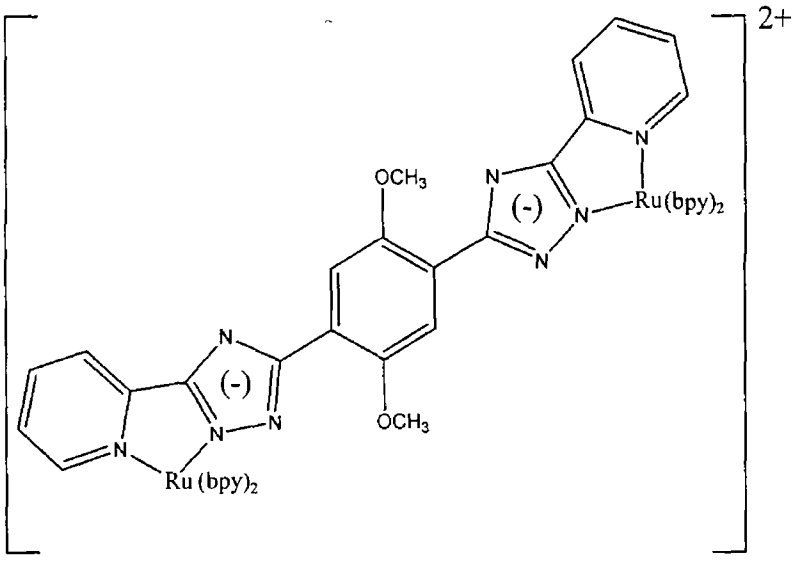

Figure 3 7 Proposed structure of the dinuclear pyrazyltriazole complex $[Ru(bpy)_2(L5)Ru(bpy)_2]^{2+}$

The mononuclear complexes 1 and 2 contain the ligands HL1 and HL2, respectively, which include an unsubstituted phenyl ring, while complexes 3 and 4 are the methoxylated mononuclear complexes containing ligands HL3 and HL4, respectively The dinuclear dimethoxy-containing complexes are complexes 5 and 6 and these compounds contain the ligands H_2L5 and H_2L6, respectively (*figure 3 7*) The complexes discussed in this chapter are important as they act as precursor compounds for the succeeding complexes described in the following chapters and are also model complexes Complexes 3 to 6 are precursor complexes, which act as the parent complexes and form the basis for the synthesis of a covey of complexes, which together provide a complete photophysical and photochemical characterisation of this genre of complex Complexes 1 and 2 are parent complexes, which provide a basis for elucidation of the photophysical and photochemical data obtained for the dimethoxyphenyl complexes Complexes 5 and 6 are homo-dinuclear complexes, which are of particular significance due to their potential to display interesting metal-metal interactions

Synthetic methods for the preparation of the ligands and the Ru (II) polypyridyl precursor complexes formed from these ligands are also provided in this chapter The ligands cited in this chapter are shown in *figure 3 6* Purity of these complexes was assessed by NMR spectroscopy and elemental analysis Once the purity of these complexes was accessed they were further characterised by emission and absorption spectroscopy and the excited state lifetimes of the various complexes have been measured and are reported in the following section The effect of the ligands on the metal centre, as well as the location of the excited state, is also accessed

Furthermore, acid-base measurements were obtained in order to investigate the nature of the lowest unoccupied molecular orbital (LUMO) This is a characteristic that varied depending on whether or not the complex contained a pyridyltriazole or a pyrazyltriazole Hence, pKa and pKa* values are presented In the case of the electrochemical characterisation, both the oxidation of the metal centre and the ligand-based reductions have been measured Finally, spectroelectrochemical data, which also vary considerably over the range of complexes and provides interesting insights into the degree of intermetallic interaction in the dinuclear complexes, are also included

The aim of this chapter is to characterise the photophysical and electrochemical properties of this group of pyrazyltriazole and pyridyltriazole complexes as these studies have not been performed previously These will then be used as model complexes for the subsequent hydroquinone and quinone complexes introduced in chapters four and five, respectively Hence, it will be demonstrated whether or not the process of electrochemically induced proton transfer, as suggested by Wang *et al*,[7] occurs within the hydroquinone complexes (*chapter four*)

3.2 Experimental Methodology

3.2.1 Synthesis of Ligands

The syntheses of the ligands, whose structure, numbering, names and abbreviations are contained in *figure 3.6*, are presented in the following section while the ^{1}H-NMR spectral analysis of the ligands HL2 and HL3 are shown in *figure 3.8*. Keyes prepared the dihydroxy-containing analogue of HL3 in her Ph.D Thesis. [7][31] The ligands HL3 and HL4 were prepared in a similar manner as this complex with the exception that dimethoxybenzoic acid was used in place of dihydroxybenzoic acid. The ligands H_2L5 and H_2L6 have also been prepared previously and the method devised by Hughes *et al.* was employed in the synthesis of these ligands. [32][33] The ligand HL1 has also been prepared previously and was synthesised in this study according to well-known literature methods. [1] The ligand HL2 was synthesised by and obtained from Claire Brennan, following the method described by Hage.[35]

3-phenyl-5- (pyridin-2''-yl)-1H-1', 2', 4'-triazole (HL1)

This ligand was prepared according to modified literature methods. [1] **^{1}H-NMR (d_6-DMSO): δ 8.56 (d, 1H, pyridyl $H^{6''}$), 8.14 (d, 1H, pyridyl $H^{3''}$), 8.10 (dd, 1H, pyridyl $H^{4''}$), 8.07 (d, 1H, phenyl $H^{6'}$), 7.89 (dd, 1H, pyridyl $H^{5''}$), 7.42 (d, 1H, phenyl $H^{2'}$), 7.38 (dd, 1H, phenyl $H^{5'}$), 7.34 (dd, 1H, phenyl $H^{3'}$), 7.30 (dd, 1H, phenyl $H^{4'}$).**

3-phenyl-5- (pyrazin-2''-yl)-1H-1', 2', 4'-triazole (HL2)

This ligand was prepared and obtained within the group via modified literature methods. [1] **^{1}H-NMR (d_6-DMSO): δ 9.38 (s, 1H, pyrazyl $H^{3''}$), 8.79 (dd, 2H, pyrazyl $H^{5''}$and pyrazyl $H^{6''}$), 8.13 (dd, 2H, phenyl $H^{2'}$ and phenyl $H^{6'}$), 7.53 (m, 3H, phenyl $H^{3'}$, $H^{5'}$, $H^{4'}$).**

3-(2',5'-dimethoxyphenyl)-5-(pyridin-2''-yl)-1H-1,2,4-triazole (HL3)

This ligand was prepared according to literature methods with the exception that 2,5-dimethoxybenzoic acid was used in place of 2,5-dihydroxybenzoic acid. [30] Yield: 3.6 g, 64 %. **^{1}H NMR (d_6-DMSO): δ 12.54 (s, 1H, -NH), 8.70 (d, 1H, pyridyl $H^{6''}$), 8.15 (d, 1H, pyridyl $H^{3''}$), 7.92 (dd, 1H, pyridyl $H^{4''}$), 7.68 (s, 1H, dimethoxy $H^{6'}$), 7.41 (dd, 1H, pyridyl $H^{5''}$), 7.31 (dd, 1H, dimethoxy $H^{4'}$), 7.06 (d, 1H, dimethoxy $H^{4'}$), 3.91 (s, H3, -OCH_3), 3.80 (s, H3, -OCH_3).**

3-(2',5'-dimethoxyphenyl)-5-(pyrazin-2''-yl)-1H-1,2,4-triazole (HL4)

The method used was the same as that described for the formation of 3-(2',5'-dimethoxyphenyl)-5-(pyridin-2''-yl)-1H-1,2,4-triazole (HL3), with the exception that 1-(2',5'-dimethoxyphenyl)-4-(pyrazin-2''-yl)-acylamidrazone was cyclised in the reaction.[30] Yield: 3.2 g, 72 %. **^{1}H NMR (d^6-DMSO): δ 9.32 (s, 1H, pyrazyl $H^{3''}$), 8.74 (s, 1H, pyrazyl $H^{5''}$), 8.68 (s, 1H, pyrazyl $H^{6''}$), 7.68 (s, 1H, dimethoxy $H^{6'}$), 7.14 (d, 1H, dimethoxy $H^{3'}$), 7.06 (d, 1H, dimethoxy $H^{4'}$), 3.91 (s, 3H, -OCH_3), 3.80 (s, 3H, -OCH_3).**

1,4-bis(5'-(pyridin-2''-yl)-1'H-1',2',4'-triazol-3'-yl)-2,5-dimethoxybenzene (H_2L5)

This ligand was prepared according to methods devised by Hughes. [32] Yield: 2.10g, 50 %. **^{1}H NMR (d_6-DMSO): δ 14.12 (s, 2H, –NH), 8.63 (d, 2H, pyridyl $H^{6''}$), 8.21 (d, 2H, pyridyl $H^{3''}$), 7.92 (d, 2H, pyridyl $H^{4''}$) and (dd, 2H, pyridyl $H^{5''}$), 7.50 (s, 2H, dimethoxy $H^{3'}$ and $H^{6'}$), 4.08 (s, 6H, –OCH_3).**

1,4-bis(5'-(pyrazin-2''-yl)-1'H-1',2',4'-triazol-3'-yl)-2,5-dimethoxybenzene (H_2L6)

The method used was the same as that described for the formation 1,4-bis(5'-(pyridin-2''-yl)-1'H-1',2',4'-triazol-3'-yl)-2,5-dimethoxybenzene (H_2L5), with the exception that 1,4-bis(acyl-pyrazin-2'-yl-amidrazone)-2,5-dimethoxy-benzene was cyclised in the reaction.[32] Yield: 1.90g, 51%. **^{1}H NMR (d_6-DMSO): δ 9.16 (s, 2H, pyrazyl $H^{3''}$), 8.54 (d, 2H, pyrazyl $H^{5''}$), 8.47 (d, 2H, pyrazyl $H^{6''}$), 7.71 (s, 2H, dimethoxy $H^{3'}$ and $H^{6'}$), 4.08 (s, 6H, 2 x –OCH_3).**

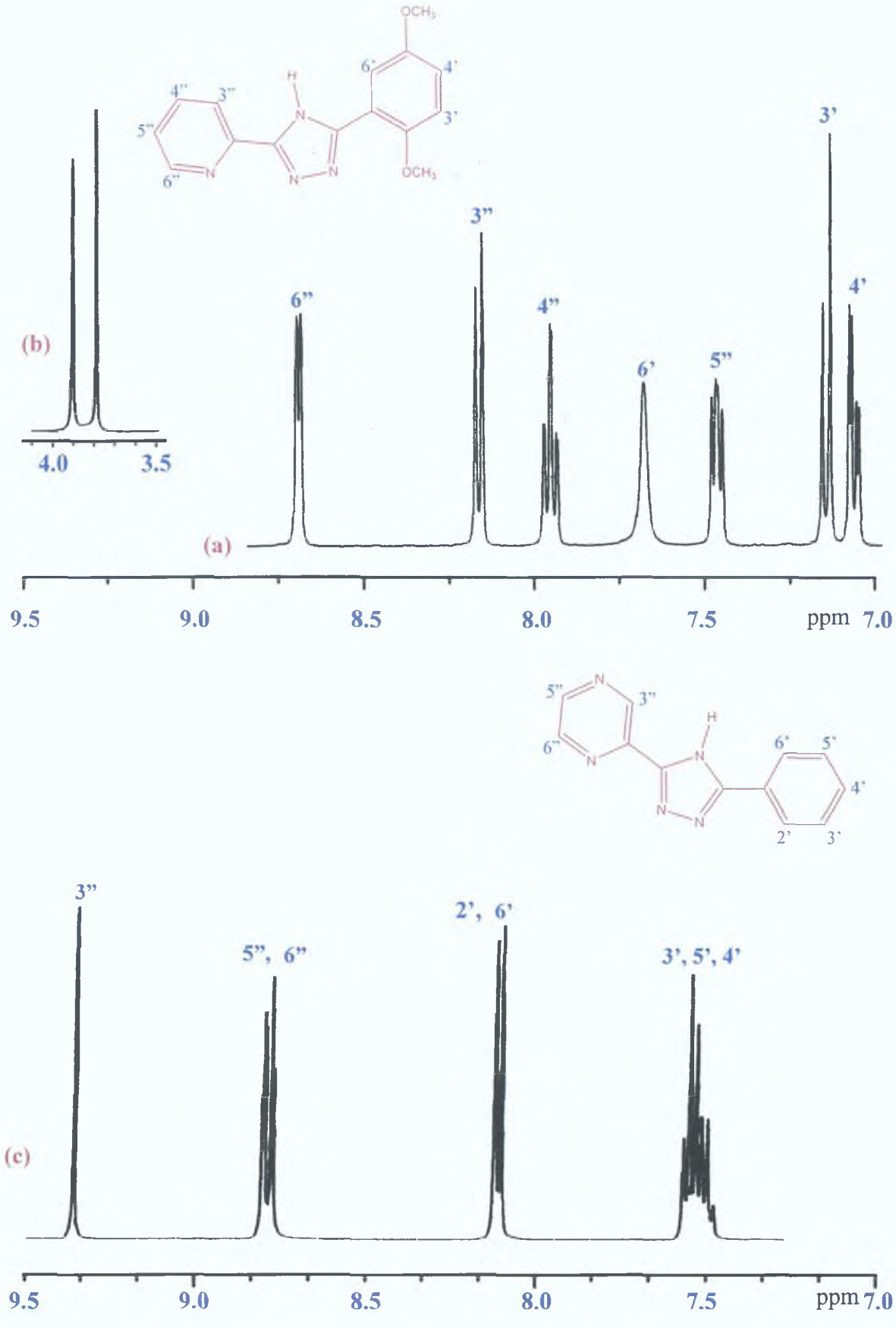

Figure 3.8 ^{1}H-NMR Spectra of the ligands (a) HL3 showing (b) $-OCH_3$ peaks inset and (c) HL2 measured in d_6-dimethyl sulphoxide (chemical shifts / ppm vs Me_4Si)

3.2.2 Synthesis of Metal Complexes

The syntheses of the Ru(II) mononuclear and dinuclear complexes of the ligands described above are presented in this section. These complexes have also been synthesised previously. However, since limited data is available on their photochemical and photophysical properties and they are precursor complexes for the compounds contained in the following chapter, it was necessary to perform their re-synthesis. $[Ru(bpy)_2Cl_2].2H_2O$ was prepared within the group according to the method described by Sullivan *et al.*[34] The ^{1}H-NMR spectra of two of the substituted phenyl complexes are presented in *figure 3.9.* Additional X-ray structure data are available for the dimethoxy-containing complexes in the thesis of Hughes. [32][33]

Complex 1: $[Ru(bpy)_2(L1)]PF_6.H_2O$

cis-$[Ru(bpy)_2Cl_2].2H_2O$ (150 mg, 0.288 mmol) and HL1 (80 mg, 0.35 mmol) were heated at reflux for 8 h in 50 cm^3 $EtOH/H_2O$ (2:1 v/v). The hot solution was filtered and evaporated to dryness after which 10 cm^3 of water was added to the dark red product. The complex was precipitated with an excess of an aqueous solution of NH_4PF_6. The product was purified by column chromatography with neutral alumina and acetonitrile as eluent. The product obtained was recrystallised from ethanol/H_2O (with 1 drop of conc. ammonia). Yield: 194 mg (82%). Calculated for $C_{33}N_8H_{27}OPF_6Ru$: C: 49.82; H: 3.16; N: 14.08 %. Anal. Found: C: 50.07; H: 2.91; N: 13.85 %.

Complex 2: $[Ru(bpy)_2(L2)]PF_6.H_2O$

The synthesis of this complex is the same as for $[Ru(bpy)_2(L1)]PF_6$ with the exception that HL2 was used in place of HL1. Yield: 190 mg (80%). Calculated for $C_{32}N_9H_{26}OPF_6Ru$: C: 48.13; H: 3.28; N: 15.78 %. Anal. Found: C: 48.03; H: 3.01; N: 15.85 %.

Complex 3: $[Ru(bpy)_2(L3)]PF_6.2H_2O$

Once again the synthesis of this complex is the same as for $[Ru(bpy)_2(L1)]PF_6.H_2O$ with the exception that HL3 was used in place of HL1. Yield: 450 mg (84%). Calculated for $C_{35}N_8H_{33}O_4PF_6Ru$: C: 49.94; H: 3.71; N: 13.31 %. Anal. Found: C: 49.67; H: 3.62; N: 13.01 %.

Complex 4: $[Ru(bpy)_2(L4)]PF_6.2H_2O$

A similar synthesis to that of $[Ru(bpy)_2(L1)]PF_6$ was employed with the exception that the HL4 ligand was used. Yield: 442 mg (81%). Calculated for $C_{35}N_9H_{32}O_4PF_6Ru$: C: 48.57; H: 3.06; N: 12.76 %. Anal. Found: C: 48.21; H: 2.97; N: 12.90 %.

Complex 5: $[Ru(bpy)_2(L5)Ru(bpy)_2](PF_6)_2.4H_2O$

The same synthetic method was again employed for this complex. However, 0.4 g (0.94 mmol) of H_2L5 was and added to 1 g (1.9 mmol) of $[Ru(bpy)_2Cl_2].2H_2O$ and refluxed in order to obtain the dimer complex. Yield: 335 mg (73%). Calculated for $C_{62}N_{16}H_{56}O_6P_2F_{12}Ru_2$: C: 45.40; H: 3.63; N: 13.66 %. Anal. Found: C: 44.80; H: 3.38; N: 13.20 %.

Complex 6: $[Ru(bpy)_2(L6)Ru(bpy)_2](PF_6)_2.4H_2O$

The synthetic method is the same as for $[Ru(bpy)_2(L5)Ru(bpy)_2](PF_6)_2.4H_2O$ with the exception that H_2L6 ligand was used in place of H_2L5. Yield: 350mg (70%). Calculated for $C_{60}N_{18}H_{54}O_6P_2F_{12}Ru_2$: C: 44.12; H: 3.40; N: 15.44 %. Anal. Found: C: 43.88; H: 2.83; N: 15.09 %.

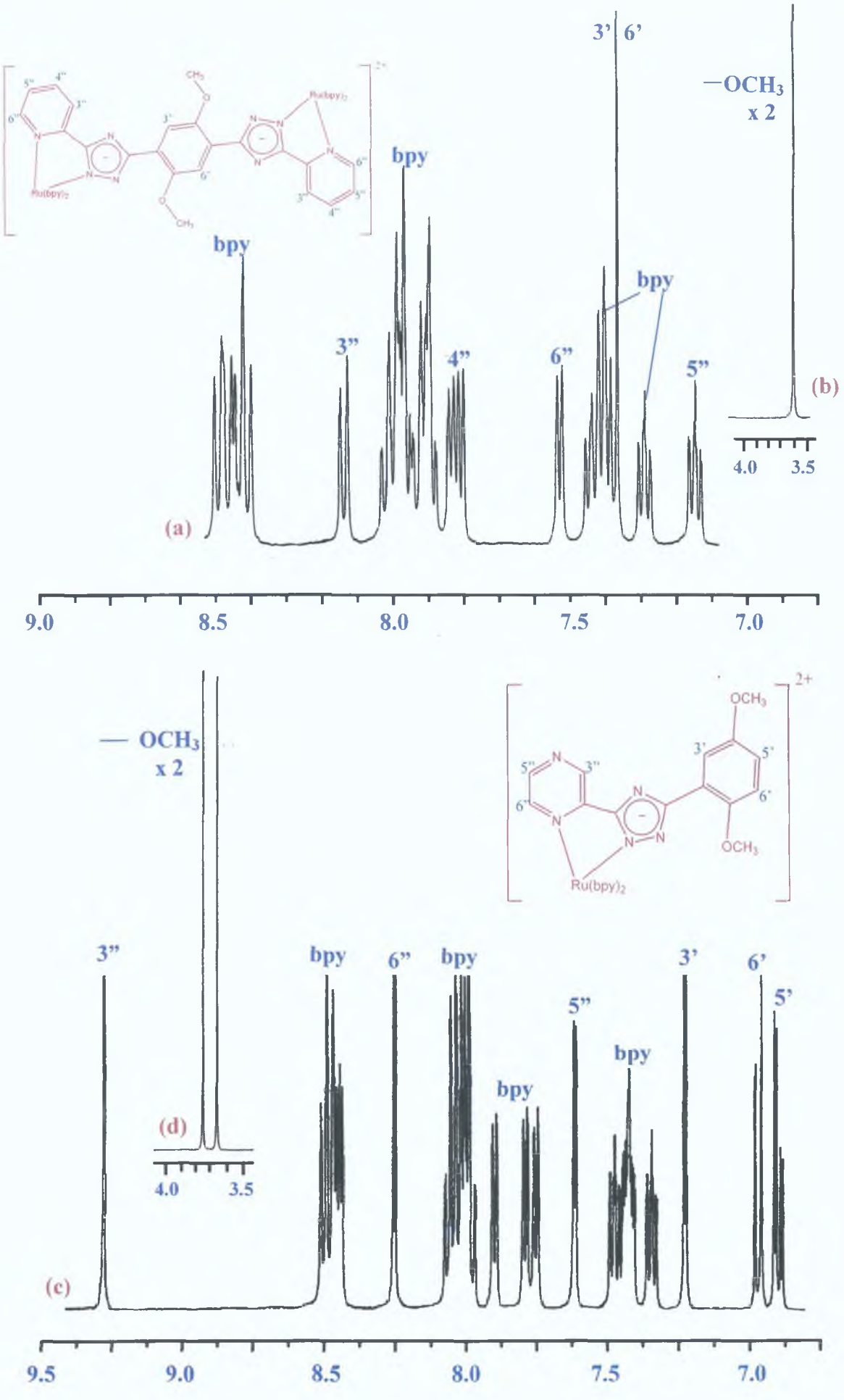

Figure 3.9 ^{1}H-NMR data of the complexes **(a)** $[Ru(bpy)_2(L5)Ru(bpy)_2](PF_6)_2.4H_2O$ with **(b)** $-OCH_3$ peak inset and **(c)** $[Ru(bpy)_2(L4)]PF_6.2H_2O$ with **(d)** $-OCH_3$ peaks inset in d_3-acetonitrile

3 3 Results and Discussion

3 3 1 Synthetic Considerations

3.3 1 1 Ligand Synthesis

The ligands HL1, HL2, HL3 and HL4 were all prepared in a similar synthetic manner with the only exception being that the synthesis of the pyrazine-containing ligands involved cyanopyrazine rather than cyanopyridine The synthesis then proceeded in the usual manner until cyclisation in ethylene glycol yielded the required product Crystals of these ligands were obtained via recrystallisation from hot ethanol and water and no further purification was required The synthesis of the ligands H_2L5 and H_2L6 was not as straightforward due to the presence of the –OMe moieties on the central phenyl ring However, unlike the preparation of the ligands from 2,5-dihydroxybenzoic acid, the synthesis of these dimethoxy precursors proved more successful and hence ligand yields were high

3 3.1 2 Complex Synthesis

The ruthenium complexes containing both the pyridine and pyrazine ligands proceeded in accordance with the standard procedure and did not prove to be problematic [35][33] Hence, reflux in ethanol / water for generally longer than three hours resulted in complex formation This process was accompanied by a colour change in which the initial deep plum colour developed to a strong burgundy In the case of the dinuclear complexes, an excess of $[Ru(bpy)_2Cl_2]\ 2H_2O$ was used in order to predominantly obtain the dual coordinated complex The complexes could then be precipitated by the addition of PF_6^- with subsequent recrystallisation from ethanol and water Purification was achieved via column chromatography on neutral alumina with acetonitrile as eluent In the case of the pyrazine-containing complexes, purification proved slightly more problematic due to the presence of the free N on the pyrazine ring, as, during column chromatography, they adhere readily to the stationary phase An acetonitrile and methanol mixture (5%) was therefore employed in these purifications A small percentage of methanol was also utilised in the column chromatography of the dinuclear complexes in order to elute the pure product

It is a well-recognised phenomenon with this nature of ligand, that the ligands deprotonate upon coordination with the metal and this is verified via the X-ray crystal structures and the CHN analyses [33] The deprotonated status of these complexes was also verified via the UV data contained following *section 3 3 2 1* A further complication associated with these syntheses is the possibility of forming isomers This is contingent with the mode of coordination of the metal with the triazole N moiety However, steric hindrance would seem to dictate a formation of a majority of the N2 isomer, as observed for many similar ligands [2][32][36-38] Furthermore, it has been shown previously that the ^{1}H-NMR spectra of the N2 and N4 bound coordination isomers are significantly different [39] Column chromatography ensured that only one isomer was isolated from the reaction, a fact substantiated by the following characterisation data

3 3 1 3 Characterisation Considerations

^{1}H-NMR spectroscopy is a necessary tool in accessing the purity and structure of complexes and it has been used extensively to identify the coordination mode of pyridyl- and pyrazyltriazole ligands [40] The proton NMR spectrum of the uncoordinated ligands HL2 and HL3 are shown in *figure 3 8* while the reasonances for coordinated ligands L1-L6 are shown in *table 3 1* The assignments of resonances due to the coordinated ligand were made by using COSY spectral data and also by comparison with the resonances of the free ligands This additional data is contained in *appendix A* Moreover, some deuterated analogues were also synthesised and these further confirm and assist in the assignment of the coordinated ligand resonances via omission of the bipyridyl resonances The synthesis of the deuterated analogues along with their CHN and the ^{1}H-NMR data are contained in *appendices A* and *C* The spectra obtained were clean and well resolved and integrate to the expected number of protons This can be clearly seen in the spectra of the mononuclear $[Ru(bpy)_2(L2)]^+$ and the dinuclear $[Ru(bpy)_2(L5)(bpy)_2Ru]^{2+}$ complexes shown in *figure 3 9* The –OMe resonances for similar dimethoxy complexes have previously been identified in the ^{1}H-NMR spectra at 3 72 ppm as singlets [41] The ^{1}H-NMR spectra of the complexes $[Ru(bpy)_2(L3)]^+$ and $[Ru(bpy)_2(L4)]^+$ also displayed two identifiable –OMe singlet peaks in this region

Resonances for coordinated ligands L1-L6
(chemical shifts / ppm vs Me_4Si)

	1	*2*	*3*	*4*	*5*	*6*
$H^{2'}$	7.36(d)	7.40(d)				
$H^{3'}$	7.28(dd)	7.20(dd)	7.22(s)	7.23(s)	7.51(s)	7.38(s)
$H^{4'}$	7.22(dd)	7.18(dd)				
$H^{5'}$	7.31(d)	7.20(dd)	6.88(dd)	6.98(dd)		
$H^{6'}$	7.85(d)	7.81(d)	6.96(d)	6.90(d)	7.51(s)	7.38(s)
$H^{3''}$	8.38(d)	9.10(s)	8.17(d)	9.26(s)	8.31(d)	9.23(s)
$H^{4''}$	8.06(d)		7.96(dd)		7.98(dd)	
$H^{5''}$	7.26(dd)	7.88(d)	7.15(dd)	7.63(d)	7.15(dd)	7.61(dd)
$H^{6''}$	7.74(dd)	8.10(d)	7.53(d)	8.26(d)	7.72(d)	8.23(d)

* For an explanation of proton numbering refer to *figure 3.9*.

Bipyridyl reasonances were observed in the following regions for:

[1] *Pyridyltriazole complexes*: 8.35-8.55(**H^3**); 7.92-8.05(**H^4**); 7.20-7.45(**H^5**); 7.85-7.92(**H^6**).

[2] *Pyrazyltriazole complexes*: 8.30-8.55(**H^3**); 7.97-8.10(**H^4**); 7.30-7.50(**H^5** / **H^6**).

Strong **–OCH_3** reasonances were observed in the following regions:

[3] *$[Ru(bpy)_2(L3)]^+$*: 3.63 (s, 3H, **-OCH_3**) and 3.74 (s, 3H, **-OCH_3**)

[4] *$[Ru(bpy)_2(L4)]^+$*: 3.65 (s, 3H, **-OCH_3**) and 3.75 (s, 3H, **-OCH_3**)

[5] *$[Ru(bpy)_2(L5)Ru(bpy)_2]^{2+}$*: 3.60 (s, 3H, **-$OCH_3$**)

[6] *$[Ru(bpy)_2(L6)Ru(bpy)_2]^{2+}$*: 3.61 (s, 3H, **-$OCH_3$**)

Table 3.1 ^{1}H-NMR data for complexes 1 – 6 measured in d_3-acetonitrile

Their characterisation as –OMe is further substantiated by their absence in the spectra of complexes $[Ru(bpy)_2(L1)]^+$ and $[Ru(bpy)_2(L3)]^+$ which differ only from the previous two complexes by their lack of –OMe substituents. In the case of the dinuclear complexes the –OMe signals are expressed as one large peak due to the equivalency of these moieties in these complexes. This is interesting to note as these dinuclear complexes are clearly highly symmetric as indicated by the presence of only one methoxy signal (*table 3.1*) and by the fact that the phenyl protons are equivalent and found as a singlet at 7.51 ppm and 7.38, respectively (*figure 3.9*).

This is in contrast to the mononuclear complexes in which the phenyl protons are not equivalent (*figure 3 9*) and is further evidence of N2 coordination within these complexes The NMR data also revealed that an upfield shift of the $H^{6'}$ proton occurs upon coordination This shift is more pronounced in the spectra of the pyridyl-containing complexes and may be attributed to the diamagnetic anisotropic interaction of the H^6 proton with the adjacent rings of the bipyridine [42] In the pyrazyltriazole complexes the H5" proton experiences a larger upfield shift than in the pyridyltriazole complexes The bipyridyl protons of the pyridyltriazole-containing complexes could be easily identified from the COSY spectra and because they fall into the normal range for previously reported, analogous systems [36][39][40]

3.3.2 Electronic and Photophysical Properties

3.3.2.1 Absorption Spectra

Table 3.2 Absorption and emission data obtained for the complexes. Unless otherwise stated, all measurements were performed in acetonitrile.

Complex	A_{max}[a] (nm) (ε x10^{-4} M^{-1} cm^{-1})	E.Quantum Yield (Φ)	E_{max} 298K[b] (nm) τ (ns)	E_{max} 77K[c] (nm) τ (μs)
$[Ru(bpy)_3]^{2+}$	452 (1.30)	0.062	608 (850)	580 (4.8)
$[Ru(bpy)_2(L1)]^{+}$	481 (1.06)	0.0038	690 (122)	612 (4.9)
$[Ru(bpy)_2(HL1)]^{2+}$	442 (1.32)	-	620 (18)	600 (5.7)
$[Ru(bpy)_2(L2)]^{+}$	453 (1.09)	0.0059	670 (220)	645 (6.7)
$[Ru(bpy)_2(HL2)]^{2+}$	440 (1.29)	-	678 (301)	618 (7.6)
$[Ru(bpy)_2(L3)]^{+}$	485 (1.07)	0.0034	685 (110)	615 (3.0)
$[Ru(bpy)_2(HL3)]^{2+}$	441 (1.43)	-	612 (8.0)	580 (5.4)
$[Ru(bpy)_2(L4)]^{+}$	456 (1.54)	0.0056	675 (167)	606 (4.0)
$[Ru(bpy)_2(HL4)]^{2+}$	440 (1.61)	-	680 (249)	616 (7.6)
$[Ru(bpy)_2(L5)Ru(bpy)_2]^{2+}$	482 (2.89)	0.0032	683 (105)	616 (2.4)
$[Ru(bpy)_2(H_2L5)Ru(bpy)_2]^{4+}$	412 (2.93)	-	612 (6)	583 (5.0)
$[Ru(bpy)_2(L6)Ru(bpy)_2]^{2+}$	454 (2.28)	0.0054	671 (160)	614 (3.9)
$[Ru(bpy)_2(H_2L6)Ru(bpy)_2]^{4+}$	440 (2.74)	-	681 (240)	626 (6.7)

[a] Protonation of the complexes achieved by addition of perchloric acid (*chapter two*).

[b] Lifetime samples at 298K underwent three freeze-pumped-thaw pre-treatments.

[c] Data at 77K were recorded in EtOH/MeOH (4:1 v/v).

[d] Emission quantum yield determination is contained in *chapter two*.

[e] Experimental errors are included in *chapter two*.

Most ruthenium (II) polypyridyl complexes exhibit similar electronic spectra. For example, the absorption spectrum of the archetypal $[Ru(bpy)_3]^{2+}$ complex shows bands at 185 nm and 285 nm which are assigned to ligand centred (LC) $\pi \rightarrow \pi^*$ transitions by comparison with the spectrum of protonated bipyridine. The band at 450 nm in this prototypical complex is assigned to a metal-to-ligand charge transfer (MLCT) $d\pi \rightarrow \pi^*$ transition, while shoulders at 322 and 344 nm are tentatively assigned to metal centred MC transitions. [22] Indeed, it is the presence of this MLCT in the visible region of the spectra that distinguishes this genus of complex and it is a common feature in the spectra of all the complexes cited in this chapter.

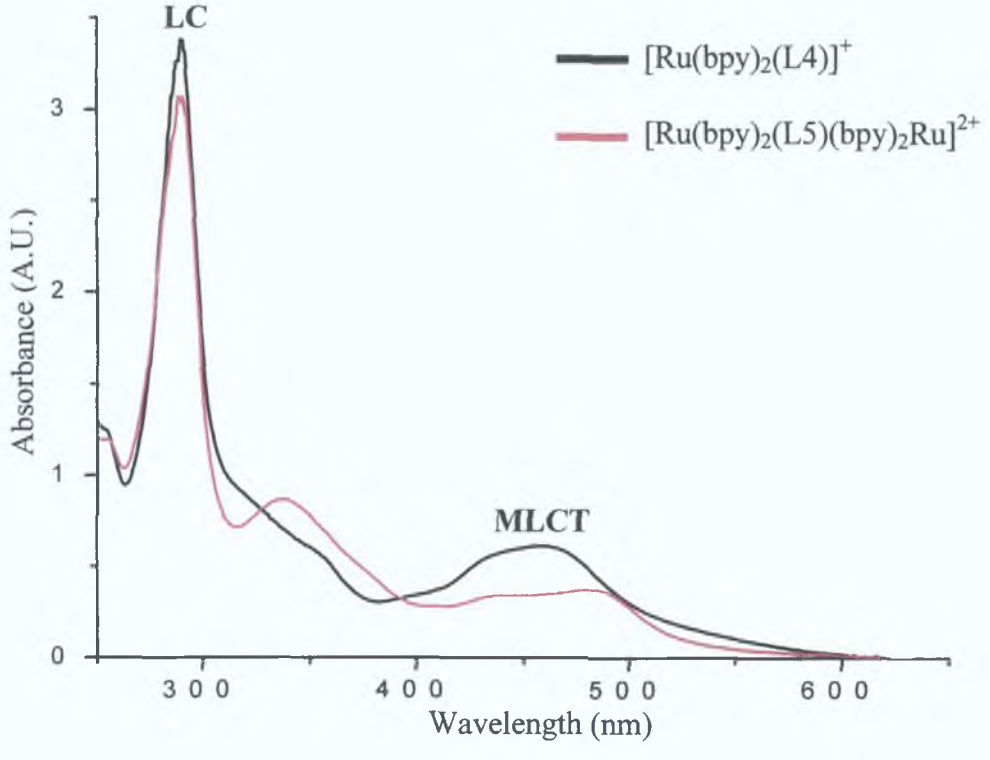

Figure 3.10 Absorption spectra of $[Ru(bpy)_2(L4)]^+$ (c. 4.56 x 10^{-5}M) and $[Ru(bpy)_2(L5)(bpy)_2Ru]^{2+}$ (c. 1.71 x 10^{-5}M) in acetonitrile at room temperature.

All UV/Vis spectra discussed in this chapter were recorded in acetonitrile. The absorption data for the mononuclear and dinuclear complexes in their protonated and deprotonated forms are recorded in *table 3.2*. As expected, two main bands were seen to dominate. The strong band at 285 nm is attributed to the ligand based $\pi - \pi^*$ transitions (*figure 3.10*), while the singlet MLCT $d\pi$-π^* transitions arise between 400 – 500 nm.

Table 3 2 also contains extinction coefficients The intensity of a transition is determined by selection rules and, in order for a transition to be fully allowed, the transition must be both Laporte and spin allowed [43] In the octahedral environs of a ruthenium complex, transition that are Laporte and spin allowed, such as LC $\pi - \pi^*$ and MLCT transitions, have extinction coefficients in the region of 10^3 and 10^5 M^{-1} cm^{-1} The complexes discussed in this chapter all display extinction coefficients in the order of 1 3 x 10^4 $M^{-1}cm^{-1}$ (*table 3 2*)

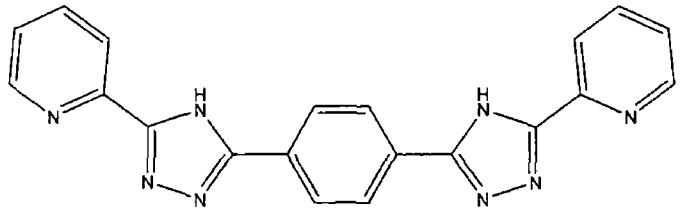

Figure 3 11 1,4-bis(pyridin-2-yl-1,2,4-triazol-3-yl)benzene [2]

In previous studies of similar ruthenium complexes, such as those discussed in the introduction by Ward and co-workers, also demonstrate comparable transitions in the electronic spectrum [21] Interestingly, substitution of the phenyl ring by dimethoxy moieties upon going from $[Ru(bpy)_2(L1)]^+$ and $[Ru(bpy)_2(L2)]^+$ to $[Ru(bpy)_2(L3)]^+$ and $[Ru(bpy)_2(L4)]^+$ evokes little difference in the absorption spectra Therefore, it can be seen that the absorption spectra of these complexes are not strongly dependant on the nature of the substituted moiety This observation is in agreement with results obtained by Ward and co-workers[21], Lehn[10][25], Paddon-Row,[8] Schanze and Sauer[26] (*figure 3 5*)

The absorption spectra of the dimer complexes described in this chapter are comparable to their analogous monomer complex Once again, substitution of the phenyl moiety has little effect on the absorption spectra Evidence for this comes from examination of the spectrum of the dinuclear complex synthesised by Weldon and co-workers, which contained the ligand depicted in *figure 3 11* [2] This represents the unsubstituted-phenyl analogue of $[Ru(bpy)_2(L5)(bpy)_2Ru]^{2+}$and similarly has an MLCT band centred at 481 nm (ε = 2 03 x 10^{-4} M^{-1} cm^{-1}) in neutral acetonitrile and at 420 nm when protonated by acid

It may also be noted however, that the MLCT of all of the complexes in neutral acetonitrile are red shifted in comparison to $[Ru(bpy)_3]^{2+}$ This is due to the effect caused by the replacement of one of the bipyridyl moieties with a ligand that possesses different properties and hence exerts a different influence on the metal centre In the case of the pyridyltriazole complexes the increased σ-donor capacity of the deprotonated ligand is manifested by a shift of approximately 30 nm to a lower energy This phenomena was also noted by Vos and co-workers in their analysis of the mononuclear Ru(II) complex of 3,5-bis(pyridin-2-yl)-1,2,4-triazole [1] In the case of their complex, which contains the ligand shown in *figure 3 12*, a shift from 475 nm (ε = 1 13x10^{-4} M^{-1} cm^{-1}) to 429 nm (ε = 1 56x10^{-4} M^{-1} cm^{-1}) upon protonation was noted, which is comparable to the shifts observed for the pyridyl-containing complexes contained in *table 3 2* [39][44]

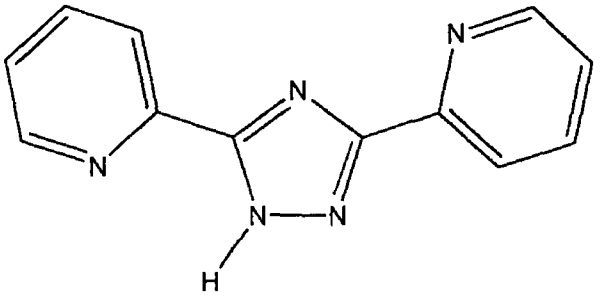

Figure 3 12 3,5-bis(pyridin-2-yl)-1,2,4-triazole (bpt)

Vos and co-workers also synthesised the pyrazyl-containing analogue of the above ligand [45] As with the pyrazyltriazole complexes contained in *table 3 2*, it was observed that this compound exhibits a less pronounced shift compared to the pyridyl analogues This may be attributed to pyrazine's stronger π-acceptor properties Electron density on the metal centre is therefore reduced by the pyrazyl ring however, the juxtaposition of the triazole moiety negates this effect and a minor red shift (circa 5 nm) in absorption is manifested The presence of the triazole ring in these complexes means that they have the potential to be protonated Protonation of the triazole ring with trifluoroacetic acid results in a change in the absorption spectra of the complex This may be attributed to the fact that protonation of the triazole ring causes a diminishing of its σ-donor properties (*figure 3 13 / table 3 2*) [46]

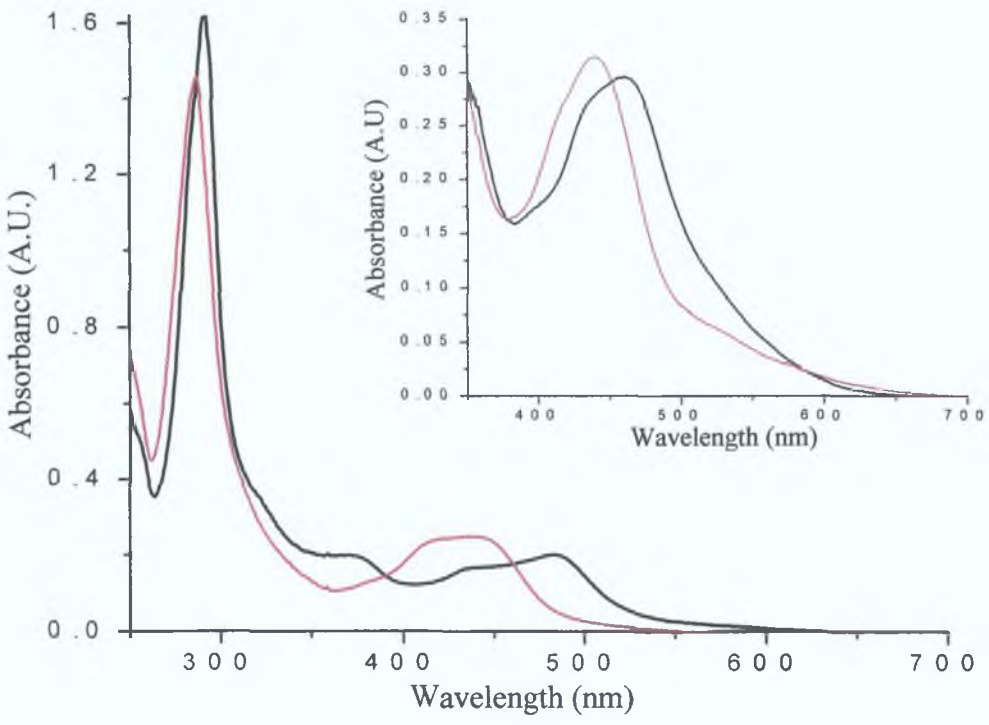

Figure 3.13 Absorption spectra of $[Ru(bpy)_2(L1)]^+$ in acetonitrile (**black line**) and after the addition of acid (**red line**) and (*Inset*) $[Ru(bpy)_2(L2)]^{2+}$ in acetonitrile (**black line**) and after the addition of acid (**red line**)

In the case of the pyridyltriazole-containing complexes, protonation results in a blue shift of the absorption by approximately 40 nm to 440 nm and a concomitant increase in the extinction coefficient. This shift is not as pronounced however in the case of the pyrazyltriazole-containing complexes and only a slight blue shift of approximately 15 nm is observed.

3.3.2.2 Luminescence Properties

Figure 3.14 contains the emission spectra of each of the complexes. The luminescence of $[Ru(bpy)_3]^{2+}$ is known to originate from a ^{3}MLCT which is therefore assigned as the lowest excited state.[1] Most of the known Ru(II) polypyridine complexes exhibit a luminescence behaviour quite similar to that of $[Ru(bpy)_3]^{2+}$, indicating that their lowest excited state is also ^{3}MLCT, for example the complexes shown in *figure 3.15*.[8][35]

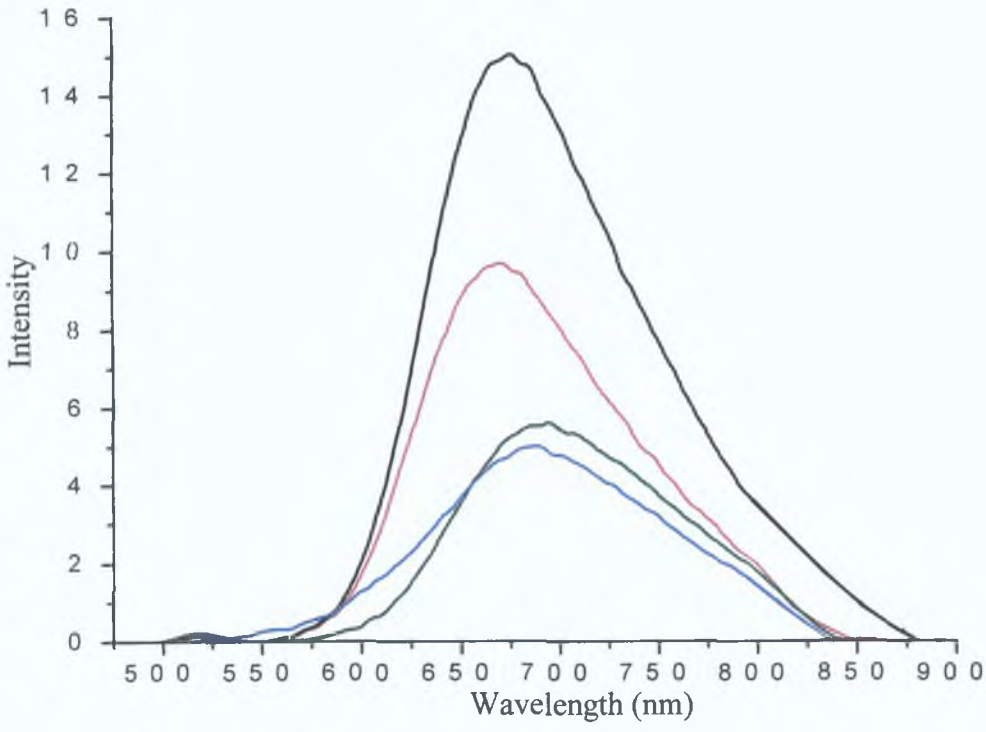

Figure 3.14 Emission spectra of $[Ru(bpy)_2(L3)]^+$ **(blue line)** $4.91x10^{-5}$ M, $[Ru(bpy)_2(L4)]^+$ **(black line)** $4.56x10^{-5}$ M, $[Ru(bpy)_2(L5)Ru(bpy)_2]^{2+}$ **(green line)** $1.71x10^{-5}$ M and $[Ru(bpy)_2(L6)Ru(bpy)_2]^{2+}$ **(red line)** $1.55x10^{-5}$ M in acetonitrile at room temperature

Each of the complexes presented in this chapter emit light at room temperature and the luminescence data for each of the complexes at room temperature and at 77 K, in the protonated and deprotonated state are contained in *table 3.2*. Examination of the data reveals a red-shift of emission of these complexes with respect to $[Ru(bpy)_3]^{2+}$. This is best explained by the effect of the triazole ring whose negative charge increases electron density on the metal centre and as a consequence the t_2g - ^{3}MLCT energy gap is reduced (*chapter one*). [44] The emission quantum yield (Φ) gives an indication of the amount of energy that is absorbed and then released as emission and in the case of the prototype complex $[Ru(bpy)_3]^{2+}$ an emission quantum yield of 0.062 was obtained (in acetonitrile). *Table 3.2* also contains the quantum yield data obtained for the range of complexes presented in this chapter. Although slightly diminished compared to the archetypal complex the quantum yields obtained are still relatively high and have values comparable to $[Ru(bpy)_2bpt]^+$ (Φ 3 x 10^{-3}) (structure of bpt ligand is depicted in *figure 3.12*).[1]

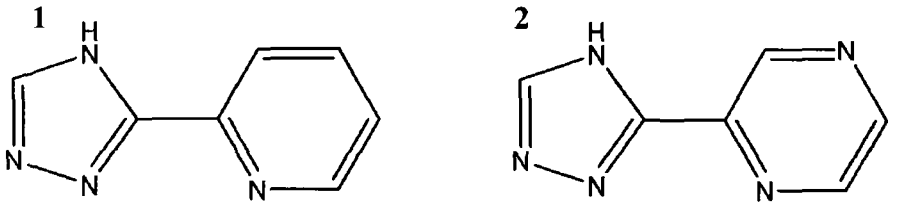

Figure 3 15 3-(pyridin-2-yl)-1,2,4-triazole (**1**) and 3-(pyrazin-2-yl)-1,2,4-triazole (**2**) [47][35]

In the case of the mononuclear pyridyltriazole complexes an emission in the region of 680 nm to 690 nm was recorded This is comparable to the complex $[Ru(bpy)_2(bpt)]^+$ (ligand in *figure 3 12*), for which luminescence was observed at 678 nm [1][39][45] The pyridyltriazole complex $[Ru(bpy)_2(L5)(bpy)_2Ru]^{2+}$ emits at 683 nm, which differs little from that of the unsubstituted complex synthesised by Weldon and co-workers, (*figure 3 11*) which was has an emission centred at 690 nm at room temperature [29] This once again shows the effect of the substituent on the phenyl ring is minor This observation is in agreement with the findings of previous studies [10][27][31] The pyrazyltriazole complexes were also observed to luminesce strongly at room temperature These complexes show a similar emission wavelength as other pyrazyltriazole complexes, such as Hage's complex $[Ru(bpy)_2(pztr)]^+$ (*figure 3 15*) which recorded an emission at 680 nm and differs only from the mononuclear complexes contained in *table 3 2* by the absence of the phenyl moiety [47]

Protonation of the complexes results in a change in the emission of the complexes The data in *table 3 2* show that, in the case of the pyridyltriazole complexes, protonation results in a decrease in intensity and a concomitant blue shift in the emission energy (circa 70 nm at 289 K) The lifetime data also display a sharp decrease upon protonation of the pyrazyltriazole complex The shifts which are noted are comparable to those observed for the analogous pyridyltriazole complexes investigated by Hage, which contain the ligand (**1**) depicted in *figure 3 15* and undergo the same shift in emission [35][47] Furthermore, the spectra obtained also bear a strong resemblance to those of the analogous unsubstituted complex prepared by Weldon and co-workers (*figure 3 11*) which emits at 690 nm at room temperature and shifts to 614 nm when protonated

The behaviour of the pyridyltriazole complexes contrasts strongly with that observed for the pyrazyltriazole complexes at room temperature. In the case of the pyrazine-containing complexes there is no such loss of emission intensity noted (*table 3.2*) and this too is noted in the room temperature lifetime data, which also do not display the same sharp decrease in value upon protonation. This phenomena was further examined during 77 K measurements.

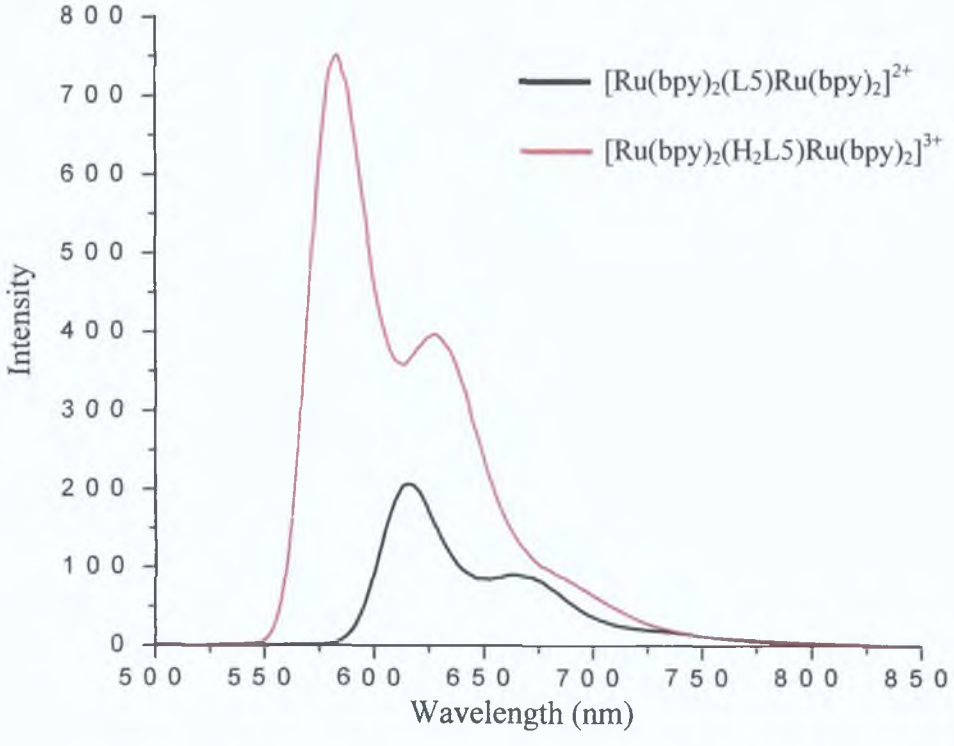

Figure 3.16 Emission Spectra of $[Ru(bpy)_2(L5)\ Ru(bpy)_2]^{2+}$ (**black line**) in EtOH/MeOH at 77 K and After the addition of 1 Drop of Acid (**red line**) at 77 K

Figure 3.16 depicts the emission spectra of $[Ru(bpy)_2(L5)Ru(bpy)_2]^{2+}$ and $[Ru(bpy)_2(H_2L5)Ru(bpy)_2]^{4+}$ at 77 K in EtOH/MeOH. Unlike in the case of the pyridyltriazole room temperature measurements, there is no longer depletion in the emission intensity. As was discussed in detail in the introductory chapter (*chapter one*) the excited state decays by way of emission or various radiationless paths. In a rigid matrix environ, which occurs at 77 K, a number of phenomena conspire to cause the observed increase in intensity. For example, vibrational decay via Ru-N is reduced within the system confines, as is the ability of oxygen to quench the excited state. Furthermore, the ^{3}MC, which is a thermally populated state (*chapter one*), becomes increasingly inaccessible as the heat of the system abates.

The spectra are also blue shifted by approximately 75 nm due to an effect known as rigidchromism. This is when solvent dipoles are immobile on the timescale of the excited state and cannot reorganise as a result of the change in electronic configuration of the excited complex. [48] The pyrazyltriazole-containing complexes have a somewhat more complicated behaviour. Unlike in the case of the pyridyltriazole complexes the pyrazine analogues do not undergo such a pronounced shift (circa 5 nm) in the emission energy upon protonation and this shift is now, conversely, to an increased energy, both at room temperature and 77 K (*figure 3.17*). Once again this is a comparable to the results obtained previously for similar complexes such as those recorded by Hage. [47][35]

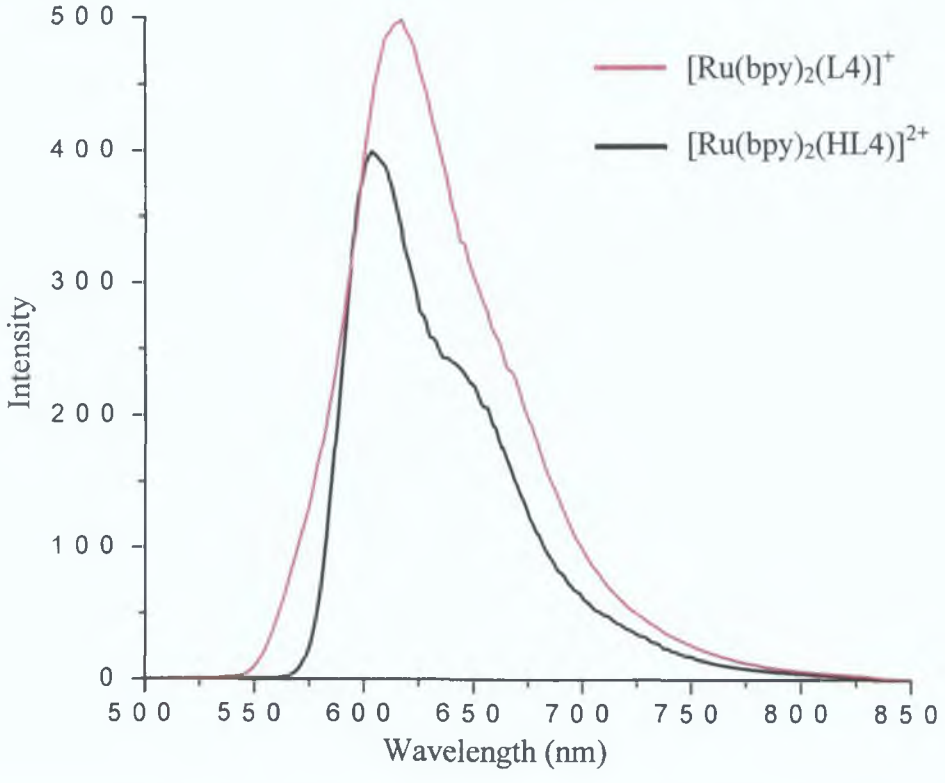

Figure 3.17 Emission spectra of $[Ru(bpy)_2(L4)]^+$ **(black line)** in neutral acetonitrile at 77 K and after the addition of 1 drop of acid (**red line**) at 77 K

These observations concur with the findings of a number of authors, who have provided temperature-dependent emission lifetime evidence, Raman studies and used partial deuteriation to show that pyrazine triazole compounds have very unusual change in the nature of the emission. [49] Their data clearly indicate that the emitting triplet state is bipyridyl-based at room temperature when the triazole is deprotonated and switches to being pyrazine-based on protonation. [50] This phenomenon is explored further in the following sections.

3 3 2 3 Lifetime Measurements

The complexity of the excited state involved in some of the complexes outlined in this chapter has already been mentioned and luminescence lifetime measurements are an additional method of characterisation The lifetime data for the range of complexes at both room temperature and low temperature in both the protonated and deprotonated states has been presented in *table 3 2* Generally, the errors that may be expected in these measurements are in the region of 10% however, in order to ensure the increased accuracy of this data, all samples underwent a freeze-pump-thaw regime prior to recording the lifetimes to mitigate the effects of oxygen in the system

In this chapter, a range of complexes is presented which display differing characteristics depending on the nature of the pendant ligand The inclusion of the additional phenyl moiety in the complex has only a very slight effect on the lifetime of the pyridyltriazole and pyrazyltriazole complexes For example, Hage's unsubstituted pyridyltriazole complex $[Ru(bpy)_2(pytr)]^+$ has a lifetime of 145 ns while the lifetime of $[Ru(bpy)_2(L1)]^+$ was recorded at 122 ns [35][33] Likewise, the analogous unsubstituted pyrazyltriazole complex $[Ru(bpy)_2(pztr)]^+$ has a lifetime of 250 ns, while the lifetime of $[Ru(bpy)_2(L2)]^+$ is 220 ns [51] Furthermore, the addition of the dimethoxy groups decreases the lifetime slightly from 122 ns for $[Ru(bpy)_2(L1)]^+$ to 110 ns for $[Ru(bpy)_2(L3)]^+$, and similiarly 220 ns for $[Ru(bpy)_2(L2)]^+$ to 167 ns for $[Ru(bpy)_2(L4)]^+$ However, these results are not surprising since, as Lehn *et al* state, dimethoxybenzene groups are not efficient quenchers of the excited state [10]

Although, it was found that the complexes display some similar characteristics replacement of the pyridyltriazole moiety by a pyrazyltriazole group does bring about differing properties Vos and co-workers, for example, have used both time resolved Raman spectroscopy and partial deuteriation techniques to show that the excited state of pyrazine-containing complexes is bipyridyl localised but that upon protonation the excited state of these complexes 'switches' to the pyrazyltriazole moiety [45][47][49][50][52][53]

It is known, for example, that deuteration of a ligand will only affect the emission lifetime of a compound when this ligand is directly involved in the emission process Therefore, if the spectator ligand is deuterated, the emission quantum yield and lifetime should not be affected Vos and co-workers showed that in the case of pyridyltriazole-containing complexes an increase in the emission lifetime of the pyridine triazole complexes is only observed upon deuteration of the polypyridyl ligands, irrespective of the protonation-state of the triazole ring [49][50] However, in the case of pyrazyltriazole-contaimng complexes, deuteration of the polypyridyl ligands does not affect the emission, while deuteration of pyrazine-containing ligand results in a twofold increase in the emission lifetime This is indicative of the fact that upon protonation of the triazole moiety the emission becomes pyrazine-based When these pyrazine complexes are not protonated however, they observed that deuteration of either bipyridyl or the pyrazyltriazole ligand has little influence on the emission lifetime at room temperature This behaviour is due to the existence of two weakly coupled excited states [49][50]

This phenomenon is also reflected in the lifetime data obtained for the complexes presented in this chapter For example, in the case of the pyridyltriazole complexes the lifetimes are seen to decrease sharply upon protonation (*table 3 2*) in conjunction with the loss in emission intensity noted in the previous section (*section 3 3 2 2*) From *table 3 2* it can be seen that at 298K the protonated pyridyltriazole complexes have a lifetime of < 20 ns These lifetimes were in fact so short that they could not be recorded on a conventional laser system due to instrumental limitations and were instead recorded on a single photon counter This decrease which is in contravention of the energy gap law [53] occurs due to the reduction of the ^{3}MLCT – ^{3}MC gap, which facilitates fast thermally activated radiationless deactivation of the emissive ^{3}MLCT excited state via population of the ^{3}MC state [39] This data concurs with the lifetime recorded by Weldon and co-workers for the unsubstituted analogue of $[Ru(bpy)_2(H_2L5)(bpy)_2Ru]^{4+}$ (*figure 3 12*) which has a lifetime of less than 20 nm when protonated [29] However, at 77 K, an increase in the emission lifetime of the protonated pyridyltriazole was recorded This increase occurs at lower temperatures due to the thermal accessibility of the ^{3}MC at 77 K [3][54]

However, as suggested by the work of Vos and co-workers, the behaviour of the pyrazyltriazole complexes differs from that of the pyridyltriazole-containing complexes. In the rigid matrix environment at 77 K a similar increase in the lifetimes, as noted for the pyridyltriazole, is again observed for the pyrazine complexes. However, it was observed that at room temperature, the protonated complex lifetimes do not undergo the sharp decrease either in the lifetimes or in the emission intensities (*section 3.3.2.2)*, as noted for the pyridyltriazoles. This suggests that these complexes undergo a switching of the excited state upon protonation, as suggested previously in the work of Vos and co-workers. [49][50] This switching of the excited state to the pyrazyltriazole moiety may be verified further by examination of the acid-base properties of the complexes, as presented in the following section.

3.3.3 Acid-Base Properties

From the previous discussions, it has become obvious that the location of the excited state in both the pyridyltriazole and pyrazyltriazole complexes is of great importance. [52] The fact that the complexes reported in this chapter contain a site on the triazole that has the potential to be protonated provides new vistas for these complexes, as differing properties may now be invoked by varying the pH. The following acid-base measurements were therefore preformed as described in the experimental chapter (*chapter two*). In ruthenium polypyridyl complexes of the type presented in this thesis, the Ru-N bond is mainly σ in nature but it is also further stabilised by back bonding between the t_{2g} and π* orbitals of the metal and the ligand, respectively (*chapter one*). Hence, determination of the acid dissociation constant (pKa value) of a complex yields information about the extent of this back bonding from the metal and also the σ-donor and π-acceptor properties of the ligands. The two types of ligand present in the complexes, pyridyl and pyrazyltriazole, therefore display quite different acid-base behaviour.

In the case of both the pyridyltriazole and pyrazyltriazole complexes reversible acid base behaviour was observed. *Figure 3.19* shows the pH-dependent absorption spectra of $[Ru(bpy)_2(L1)]^+$ in Britton-Robinson buffer from pH 2 to pH 6.

This spectrum is typical of the pyridyltriazole complexes and contains three well-defined isobestic points at 457 nm, 390 nm and 308 nm. From an examination of this figure it can be seen that at pH 2, where the complex is protonated, a λ_{max} of 440 nm is observed. This λ_{max} is gradually shifted to a reduced energy value of 465 nm as the pH is increased to 6. Addition of more NaOH produced no further change in the λ_{max} noted. The change in absorption intensity at 440 nm was then plotted against the changing pH and the resulting graph is shown *inset* in *figure 3.19*. A sigmoidal curve was then fitted to the graph to give a point of inflection, which is equivalent to the pKa value of the complex. *Table 3.3* contains the ground state pKa values, obtained in this manner, for all of the pyridyltriazole complexes.

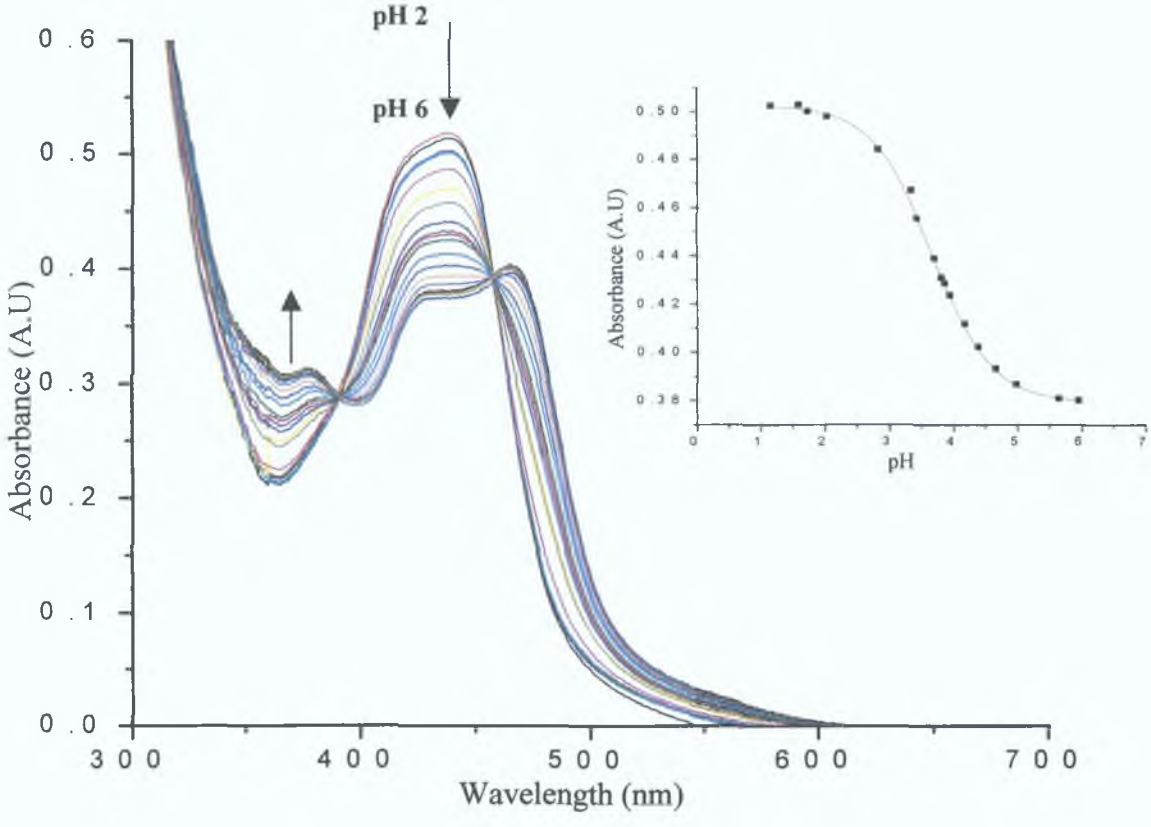

Figure 3. 19 pH dependence of the absorption spectra of $[Ru(bpy)_2(L1)]^+$ in Britton-Robinson buffer. Fitted sigmoidal curve (*inset*) of absorbance (at 440nm) versus increasing pH

The pH dependence of the absorption spectra of the pyrazyltriazole complexes was also obtained by monitoring the spectral changes in Britton-Robinson buffer with varying pH. The pH dependence spectra of these complexes differs somewhat to that of the pyridyltriazole complexes. The spectra of $[Ru(bpy)_2(L4)]^+$ are typical of the pH spectra obtained for the pyrazyltriazole complexes. Once again, three well-defined isobestic points were observed but they were now located at 556 nm, 420 nm and 355 nm. At a pH of 1.50 the λ_{max} is observed at 454 nm and as the pH increases the λ_{max} gradually shifts to 446 nm at pH 5.48. Continued addition of NaOH produced no further change in the λ_{max} value. This red shift in the absorption maxima is comparable to that noted for the pyridyltriazole complexes, however, in the case of the pyrazyltriazoles complexes the shift is considerable less pronounced. This trend is comparable to that reported by Hage in his analysis of the coordinated ligands depicted previously in *figure 3.15* and was therefore unsurprising and relates to the σ-donor properties of the complexes. [35][47] The pKa values of all the pyrazyltriazole complexes are contained in *table 3.3*.

Complex	pKa	pHi	pKa*
$[Ru(bpy)_2(L1)]^+$	3.7	2.7	2.8 (3.6)
$[Ru(bpy)_2(L2)]^+$	2.9	4.0	4.1 (5.3)
$[Ru(bpy)_2(L3)]^+$	4.0	2.7	3.0 (3.7)
$[Ru(bpy)_2(L4)]^+$	2.9	3.9	4.2 (5.3)
$[Ru(bpy)_2(L5)Ru(bpy)_2]^{2+}$	3.9	2.6	3.0 (3.5)
$[Ru(bpy)_2(L6)Ru(bpy)_2]^{2+}$	2.8	3.8	4.0 (5.2)

Table 3.3 Ground State and Excited State pKa Values for the Mononuclear and Dinuclear Complexes. pKa* Values Were Obtained Using Eqn. 1 (**in Blue**) and Eqn 2 (*vide post* pg 81 and 82)

These results show that the pKa values obtained for the pyridyltriazole complexes are comparable to those obtained for preceding analogous complexes. For example, the unsubstituted pyridyltriazole complex which contains the ligand depicted in *figure 3.15* also has a pKa value of 4.1 while the dinuclear analogue of $[Ru(bpy)_2(L5)(bpy)_2Ru]^{2+}$, in *figure 3.12*, has a similar pKa value of 3.6.[29]

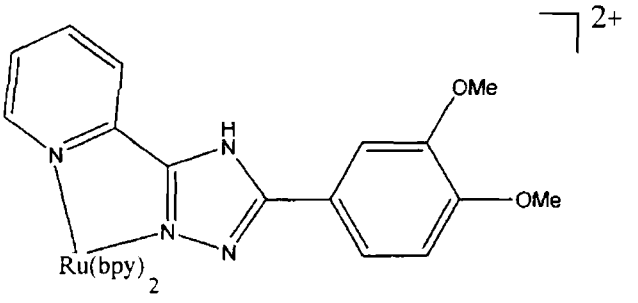

Figure 3 21 $[Ru(bpy)_2(3\text{-}(1',2'\text{-dimethoxyphenyl})\text{-}5\text{-}(pyridin\text{-}2\text{-}yl)\text{-}1,2,4\text{-}triazole)]^{2+}$ [31]

O'Brien *et al* synthesised a mononuclear ruthenium complex which also contains two dimethoxy substituents on the phenyl moiety (*figure 3 21*) This mononuclear complex bears a strong resemblance to $[Ru(bpy)_2(L3)]^+$ however, the dimethoxy substituents are in different positions on the phenyl ring This complex too has a similar pKa value of 4 1 [31]

The pyrazyltriazole complexes however, have a slightly more complicated acid-base chemistry since the non-coordinated N on the pyrazine ring may also be protonated [55] This process occurs at very low pH values (typically in the region of –1 2 [56]) however, and is hence not witnessed within the pH window of these measurements Furthermore, the pKa values obtained for the pyrazyltriazole complexes are significantly lower than those of the pyridyltriazole complexes This is indicative of the fact that pyrazine-containing complexes have a substantially weaker σ-donor capacity than the pyridyl analogues This has been noted previously for other pyrazyl-containing complexes and is an important observation for the following electrochemical section [56] The fact that the pyrazine-based complexes are more acidic than the analogous pyridine based complexes, due to the greater electron withdrawing nature of the pyrazine ring, has been noted previously for pyrazine-containing complexes For example, Browne *et al* examined a number of mononuclear and dinuclear pyridyltriazole and pyrazyltriazole complexes and in each case they found that the pyrazyltriazole complexes were more acidic [5][57] The values obtained for the pyrazyltriazole complexes are also similar to that (pKa = 3 1) obtained by S Killeen for the ruthenium complex of the ligand shown in *figure 3 22* [58]

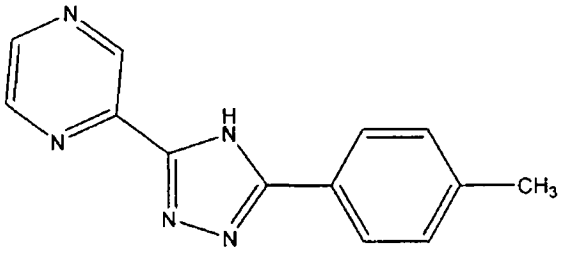

Figure 3 22 3-(2'-pyrazyl),5-(4''-tolyl)-1,2,4-triazole [58]

Finally, it may also be noted that in the case of the dinuclear complexes, which have two possible protonatable triazole rings, a two-step protonation is possible Only one protonation step with a pKa value of 3 9 and 2 8 respectively, for $[Ru(bpy)_2(L5)(bpy)_2Ru]^{2+}$ and $[Ru(bpy)_2(L6)(bpy)_2Ru]^{2+}$ was observed in the range pH 1 5 to pH10 This indicates that in this media both protonation steps occur at effectively the same pH and mdicates weak metal-metal interaction as suggested by the previous absorption data in *section 3 3 2 1* [29][33] Again, this is not unlike the situation noted for the unsubstituted version of $[Ru(bpy)_2(L5)(bpy)_2Ru]^{2+}$ synthesised by Weldon and co-workers and depicted in *figure 3 12*, which also demonstrated simultaneous protonation with a pKa value of 3 6 [2]

The pKa data obtained so far yield information regarding the ground state acid-base properties of the complexes, viz the amount of electron donation from the ligand to the metal Hence, upon manipulation of the pyridyl- and pyrazyl-triazole moiety, the ground state pKa value can provide information on both the extent of this back bonding from the metal as well as the σ-donor and π-acceptor properties of the ligand [59][60][61] However, further information can be obtained via the determination of the excited state pKa* value This offers an insight into the nature of the emitting state and hence the pKa* value for each of the complexes was determined Additional information may be obtained by investigation of the dependence of the emission spectra on pH If for example, the excited state is located on the triazole ring there will be an increased negative charge here caused by the excited electron This, in turn decreases its ability to deprotonate which will result in a higher pKa* value in the excited state than in the ground state

However, if the excited state is located on the other bipyridyl ligand, deprotonation becomes more favourable and the resultant pKa* value is less than the pKa value This data was achieved by monitoring the changes in the emission spectra of the complexes with varying pH Emission titrations were achieved by exciting the complex at an appropriate isobestic point determined from the absorption spectra [62]

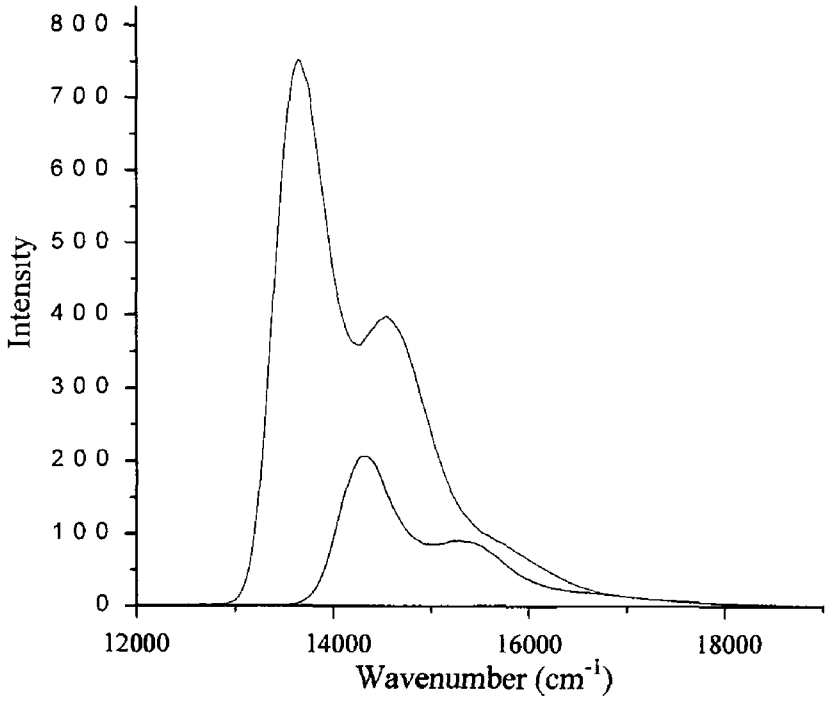

Figure 3. 23 Emission spectra of $[Ru(bpy)_2(L5)Ru(bpy)_2]^{2+}$ in neutral EtOH/MeOH (**black line**) and with 1 drop of acid (**red line**) at 77K in cm^{-1}

The excited state pKa value may then be evaluated in two distinct manners, by either the Forster method or via the Ireland and Wyatt technique [62] The Forster cycle is an indirect method of determination of excited state equilibriums based on ground state thermodynamics and electronic transition energies [63] With this method the excited state pKa* value of a complex can be estimated from its ground state properties via the following equation

$$pKa^* = pKa + \frac{0.625\,(\nu_b - \nu_a)}{T} \qquad (Eqn\ 1)$$

Where ν_a and ν_b are the $E_{0\text{-}0}$ values (in cm^{-1}) of the protonated and deprotonated complexes, respectively. These values are best obtained from the λ_{max} value of the emission spectra (in cm^{-1}) at 77 K, as they are the most accurate means of obtaining an estimate for the energy difference involved in the 0-0 transitions (*figure 3.23*). However, it is also important to note that when employing the Forster equation as a method for determining the pKa^* value small errors in the assessment of $E_{0\text{-}0}$ for ν_a and ν_b produce considerable errors in the pKa* value. [62] The second method was devised by Ireland and Wyatt and is based on a kinetic model in which pKa* value is calculated from the fluorescence lifetimes of the protonated (τ_a) and deprotonated (τ_b) complexes and the point of inflection (pH_i).

$$pKa^* = pH_i + \log\left(\frac{\tau_a}{\tau_b}\right) \qquad (Eqn.\ 2)$$

The point of inflection is determined by plotting emission intensity against pH in much the same way as the pKa values were determined. Equation 2 depicts the relationship between the lifetimes, the point of inflection and the pKa* value.

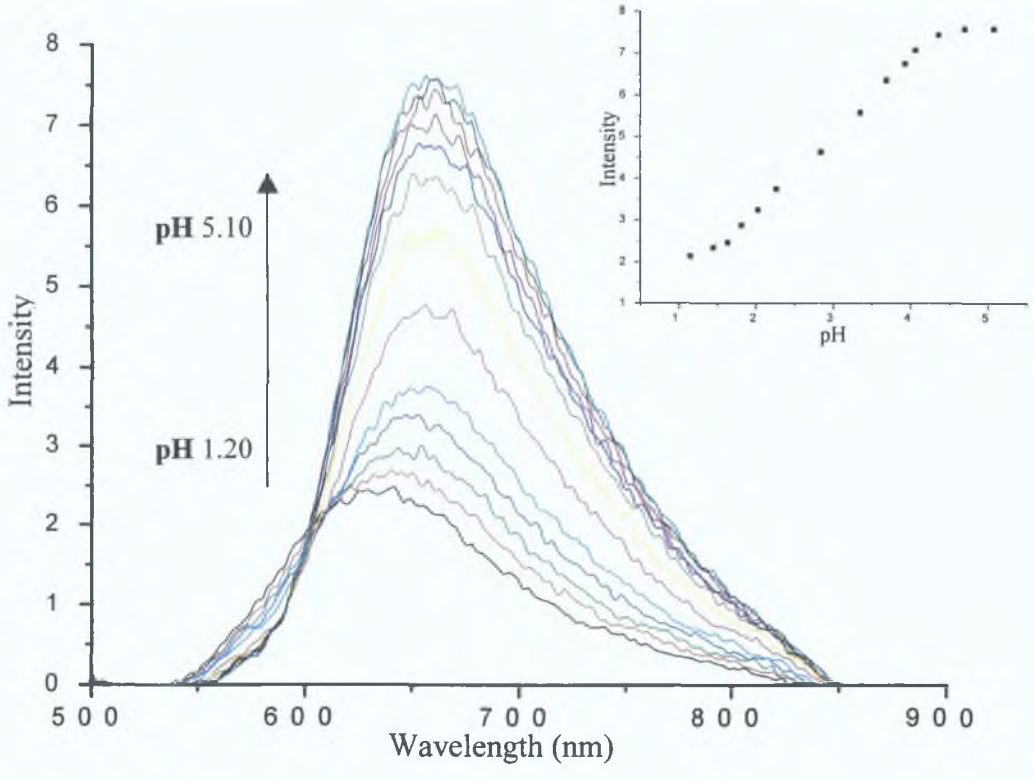

Figure 3. 24 pH dependence of the emission spectra of $[Ru(bpy)_2(L5)Ru(bpy)_2]^{2+}$ in Britton-Robinson buffer. (Inset) sigmoidal curve of emission intensity versus increasing pH.

Figure 3 24 depicts the pH dependence emission spectra of $[Ru(bpy)_2(L5)Ru(bpy)_2]^{2+}$ This figure is typical of those exhibited by these triazole complexes From an examination of *figure 3 24,* it can be seen that the λ_{max} value at pH 1 20 is 634 nm, which is seen to shift gradually as the acidity decreases At pH 5 10 the λ_{max} has red-shifted to 660 nm with a concomitant increase in the emission intensity An isobestic point at 603 nm is also observed A graph of pH versus intensity at λ_{max} is also included (inset on *figure 3 21*) Fitting a sigmoid curve to this plot yields a value for pH_i (point of inflection)

In comparison, the emission intensities of the pyrazyltriazole complexes in aqueous media are weaker (*table 3 3*) [35] At a pH value of 1 98 emission is practically non-existent and the λ_{max} of emission is circa 707 nm As NaOH is added the emission intensity increases and the λ_{max} reduces in energy to 720 nm at pH 5 80 A plot of intensity versus pH was then obtained and hence a value for the pH_i was found The pKa* values for the range of complexes described in this chapter were then calculated using both equations 1 and 2 However, equation 2 is generally considered to be a more accurate method of calculating pKa* value This is due to the fact that the lifetime values are used instead of emission values and these are more accurate [62]

In the case of the pyridyltriazole complexes it is seen that the pKa values are higher than the pKa* values This was the case for both the mononuclear and dinuclear pyridyltriazole complex and is a very significant observation as it is indicative of the fact that the pyridyltriazole moieties are spectator ligands and do not actively participate in the emission processes This behaviour correlates well with both the luminescence and lifetime data obtained previously for these pyridyltriazole complexes (section 3 3 2) Hence, since the excited state is more acidic than the ground state, this implies that the LUMO is not located on the triazole moiety and instead is bipyridyl based This trend is in agreement with that witnessed for previous pyridyltriazole complexes For example, the pKa value of $[Ru(bpy)_2(pytr)]^+$, which contains the ligand depicted in *figure 3 15* (1), is 4 1 while the pKa* value is 3 4 [35]

However, these results are at variance with that experienced in the case of the pyrazyltriazole-containing complexes In the case of these complexes the pKa* values are now higher than the pKa values [64] For example, the pKa value of $[Ru(bpy)_2(pztr)]^+$, which contains the deprotonated form of the ligand depicted in *figure 3 15* (2), is 3 7 while the excited state pKa value (pKa*) is 3 8 [35] Since, the excited state acidity is related to the nature of the emitting state this observation is very important as it shows that the electron resides on the pyrazyltriazole ligand after excitation of the complex After excitation, the electron-rich pyrazine ring can bind a proton much easier than in the ground state and is therefore more basic Hage and co-workers[52][65] and Vos and co-workers[45][53] have studied such excited state behaviour for similar pyrazine-containing complexes in depth Their work too indicated that the emitting state is bipyridyl-based when the triazole ring is deprotonated, but that when the triazole is protonated the emitting state switches to the pyrazine moiety Hence, these pKa* measurements provide further evidence that the excited state emanates from the triazole moiety and hence the excited state does experience a switching from the bipyridyl group as suggested previously in *section 3 3 2* Furthermore, these findings are of particular interest for the electrochemical measurements contained in the following section

3.3.4 Electrochemical Properties

Electrochemical measurements were performed to further investigate the electronic properties of the ruthenium (II) polypyridyl complexes. The oxidation and reduction potentials for the complexes contained in this chapter are summarised in *table 3.4*.

Complex	*Oxidation Potentials (V)*[a,b]		*Reduction Potentials (V)*[c]
	Ru^{II}/Ru^{III}	Ligand	
$[Ru(bpy)_3]^{2+}$	1.26	-	-1.33,-1.55, -1.80
$[Ru(bpy)_2(L1)]^{+}$	0.84	-	-1.47, -1.74
$[Ru(bpy)_2(HL1)]^{2+}$	1.14	-	-1.49, -1.75
$[Ru(bpy)_2(L2)]^{+}$	0.94	-	-1.43,-1.67, -2.01
$[Ru(bpy)_2(HL2)]^{2+}$	1.25	-	*d*
$[Ru(bpy)_2(L3)]^{+}$	0.80	1.20, 1.40	-1.48, -1.76
$[Ru(bpy)_2(HL3)]^{2+}$	1.20	1.45	*d*
$[Ru(bpy)_2(L4)]^{+}$	0.90	1.12, 1.20	-1.46,-1.67,-1.98
$[Ru(bpy)_2(HL4)]^{2+}$	1.21	1.38	*d*
$[Ru(bpy)_2(L5)Ru(bpy)_2]^{2+}$	0.82	1.26, 1.45	-1.48, -1.73
$[Ru(bpy)_2(H_2L5)Ru(bpy)_2]^{4+}$	1.25	1.50	-1.49, -1.73
$[Ru(bpy)_2(L6)Ru(bpy)_2]^{2+}$	0.92	1.18, 1.28	-1.44,-1.68,-1.96
$[Ru(bpy)_2(H_2L6)Ru(bpy)_2]^{4+}$	1.24	1.43	*d*

[a] Values standardised with respect to the redox potential of ferrocene (+0.38 V *vs.* SCE) under equivalent experimental conditions as a secondary electrode. [66]

[b] Protonation was achieved via addition of 1 drop of conc. $HClO_4$.

[c] All measurements were carried out under a constant flow of nitrogen. Cathodic samples also underwent deaeration by purging with argon for 15mins.

[d] Surface effects arise in acidic solutions making reduction potentials difficult to obtain.[35]

Table 3.4 Electrochemical data for the Ru (II) complexes in acetonitrile with 0.1M TEAP versus SCE

The electrochemical measurements reported in this chapter were carried out under strict experimental conditions outlined in *chapter two* The most pertinent solvent environs as well as the most judicious choice of electrode system were ascertained following exhaustive electrochemical studies (*Appendix B*)

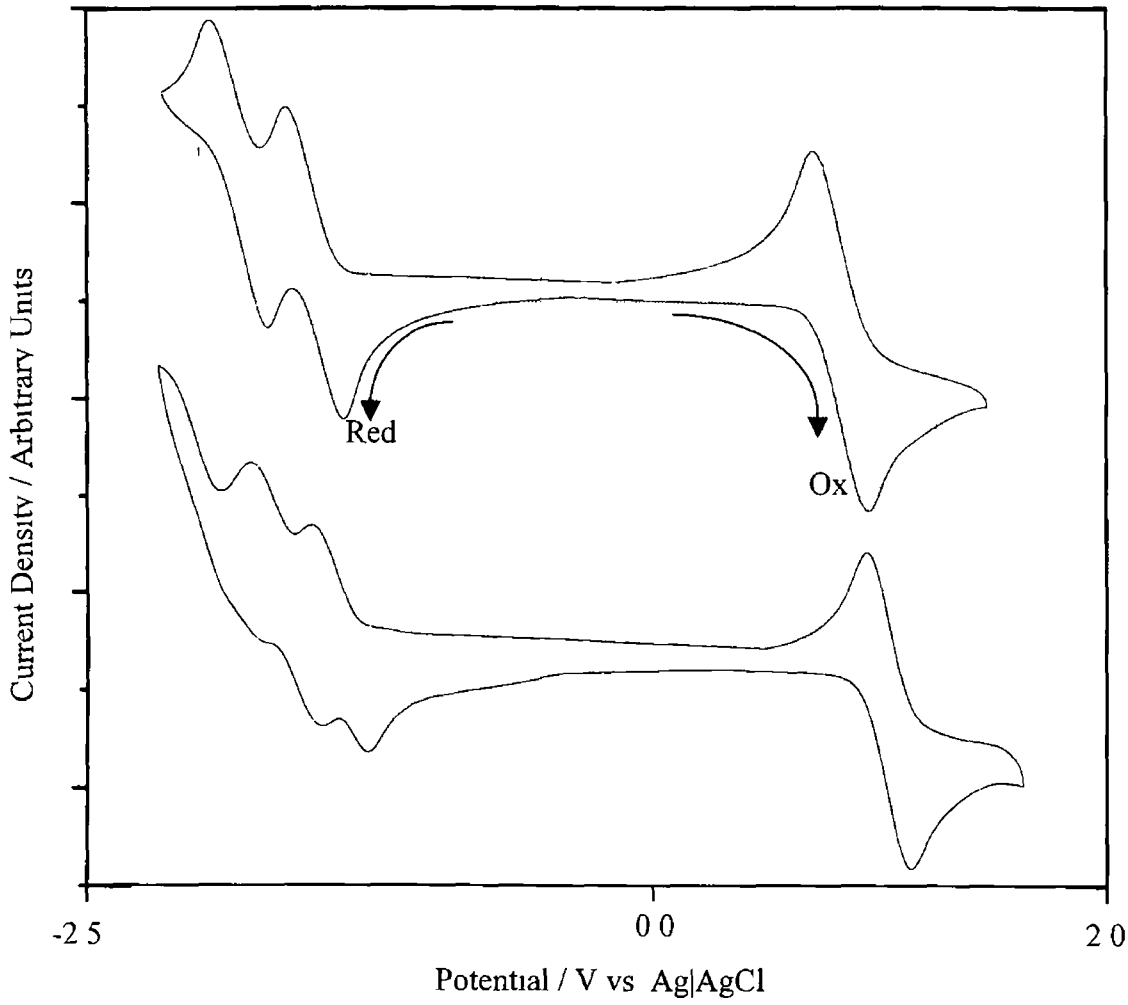

Figure 3 25 Cyclic Voltammograms of $[Ru(bpy)_2(L1)]^+$ **(red line)**, $[Ru(bpy)_2(L2)]^+$ **(black line)** in MeCN with 0 1M TEAP in Volts Versus SCE (*scan rate* 0 05V/s)

The electrochemical behaviour of these complexes is characterised by metal-based oxidations and ligand based reductions *Figure 3 25* depicts the cyclic voltammogram which was obtained for $[Ru(bpy)_2(L1)]^+$ and the pyrazyltriazole containing $[Ru(bpy)_2(L2)]^+$ complexes The data obtained are typical of ruthenium (II) polypyridyl complexes and at positive potentials is uncomplicated by ligand processes and hence, facilitated elucidation of the voltammetry of the subsequent dimethoxy containing complexes

By examination of the voltammograms it can be seen that in the case of both $[Ru(bpy)_2(L1)]^+$ and $[Ru(bpy)_2(L2)]^+$ the redox process observed in the anodic portion of the voltammogram is a reversible metal (Ru^{II}/Ru^{III}) process This is comparable to the data obtained for analogous complexes For example, the mononuclear ruthenium complex of 3,5-bis(pyridin-2-yl)-1,2,4-triazole (*figure 3 11*) which has one redox wave at 0 85 V versus SCE The ruthenium bipyridyl complex containing a pyridyltriazole complex, as synthesised by Hage (*figure 3 15* (**1**)), also reported a $Ru^{II/III}$ redox potential at 0 83 V and its pyrazyltriazole contemporary (*figure 3 15* (**2**)), which has an oxidation potential at 0 95 V [1][35] It is logical to conclude therefore, by comparison of these potentials for the oxidation of similar Ru (II) polypyridyl complexes containing pyridyltriazole or pyrazyltriazole ligands, that the first reversible oxidation steps at 0 84 V and 0 94 V versus SCE for the pyridyltriazole and the pyrazyltriazole complexes respectively, result from a metal centre coordinated to a deprotonated triazole ring [16][24]

However, it may also be noted upon examination of the data in *table 3 4* that there is a notable difference between the oxidation potentials obtained for the pyridyltriazole and pyrazyltriazole containing complexes and for that of the archetypal $[Ru(bpy)_3]^{2+}$ The extent of this difference varies and is less pronounced in the pyrazyltriazole containing complexes This arises from the substitution of one of the bipyridyl moieties by a ligand with differing properties Since the triazole moiety is a σ-donor there is an increase in the electron density on the metal centre which is expected to reduce the oxidation potential However, the pyridine and pyrazine moieties have π-acceptor properties and hence, a concurrent reduction of electron density on the metal centre results causing an increase in oxidation potential These two factors combined result in the slightly decreased oxidation potential with respect to $[Ru(bpy)_3]^{2+}$ observed for both the pyridyl- and pyrazyl-triazole complexes [1] *Figure 3 25* also shows the cathodic region of the CVs This region of the voltammogram differs for the pyrazyltriazole and the pyridyltriazole In the case of $[Ru(bpy)_2(L1)]^+$ the first reduction observed in the cathodic region of the voltammogram is bipyridine based by comparison with previously reported pyridyltriazole complexes such as that depicted in *figure 3 15*(**1**) [35]

This is not the case however, for $[Ru(bpy)_2(L2)]^+$. The difference is due to the electron accepting nature of the pyrazine ring (pz). In $[Ru(bpy)_2(L2)]^+$ the first reversible reduction observed is assigned as pyrazine based while the second reversible reduction is bipyridine centred. This too is a well-documented phenomenon and is again comparable to the potentials obtained for the ruthenium complex containing the pyrazyltriazole ligand depicted in figure 3.15(**2**)[1][65] and other pyrazyltriazole containing complexes. [58]

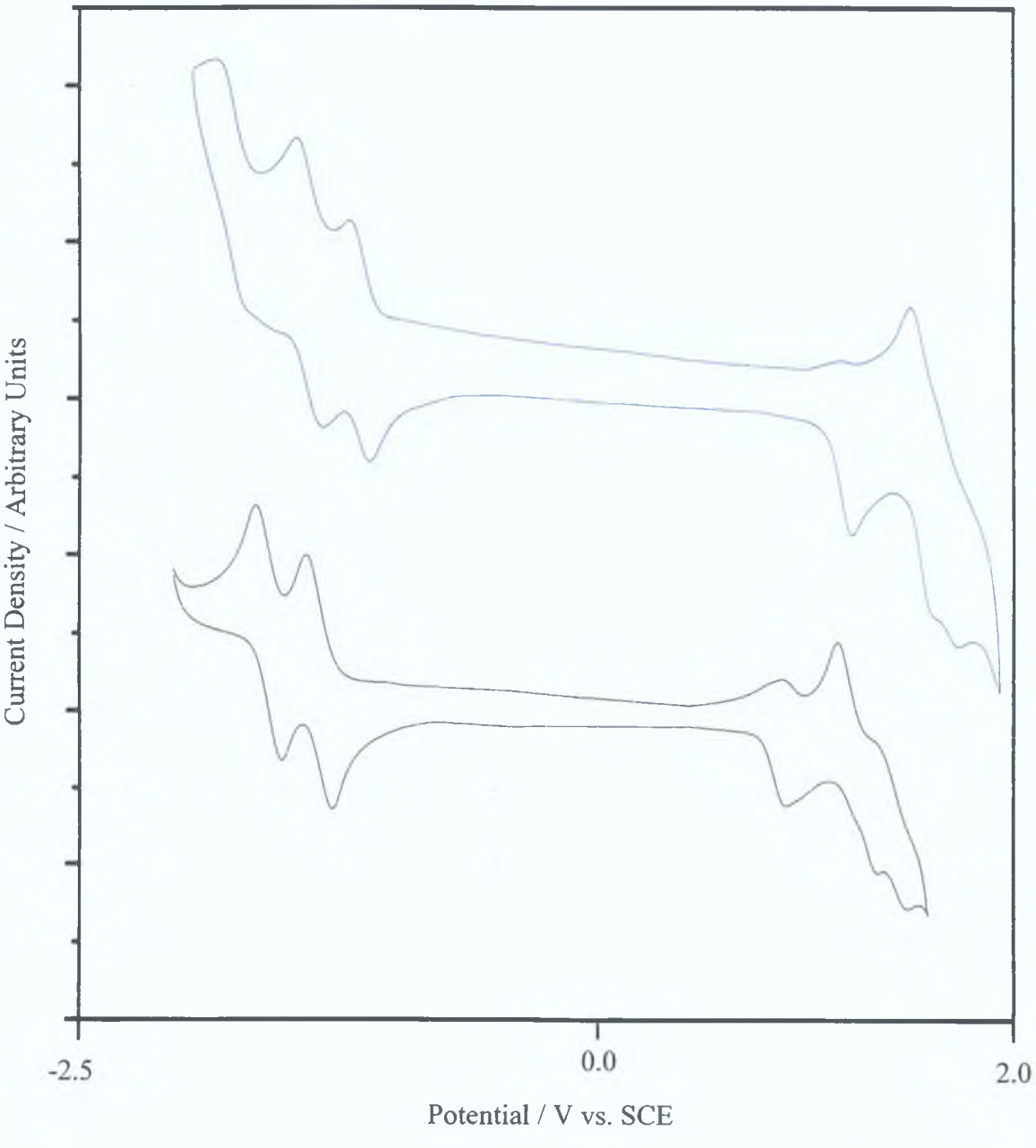

Figure 3. 26 Cyclic Voltammograms of $[Ru(bpy)_2(L4)]^+$ **(blue line)**, $[Ru(bpy)_2(L3)]^+$ **(black line)** in Neutral MeCN with 0.1M TEAP in Volts Versus SCE (scan rate 0.10V/s)

The cyclic voltammogram of the mononuclear complexes $[Ru(bpy)_2(L4)]^+$ and $[Ru(bpy)_2(L3)]^+$ were obtained under similar experimental conditions (*figure 3 26*) These voltammograms are similar to those of $[Ru(bpy)_2(L1)]^+$ and $[Ru(bpy)_2(L2)]^+$ and once again the first reversible oxidations at 0 90 V for $[Ru(bpy)_2(L4)]^+$ and 0 80 V for $[Ru(bpy)_2(L3)]^+$ versus SCE have been assigned as metal centred $Ru^{II/III}$ processes The reversible reductions are once again bipyridine based in the case of the pyridyltriazole containing $[Ru(bpy)_2(L3)]^+$ and pyrazyltrizole followed by bipyridine processes for $[Ru(bpy)_2(L4)]^+$, as was the case for $[Ru(bpy)_2(L1)]^+$ and $[Ru(bpy)_2(L2)]^+$

Complexes 3 to 6 contain a dimethoxyphenyl group and the oxidation processes of these moieties needs to be considered The complexes $[Ru(bpy)_2(L3)]^+$ and $[Ru(bpy)_2(L4)]^+$ and the dinuclear analogues display further processes in the anodic region of the CV These quasi-reversible processes have been identified as dimethoxy processes and occur subsequent to the metal redox processes (*figure 3 26*) [33] Such ligand processes have been noted previously for similar dimethoxy containing complexes For example, the ruthenium complex synthesised by Shukla *et al* , contains the ligand depicted in *figure 3 27*

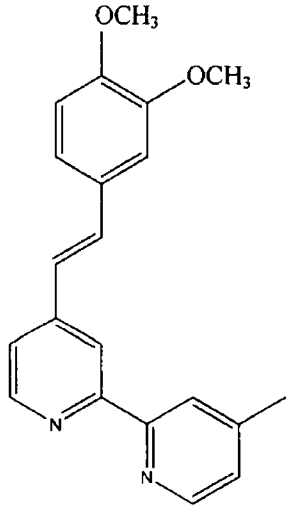

Figure 3 27 4-methyl-4'-[1-(3,4-dimethoxyphenyl)-ethen-2-yl]-2,2'-bipyridine [27]

This complex contains two methoxy moieties and the electrochemistry is similar to that obtained for $[Ru(bpy)_2(L3)]^+$ with a $Ru^{II/III}$ couple, at 0 84 V and additional quasi-reversible oxidations after the metal processes at 0 97 V which they ascribe to the pendant dimethoxyphenyl group [27]

O'Brien *et al* synthesised a similar complex containing the ligand depicted in *figure 3 21*, which was also found to exhibit similar behaviour with the metal process occurring at 0 71 V versus Ag | AgCl prior to the oxidation of the dimethoxy moieties at 1 20 V versus Ag | AgCl [31]

The cyclic voltammograms of the dinuclear complexes were also obtained It is interesting to note by comparison with the mononuclear analogues that the CVs of these complexes show only one oxidation wave of positive potential, which may by associated with the metal redox process This peak, which occurred at 0 82 V and 0 92 V for the dinuclear pyridyltriazole and pyrazyltriazole complexes respectively, could not be resolved with differential pulse voltammetry This was the case for both the pyridyltriazole containing and the pyrazyltriazole containing complexes and may be attributed to the simultaneous two-electron oxidation of the two metal units This result was also not entirely unexpected as it was noted for the analogous unsubstituted pyridyltriazole complex synthesised by Weldon and co-workers (*figure 3 12*) In this complex a similar oxidation of 0 84 V vs SCE was obtained under comparative experimental conditions and it also displayed only one reversible redox process associated with the simultaneous oxidation of the metal centres [2] Furthermore, examination of the larger peak-to-peak separation (E_p) in the first oxidation wave of the dinuclear complexes compared to those of the mononuclear complexes reflects the bielectromc process involved in the metal oxidation [33]

The thermodynamic stability of a mixed-valence species relative to the reduced and oxidised isovalent ones can be evaluated through the comproportionation constant, K_c as defined by *Eqn 3* at T = 298K [67]

$$K_c = e^{\Delta E(mV) / 25\,69} \qquad \textit{(Eqn 3)}$$

The absence of a significant difference in the two metal-based oxidations of the dinuclear complexes seems to suggest that there is little electronic coupling between the two metal centres in the ground state (*vide infra*), and the value of K_c for the dinuclear complexes is therefore reported to be less than 5 [68][69] Indeed, this phenomenon is known to occur in molecules that contain a number of identical, non-interacting centres [70]

If the interaction between the metal centres was strong this would ultimately result in stabilisation of the mixed-valence complex and result in the presence of discrete oxidation waves for each of the metal centres [71] The first oxidation potential of the dinuclear complexes are comparable to their analogous mononuclear complement i e , $[Ru(bpy)_2(L3)]^+$ and $[Ru(bpy)_2(L4)]^+$ They are also comparable to the oxidation potentials observed for the mononuclear complexes of the unsubstituted $[Ru(bpy)_2(L1)]^+$, $[Ru(bpy)_2(L2)]^+$, and the complexes containing the ligands depicted in *figure 3 15* The properties of the dinuclear complexes are hence similar to those of their mononuclear counterparts, which further indicate the independent behaviour of each of the two metal centres This is in stark contrast to the behaviour observed for dinuclear complexes, such as $[(Ru(bpy)_2)_2(bpt)]^{3+}$ and $[(Ru(bpy)_2)_2(bpzt)]^{3+}$ in which separate metal oxidations were observed as the metal units were found to interact quite strongly [4]

As with the unsubstituted dinuclear complex containing the ligand depicted in *figure 3 12* the reduction waves of $[Ru(bpy)_2(L5)Ru(bpy)_2]^{2+}$ are bipyridyl based The reduction processes noted for $[Ru(bpy)_2(L6Ru(bpy)_2]^{2+}$ are again comparable to those of the mononuclear complex with the pyrazyltriazole wave occurring prior to those of the bipyridyls [29] The effect of substituting one of the bipyridyl moieties of $[Ru(bpy)_3]^{2+}$ by a pyridyltriazole or a pyrazyltriazole type ligand has already been discussed and the effect that this substitution has on the oxidation potential of these complexes has been investigated

The oxidation potential of these complexes may be altered by changing the pH of the solvent environment Hence, the effect that protonation of the triazole ring, with acid, has on the oxidation potential of the metal centre was also investigated In the cyclic voltammograms of the protonated complexes it was observed that a shift in the oxidation potentials, with respect to the unprotonated analogues, can occur In the case of the pyridyltriazole complexes a shift of approximately 400 mV is observed while a less pronounced shift of circa 300 mV is noted for the pyrazyltriazole complexes (*table 3 4*)

This mirrors the results obtained for similar complexes, such as the ruthenium complex of pyrazyltriazole (*figure 3 15*(**2**)) where the oxidation shifts to 1 30 V versus SCE when protonated, and the ruthenium pyridyltriazole complex (*figure 3 15*(**1**) which shifts to 1 14 V upon protonation [1][65]

This anodic shift is due to the fact that the σ-donor capacity of the triazole is decreased upon protonation Hence there is a decreased electron density on the metal centre and there is a concomitant increase in the oxidation potential of the metal to such an extent that it is almost comparable to that of $[Ru(bpy)_3]^{2+}$ The reduction potentials of the protonated complexes were difficult to obtain This situation has been noted previously and may be attributed to both the fact that some adsorption on to the electrode surface occurs as well as the fact that deprotonation of the protonated complexes may occur upon scanning to negative potentials [35]

The electrochemical results discussed in this section have provided much useful information concerning the electronic properties of the complexes presented in this chapter The data obtained in relation to the dinuclear complexes appear to indicate weak or no communication between the metal centres This conclusion is largely based on the K_c values obtained for these complexes This value however, while providing an indication of the electronic interaction between two metal sites in a binuclear complex is not as direct a method of determining metal-metal electronic coupling as the analysis of the intervalence transition (IT) bands Indeed, one of the most reliable and direct methods of determining the amount of intercomponent electronic communication in bimetallic systems is by the study of the IT band [72] Hence, the following section, examines the oxidative spectroelectrochemical properties of this group of complexes

3 3 5 Spectroelectrochemistry

Spectroelectrochemistry is a powerful technique that may be used to further elucidate and explore the electrochemical properties and hence, electronic properties of ruthenium (II) polypyridyl complexes such as, those presented in this chapter Spectroelectrochemistry encompasses a range of techniques that arise from the marriage of two or more methods In this study the spectroelectrochemical techniques used involved the amalgamation of two separate characterisation methods, which have already discussed in earlier sections of this chapter

3 3 5 1 Absorption Spectroelectrochemistry

Absorption spectroelectrochemistry is a procedure used to examine the electrochemical and electronic absorption spectroscopy of compounds that are stable in a number of oxidation states [73] As discussed in the previous section the electrochemical behaviour of these complexes are characterised by metal-based oxidations and ligand-based reductions [40][39] The experimental conditions utilised during the course of this study are outlined in *chapter two*

This technique is particularly interesting for the examination of the dinuclear complexes introduced in this chapter The previous electrochemical data indicates that there is only very weak interaction between the metal centres in both the pyridyltriazole and pyrazyltriazole containing dinuclear complexes As reported in the introductory chapter intervalence transition (IT) bands, which may occur in mixed valence complexes, can provide an indication of the level of communication present between two metal centres [72] Since, in these dinuclear complexes there appears to be localised valences and weak metal-metal interactions, the treatment given by Hush was applied to the properties of the IT band [74]

It has already been shown in the previous section that oxidation of these complexes is metal centred It follows then that the energy of a transition involving this orbital is dramatically altered when the complex is oxidised This is reflected in the absorption spectrum of the complex For example, *figure 3 28* shows the spectroelectrochemical analysis of $[Ru(bpy)_2(L2)]^+$

The absorption spectrum of this complex is shown (**in black**) before a potential was applied to the system and then (in red) after 30 minutes at a potential of 1.10 V. The spectra depicted in *figure 3.28* are typical of those obtained for ruthenium (II) polypyridyl complexes.

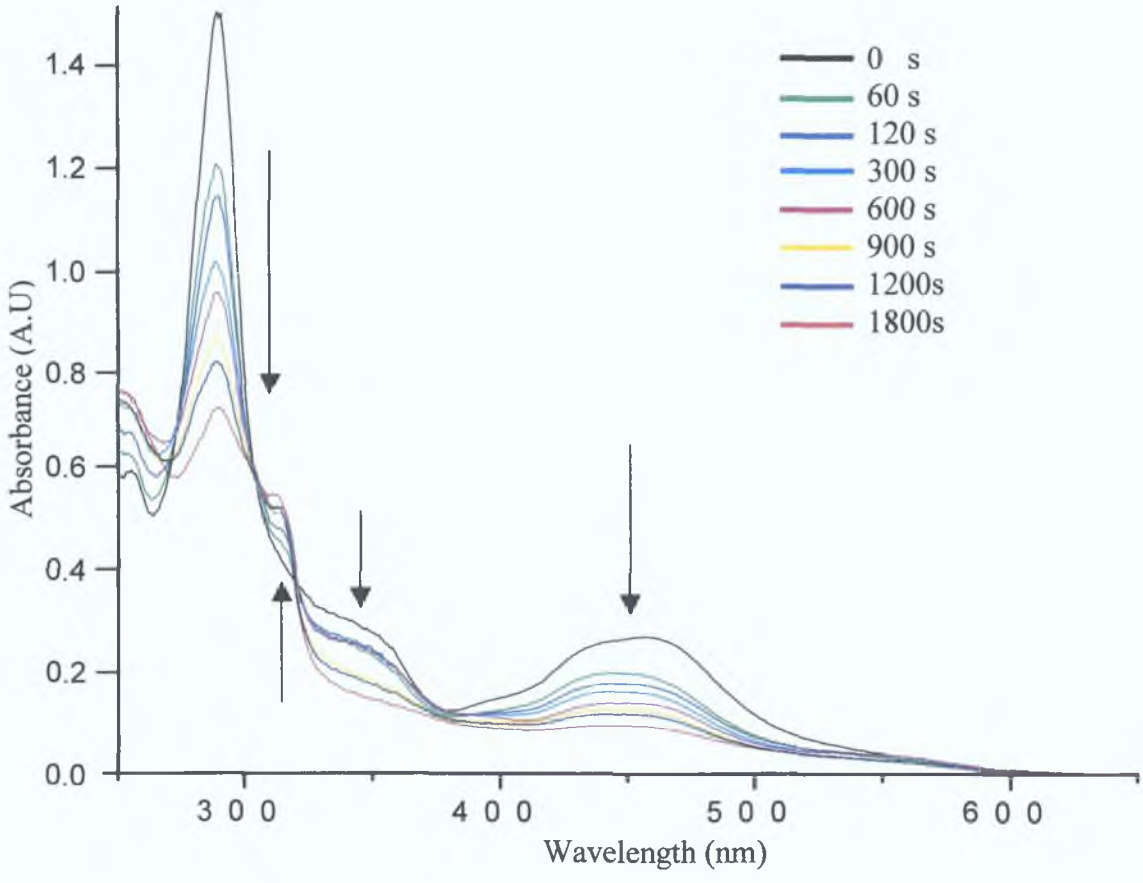

Figure 3.28 Spectroelectrochemical analysis of $[Ru(bpy)_2(L2)]^+$ at a potential of 1.10 V in neutral acetonitrile with 0.1 M TEAP vs. Ag|AgCl.

It can be seen from the above spectrum that the MLCT is strongly affected by the oxidation process and there is a dramatic shift in this transition and indeed the transition bleaches over the course of the oxidation. The increasingly positive nature of the ruthenium metal centre also lowers the energy of the π^* orbital of the ligands and this results in the slight red shift of the ligand $\pi - \pi^*$ transitions. Indeed, this characteristic splitting and shift to lower energy is synonymous with the oxidation of metal centres that are bound to 2,2'-bipyridyl ligands. [75]

As a complex is electrochemically oxidised new transitions may also appear. In the above figure, for example, a new shoulder is formed at 316 nm. This shoulder is characteristic of ruthenium (III) polypyridyl complexes. There is also some 'tailing' noticeable at approximately 600 nm. These weak long-wavelength shoulders are assigned to ligand-to-ligand charge transfer (LLCT) transitions. [76] In some cases, however, newly formed transitions are shifted completely outside the UV-vis region of the spectrum.

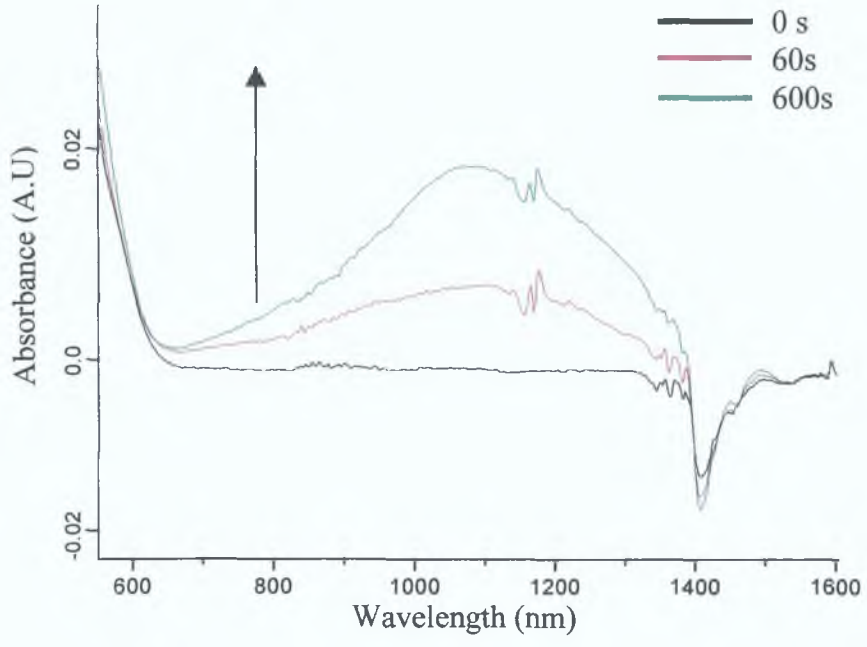

Figure 3.29 Spectroelectrochemical analysis of $[Ru(bpy)_2(L3)]^+$ in acetonitrile with 0.1M TEAP at a potential of 1.10 V vs. Ag|AgCl

For this reason spectroelectrochemical analysis from 360 nm to 2200 nm was also obtained for each complex and *figure 3.29* shows the oxidative spectroelectrochemical analysis of $[Ru(bpy)_2(L3)]^+$ in the region of 580 nm to 1600 nm. Some clear changes were noted in this area of the spectrum as the complex was electrochemically oxidised and a transition is seen to appear as the metal centre is oxidised. Due to its position and since, it is seen to deplete again once the potential is returned to 0 V, this transition is most likely associated with a new, bpy(π) – Ru d(π), ligand to metal charge transfer (LMCT) arising as the metal is oxidised.

This transition, centred at approximately 1080 nm, was seen to form in the absorption spectra of each of the mononuclear complexes, as they were electrochemically oxidised. Finally, the potential was then returned to 0 V and the new spectrum, of the ground state complex after the oxidation process, was obtained. Clean isobestic points were maintained throughout the oxidation process indicating the occurrence of a single oxidation process. The initial spectrum at 0 V and this new spectrum were then compared and it was consequently found that this metal-based oxidation was almost 100 % reversible. Each of the mononuclear complexes was found to display similar characteristic and similar reversible behaviour.

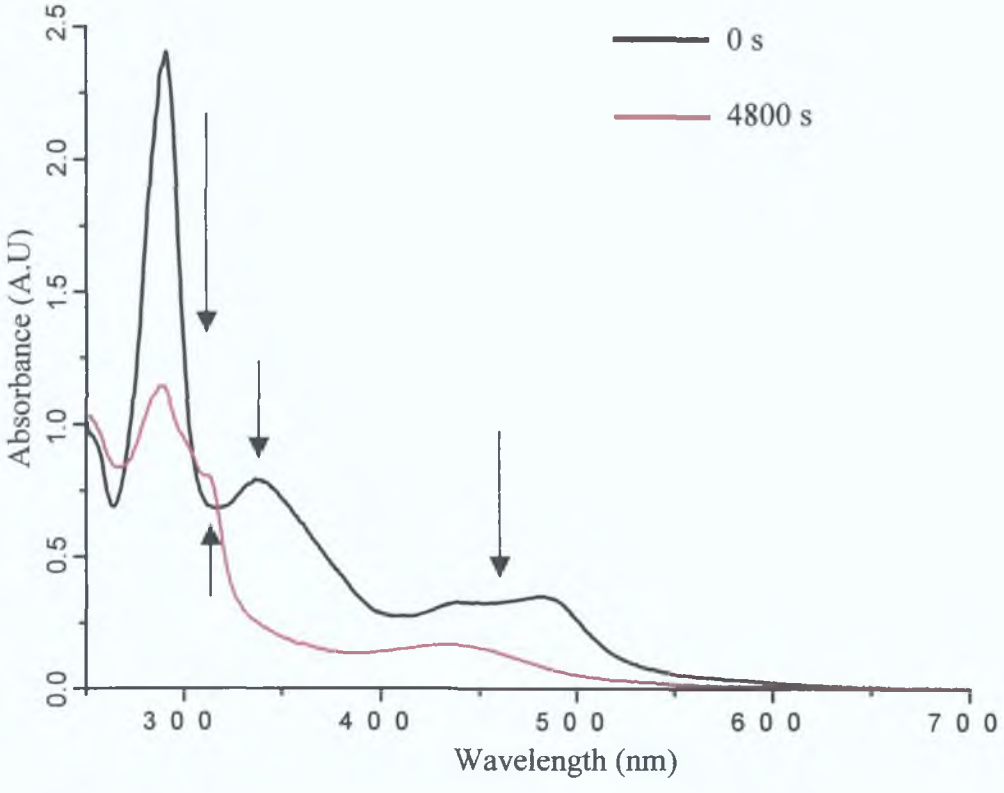

Figure 3.30 Spectroelectrochemical analysis of $[Ru(bpy)_2(L5)Ru(bpy)_2]^{2+}$ at a potential of 1.10 V in neutral acetonitrile with 0.1 M TEAP vs. Ag|AgCl

The analysis of the dinuclear complexes, although similar to that of the mononuclear compounds, is more complex. The oxidative spectroelectrochemical analysis of $[Ru(bpy)_2(L5)Ru(bpy)_2]^{2+}$ is depicted in *figure 3.30*. Once again, oxidation of the complex to a potential of 1.10 V vs. Ag|AgCl, results in significant changes of the absorption spectrum.

The MLCT at 480 nm is again seen to deplete as Ru(II) oxidises to Ru(III). The characteristic shoulder also associated with the formation of the Ru(III) polypyridyl species at 316 nm, was observed. Oxidation of the metal centre also lowered the energy of the π^* orbital of the ligand moieties as a small red shift of the ligand π– π^* at 280 nm was also noted. The ligand transitions between 250 nm and 380 nm also decrease in intensity as the metal centre oxidises as expected for metal centres bound to polypyridyl ligands. Once again, an LMCT appears as the metal centres oxidise at around 1080 nm. This oxidation was found to be reversible upon returning to 0 V, however, this reversibility of the system is lost if the potential is increased to beyond the ligand oxidations at 1.20 V as these are irreversible processes in this aprotic solvent environment. [27] This is reminiscent of the redox behaviour noted by Shukla *et al.* for the ruthenium dimethoxy complex of the ligand depicted in *figure 3.27.*

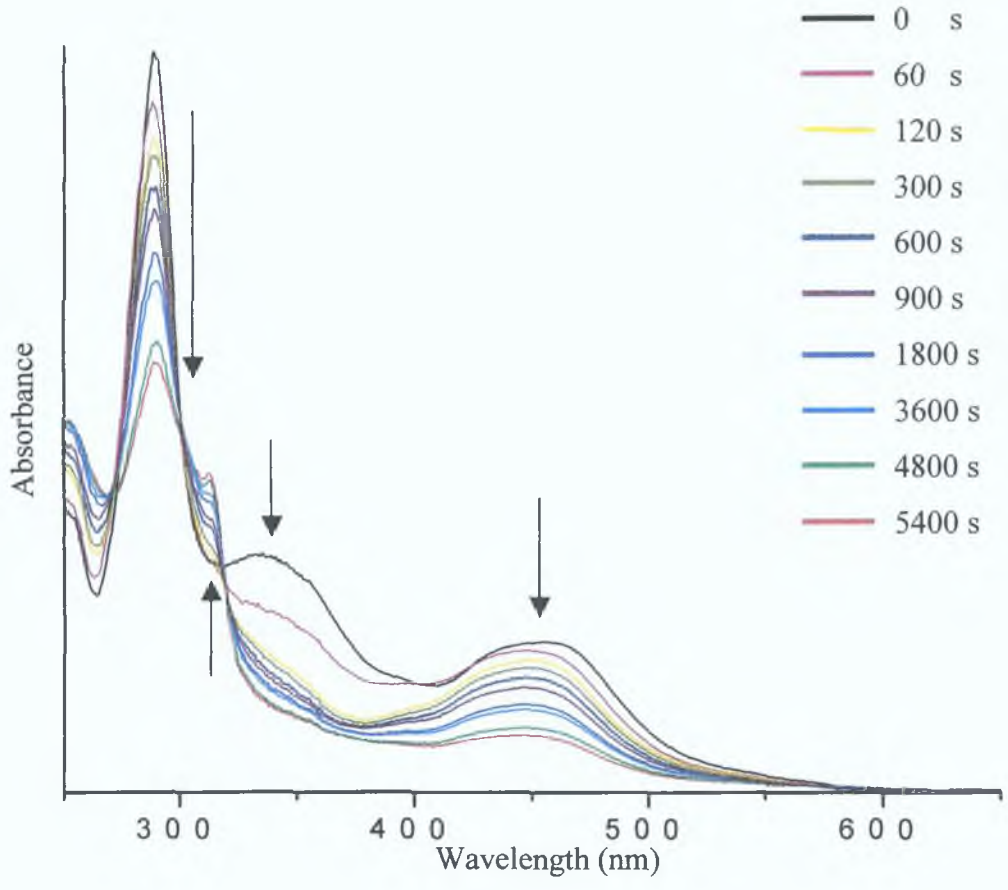

Figure 3.31 Spectroelectrochemical analysis of $[Ru(bpy)_2(L6)Ru(bpy)_2]^{2+}$ at a potential of 1.22 V in neutral acetonitrile with 0.1 M TEAP vs. Ag|AgCl

Similar behaviour was noted in the spectra of the pyrazyltriazole dinuclear complex The oxidative spectroelectrochemical analysis of the dinuclear pyrazyltriazole-containing complex $[Ru(bpy)_2(L6)Ru(bpy)_2]^{2+}$ is shown in *figure 3 31* Application of a potential of 1 12 V over 5400 s resulted in a number of spectral changes associated with the oxidation of a metal centre with bipyridyl ligands The MLCT is again seen to change dramatically as it is this transition that is involved in the oxidation process The bpy $\pi - \pi^*$ transition is seen to change as observed in the pyridyl complex This ligand transition also undergoes a slight red shift in energy as the metal centre oxidises and becomes more positive, stabilising the π^* bpy orbital As a new Ru(III) polypyridyl complex is formed a characteristic shoulder associated with this species is seen to form at 316 nm As with previous complexes, the ligand centred transitions at 340 nm also deplete as the nature of the metal orbitals change These processes were found to be reversible upon obtaining the spectrum of the complex after the potential was returned to 0 V However, scanning beyond the ligand oxidations resulted in the loss of this reversibility as described previously, since the ligand oxidations are not reversible in this solvent environ [27]

Oxidative spectroelectrochemical analysis was also carried out in the IR/near IR region from 600 nm to 2200 nm *Figure 3 32* shows the near IR spectral data obtained for $[Ru(bpy)_2(L5)Ru(bpy)_2]^{2+}$ As discussed previously oxidation of the mononuclear complex $[Ru(bpy)_2(L3)]^+$ resulted in the disappearance of the MLCT bands and the appearance of bands in the region 800 nm to 1400 nm *(figure 3 29)* These new bands were assigned as ligand-to-metal charge transfer bands (LMCT) on the basis of their energetic positions and intensities and by comparison with related complexes such as those studied by Hage *et al* and Vos and co-workers [33][57][77][78] For the dinuclear complex $[Ru(bpy)_2(L5)Ru(bpy)_2]$ similar changes occur in the UV-Vis-NIR spectra upon full (metal-centred) oxidation however additional bands are also observed during the oxidation process *(figure 3 32)* This additional feature emerges as a broad but very weak band centred at 1540 nm Initial oxidation leads to the appearance of this absorption band but as the oxidation progresses this band is seen to decrease in intensity

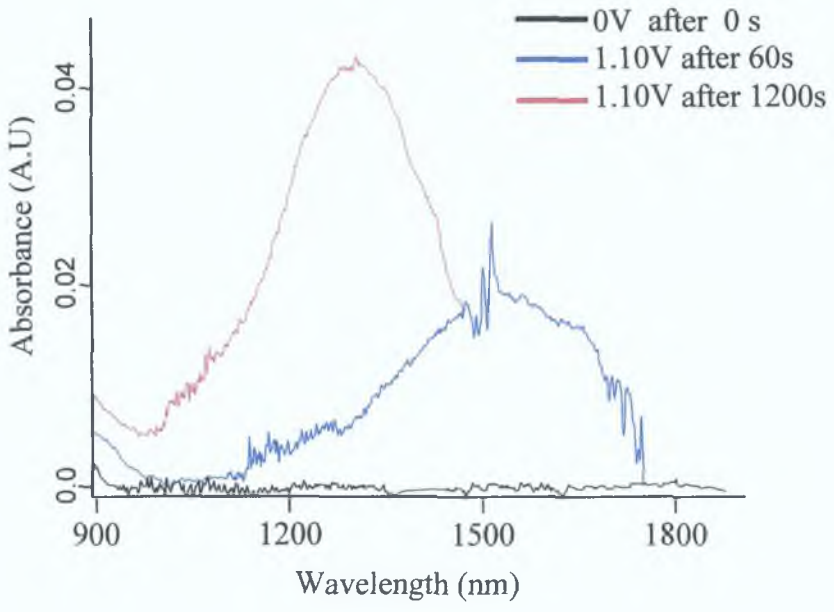

Figure 3.32 Near-IR oxidative spectroelectrochemical analysis of $[Ru(bpy)_2(L5)Ru(bpy)_2]^{2+}$ in acetonitrile with 0.1M TEAP

When this band decreases in intensity a more intense LMCT band develops at 1220 nm. Since this band is very similar to that found for the mononuclear analogue (*figure 3.29*) and it persists in the fully oxidised species, it is attributed to a charge transfer from the bridging ligand to the Ru(III) centres.[57] Further evidence for the LMCT nature of this band comes from comparison with the analogous dinuclear ruthenium complex, which is not dimethoxy, substituted (*figure 3.12*) and also has an LMCT centred at circa 1000 nm. [2] The increase and subsequent decrease of the NIR band (1540 nm) during the oxidation process, together with its position and intensity, strongly suggests that this absorption feature represents an intervalence transition (IT).[79][80][57] The original spectra recorded at 0 V (**black** line, *figure 3.32*) is therefore representative of $[Ru^{II}(bpy)_2(L5)Ru^{II}(bpy)_2]^{2+}$, while the band that forms (LMCT) and persists after 1200 s at 1.20 V may be attributed to the $[Ru^{III}(bpy)_2(L5)Ru^{III}(bpy)_2]^{2+}$ redox state. Finally the band (IT) that appears at 1.20 V and then disappears may be associated with the mixed valence $[Ru^{II}(bpy)_2(L5)Ru^{III}(bpy)_2]^{2+}$ species (*figure 3.32*).[33]

Oxidative spectroelectrochemical analysis of the dinuclear pyrazyltriazole complex $[Ru(bpy)_2(L6)Ru(bpy)_2]^{2+}$ complex was also performed in this region.

Although it was expected that comparable IT bands would be observed for this complex, none were noted in the NIR spectra This is unexpected as structurally similar complexes, such as the dinuclear pyrazine complexes studied by Hage and co-workers and Vos and co-workers, were found to yield IT bands [81][57] However, other dinuclear ruthenium complexes were also found to be lacking in any observable IT bands For example Browne *et al* examined a pyrazine bridged ruthenium dinuclear complex in which IT bands were found to be absent [82] However, it is possible that these bands were undetectable due to their inherent weak nature The extent of the intercomponent interaction detected in these complexes is of central importance in the area of supramolecular chemistry as discussed previously in *chapter one* and therefore the following section examines the extent of this interaction for the dinuclear pyridyltriazole complex in which an IT band was detected

3 3 5 2 Intervalence Transfer Properties

Accordingly, analysis of the IT band can yield information about the interaction between the metal centres in a dinuclear complex The Hush treatment assumes localised valences and relatively weak metal-metal interactions and therefore this procedure is suitable for the dinuclear complexes presented in this chapter as the electrochemical data discussed earlier suggests the presence of weak intermetallic communication within these dinuclear complexes [74] The dinuclear complexes considered in this chapter have symmetric bridging ligands and therefore the following calculations have assumed that the free energy change for electron transfer (ΔG) within these systems equals zero Furthermore, the intervalence band was not complicated by being in a precarious juxtaposition with the MLCT transition or other transitions on the time scale of the appearance of the IT bands However, since artefacts arose in the spectra of the IT bands as a result of the solvent absorption exceeding the compensation capability of the spectrophotometer, the spectra underwent Gaussian deconvolution in order to obtain a well-resolved IT band, which then permitted evaluation of the coupling parameter using the simple Hush procedure [83][84] Hence, assuming a Gaussian band shape, a lower limit for the bandwidth at room temperature could be calculated from [74][85]

$$\bar{\nu}_{max} = (\bar{\nu}_{1/2})^2 / 2.31) \qquad \textit{(Eqn. 4)}$$

Where $\bar{\nu}_{max}$ (in cm^{-1}) is the energy at the band maximum and $\bar{\upsilon}_{1/2}$ (in cm^{-1}) is the bandwidth at half height. A theoretical bandwidth may be calculated as follows:

$$\bar{\nu}_{1/2} = (2310.\bar{\nu}_{max})^{1/2} \ cm^{-1} \qquad \textit{(Eqn. 5)}$$

As stated in the introductory chapter three classes of systems may be distinguished depending on the magnitude of the interaction between the metal centres. In class I systems there is no interaction between the metal centres and hence no IT band would be observed in the spectrum of the oxidised complex. Therefore, this system may either be classed as class II or class III. In order to differentiate between the two classes the above calculations may be invoked. According to Hush's model, a simple and useful criterion to estimate the delocalisation degree of a system is given by the comparison between the theoretical and the experimentally measured spectral half-bandwidth, where the broader the experimental one is in relation to the calculated one, the more valence trapped the system is (i.e. class II). The limit situation (full delocalisation) is reached when the measured $\upsilon_{1/2}$ is substantially narrower than the calculated value.[67] *Table 3.5* contains the data calculated for $[Ru(bpy)_2(L5)Ru(bpy)_2]^{2+}$ and it can therefore, be seen upon comparison of the theoretically calculated bandwidth (3886 cm^{-1}) and the experimentally generated value (5100 cm^{-1}) that this system does conform to class II parameters, as the experimental bandwidth is clearly broader than the calculated value.

Complex	υ_{max} (E_{op}) (cm^{-1})	$\Delta\upsilon_{1/2}$ (calc) (cm^{-1})	$\Delta\upsilon_{1/2}$ (exp) (cm^{-1})	ε_{max} ($M^{-1}cm^{-1}$)	V_{ab} (cm^{-1})	α^2 (cm^{-1})
$[Ru(bpy)_2(L5)(bpy)_2Ru]^{2+}$	6470	3866	5100	2034	443	0.005

Table 3.5 **Intervalence transfer properties of the electrochemically generated $[Ru(bpy)_2(L5)Ru(bpy)_2]^{2+}$ mixed-valence complex in acetonitrile with 0.1 M TEAP**

Further calculations may also be carried out in order to explore further the IT properties of this complex However, some estimates must be made in order to carry out these computations For example, it was noted in the previous section 3 3 5, the metal oxidation peaks of the dinuclear complexes are irresolvable and this suggests that the metal interaction is very weak and hence K_c, which provides a measure of the thermodynamic stability of a mixed-valence species relative to the reduced and oxidised isovalent ones, was deemed to be less than 5 [68][69] This implies that oxidation of half of the ruthenium in the dinuclear complex forms a solution containing half of the dinuclear species as the mixed valence species while the remaining solution is an equimolar mixture of the homovalent species Hence, a considerable error would arise in the calculations if the concentration of the mixed-valence species were taken to equal the total dinuclear content K_c was hence estimated at 4 as it has been shown that when the metal-metal distance reaches 12Å K_c is near the statistical limit [29] For this reason the extinction coefficient for the IT band has been corrected by a factor of $(2 + (K_c)^{1/2})/(K_c)$ to account for comproportionation [67]

Furthermore, as no crystal structure data was available for the dinuclear complexes the metal-metal distance used in the calculations was obtained by molecular mechanics geometry optimisation calculations using the Chem3D Ultra package and refers to 'rigid' coordination modes, which do not take into account fluxional behaviour From these calculations a metal-metal distance of approximately 12 Å was deduced for $[Ru(bpy)_2(L5)Ru(bpy)_2]^{2+}$ While the following calculations are therefore approximations, nevertheless the results obtained in the calculation do provide a general estimate of the behaviour of the dinuclear system

Hence, by using the following formalism the magnitude of the electronic coupling, V_{ab}, and the electron delocalisation from Ru^{II} to Ru^{III}, and α^2, related to the mixed valence state could also be estimated from the properties of the IT bands via the following formulae

$$\alpha^2 = \frac{(4.2 \times 10^{-4})\ \varepsilon_{max}\ \bar{\nu}_{1/2}}{d^2\ \bar{\nu}_{max}} \qquad \textit{(Eqn 6)}$$

where, α^2 is the extent of delocalisation, $\bar{\nu}_{max}$ (in cm^{-1}) is the energy at the band maximum, $\bar{\upsilon}_{1/2}$ (in cm^{-1}) is the bandwidth at half height, ε_{max} is the extinction coefficient of the IT band (ε in $dm^3\ mol^{-1}\ cm^{-1}$) and d is the distance between the ruthenium centres The experimental α^2 value is the average of α^2 values for the ground and mixed-valence excited states If delocalisation is small the electronic wave functions used for overlap are relatively unperturbed and α^2 is a direct measure of delocalisation in the ground state hence, the larger the value of α^2 the higher the extent of electron delocalisation [74]

The extent of intermetallic interaction may be computed via the following formula [67][84]

$$V_{ab} = 2.05 \times 10^{2} (\varepsilon_{max} \bar{\upsilon}_{max} \bar{\upsilon}_{1/2}) / R_{MM} \qquad (Eqn\ 7)$$

Where V_{ab} is the coupling (in cm^{-1}), ε_{max} is the maximum extinction coefficient, $\bar{\upsilon}_{max}$ is the band position in cm^{-1}, $\bar{\upsilon}_{1/2}$ is the width at half maximum (cm^{-1}), and R_{MM} is the metal-metal distance in Å

These calculations were preformed and V_{ab} was found to equal 443 cm^{-1} while α^2 was found to be 0 005 cm^{-1} These results provide further evidence that, while it is relatively weak, some degree of interaction between the two metal centres This once again, confirms the status of this complex as a class II complex This result is comparable with literature examples of other class II systems For example the dinuclear ruthenium complex reported by Rocha *et al* which was found to be a class II complex under acidic conditions and reported a delocalisation value (α^2) of 0 004 cm^{-1} and an interaction value (V_{ab}) of 425 cm^{-1} The extent of intermetallic interaction (V_{ab} = 755 cm^{-1}) and electron delocalisation (α^2 = 0 012 cm^{-1}) in this type of complex under neutral conditions increases considerably as the complex becomes class III in nature [67] The extent of electron delocalisation and the intermetallic coupling in $[(Ru(bpy)_2)_2(bpt)]^{3+}$ (α^2 = 0 016 cm^{-1}, V_{ab} = 700 cm^{-1}) is considerably higher than in $[Ru(bpy)_2(L5)Ru(bpy)_2]^{2+}$ This can be rationalised on the basis that the metal-metal distance is increased appreciably in $[(Ru(bpy)_2)_2(bpt)]^{3+}$ and a phenyl spacer is also presenting this complex which has been shown previously to preclude strong electronic communication [86][87]

Finally, it must also be noted that in the analogous ruthenium dinuclear complex which does not contain dimethoxy groups on the phenyl spacer (*figure 3 12*), V_{ab} was found to be 295 cm^{-1} while α^2 can be estimated at 0 0014 cm^{-1} [2] In the case of the protonated dinuclear pyridyltriazole complex, no IT band is observed The absence of this band and the single bielectronic redox wave therefore confirm this complex to have no intermetallic interaction and it is, therefore, best described as type I [33]

3 3 5 3 Luminescence Spectroelectrochemistry

According to Kirchoff luminescence spectroscopy is well recognised for its improved selectivity and sensitivity relative to absorption spectroscopy When luminescence spectroscopy is coupled to electrochemistry, it provides the opportunity to selectively probe the excited state properties of *in situ* generated chromophores [88] Due to the increased sensitivity of this method compared to absorption spectroelectrochemistry, luminescence spectroelectrochemical analyses were also undertaken

When an oxidising potential was applied to the complexes presented in this chapter under the conditions outlined in *chapter two*, a depletion of the emission quantum yield was noted In the case of each complex the oxidising potential applied during these analyses was associated with the first redox process observed in the cyclic voltammogram of that complex i e the metal-based oxidations For example, *figure 3 33* shows the luminescence spectroelectrochemical data obtained for $[Ru(bpy)_2(L5)Ru(bpy)_2]^{2+}$ at 1 10 V This figure is typical of the spectra obtained for these complexes

Also, for $[Ru(bpy)_2(L1)]^+$ and $[Ru(bpy)_2(L2)]^+$ a reversible depletion in the luminescence was noted upon the application of an oxidising potential The analysis of these complexes are not complicated by the presence of substituents on the phenyl spacer and hence careful selection of the oxidising potential was not necessary and the depletion noted could therefore be assigned as resulting from the oxidation of Ru^{II} to Ru^{III}

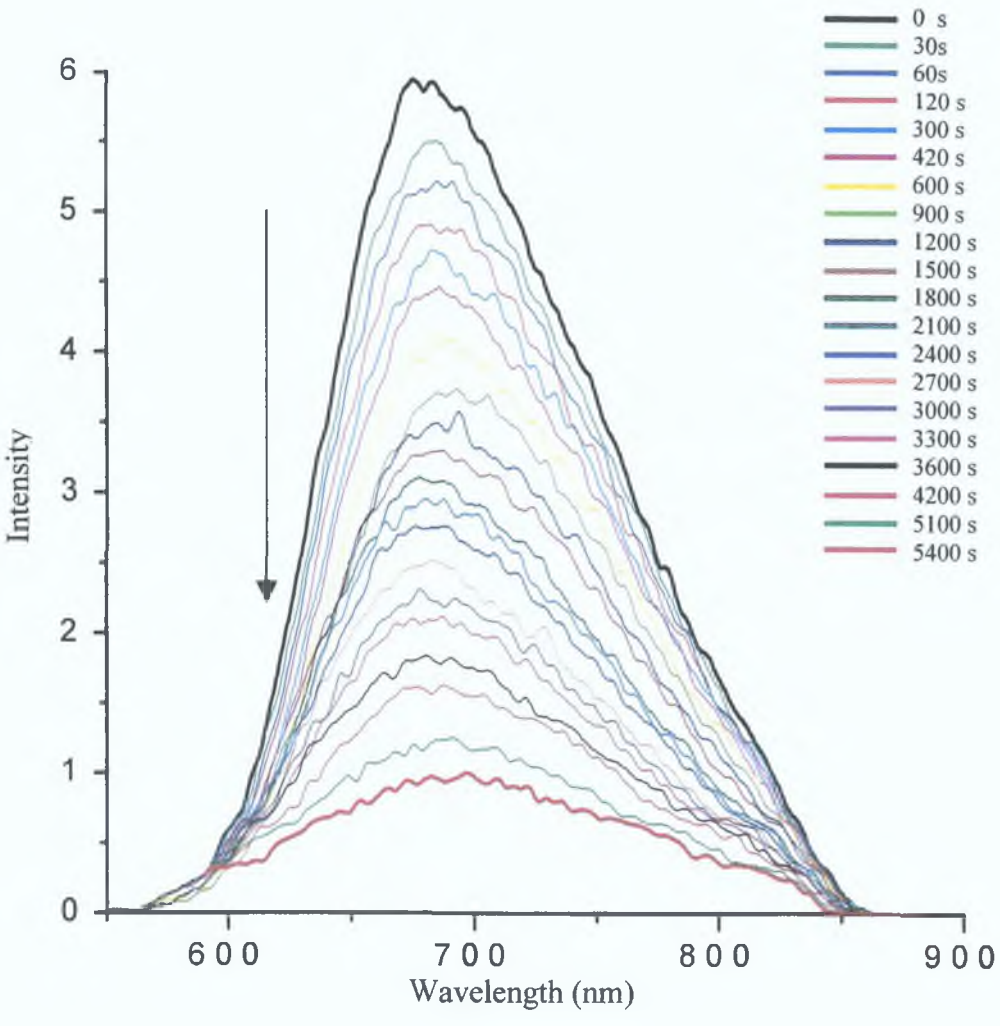

Figure 3.33 Luminescence spectroelectrochemical analysis of $[Ru(bpy)_2(L5)Ru(bpy)_2]^{2+}$ in neutral acetonitrile with 0.1 M TEAP at a potential of 1.10 V vs. Ag|AgCl

In the case of the other dimethoxy containing complexes application of an oxidising potential of 1.10 V associated with the first redox process (i.e. the metal redox process) observed in the CV of the complex resulted once again, in a reversible depletion of the luminescence. By comparison with the unsubstituted complexes $[Ru(bpy)_2(L1)]^+$ and $[Ru(bpy)_2(L2)]^+$, this depletion was deemed to arise due to the oxidation of the metal centre(s). The fact that this process was found to be reversible suggests that the metal oxidation is the only process occurring and provides further evidence that the final species noted during the absorption spectroelectrochemical analyses of the dinuclear complexes were indeed Ru^{III} and Ru^{III}/Ru^{III} in nature for the mononuclear and dinuclear complexes, respectively.

However, if the potential was increased beyond the first redox potential there was a subsequent loss of reversibility of the system. This is consistent with the oxidation of the dimethoxy moieties, which are irreversible in aprotic solvents. [27] These measurements provide further conformation of the nature of the oxidations occurring within these complexes and further confirm that reversible metal centred oxidations occur prior to the ligand oxidations.

3.4 Conclusion

The synthesis, electrochemical and spectroscopic characterisation of a number of Ru(II) polypyridyl complexes containing the ligands 3-phenyl-5-(pyridin-2''-yl)-1H-1',2',4'-triazole (HL1), 3-phenyl-5-(pyrazin-2''-yl)-1H-1',2',4'-triazole (HL2), 3-(2',5'-dimethoxyphenyl)-5-(pyridin-2''-yl)-1H-1',2',4'-triazole (HL3), 3-(2',5'-dimethoxyphenyl)-5-(pyrazin-2''-yl)-1H-1',2',4'-triazole (HL4), 1,4-bis(5'-(pyridin-2''-yl)-1'H-1',2',4'-triazol-3'-yl)-2,5-dimethoxyphenyl (H_2L5) and 1,4-bis(5'-(pyrazin-2''-yl)-1'H-1',2',4'-triazol-3'-yl)-2,5-dimethoxyphenyl (H_2L6) were presented in this chapter.

$[Ru(bpy)_2(L1)]^+$ and $[Ru(bpy)_2(L2)]^+$ are model systems for the elucidation of the properties of the dimethoxy substituted complexes and the subsequent dihydroxyphenyl and quinone containing complexes contained in the following chapters. $[Ru(bpy)_2(L3)]^+$, $[Ru(bpy)_2(L4)]^+$, $[Ru(bpy)_2(L5)Ru(bpy)_2]^{2+}$ and $[Ru(bpy)_2(L5)Ru(bpy)_2]^{2+}$ are precursor molecules for the synthesis of the subsequent group of hydroquinone and quinone containing complexes in chapters four and five. They also provide a basis for the investigation of these ensuing complexes in which the electrochemical and spectroelectrochemical measurement are complicated by the fact that the ligand oxidations occur prior to the metal redox process(es).

The ligands (*figure 3.6*) were synthesised via literature methods. These ligands were then coordinated to ruthenium via literature methods to yield the subsequent mononuclear and dinuclear complexes (complexes 1-6). The structure and purity of these ligands was assessed via NMR spectroscopy and elemental analyses.

The NMR spectra of the ligands HL3 – H_2L6 and the complexes 3-6 showed the presence of dimethoxy peaks between 3.5 ppm and 4.0 ppm. In the case of HL3, HL4, complex 3 and complex 4, two dimethoxy peaks were observed in the NMR spectra while H_2L5, H_2L6 and complexes 5 and 6 displays one strong dimethoxy peak due to the highly symmetric nature of these compounds.

The absorption data obtained for the complexes are similar to the archetypal $[Ru(bpy)_3]^{2+}$ complex with an MLCT between 400 and 500 nm and ligand centred bands at lower wavelengths. However, for each of the complexes the MLCT band was red shifted in comparison with $[Ru(bpy)_3]^{2+}$ due to the replacement of one of the bipyridyl moieties. Protonation of these complexes resulted in a blue shift of the λ_{max} of each of the complexes. This shift was less pronounced in the case of the pyrazyltriazole complexes. The absorption data for the dinuclear complexes provided evidence that there is a lack of intermetallic communication in these complexes as they behave in much the same manner as the mononuclear analogues. The luminescence observed for each of these complexes was also comparable to that of $[Ru(bpy)_3]^{2+}$ indicating that the lowest excited state is ^{3}MLCT in character for these complexes at room temperature. Protonation of the complexes at room temperature caused the pyridyltriazole complexes to decrease in emission intensity due to the formation of ligands with lower σ-donation and hence an increased ability to populate the ^{3}MC at room temperature. This phenomenon was also supported by the lifetime data. This decrease was accompanied by a shift in the emission to lower wavelengths. The pyrazyltriazole complexes did not behave in the same manner and protonation resulted in a shift to higher wavelengths and no comparable loss in emission intensity was observed. A change in the nature of the LUMO was also evoked by protonation of the triazole moiety in these complexes. These observations were also substantiated by the lifetime measurements.

The pH data obtained for the pyridyltriazole complexes further substantiated the fact that the excited state is always bipyridyl based in these complexes, regardless of the protonation state of the triazole moiety. The pH data for the pyrazyltriazole complexes provided further evidence of switching of the excited state in these complexes upon protonation of the triazole moiety.

Electrochemical measurements showed that the oxidation of the metal from Ru^{II} to Ru^{III} occurs prior to the dimethoxy oxidations in each of the complexes A single bielectronic redox wave was noted for the dinuclear complexes further confirming the weak intermetallic interaction in these complexes The cathodic region of the pyridyltriazole complexes depicted bipyridyl processes at approximately –1 48 V and –1 75 V, while the pyrazyltriazole complexes display additional pyrazyl processes prior to those of the bipyridyl groups at approximately –1 45 V Spectroelectrochemical techniques further confirmed the occurrence of metal redox processes prior to the ligand processes LMCT bands were also noted m the spectra of the complexes upon application of an oxidising potential and in the case of $[Ru(bpy)_2(L5)Ru(bpy)_2]^{2+}$ an IT band was observed Calculations performed on this IT band confirmed this complex to be class II No observable IT band was noted in the case of $[Ru(bpy)_2(L6)Ru(bpy)_2]^{2+}$ Luminescence spectroelectrochemical measurements further confirmed that the metal redox processes occur prior to those of the dimethoxy ligand processes

The next chapter contains the synthesis of the hydroquinone analogues of complexes 3 – 6 The results obtained for this new group of complexes will be discussed in light of the observations made for the complexes contained in this chapter

3.5 Bibliography

1 F Barigelletti, L De Cola, V Balzani, R Hage, J G Haasnoot, J Reedijk, J G Vos, *Inorg Chem*, **1989**, 28, 4344

2 F M Weldon, J G Vos, *Inorg Chim Acta*, **2000**, 307, 13

3 R Hage, J H van Diemen, G Ehrlich, J G Haasnoot, D J Stufkens, T L Snoeck, J G Vos, J Reedijk, *Inorg Chem*, **1990**, 29, 988

4 R Hage, J G Haasnoot, H A Nieuwenhuis, J Reedijk, D J A De Ridder, J G Vos, *J Am Chem Soc*, **1990**, 112, 9245

5 W R Browne, C M O'Connor, H P Hughes, R Hage, O Walter, M Doering, J F Gallagher, J G Vos, *J Chem Soc, Dalton Trans*, **2002**, 4048

6 J R Bolton, J A Schmidt, T Ho, J Liu, K J Roach, A C Weedon, M D Archer, J H Wilford, V P Y Gadzekpo, *Adv Chem Sens*, **1991**, 228, 117

7 R Wang, T E Keyes, R Hage, R H Schmehl, J G Vos, *J Chem Soc, Chem Comm*, **1993**, 1652

8 P T Gulyas, T A Smith, M N Paddon-Row, *J Chem Soc, Dalton Trans*, **1999**, 1325

9 M E Peover, *Nature*, **1972**, 191, 782

10 V Goulle, A Harriman, J -M Lehn, *J Chem Soc, Chem Commun*, **1993**, 1034

11 M Haga, E Dodsworth, A B P Lever, *Inorg Chem*, **1986**, 25, 447

12 M D Ward, J A McCleverty, *J Chem Soc, Dalton Trans*, **2002**, 275

13 F N Rein, R C Rocha, H E Toma, *J Electroanal Chem*, **2000**, 494, 21

14 M Barthram, M D Ward, *New J Chem*, **2000**, 24, 510

15 R S da Silva, S I Gorelsky, E S Dodsworth, E Tfouni, A B P Lever, *J Chem Soc, Dalton Trans*, **2000**, 4078

16 H Masui, A P B Lever, P A Auburn, *Inorg Chem*, **1991**, 30, 2402

17 M Haga, E S Dodsworth, A P B Lever, *Inorg Chem*, **1986**, 25, 447

18 D J Stufkens, T L Snoeck, A P B Lever, *Inorg Chem*, **1988**, 27, 953

19 A P B Lever, P A Auburn, E S Dodsworth, M Haga, W Liu, M Melnik, W A Nevin, *J Am Chem Soc*, **1988**, 110, 8076

20 M Barthram, Z R Reeves, J C Jeffery, M D Ward, *J Chem Soc, Dalton Trans*, **2000**, 3162

21 D Bardwell, J C Jeffery, L Joulie, M D Ward, *J Chem Soc, Dalton Trans*, **1993**, 2255

22 J C Jeffery, D J Liard, M D Ward, *Inorg Chim Acta*, **1996**, 251, 9

23 M Bond, F Marken, C T Williams, D A Beattie, T E Keyes, R J Forster, J G Vos, *J Phys Chem B*, **2000**, 104, 1977

24 B M Holligan, J C Jeffery, M K Norgett, E Schatz, M D Ward, *J Chem Soc, Dalton Trans*, **1992**, 3345

25 V Goulle, A Harriman, J -M Lehn, *J Chem Soc, Chem Commun*, **1993**, 1034

26 K S Schanze, K Sauer, *J Am Chem Soc*, **1988**, 110, 1180

27 A D Shukla, B Whittle, H C Bajaj, A Das, M D Ward, *Inorg Chim Acta*, **1999**, 285, 89

28 S Fanni, T E Keyes, S Campagna, J G Vos, *Inorg Chem*, **1998**, 37, 5933

29 F M Weldon, *Ph D Thesis*, **1998**, Dublin City University

30 T E Keyes, *Ph D Thesis*, **1994**, Dublin City University

31 L O'Brien, M Duati, S Rau, A L Guckian, T E Keyes, N M O'Boyle, A Serr, H Gorls, J G Vos, *J Chem Soc, Dalton Trans*, **2004**, 514

32 D Hughes, *Ph D Thesis*, **1999**, Dublin City University

33 P Passaniti, W R Browne, F C Lynch, D Hughes, M Nieuwenhuyzen, P James, M Maestri, J G Vos, *J Chem Soc, Dalton Trans*, **2002**, 1740

34 B P Sullivan, D J Salmon, T J Meyer, *Inorg Chem*, **1978**, 17, 3334

35 R Hage, *Ph D Thesis*, **1991**, Leiden University, The Netherlands

36 P J Steel, F Lahousse, D Lerner, C Marzin, *Inorg Chem*, **1983**, 22, 1488

37 E M Ryan, R Wang, J G Vos, R Hage, J G Haasnoot, *Inorg Chim Acta*, **1993**, 208, 49

38 B Buchanan, *Ph D Thesis*, **1989**, Dublin City University

39 R Hage, A H J Dijkhuis, J G Haasnoot, R Prins, J Reedijk, B E Buchanan, J G Vos, *Inorg Chem*, **1988**, 27, 2185

40 R Hage, R Prins, J G Haasnoot, J Reedijk, J G Vos, *J Chem Soc, Dalton Trans*, **1987**, 1387

41 R A Metcalfe, A B P Lever, *Inorg Chem*, **1997**, 36, 4762

42 P Ballesteros, R M Claramunt, C Escolastico, M D Santa Maria, *J Org Chem*, **1992**, 57, 1873

43 E Kochanski, *Mathematical and Physical Sciences*, **1992**, Series C, Kluwer Acedemic Publishers, Dorderecht, 376

44 S Serroni, S Campagna, G Denti, T E Keyes, J G Vos, *Inorg Chem*, **1996**, 35, 4513

45 C G Coates, T E Keyes, H P Hughes, P M Jayaweera, J J McGarvey, J G Vos, *J Phys Chem A*, **1998**, 102, 5013

46 J G Vos, J G Haasnoot, G Vos, *Inorg Chim Acta*, **1983**, 71,155

47 H A Nieuwenhuis, J G Haasnoot, R Hage, J Reedijk, T L Snoeck, D J Stufkens, J G Vos, *Inorg Chem*, **1991**, 30, 48

48 M Wrighton, D L Morse, *J Am Chem Soc*, **1974**, 96, 998

49 S Fanni, T E Keyes, C M O'Connor, H Hughes, R Y Wang, J G Vos, *Coord Chem Rev*, **2000**, 208, 77

50 T E Keyes, C M O'Connor, U O'Dwyer, C G Coates, P Callaghan, J J McGarvey, J G Vos, *J Phys Chem A*, **1999**, 103, 8915

51 W R Browne, D Hesek, J F Gallagher, C M O'Connor, J S Killeen, F Aoki, H Ishida, Y Inoue, C Villani, J G Vos, *Dalton Trans*, **2003**, 2597

52 R Hage, J G Haasnoot, H A Nieuwenhuis, J Reedijk, R Wang, J G Vos, *J Chem Soc, Dalton Trans*, **1991**, 3271

53 C G Coates, T E Keyes, J J McGarvey, H P Hughes, J G Vos, P M Jayaweera, *Coord Chem Rev*, **1998**, 171, 323

54 J M de Wolf, R Hage, J G Haasnoot, J Reedijk, J G Vos, *New J Chem*, **1991**, 15, 501

55 R J Crutchley, A B P Lever, *Inorg Chem*, **1982**, 21, 2277

56 R Hage, J G Haasnoot, J Reedijk, R Wang, J G Vos, *Inorg Chem*, **1991**, 30, 3263

57 W R Browne, F Weldon, A Guckian, J G Vos, *Collect Czech Chem Commun*, **2003**, 1467

58 J S Killeen, *Ph D Thesis*, **2003**, Dublin City University

59 D E Morris, Y Ohsawa, *Inorg Chem*, **1984**, 23, 3010

60 P J Giordano, C R Bock, *J Am Chem Soc*, **1978**, 100, 6960

61 P H Xie, Y J Hou, B W Zhang, Y Cao, *J Photochem Photobio A Chem*, **1999**, 3, 169

62 J G Vos, *Polyhedron*, **1992**, 11, *18*, 2285

63 *IUPAC Compendium of Chemical Terminology*, **1996**, 68, 2243

64 P Ford, D F Rudd, R Gaunder, H Taube, *J Am Chem Soc*, **1968**, 90, 1187

65 H A Nieuwenhuis, J G Haasnoot, R Hage, J Reedijk, T L Snoeck, D J Stufkens, J G Vos, *Inorg Chem*, **1991**, 30, 48

66 N G Connelly, W E Geiger, *Chem Rev*, **1996**, 96, 877

67 R C Rocha, H E Toma, *Inorg Chem Commun*, **2001**, 230

68 J C Curtis, J S Bernstein, T J Meyer, *Inorg Chem*, **1985**, 24, 385

69 D E Richardson, H Taube, *Inorg Chem*, **1981**, 20, 1278

70 J B Flanagan, S Margel, A J Bard, F C Anson, *J Am Chem Soc*, **1978**, 100, 4248

71 C Creutz, H Taube, *J Am Chem Soc*, **1969**, 91, 3988

72 C Creutz, Prog *Inorg Chem*, **1983**, 30, 1

73 G A Heath, L J Yellowlees, *J Chem Soc, Chem Comm*, **1981**, 287

74 R W Callaghan, F R Keene, T J Meyer, D J Salmon, *J Am Chem Soc*, **1977**, 99,1064

75 E Brauns, S W Jones, J A Clark, S M Molnar, Y Kawanishi, K J Brewer, *Inorg Chem*, **1996**, 35, 1737

76 V Kasack, W Kaim, H Binder, J Jordanov, E Roth, *Inorg Chem*, **1995**, 34, 1924

77 R Hage, J G Haasnoot, H A Nieuwenhuis, J Reedjik, D J A Rider, J G Vos, *J Am Chem Soc*, **1990**, 112, 9245

78 C Di Pietro, S Serroni, S Campagna, M T Gandolfi, R Ballardini, S Fanni, W R Browne, J G Vos, *Inorg Chem*, **2002**, 41, 2871

79 J Bonvoisin, J P Launay, M van der Auweraer, F C de Schryver, *J Phys Chem*, **1994**, 98, 5052

80 J Bonvoisin, J P Launay, M van der Auweraer, F C de Schryver, *J Phys Chem*, **1996**, 100, 18006

81 R Hage, H E B Lempers, J G Haasnoot, J Reedijk, F M Weldon, J G Vos, *Inorg Chem*, **1997**, 36, 3139

82 W R Browne, N M O'Boyle, W Henry, A L Guckian, S Horn, T Fett, C M O'Connor, M Duati, L DeCola, C G Coates, K L Ronayne, J J McGarvey, J G Vos, *J Am Chem Soc*, **2005**, 127, 1229

83 A C Ribou, J P Launay, M L Sachtleben, H Li, C W Spangler, *Inorg Chem*, **1996**, 35, 3735

84 A C Ribou, J P Launay, K Takahashi, T Nihira, S Tarutani, C W Spangler, *Inorg Chem* , **1994**, 33, 1325

85 R W Callaghan, T J Meyer, *Chem Phys Letts* , **1976**, 39, 1

86 R Hage, J G Haasnoot, J Reedijk, R Wang, E M Ryan, J G Vos, A L Spek, A J M Duisenberg, *Inorg Chim Acta*, **1990**, 174, 77

87 L Hammarstrom, F Barigelletti, L Flamigni, N Armaroli, A Sour, J P Collin, J P Sauvage, *J Am Chem Soc* , **1996**, 118, 11972

88 J R Kirchhoff, *Current Sep* , **1997**, 16, 11

Chapter Four

Mono- and Dinuclear Ruthenium(II) Complexes Containing Dihydoxyphenyl Moieties

The synthesis, photophysical and electrochemical properties of a group of mononuclear and dinuclear ruthenium(II) complexes are presented in this chapter The complexes contained in this chapter are the successors of the compounds that have already been discussed in chapter three and are characterised by the presence of pyridyl-1,2,4-triazole or pyrazyl-1,2,4-triazole unit(s) and dihydroxyphenyl moieties

4.1 Introduction

In *chapter one,* the processes entailed in natural photosynthesis were presented. There has been considerable interest in the elucidation and emulation of these natural processes over the past number of years and this has led to a general growth in the interest in quinonoid species and particularly the hydroquinone / quinone redox couple for a number of incongruous reasons.[1-5]

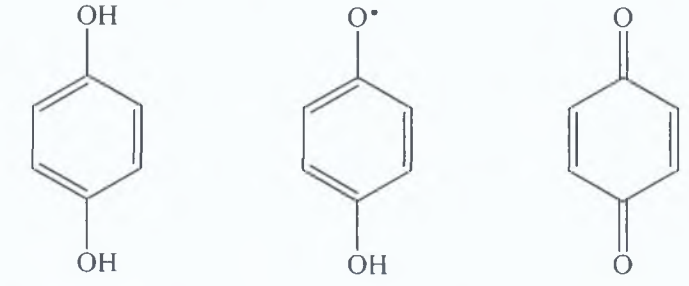

Figure 4.1 Structure and nomenclature of quinonoid species. [6]

This is attributable to the fact that quinoid complexes comprise a redox reaction of classical and current importance as they represent one of the oldest and most basic redox processes. [1][2] For instance, they play a pivotal role within photosynthesis. In the type-two reaction centre of *Rhodopseudomonas viridis*, for example, there is a light-induced charge separation between a pigment electron donor and a pigment electron acceptor in which a hydroquinone is oxidised to a quinone. [7][8] The role of hydroquinones in natural photosynthesis has therefore, led to its inclusion as an electron donor in biomimetic systems particularly in the field of hydroquinone-linked porphyrin systems.[9-12] The structure and nomenclature of the various quinonoid species mentioned in the text are depicted in *figure 4.1.*

Central to the understanding of the processes involved in photosynthesis is the examination of the behaviour of the hydroquinone / quinone redox couple. Hydroquinones and catechols (1,2-dihydroxybenzene) display rather complicated electrochemical behaviour in aqueous solutions. This is due to the occurrence of secondary reactions and to the formation of dinuclear and hydroxylated products.[13][14] This behaviour is dependant upon the ligand concentration, pH value and applied potentials. [15]

Laviron has treated the roles of protonation and deprotonation on the electrochemical mechanisms, which interconvert quinone and hydroquinone, and their self-exchange reaction, quantitatively. [16-18] In an effort to explicate the elementary steps of quinone / hydroquinone electron transfer Laviron proposed a "scheme of squares" (*figure 4.2*). This scheme applies to hydroquinone and catechol oxidation on Pt with the order of proton and electron transfer depending on pH value. [17]

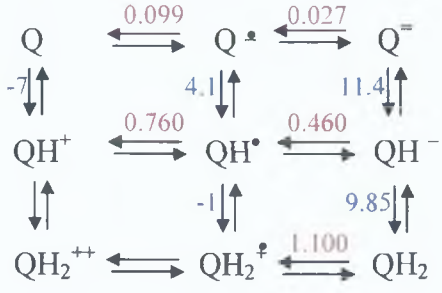

Figure 4.2 The "scheme of squares" for the quinone (Q) / hydroquinone (HQ) redox couple as described by Laviron.[17]

The redox potentials (vs. NHE at 25°C) (in red) for the successive one-electron couples that connect quinone and hydroquinone and pK_a values (in blue) for the various components are also shown in the above scheme. The potential and pK_a data, illustrate the profound effect that changes in oxidation state can have on acid-base properties. [19] In general, however, when the electrochemical work is carried out in organic solutions, as it mostly is in this chapter, the complications from chemical reactions coupled with electron transfer processes are found to be much less critical. [20]

The intriguing electrochemical behaviour is particularly evident in metal-quinonoid complexes. Over the past few years considerable attention has been paid to ruthenium polypyridyl complexes bound to catechol / hydroquinone moieties (*figure 4.3*). [21][22-29] Generally these complexes involve a bidentate coordination mode through the two vicinal phenolate oxygen atoms. [15] However, a number of studies by such authors as Haga[22], Lever[29], Ward[30-34] and co-workers involve coordination via nitrogen and oxygen moieties. Keyes and co-workers, for example, have prepared a range of O, N coordinated complexes. [35-37]

While Ernst *et al* have also reported coordination of ruthenium polypyridyl moieties via a diphenylphosphino and a hydroxyl moiety [38]

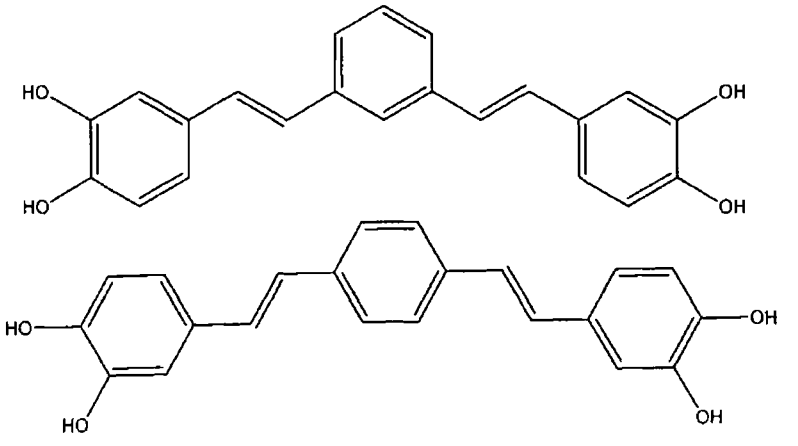

Figure 4 3 Catecholate ligands used in the preparation of the ruthenium dimer complexes [24]

This interest in such complexes centres on the fact that it has been shown that within these complexes there is a strong degree of orbital mixing between d(π) and ligand p(π) frontier orbitals [39] Interesting characteristics are invoked by the metal-ligand orbital mixing as this generates an opportunity for considerable covalency between the redox-active metal centre and coordinated redox-active ligand This leads to the possibility of using these kinds of systems as building blocks for molecular electronic devices [40][41]

A number of interesting ruthenium complexes containing ligands with hydroquinone / catechol or phenol moieties have also been reported [42-49] Perhaps the most intriguing of these studies was carried out by Lehn and co-workers, in which they were interested in exploiting the reversible electrochemical interconversion in protic media of the hydroquinone / quinone redox couple by the exchange of two protons and two electrons Their complex represented an excellent example of an electro-photoswitching device as the quinone unit quenched the luminescence of the ruthenium polypyridyl moiety while the hydroquinone moiety did not [48] The phenomena of electrochemically induced proton transfer from a hydroquinone moiety to an attached triazole ring have also been investigated (*scheme 4 1*) [43]

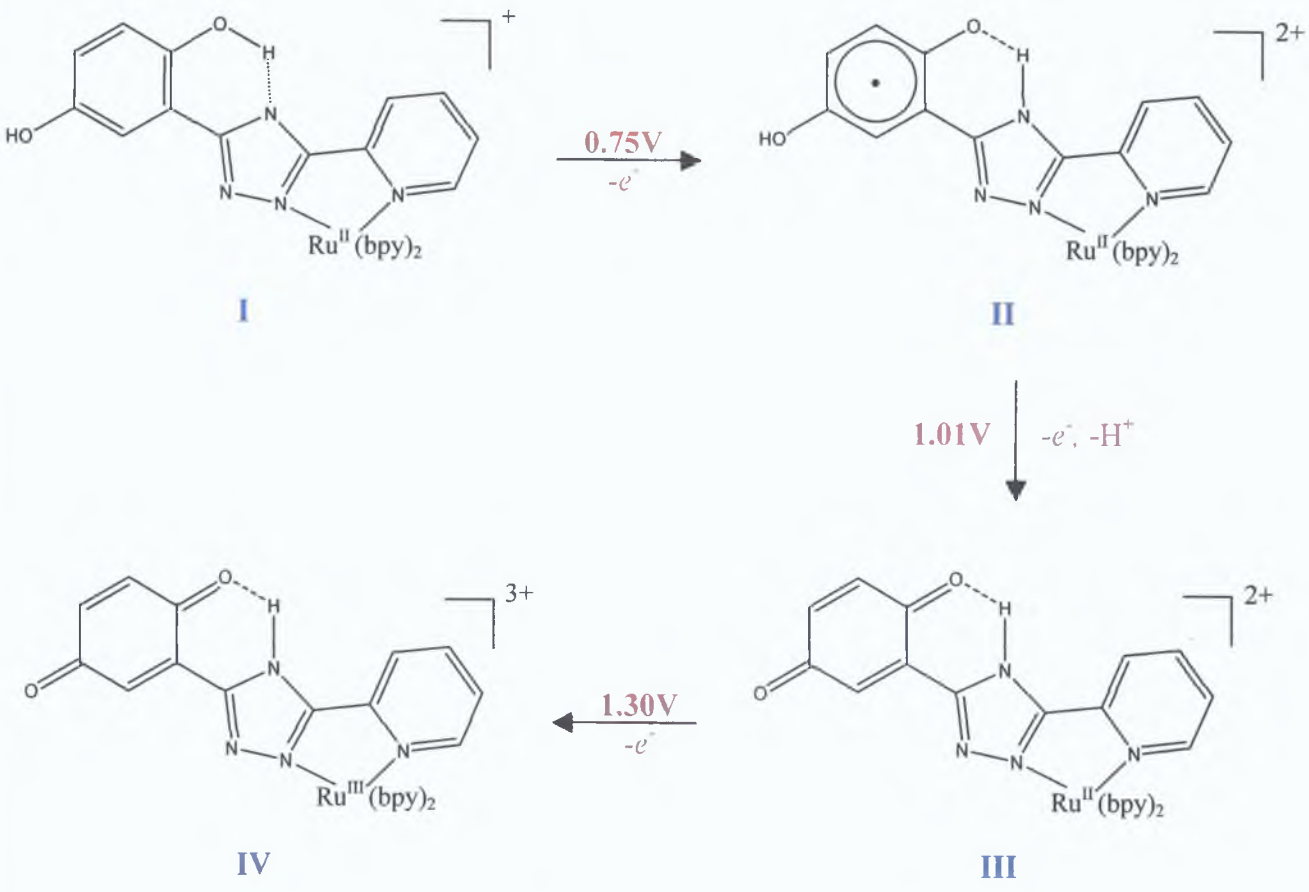

Scheme 4.1 Scheme proposed by Wang *et al.* for a reversible, electrochemically induced proton transfer reaction from a hydroquinone group to the attached triazole ring. [43]

In most of these cases however, long-lived photoinduced charge separation is perturbed by rapid electron back-transfer probably due to the fact that the hydroquinone moiety is bound to the ruthenium centre via polypyridyl ligands.[46][48][60] Vos and co-workers however, have taken a different approach to this problem by the inclusion of non-polypyridyl, non-luminescent spectator ligands such as, the negatively charged pyridyltriazole, 3-(pyridin-2'-yl)-1,2,4-triazole. [43] Complexes containing either hydroquinone or catechol moieties have been prepared by Keyes, Weldon, O'Brien and co-workers with the aim of the investigations to study electron and energy transfer processes between photoactive components via a negatively charged triazolate bridge. [42][43][45][49] *Scheme 4.1* was proposed by Wang *et al.* It depicts an electrochemically induced, reversible proton transfer involving a quinone / hydroquinone redox couple. They suggest that this proton transfer occurs intramolecularly via hydrogen-bridge formation between the hydroquinone and the triazole. [43]

The complexes presented in this chapter are analogous to those in *chapter three* however, they contain a dihydroxyphenyl moiety in place of the dimethoxyphenyl group The structures of these complexes are shown in *figure 4 4* They have been synthesised by the direct demethylation of the complexes contained in *chapter three* Hence, they represent the second group of complexes in this continuing series aimed at ultimately understanding the interaction between hydroquinone / quinone groups coupled to a *ruthenium* centre(s) via a negatively charged bridge An investigation as to whether or not the process of electrochemically induced proton transfer (*scheme 4 1*) occurs, within the hydroquinone complexes presented here, will also be considered in this chapter [43]

First, the synthetic factors involved in the demethylation of these complexes are presented The compounds were prepared via modified literature methods and their purity was then assessed by NMR spectroscopy and elemental analysis These results are contained in the following experimental section Following the establishment of the purity of these complexes they were further characterised by emission and absorption spectroscopy and the ground and excited state lifetimes of the various complexes were measured and reported in the subsequent section In order to investigate changes in the electrochemical behaviour of these complexes upon demethylation, electrochemical characterisation of both the oxidation of the metal centre and the ligand-based reductions has also been undertaken and the results are discussed in the electrochemical section Acid-base measurements are presented in order to investigate the nature of the *lowest unoccupied molecular* orbital (LUMO) This is a characteristic that once again, varied depending on whether the complex contained a pyridyltriazole or a pyrazyltriazole These values along with relevant pKa and pKa* values are also quoted within this chapter

Finally, since the dinuclear complexes may have interesting intermetallic interactions invoked by the presence of the hydroquinone moieties, in depth spectroelectrochemical data are presented Hence, a comprehensive set of data for these hydroquinone-containing complexes are collated within this chapter and discussed with particular reference to their analogous dimethoxy-containing complexes previously considered in *chapter three*

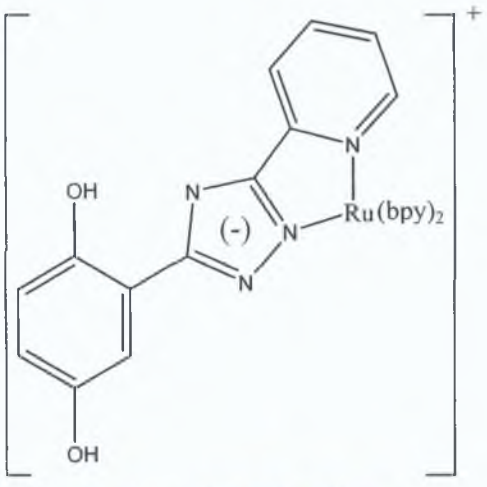

$[Ru(bpy)_2(L7)]PF_6.2H_2O$

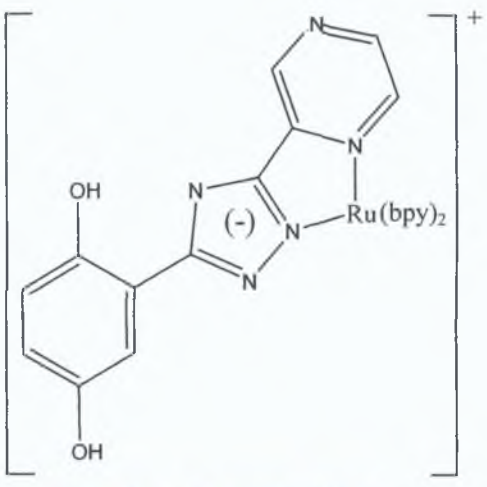

$[Ru(bpy)_2(L8)]PF_6.2H_2O$

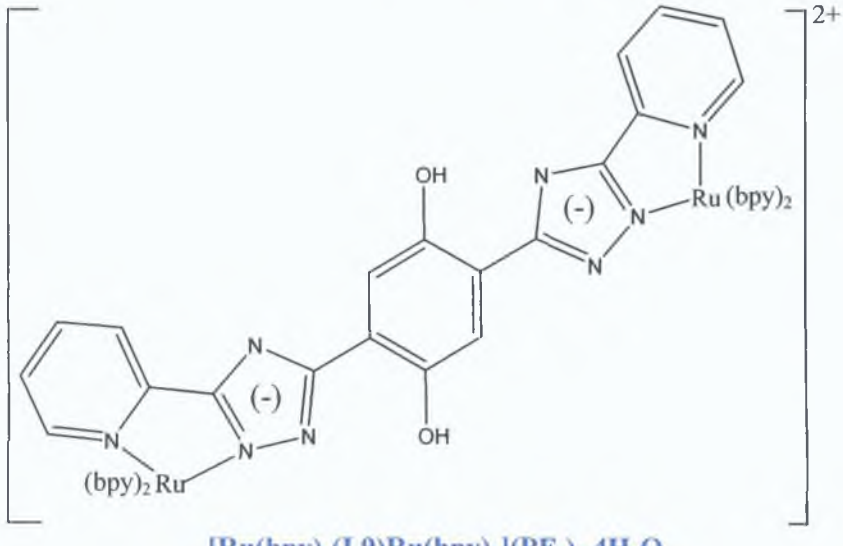

$[Ru(bpy)_2(L9)Ru(bpy)_2](PF_6)_2.4H_2O$

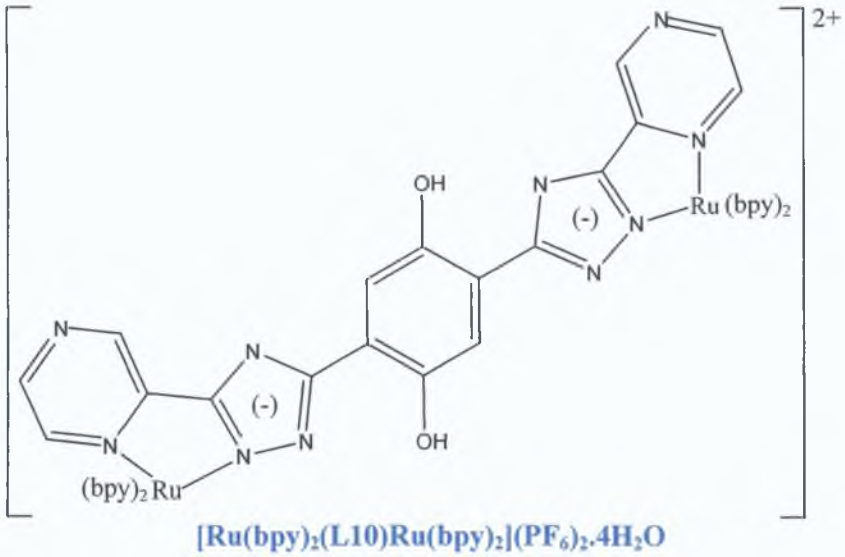

$[Ru(bpy)_2(L10)Ru(bpy)_2](PF_6)_2.4H_2O$

Figure 4.4 Structures of mononuclear and dinuclear complexes cited in this chapter.

4.2 Experimental Methodology

4.2.1 Synthetic Methods

The synthesis of the daughter Ru(II) complexes containing dihydroxy moieties, prepared by the demethylation of the precursor complexes in *chapter three*, are presented in this section. These complexes have been synthesised previously, [44] however, since no data were available on their photochemical and photophysical properties and since, they are precursor complexes for the compounds contained in the following chapter, it was necessary to perform their re-synthesis. The deprotection of the ligand HL3 was also undertaken in order to aid in the elucidation of the electrochemical results presented in a subsequent section. Hence, the novel synthesis and NMR spectral characteristics of this ligand are also presented in this section. The ^{1}H-NMR spectra of the $[Ru(bpy)_2(L9)Ru(bpy)_2](PF_6)_2.4H_2O$ complex, which is typical of that obtained for these complexes, is presented in *figure 4.5*. A modification of the demethylation techniques and reaction methodologies developed by O'Brien *et al.* was utilised for the synthesis of the following complexes. [45]

Complex 7: $[Ru(bpy)_2(L7)]PF_6.2H_2O$

$[Ru(bpy)_2(L3)]PF_6.H_2O$ (200 mg, 0.24 mmol) was added to dry dichloromethane (3 cm^3) and brought to – 80° C in an acetone / liquid nitrogen slush bath under a constant flow of N_2. An excess of 1.0 M boron tribromide (10 cm^3) was then introduced into the nitrogen-saturated chamber. The nitrogen stream was then removed and the flask sealed. The mixture was then allowed to attain room temperature and the reaction was allowed to proceed over a 12 h period with constant stirring. The reaction mixture was then poured onto ice water and stirred for 30 min. This mixture was then transferred to a separating funnel and the organic layer removed. The remaining aqueous layer was neutralised with a saturated sodium bicarbonate solution. A small quantity of ammonium hexafluorophosphate was then added and a red deprotected ruthenium complex precipitated. The solid product was collected by vacuum filtration and washed with water and ether. The product was then recrystallised from hot ethanol / water (2:1 v/v). Demethylation was verified by TLC and NMR spectral techniques as the $-OCH_3$ singlet peaks (3.5 – 4.0 ppm) were found to be absent.

Purity was established by the ^{1}H-NMR spectrum and analytical HPLC. Yield = 62 mg (31 %). Calculated for $RuC_{33}N_8H_{29}O_4PF_6$: C: 46.76; H: 3.45; N: 13.22 %. Anal. Found: C: 47.32; H: 3.12; N: 12.71 %.

Complex 8: $[Ru(bpy)_2(L8)]PF_6.2H_2O$

$[Ru(bpy)_2(L4)]PF_6.H_2O$ was demethylated with BBr_3 in a similar manner to that described previously for $[Ru(bpy)_2(L7)]PF_6.H_2O$ with the exception that 200 mg (0.196 mmol) of $[Ru(bpy)_2(L4)]PF_6.H_2O$ was used in place of $[Ru(bpy)_2(L3)]PF_6.H_2O$. The product was recrystallised from hot ethanol / water (2:1 v/v) and demethylation was verified by TLC and NMR spectral techniques in which the $-OCH_3$ singlet peaks (3.5 – 4.0 ppm) were again found to be absent. Purity was established by the ^{1}H-NMR spectrum and analytical HPLC. Yield = 134 mg (67 %). Calculated for $RuC_{32}N_9H_{28}O_4PF_6$: C: 43.83; H: 3.13; N: 13.38 %. Anal. Found: C: 44.07; H: 2.81; N: 13.69 %.

Complex 9: $[Ru(bpy)_2(L9)Ru(bpy)_2](PF_6)_2.4H_2O$

$[Ru(bpy)_2(L9)Ru(bpy)_2](PF_6)_2.4H_2O$ was, once again, prepared by an analogous method as that outlined for $[Ru(bpy)_2(L7)]PF_6.H_2O$. During the preparation of this complex, however, $[Ru(bpy)_2(L5)Ru(bpy)_2](PF_6)_2.4H_2O$ (400 mg, 0.26 mmol) was demethylated with BBr_3 in dichloromethane. Recrystallised was achieved from hot ethanol / water (2:1 v/v) and demethylation was verified by TLC and NMR spectral techniques in which the $-OCH_3$ singlet peaks (3.5 – 4.0 ppm) were again found to be absent. Purity was established by the ^{1}H-NMR spectrum and analytical HPLC. Yield = 296 mg (74 %). Calculated for $Ru_2C_{60}N_{16}H_{52}O_6P_2F_{12}$: C: 42.65; H: 2.31; N: 12.44 %. Anal. Found: C: 42.93; H: 2.62; N: 12.68 %.

Complex 10: $[Ru(bpy)_2(L10)Ru(bpy)_2](PF_6)_2.4H_2O$

The protected complex $[Ru(bpy)_2(L6)Ru(bpy)_2](PF_6)_2.4H_2O$ was demethylated with BBr_3 in a similar manner as described for $[Ru(bpy)_2(L7)]PF_6.H_2O$. However, 400 mg (0.26 mmol) of $[Ru(bpy)_2(L6)Ru(bpy)_2](PF_6)_2.4H_2O$ was dissolved in dichloromethane prior to the addition of BBr_3. The solid product that was precipitated was recrystallised from hot ethanol / water (2:1 v/v) and demethylation was verified by TLC and NMR spectral techniques in which the $-OCH_3$ singlet peaks (3.5 – 4.0 ppm) were again found to be absent.

Purity was established by the ^{1}H-NMR spectrum and analytical HPLC. Yield = 248 mg (62 %). Calculated for $Ru_2C_{58}N_{18}H_{50}O_6P_2F_{12}$: C: 41.94; H: 2.89; N: 15.91 %. Anal. Found: C: 41.38; H: 2.54; N: 15.40 %.

3-(2',5'-dihydroxyphenyl)-5-(pyridin-2''-yl)-1H-1,2,4-triazole (H3L3)

This ligand was prepared using the cerium ammonium nitrate (CAN) method described in *chapter five,* however, the hydroquinone ligand was obtained. Yield: 300 mg, 85 %. **^{1}H-NMR (d_6-DMSO): δ 10.05 (s, 2H, -OH), 8.83 (d, 1H, pyridyl H$^{6''}$), 8.49 (d, 1H, pyridyl H$^{3''}$), 7.83 (d, 1H, pyridyl H$^{4''}$), 7.82 (s, 1H, phenyl H$^{6'}$), 7.78 (dd, 1H, pyridyl H$^{5''}$), 7.49 (m, 2H, phenyl H$^{3'}$ and H$^{4'}$).**

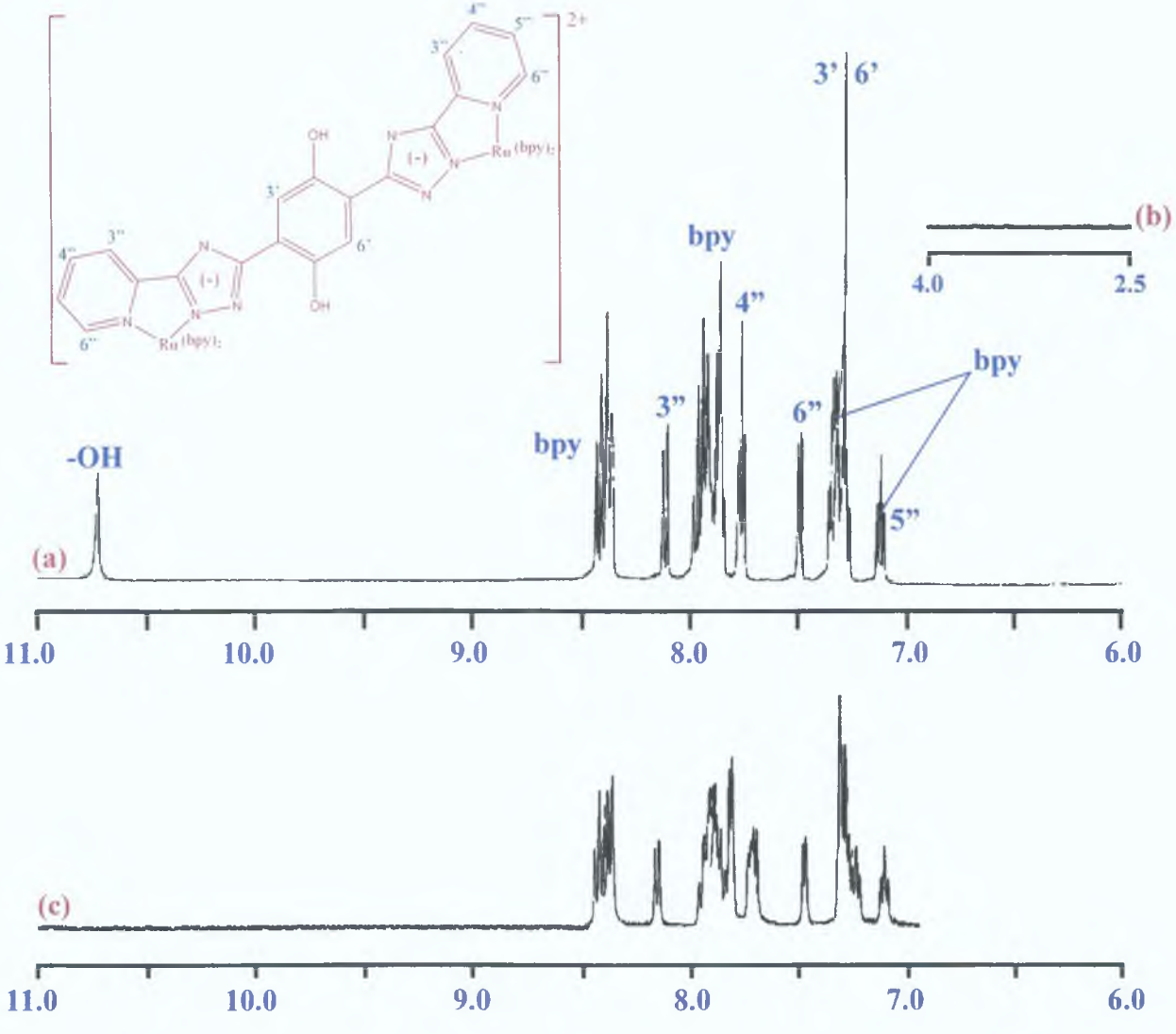

Figure 4.5 ^{1}H-NMR spectra of (a) $[Ru(bpy)_2(L9)Ru(bpy)_2](PF_6)_2.4H_2O$ (b) the $-OCH_3$ region inset and (c) $[Ru(bpy)_2(L9)Ru(bpy)_2](PF_6)_2.4H_2O$ with1 drop of D_2O in d_3-acetonitrile

4.3 Results and Discussion

4.3.1 Synthetic Considerations

Numerous synthetic methodologies have been employed in the synthesis of ruthenium complexes containing hydroquinone or catechol moieties. In 2000, for example, Spyroudis published a complete exegesis on the various methods developed for the synthesis of hydroquinone and related complexes. [46] A number of complexes similar to those cited in this chapter have also been described previously. [42][43] Various methods of synthesis may be employed in the formulation of such complexes. Vos and co-workers for example, have prepared these complexes in two discrete manners. The initial approach was via the direct preparation of the dihydroxy-containing ligands followed by complexation to the ruthenium centre(s). [35][37][42][43] Weldon *et al.* for example, prepared a hydroquinone-containing ligand (*figure 4.6*), which was then coordinated to yield the dinuclear ruthenium complex. [42] However, although this approach did successfully yield the required complexes, there are a number of disadvantages to this technique including complicated semi-preparative HPLC purification requirements and hence reduced product yields. [47]

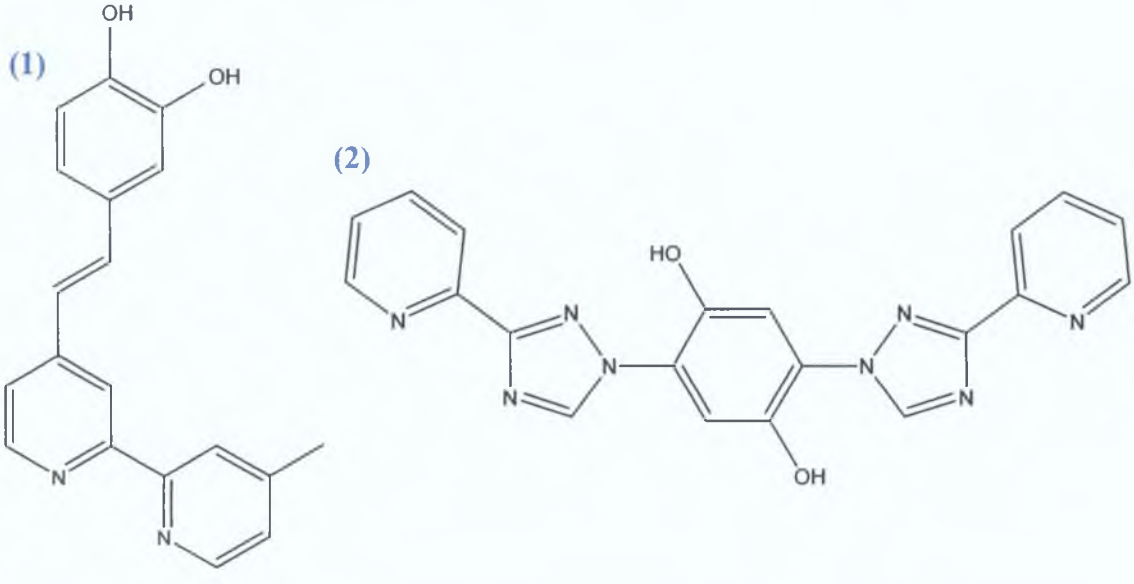

Figure 4.6 Structure of (1) the catechol-containing ligand synthesised by Shukla *et al.* and (2) the hydroquinone-containing ligand synthesised by Weldon *et al.* [42][48]

A similar but alternative approach to the synthesis of such complexes is to deprotect a methylated ligand prior to its coordination to a metal centre.

Sauvage[50] and Ward[32][48][49] and co-workers for example, adopted such an approach and they created their hydroquinone-containing complexes by first deprotecting the dimethoxy ligand with molten pyridinium chloride followed by the subsequent coordination to the metal. This approach, however, does not solve the problem of yields and purification difficulties. Hence, a novel approach to the complexes was developed which involved the conversion of the methylated complex to the analogous hydroquinone-containing complex subsequent to complexation. [45] This has a number of benefits including more facile purification techniques and greater overall yields coupled to the advantage of having the analogous deprotected complexes for comparison purposes. [47]

The oxidation of p-dimethoxybenzene derivatives to the corresponding hydroquinone has been accomplished using a variety of oxidising agents particularly nitric acid and argentic oxide. [51-53] Iodotrimethylsilane has also been suggested as a possible demethylating agent, however, varying degrees of success has been reported for ruthenium polypyridyl complexes. [54] A rather more successful method for the deprotection of such species, however, has been extensively reported via the utilisation of boron tribromide. [46] A number of authors including Ward, Yellowlees and Vos and co-workers have, therefore, utilised this agent for the deprotection of methylated species in order to obtain their target hydroquinones (or catechols). [24][55][45][56][57][58][59]

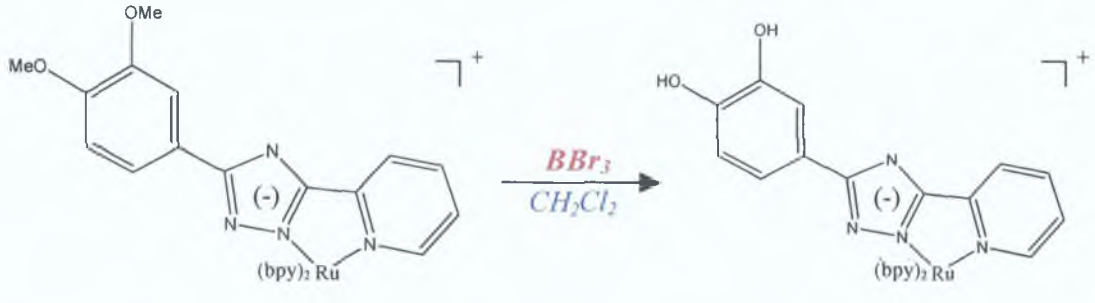

Figure 4.7 Demethylation process utilised by O'Brien *et al.* for the preparation of catechol complexes. [45]

Lehn and co-workers, in their paper on the preparation of an electro-photoswitch discussed in the introductory section, demethylated their dimethoxy-containing ruthenium complex with boron tribromide. [60] O'Brien *et al.* also obtained their catechol-containing complexes with boron tribromide as shown in *figure 4.7*.

As this BBr_3 method was found to generate good product yields and no further purification techniques were required with this methodology. Hence, it was employed in the synthesis of the complexes presented in this chapter. [45] It must be noted, that there are number of factors which must be taken into consideration for this procedure. BBr_3 is a fairly noxious agent and was obtained as a solution in dichloromethane in an airtight container and stored under a blanket of argon. This is due to its propensity to rapidly hydrolyse upon contact with air.

In this case the moisture in the air causes it to fume vigorously and release heat with a concomitant change in the colour of the solution from a clear liquid to a muddy brown colour as it hydrolyses to boric acid. Even under the best storage conditions this solution is generally partially hydrolysised and hence, light brown in colour upon syringing into the experimental flask. For this reason a ten-fold excess of BBr_3 was used. This excess coupled with longer reaction times than previously reported ensured complete demethylation to the required product. Careful handling and storage of this hazardous solution was, therefore, also implemented. Furthermore, all glassware and the dichloromethane solvent employed during the synthesis were dry and the reaction was carried out under a constant flow of nitrogen. To ensure that the reaction flask was maintained at a constant temperature of approximately $-80^{o}C$, an acetone / liquid nitrogen cryostatic ice bath was utilised. When the reaction had reached completion it was quenched with water with the subsequent formation of HBr. The acidity of the solution was then dissipated by the addition of the alkaline sodium carbonate solution. This process of neutralisation was performed with care with the intention that the solution was not over acidified ($pH > 9$), which would lead to the production of irreversible semiquinone species. The overall reaction was also accompanied by a colour change in which the initial strong burgundy colour of the starting complex developed to yield the strong red colour of the hydroxylated product. Upon neutralisation some precipitate was observed to form, however, further precipitation was achieved by adding a small quantity of NH_4PF_6. The target complex was then successfully obtained after recrystallisation from a 2:1 solution of hot ethanol/water. No further purification was required and the purity of the complex was confirmed via the following characterisation data.

4.3.2 Characterisation Considerations

^{1}H-NMR spectroscopy was utilised in the assessment of the purity and structural assignment of the complexes presented in this chapter. *Table 4.1* contains the NMR data for the coordinated ligands in each complex while the proton NMR spectrum of the complex $[Ru(bpy)_2(L9)Ru(bpy)_2](PF_6)_2.4H_2O$ in d_3-acetonitrile and of the same complex in d_3-acetonitrile with 1 drop of D_2O are shown in *figure 4.5*. These spectral tools along with the spectra obtained for the previous methoxy complexes allowed for successful elucidation of the structure of these hydroxylated complexes. COSY spectral data were also obtained to further support these assignments for each complex and supplementary data are provided in *appendix A*. The ^{1}H-NMR spectrum of $[Ru(bpy)_2(L9)Ru(bpy)_2](PF_6)_2.4H_2O$ is shown in *figure 4.5* and is typical of the spectra obtained for these hydroxylated complexes. The spectra are clean and well resolved and integrate to the expected number of protons and are, therefore, consistent with the expected structure. Sharp, well-defined reasonances were observed for all complexes, confirming the presence of Ru^{II} and the absence of semiquinone radicals. [35]

Reasonances for coordinated ligands L7-L10

(chemical shifts / ppm vs Me_4Si)

	7	*8*	*9*	*10*
$H^{3'}$	7.66(d)	7.30(d)	7.39(s)	7.42(s)
$H^{5'}$	6.63(m)	6.62(m)		
$H^{6'}$	6.55(d)	6.64(d)	7.39(s)	7.42(s)
$H^{3'''}$	8.12(d)	9.20(s)	8.22(d)	9.34(s)
$H^{4'''}$	7.90(dd)		7.83(dd)	
$H^{5'''}$	7.21(dd)	7.60(d)	7.21(dd)	7.68(d)
$H^{6'''}$	7.55(d)	8.20(d)	7.57(d)	8.29(d)
-OH	10.66	10.68	10.65	10.64

* For an explanation of proton numbering refer to *figure 4.5*.

Bipyridyl reasonances were observed in the following regions for:

[1] *Pyridyltriazole complexes*: 8.30-8.90(**H**^{3}); 7.90-8.20(**H**^{4}); 7.20-7.35(**H**^{5}); 7.40-7.60(**H**^{6}).

[2] *Pyrazyltriazole complexes*: 8.38-8.55(**H**^{3}); 7.80-8.15(**H**^{4}); 7.25-7.45(**H**^{5} / **H**^{6}).

Table 4.1 ^{1}H-NMR data for complexes 7 – 10 measured in d_3-acetonitrile

In the previous chapter it was seen that in the spectra of the protected complexes the –OMe reasonances were observed in the ^{1}H-NMR spectra of the mononuclear complexes as two identifiable –OMe peaks and as strong singlets in the dinuclear complexes in the region between 3 50 and 4 00 ppm As complexes *7-10* differ only from complexes *3-6* by the replacement of the -OMe groups by –OH moieties then these peaks must necessarily be absent from the spectra of the demethoxylated complexes Indeed, no peaks were observed in the aliphatic region of any of the –OH containing complexes This is comparable to the NMR data reported by Shukla *et al* who also noted that for their dimethoxy complexes the two methyl groups of the dimethoxyphenyl at 3 84 and 3 88 ppm are absent in the spectrum of dihydroxy complex (*figure 4 6*) [21]

Furthermore, the presence of an additional peak associated with the –OH group was observed in the spectra of complexes 7-10 above 10 50 ppm The –OH nature of this peak was further verified by the addition of 1 drop of D_2O which resulted in the loss of this broad peak This is due to the lability of the –OH proton which readily exchanges with labile deuterons from the solvent effectively removing them from the spectra Furthermore, the fact that the –OH proton is shifted significantly downfield (e g to approximately 10 65 ppm m the case of $[Ru(bpy)_2(L9)Ru(bpy)_2](PF_6)_2$ $4H_2O$ presented in *figure 4 5*) suggests the presence of an intramolecular hydrogen bond between the uncoordinated -OH and the adjacent triazole The result is not unexpected as various studies have reported evidence for the presence of intermolecular hydrogen bonding involving the hydroxyl groups and the free N atoms of the triazole rings in similar ruthenium(II)-polypyridyl complexes containing triazole ligands with phenol or hydroquinone moieties [35][43][61]

Finally, it can be seen by comparison of the proton reasonances for the protected complexes in *chapter three* and the deprotected complexes reported here, that there are small but significant changes in the position of these resonances Firstly, the upfield shift of the H^6 proton which was noted in the spectra of the dimethoxy-containing complexes and was attributed to diamagnetic anisotropic interaction of the H^6 proton with the adjacent rings of the bipyridine is, unsurprisingly, again noted in the spectra of these hydroquinone complexes [34]

This further confirms that the ^{1}H-NMR spectral reasonances alter very little upon demethylation, a fact previously noted by both Shukla *et al.* and O'Brien *et al.* upon demethylation of their dimethoxy complexes (*figure 4.6 / 4.7*). Secondly, it may be seen that for the hydroquinone complexes the proton reasonances of the coordinated ligand are shifted to higher field by approximately 0.1 to 0.2 ppm compared to the methoxy analogues. This is particularly evident in the case of the phenyl protons. This is a similar observation as was noted in the case of comparable catecholate complexes reported by O'Brien *et al.* and once again, provides further confirmation of the loss of the methoxy moieties. [45] A comparison of the protons shifts in the NMR spectra of these complexes compared to the methoxy and quinone analogues can be found in *figure 5.11* in *chapter five* and in *appendix A*.

4.3.3 Computational Results

The computational chemistry program Gaussian 03 was used to carry out density functional theory (DFT) calculations on the complex $[Ru(bpy)_2(L7)]^+$.[62] These calculations were performed by my colleague Dr. Noel O'Boyle. Gausssum 0.6 was also used to performed calculations on the contributions of different groups to each molecular orbital. [63] The initial structure for the geometry optimisation was taken from crystallographic data previously obtained for this complex. [44]

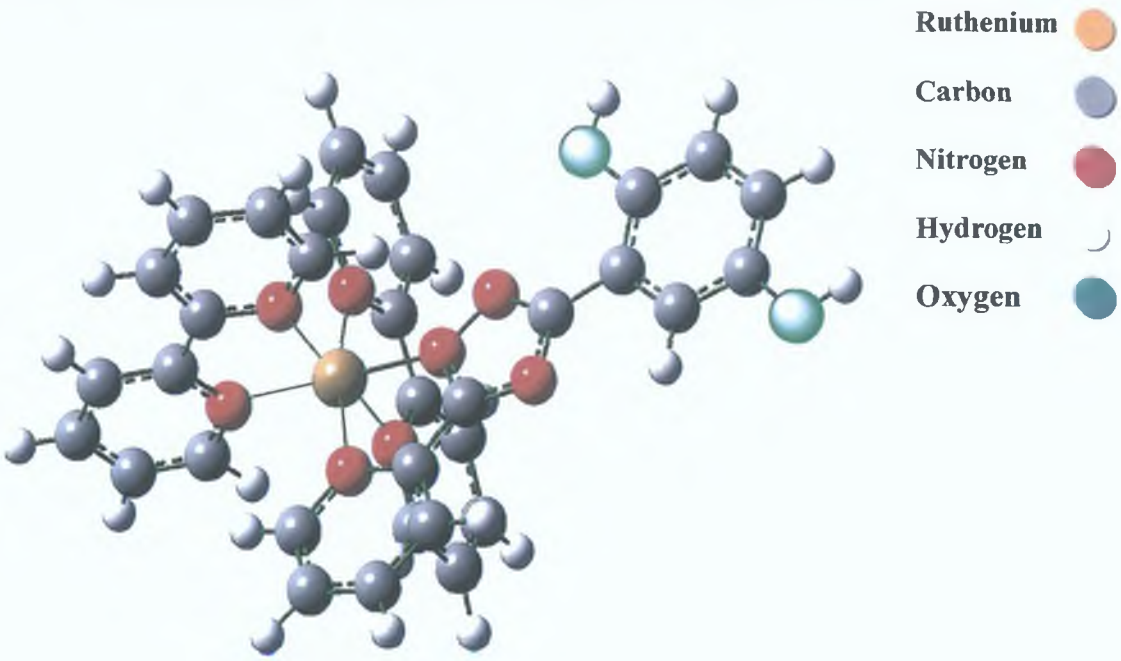

Figure 4.8 Geometry-optimised molecular structure of $[Ru(bpy)_2(L7)]^+$.

The optimised geometry is shown in *Figure 4.8*. The image is intended to provide an optical aid to the reader in the visualisation of the molecule being discussed and hence, helps in the elucidation of the following characterisation data. It, therefore, complements the following experimental data rather than replacing it.

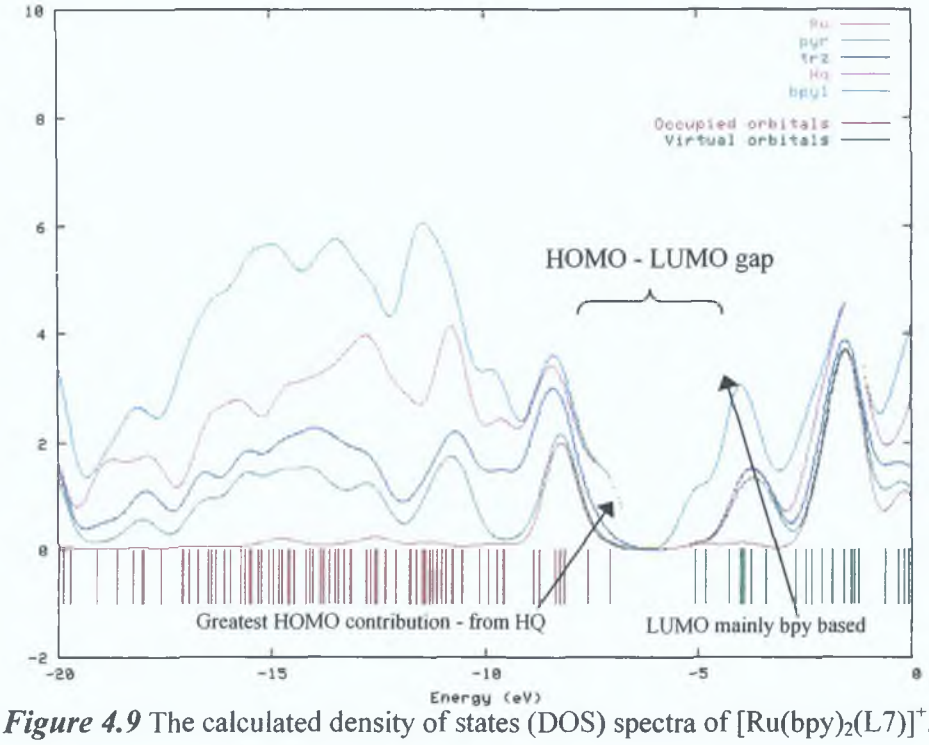

Figure 4.9 The calculated density of states (DOS) spectra of $[Ru(bpy)_2(L7)]^+$.

Figure 4.9 above was then created which shows the calculated density of states (DOS) spectra of this complex. The groups used are labelled in *Figure 4.9* as follows: HQ, hydroquinone moiety; Ru, the ruthenium metal atom; pyr, pyridine group; trz, the triazole ring; bpy 1 and bpy 2, the two bipyridyl ligands. Calculated DOS spectra have been shown to be a useful visualization method for the spatial distribution of the electronic structure of complexes. [64] In particular, where there are several close-lying energy levels in the frontier region, DOS spectra give a better picture of the contributions of the various moieties to the HOMO and LUMO, compared to the examination of individual energy levels. [45] Across the bottom of the graph are a series of brown and green lines that are representative of the closely spaced molecular orbitals of the complex. The 'gap' in the orbitals occurs between the HOMO and the LUMO state. Each line on the upper part of the graph illustrates the contribution of each moiety to the molecular orbitals in a particular energy region.

LUMO + 2	*LUMO + 1*
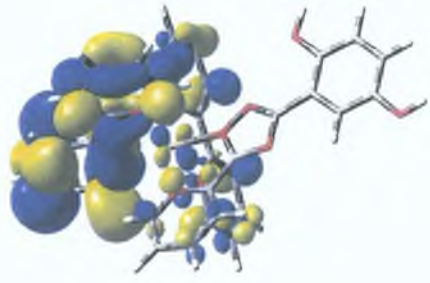	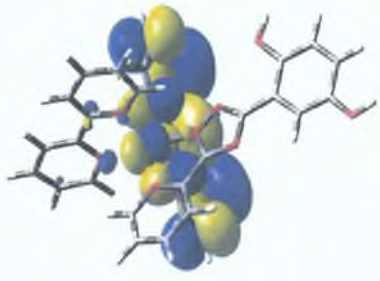
LUMO	*HOMO*
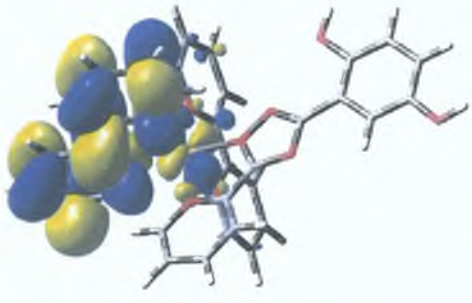	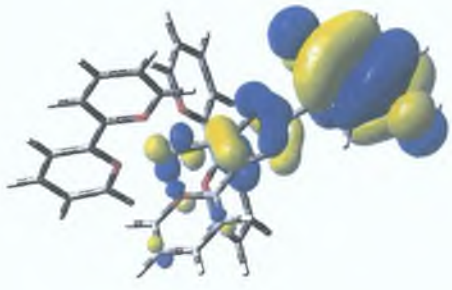
HOMO - 1	*HOMO - 2*
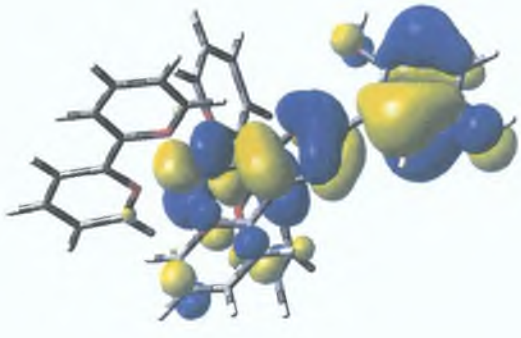	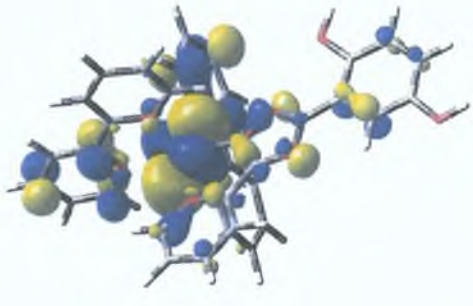
HOMO - 3	*HOMO - 4*
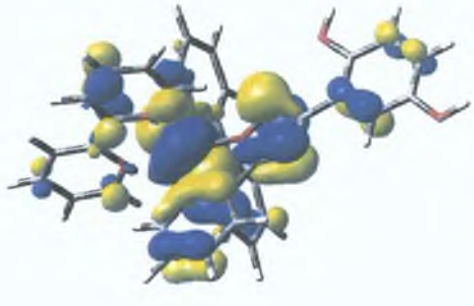	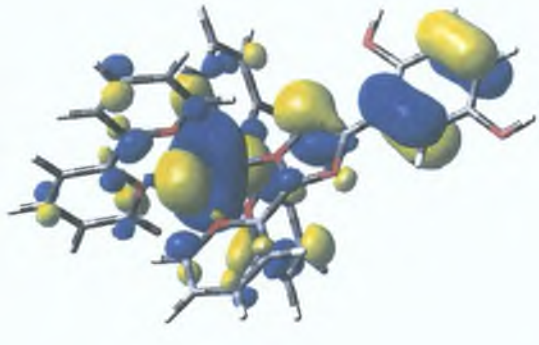

Table 4.2 Calculated isosurface images of the frontier orbitals of $[Ru(bpy)_2(L7)]^+$.

From *figure 4 9* it can be seen that in the HOMO region, there is a large contribution from the hydroquinone moiety of the pyridyltriazole ligand, and at slightly lower energy, a significant metal-based contribution from the ruthenium There is also a significant contribution from the triazole moiety of pyridyltriazole to the HOMO region at lower energy Very little bipyridyl donation is observed in this region Conversely the LUMO region is strongly bipyridyl in character At slightly higher energy, there is a roughly equal contribution to the LUMO region from the pyridyl moiety of the pyridyltriazole ligand In this region, there is little or no metal contribution

The electronic structures of the HOMO and LUMOs of $[Ru(bpy)_2(L7)]^+$ were then generated and are contained in *table 4 2* The table contains isosurface visual representations of the graphical data in *figure 4 9* The first images, therefore, show the ***LUMO + 2***, ***LUMO + 1*** and the ***LUMO*** states Upon an examination of these diagrams it is, once again, clear that the LUMO is strongly bipyridyl based For example, the ***LUMO*** state is concentrated on the first bipyridyl moiety while the ***LUMO + 1*** is found mainly on the second of the bipyridyl moieties This is due to the fact that the two bipyridyl moieties differ slightly in energy with one having slightly higher energy than the other (*figure 4 9*) The subsequent diagrams show the HOMO states It is now clear that the pyridyltriazole moieties, specifically the hydroquinone group, play a very large role in the HOMO of this complex For example, in the ***HOMO*** diagram there is a strong concentration on the hydroquinone moiety The ***HOMO – 1*** also appears to be strongly hydroquinone influenced while the HOMO then appears to deviate towards a more metal based character as we progress to ***HOMO - 3 and HOMO – 4*** The bipyridyl moieties also appear to have no significant role in these HOMO states (*table 4 2*) The computer-generated data provide a useful theoretical basis for the following experimental characterisations

4 3 4 Electronic and Photophysical Properties

4 3 4 1 Absorption Spectra

The UV/Vis spectra discussed in this chapter were recorded in acetonitrile and the absorption data for all of the mononuclear and dinuclear complexes in both their protonated and deprotonated forms are recorded in *table 4 3*

In the previous chapter it was noted that the electronic spectra of the dimethoxy-containing were similar to the spectra obtained for a plethora of ruthenium (II) complexes. Once again, the absorption spectra obtained for the hydroquinone-containing complexes presented in this chapter are comparable with the prototypical $[Ru(bpy)_3]^{2+}$ [27] and demethylation of the dimethoxy groups has no significant effect on the spectrum. This was also the case in studies of comparable complexes, for example Shukla *et al.*, who also reported little change in the absorption spectra upon demethylation of their hydroquinone complex (*figure 4.6*). [48]

Table 4.3 Absorption and emission data obtained for the complexes. Unless otherwise stated, all measurements were performed in acetonitrile.

Complex	λ_{max}[a] (nm) (ε x10^{-4})	E.Quantum Yield (Φ)	E_{max} 298K[b] (nm) τ (ns)	E_{max} 77K (nm) τ (μs)
$[Ru(bpy)_2(L7)]^+$	476 (1.10)	0.0052	675 (166)	612 (2.8)
$[Ru(bpy)_2(HL7)]^{2+}$	438 (1.32)	-	612 (<20)	580 (5.5)
$[Ru(bpy)_2(L8)]^+$	452 (1.51)	0.0054	660 (165)	612 (3.7)
$[Ru(bpy)_2(HL8)]^{2+}$	441 (1.59)	-	667 (240)	617 (7.5)
$[Ru(bpy)_2(L9)Ru(bpy)_2]^{2+}$	474 (2.82)	0.0047	677 (151)	613 (2.7)
$[Ru(bpy)_2(H_2L9)Ru(bpy)_2]^{4+}$	436 (2.96)	-	614 (<20)	582 (5.2)
$[Ru(bpy)_2(L10)Ru(bpy)_2]^{2+}$	451 (2.30)	0.0051	661 (156)	612 (3.6)
$[Ru(bpy)_2(H_2L10)Ru(bpy)_2]^{4+}$	440 (2.71)	-	670 (232)	618 (6.6)

[a] Protonation of the complexes achieved by addition of perchloric acid.

[b] Data at 77 K were recorded in EtOH/MeOH (4:1 v/v).

Hence, the spectra of the complexes contained in this chapter are dominated in the visible region between 450 nm – 480 nm by a $d\pi$-π^* metal-to-ligand charge transfer (MLCT) transition. The MLCT bands observed also exhibit a low energy shoulder at the λ_{max} characteristic of 1,2,4-triazole systems. [42]

These transitions are typical of these types of complexes and were also seen in the previous chapter. [27] Intense π-π^* transitions were also observed in the UV region at approximately 280 nm, which are associated with the pyridyltriazole or the pyrazyltriazole and the bipyridyl ligands, respectively. There are also features in the absorption spectra around 330-350 nm which are associated with π-π^* transitions in the hydroquinone moieties. These absorptions have been noted previously in similar complexes containing hydroquinone moieties. [35][42][43] Typical absorption spectra obtained for these hydroquinone-containing complexes are shown in *figure 4.10*. This shows the spectra of the ruthenium pyridyltriazole and pyrazyltriazole complexes $[Ru(bpy)_2(L7)]^+$ and $[Ru(bpy)_2(L8)]^+$. It can be seen from an examination of these spectra that the MLCT of these complexes occur at 476 nm and 452 nm, respectively. There is a slight shift in the λ_{max} of the hydroquinone complexes compared to the methylated analogues. For example, $[Ru(bpy)_2(L7)]^+$ now has a λ_{max} of 476 nm compared to its methylated counterpart $[Ru(bpy)_2(L3)]^+$ which imparted a λ_{max} of 485 nm. (For a comparison of the UV spectra of the dimethoxy, dihydroxy and quinone complexes see *figure 5.14, chapter five*.)

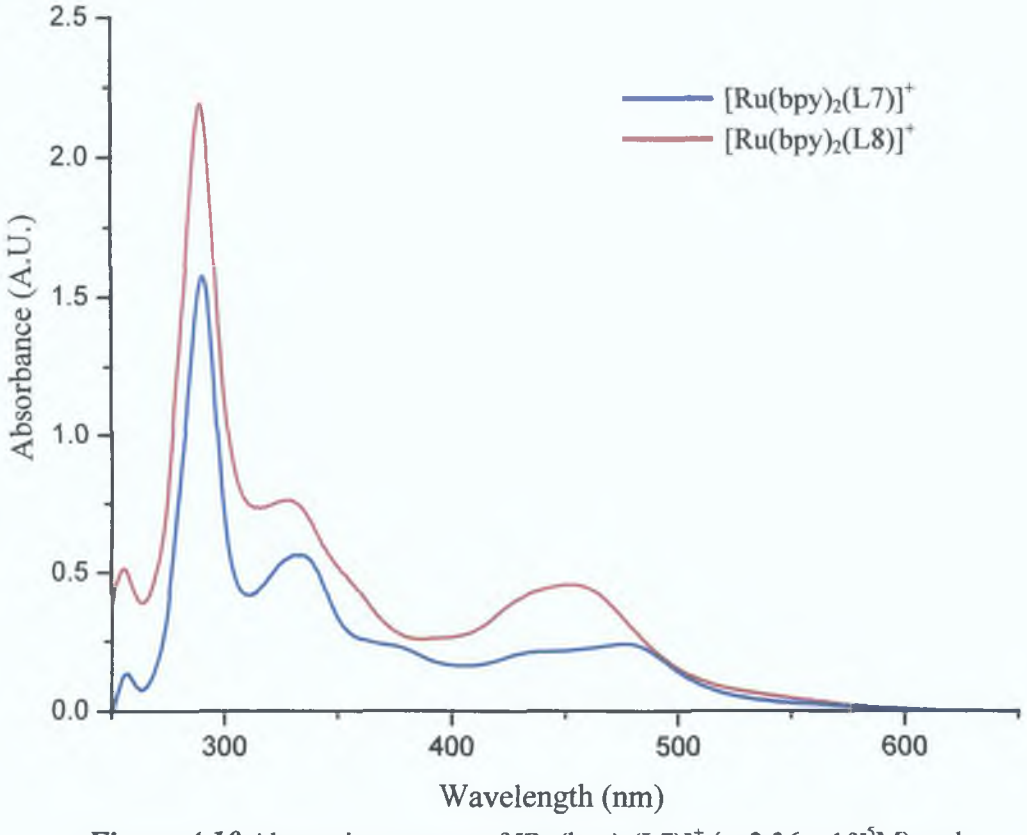

Figure 4.10 Absorption spectra of $[Ru(bpy)_2(L7)]^+$ (c. 2.36 x 10^{-5}M) and $[Ru(bpy)_2(L8)]^+$ (3.02 x 10^{-5}M) in neutral acetonitrile at room temperature.

This shift (circa 5 nm) can contributed to the loss of the more strongly electron donating methoxy substituent [65] The shifts in the pyrazyltriazole complexes are slightly less and are possibly due to the counteraction of the pyrazine's strong π-acceptor properties compared to pyridine [66] The data obtained for these complexes are comparable to similar hydroquinone / phenol or catechol-containing complexes [43][45] For example, *figures 4 11* and *4 7* contain pyridyltriazole ligands with catechol or phenol moieties which were used in the synthesis of similar ruthenium polypyridyl complexes [45][61] The complexes containing the ligands shown in *figure 4 11* and *4 7* reported similar absorption spectra as the pyridyltriazole complexes reported in this chapter with λ_{max} centred at 476 nm and 481 nm, respectively [61][67] Similarly, the ruthenium complex containing the pyrazyltriazole analogue of the ligand in *figure 4 11* also reported a λ_{max} at 455 nm, which is comparable to the values obtained for the pyrazyltriazole complexes listed in *table 4 3* [67] It was also noted in the previous chapter that the MLCT of the methylated analogues are red-shifted with respect to $[Ru(bpy)_3]^{2+}$ [68] This red shift is again noted in the spectra of the hydroquinone complexes (to a lesser extent in the case of the pyrazyltriazole complexes) and is attributable to the strong σ-donation of the deprotonated pyridyltriazole or pyrazyltriazole moiety (*table 4 3*)

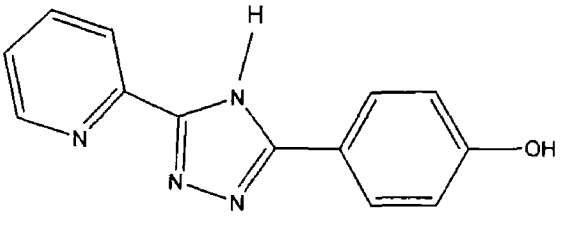

Figure 4 11 Ligand contained in the ruthenium complexes synthesised by Hage *et al* [61]

For example, from an examination of the data in *table 4 3* it can be seen that the pyridyltriazole complexes manifest a shift of approximately 25 nm to a lower energy This shift was also observed in the spectra of other similar ruthenium complexes containing dihydroxy moieties [45][48]

The pyrazyltriazole complexes, however, undergo a significantly smaller shift than the pyridyl analogues as the pyrazine has increased π-acceptor properties (*table 4.3*). These strong π-acceptor properties, however, are negated by the presence of the triazole moiety and hence, only a slight shift in MLCT occurs. This phenomenon has also been noted previously in the case of the analogous pyrazyltriazole version ligand depicted in *figure 4.11*. [67]

The deprotonated status of the triazole ring in these complexes is supported by the λ_{max} value of the lowest energy ^{1}MLCT transition, for example, 476 nm in the case of the mononuclear pyridyltriazole complex. The presence of the triazole ring in these complexes means that they have the ability to be protonated, which resulted in a blue shift of the λ_{max} of the complexes (*table 4.3*). [69][70][71]

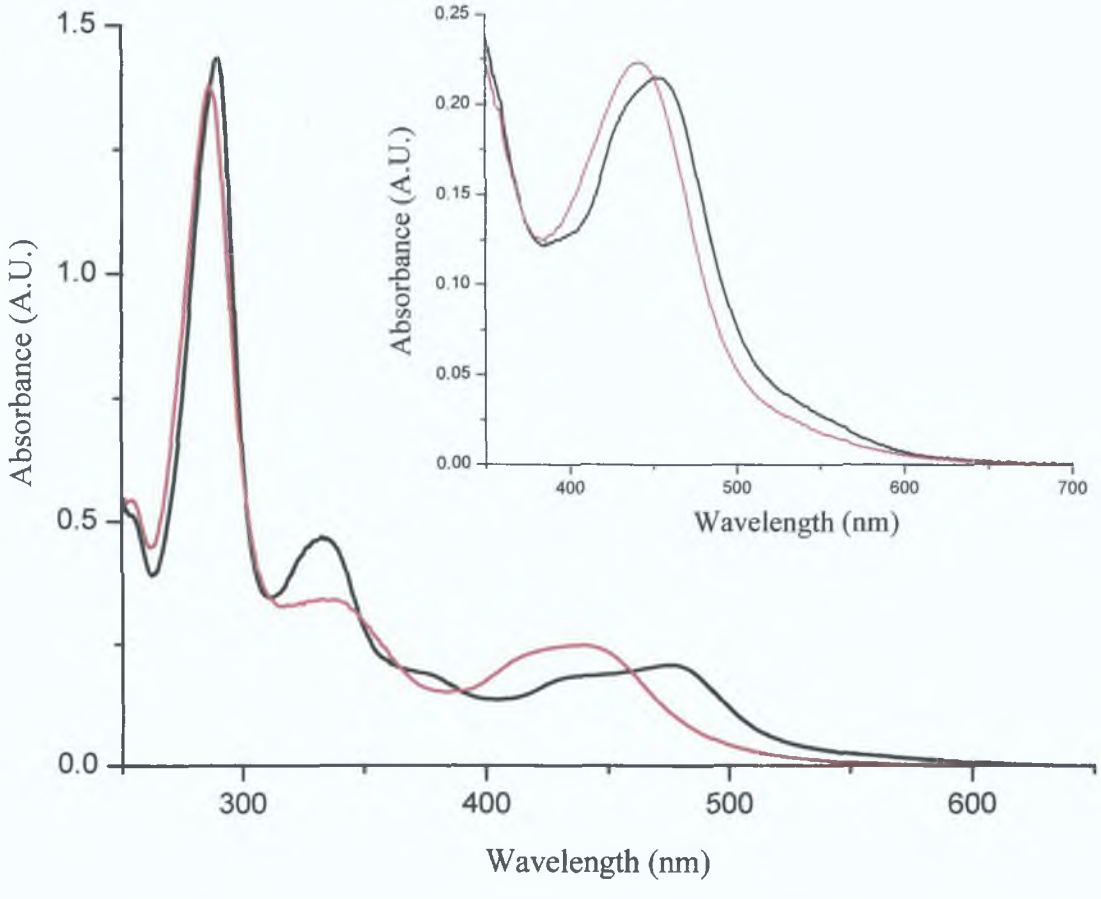

Figure 4.12 Absorption spectra of $[Ru(bpy)_2(L7)]^+$ in neutral acetonitrile (**black line**) and after the addition of 1 drop of trifluoroacetic acid (red line) and (*Inset*) $[Ru(bpy)_2(L8)]^{2+}$ in neutral acetonitrile (**black line**) and after the addition of 1 drop of TFA (red line)

When the triazole was protonated by the addition of acid the absorption spectra of both the pyridyltriazole and pyrazyltriazole complexes are seen to undergo a shift of the MLCT band as the σ-donor properties of the triazole ring are lessened This transformation can be observed in the absorption spectrum of $[Ru(bpy)_2(L7)]^+$ and $[Ru(bpy)_2(L8)]^+$ which are shown in *figure 4 12* in neutral acetonitrile and after the addition of 1 drop of acid The protonated pyridyltriazole complexes experience a blue shift of the absorption band by approximately 35 nm accompanied by a concomitant increase in the extinction coefficient (*figure 4 12*) However, in the case of the pyrazyltriazole complexes the presence of the π-acceptor pyrazine moiety again results in a less pronounced shift of λ_{max} (by approximately 10 nm) This shift upon protonation was observed for all these complexes and has also been reported previously for similar dihydroxy-containing complexes [45][61][67]

In the case of the hydroquinone complexes, however, there is now also a simultaneous decrease in the bands associated with the hydroquinone moieties (circa 330 nm) Since, these changes are not totally reversible upon addition of a drop of base, it is likely that they are associated with the formation of semiquinone species These species may then in turn undergo disproportionation to form a mixture of hydroquinone and quinone species [72] This phenomenon was proposed previously for similar hydroquinone complexes and this will be explored in more detail in the following chapter, which contains the quinone analogues [42]

It is also of interest to note that there is no real difference between the behaviour noted for the mononuclear and that observed for the dinuclear complexes in both their protonated and deprotonated forms This would seem to indicate that there is very little, if any, interaction between the metal centres This was also noted in the case of the methoxy-containing analogues, indicating that the replacement of the dimethoxy moieties by dihydroxy groups does not invoke a change in the level of communication between the metal centres This phenomenon, however, will be explored in more detail in the following sections

4.3.4.2 Luminescence Properties

The luminescence data for the hydroquinone complexes discussed in the chapter are presented in *table 4.3*. Room temperature measurements were performed in neutral acetonitrile while measurements at 77 K were undertaken in an ethanol-methanol solution. In both cases protonation was achieved by the addition of 1 drop of trifluoroacetic acid. In the case of each of the complexes measured the emission was much weaker than that of $[Ru(bpy)_3]^{2+}$ (Φ = 0.062), however, the luminescence is quite clear and is characteristic of emission from the lowest ^{3}MLCT ($d\pi$ Ru → π^* bpy) excited state (*figure 4.13*).[73] This mirrors the luminescence data obtained by Schanze and Sauer[55] and Shukla *et al.* [48] who also reported this decreased emission from the ^{3}MLCT excited state for their dihydroxy complexes. There is also a similar distinct red-shift of emission in these complexes compared to $[Ru(bpy)_3]^{2+}$ due to the effect of the triazole ring whose negative charge increases electron density on the metal centre and reduces the t_2g - MLCT energy gap. [74]

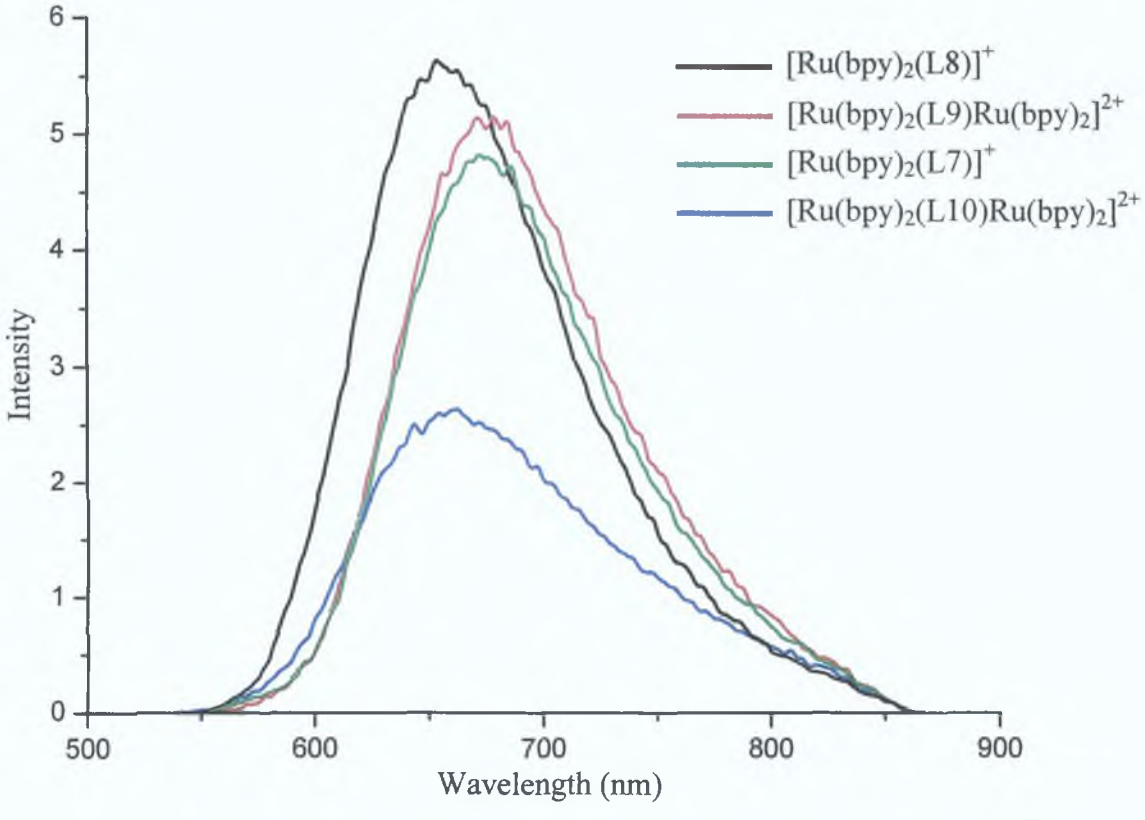

Figure 4.13 Emission Spectra of $[Ru(bpy)_2(L7)]^+$ (conc. 2.36 x 10^{-5}M), $[Ru(bpy)_2(L8)]^+$ (conc. 3.02 x 10^{-5}M), $[Ru(bpy)_2(L9)Ru(bpy)_2]^{2+}$ (conc. 2.11 x 10^{-5}M) and $[Ru(bpy)_2(L10)Ru(bpy)_2]^{2+}$ (conc. 1.51 x 10^{-5}M) in acetonitrile at room temperature

Figure 4 13 contains the emission spectra of both the mononuclear and dinuclear pyrazyltriazole and pyridyltriazole complexes in neutral acetonitrile at room temperature The pyridyltriazole complexes have emission maxima centred at around 676 nm These values differ very little from the data obtained for the dimethoxy analogues in *chapter three* However, slight changes in the emission values of the deprotected complexes compared to the protected analogues may, once again, be attributed to the replacement of the –OMe groups by the less strongly electron electron donating –OH substituents [65]

In previous studies involving ruthenium complexes with hydroquinone moieties some quenching of emission was observed which was associated with the hydroxy moiety(ies) [75] However, generally in these studies the hydroquinone moiety was in close proximity to the metal centre i e attached via the polypyridyl moieties [55][75] In the case of the hydroquinone complexes presented in this chapter there is no such decrease in the emission of the demethylated complexes (*table 4 3*) This may be attributed to the insulating effect of the triazole ring, which is incorporated into the pyridyl or pyrazyl ligands and weakens direct electronic coupling between the electron donating hydroquinone group and the ruthenium sensitiser [76] Previous studies involving similar complexes such as, the ruthenium complex containing the catechol shown in *figure 4 7* also reported little obvious quenching of luminescence upon demethylation [45] This was further confirmed by the lifetime data (see *table 4 3* and *table 3 2*)

This illustrates the fact that demethylation has no significant effect on the spectrum and the slight shift noted in the specta upon demethylation (approximately 10 nm) arises only as a result of the decreased electron donating effect of the hydroquinone moiety compared to the –OMe group [21][65][77] Once again, this was the same behaviour as noted by Shukla *et al* (*figure 4 6*) and O'Brien *et al* (*figure 4 7*) for their dihydroxy-containing complexes [21][45] Correspondingly, the pyrazyltriazole type complexes were observed to emit at approximately 660 nm Once again, the emission spectra are comparable to their methoxylated analogues [21][65][77]

These data are comparable to the data achieved for the ruthenium complex containing the pyrazyltriazole ligand analogue of *figure 4.11*. [67]

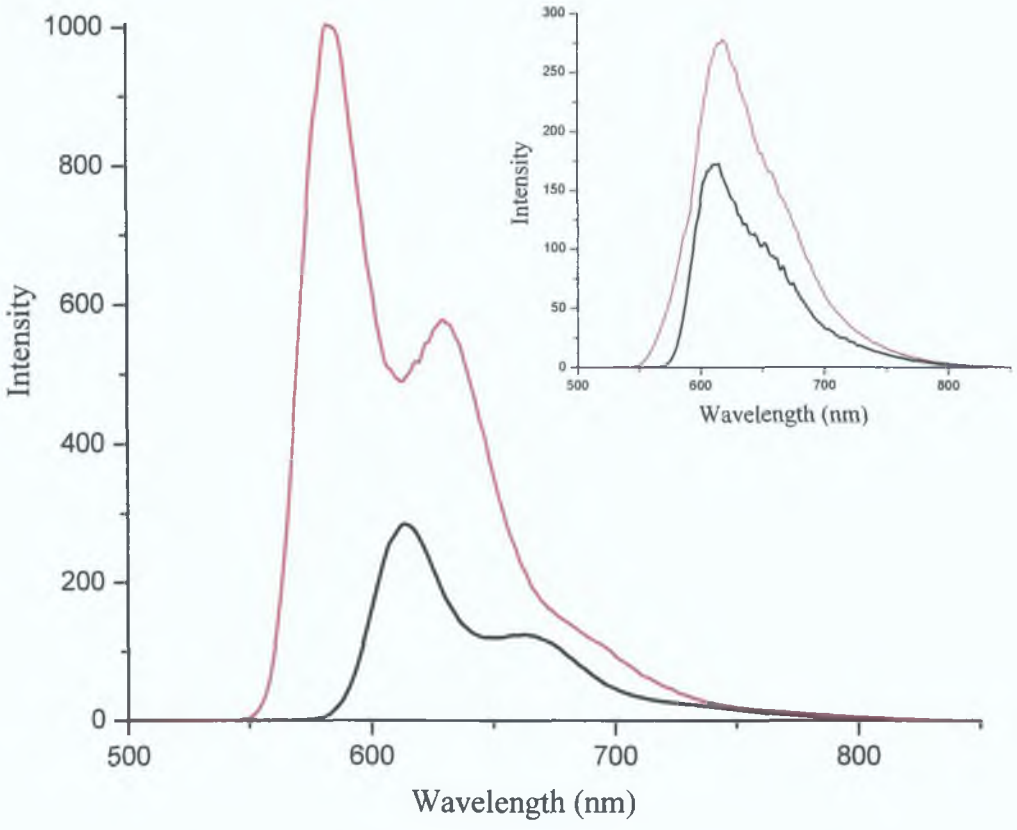

Figure 4.14 Emission spectra of $[Ru(bpy)_2(L9)Ru(bpy)_2]^{2+}$ in EtOH/MeOH at 77 K (**black line**) and after the addition of 1 drop of acid at 77 K (**red line**) and (*Inset*) spectra of $[Ru(bpy)_2(L10)Ru(bpy)_2]^{2+}$ in EtOH/MeOH at 77 K (**black line**) and after the addition of 1 drop of acid at 77 K (**red line**).

The complexes were protonated via the addition of 1 drop of trifluoroacetic acid in order to obtain the protonated room temperature and 77 K results contained in *table 4.3*. The low temperature emission spectra of $[Ru(bpy)_2(L9)Ru(bpy)_2]^{2+}$ and $[Ru(bpy)_2(L10)Ru(bpy)_2]^{2+}$ and their protonated data are shown in *figure 4.14*. Protonation of the hydroquinone complexes results in similar behaviour as noted in the case of the protected analogues. For example, the pyridyl based complexes containing the ligand depicted in *figure 4.11* and the complex in *figure 4.7* shift by approximately 65 nm upon protonation (at room temperature). [45][61] However, as observed for the protected analogues in the previous chapter, this shift is also accompanied by a decrease in the emission intensity of the pyridyltriazole complexes.

This decrease has been noted previously for similar pyridyltriazole-hydroquinone-containing complexes and is associated with the lower σ-donation ability of the ligand causing a decrease in the ligand field splitting and hence, increased thermal population of the ^{3}MC and hence, faster radiationless decay [43] The pyrazyltriazole complexes shift to a reduced energy (circa 8 nm) upon protonation and do not display the same loss of emission intensity as the pyridyltriazole complexes Again this is analogous to the behaviour noted in *chapter three* for the protected pyrazyltriazole complexes and for similar pyrazyltriazole complexes studied previously [78][66] The phenomenon was explored further in the lifetime section and in the spectra obtained at low temperatures

The emission spectra of the complexes at 77 K appear different to the room temperature spectra due to the emergence of the vibrational structure coupled to an increase in intensity caused by the rigid matrix created within the solid environs of the EtOH/MeOH alcoholic glass, as this environment somewhat hinders the excited state This was seen previously in the case of the protected complexes and may, once again, be attributed to solvent rigidchomism and the fact that the strongly deactivating ^{3}MC level is inaccessible at lower temperatures (*figure 4 14*) [79] At this decreased temperatures the pyridyltriazole complexes are, once again, seen to blue shift upon protonation by approximately 30 nm However, at these lower temperatures there is a decreased in the availability of the thermally accessed ^{3}MC Hence, the decrease in the emission intensity witnessed at room temperature is no longer apparent and instead the intensity increases as observed for the protected analogues (*figure 4 14*) Once again, this behaviour has been observed previously for similar hydroquinone-containing complexes [43] The pyrazyltriazole complexes again display similar behaviour to that of their methylated analogues They do not undergo as pronounced a shift as the pyridyltriazole complexes (circa 5 nm) Furthermore, this shift is to a lower energy and is accompanied by an increase in the emission intensity This shift occurs due to switching of the excited state upon protonation as described previously (*figure 4 14*) *Table 4 3* contains lifetime data at room temperature and at 77 K and in neutral and protonated media, which were obtained for the hydroquinone complexes presented in this chapter

All samples were freeze-pump-thawed prior to obtaining a measurement in order to achieve accurate results and to negate the effects of oxygen within the system These results are particularly interesting as the presence of the –OH moieties may have been expected to quench the lifetime of the excited state as this was observed to occur in a number of hydroxy-containing complexes [75][60] For example, Lehn and co-workers found that the lifetime of their ruthenium hydroquinone complex was found to be 0 98 μs compared to 1 08 μs for the analogous –OMe complex They attributed this slightly shorter lifetime to inefficient intramolecular electron transfer from the hydroqumone unit toward the triplet state of the chromophore [60] However, in ruthenium hydroqumone complexes of the type discussed in this chapter, the presence of the triazole moiety seems to negate this electron transfer effect (see *tables 3 2* and *4 3*) The hydroquinone complexes presented in this chapter do not undergo any quenching of the excited state in agreement with similar triazolate complexes For example, Weldon *et al* reported a room temperature lifetime of 210 ns for their dinuclear hydroquinone-containing complex (the ligand contained in this complex is depicted in *figure 4 6*)

In fact, upon an examination of the lifetime data contained in *table 4 3*, it may be seen that the mononuclear and dinuclear complexes have relatively long-lived excited states compared to complexes containing neutral triazole ligands [71] For example, the lifetime of $[Ru(bpy)_2(L7)]^+$ was found to be 166 ns at room temperature compared to 110 ns for the analogous dimethoxy complex (*table 3 2*) This seems to suggest that the hydroquinone moiety plays a significant role in determining the excited state properties of these complexes [42]

The pyridyltriazole ligands are σ-donors and the excited state is expected to be located on the bipyridyl moiety rather than on the pyridyltriazole ligand From the previous UV/Vis and luminescence data it appears that this is also the location of the excited state when the triazole is protonated Indeed, when protonated the lifetimes of the pyridyltriazole complexes decrease so sharply (< 20 ns) that they were no longer measurable on the conventional laser set-up This was also the case for the analogous dimethoxy complexes

However, pyrazyltriazole complexes differ from the pyridyltriazole analogues as protonation of the triazole moiety causes the excited state to switch from bpy to the pyrazine moiety [76] This is reflected in the lifetime data, which unlike the pyridyltriazole complexes do not undergo a rapid decrease (*table 4 3*) Vos and co-workers reported a comparable result for the ruthenium complex containing the pyrazyltriazole analogue of *figure 4 11* [68] It was noted that for this complex the lifetime increased from 126 ns in neutral acetonitrile to 558 ns when protonated [67] This will, however, be further discussed in light of the acid-base properties of the complexes outlined in the following section Finally, at 77 K there is a considerable increase in the lifetimes of all of the complexes This was also reported previously for the analogous methoxylated complexes (*chapter three*)

4.4 Acid-Base Properties

The presence of the triazole moiety in these complexes has been shown to lend interesting characteristics to this group of compounds. This is particularly apparent in the case of the pyrazyltriazole complexes in which the location of the excited state has been shown to switch depending on the pH value of the solution.[80][81][82] The following pKa measurements were, hence, performed in order to ascertain the nature of the excited state in each of these complexes. It may, however, be recalled from the introduction that the behaviour of these hydroquinone-containing complexes is somewhat intricate in aqueous media. [20] Nonetheless, the following table 4.4 contains the pKa and pKa* values obtained in Britton-Robinson buffer. The data obtained during the course of these acid-base measurements are presented in the following section (*figure 4.15* and *figure 4.16*). Experimental conditions and errors are reported in *chapter two*. The pKa* value calculations were obtained as described previously in *section 3.3.3, chapter three*.

Complex	pKa	pHi	pKa*
$[Ru(bpy)_2(L7)]^+$	3.2	2.6	2.9 (4.2)
$[Ru(bpy)_2(L8)]^+$	2.8	4.7	5.0 (3.9)
$[Ru(bpy)_2(L9)Ru(bpy)_2]^{2+}$	3.1	2.7	3.0 (4.0)
$[Ru(bpy)_2(L10)Ru(bpy)_2]^{2+}$	2.9	4.5	4.8 (4.2)

Table 4.4 Ground state and excited state pKa values for the mononuclear and dinuclear complexes. pKa* values were obtained using both the Forster equation (**in Blue**) and the Ireland and Wyatt method. [85]

Figure 4.15 contains the absorption spectra of $[Ru(bpy)_2(L7)]^+$ over a range of pH values from 1.91 to 5.08. For both the pyridyltriazole and pyrazyltriazole complexes reversible acid-base behaviour was observed in the pH value range examined. Clear isobestic points can be seen at 458 nm, 390 nm and 358 nm in this pH value range. The isobestic point (458 nm) was subsequently utilised in the emission measurements to obtain the pHi value. A λ_{max} value of 438 nm can be noted in *figure 4.15* at a pH value of 1.91 when the complex is protonated. As the pH value is increased to 5.08 the λ_{max} value is progressively shifted to a lower energy (464 nm).

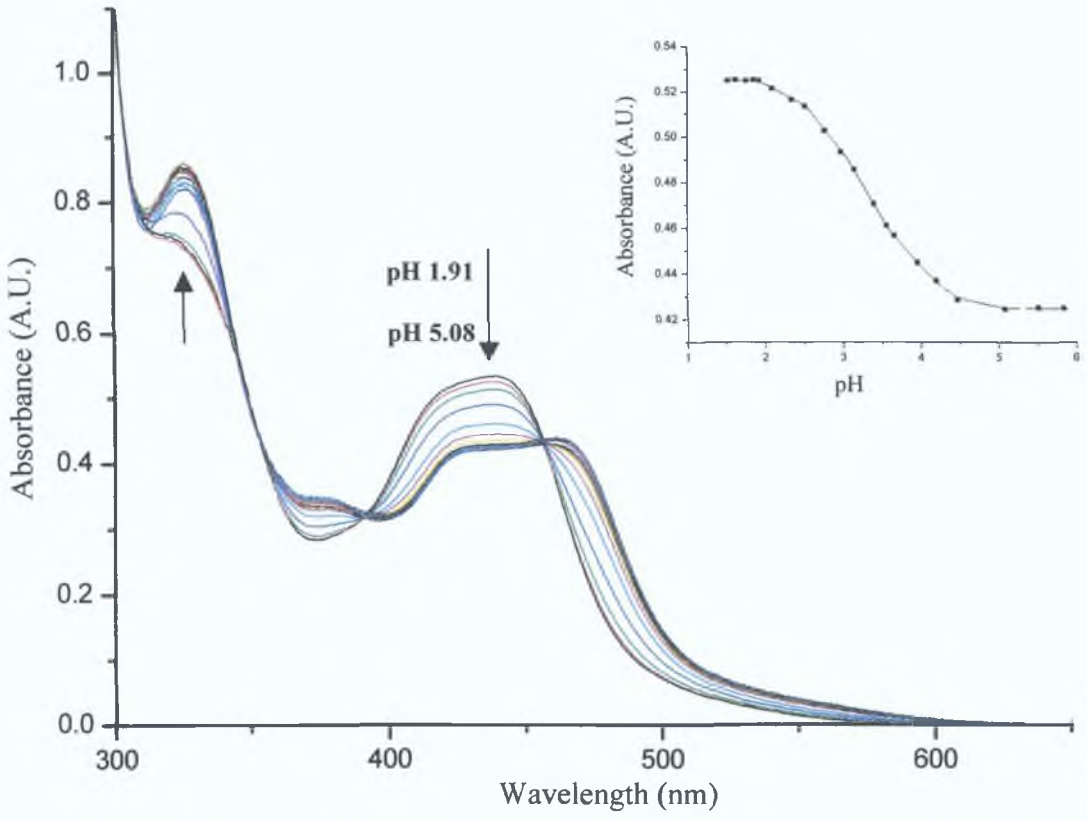

Figure 4. 15 pH dependence of the absorption spectra of $[Ru(bpy)_2(L7)]^+$ in Britton-Robinson buffer. *Inset* fitted sigmoidal curve of absorbance (at 440 nm) versus pH.

Inset (*figure 4.15*) is a graph of pH value versus absorbance to which a sigmoidal curve is fitted and hence, a point of inflection could be obtained which corresponds to the pKa value of the complex. *Table 4.4* shows that the pKa values obtained for the pyridyltriazole complexes are considerably lower than those obtained for the analogous dimethoxy-containing complexes in *chapter three*. For example, the pKa value obtained for $[Ru(bpy)_2(L3)]^+$ was 4.0 while that of $[Ru(bpy)_2(L7)]^+$ was found to be 3.2 which is a significant reduction (*table 3.3*). It is possible that this decrease in the pKa value may be attributable to the hydroxy moieties as this is the only difference between the two complexes. Interestingly O'Brien and co-workers, who examined the analogous catechol complex shown in *figure 4.7*, did not observe this decrease in the pKa value upon deprotecting the catechol complex. It is, therefore, possible that this further decrease in the pKa value is associated with hydrogen bridge formation between the triazolic protonatable nitrogen and the hydroxyl moiety.

This bridging was suggested by Wang *et al* and was discussed in the introduction (*scheme 4 1*) [43] Keyes also reported similar pKa behaviour for this hydroquinone complex in her Ph D thesis [83] On the basis of this evidence, it is possible that the triazolic nitrogen is slightly more acidic as a result of its interaction with the neighbouring –OH moiety Furthermore the catechol complex reported by O'Brien *et al*, in which there is no such reduction m the pKa value upon demethylation, has a different positioning of the –OH groups It is possible that due to the repositioning of the –OH groups no such H-bridge could form between the triazole and the hydroxyl groups This could be further confirmation of an intramolecular bridge hypothesis [45]

The pH value dependence of the absorption spectra of the pyrazyltriazole complexes was also obtained in aqueous Britton-Robinson buffer (*table 4 4*) Again clear and well-defined isobestic points were observed at approximately 560 nm, 422 nm and 358 nm A similar, although less pronounced, shift in the λ_{max} value as observed for the pyridyltriazole complexes For example, at a pH value of 2 0 the λ_{max} is observed at 454 nm and steadily shifts to 447 nm as the pH value is increased to 6 30 This shift is less pronounced than noted for the pyridyltriazole complexes as observed previously for analogous methylated pyrazyltriazole complexes in *chapter three* [84] It may also be seen, upon comparison with the protected complexes, that the pKa values obtained for the hydroquinone complexes are very similar to those of their methoxolated counterparts On the basis of these data it would seem to indicate that either intermolecular H-bonding is not present in these complexes or that the effects of such a phenomena on the pKa values are not as obvious due to the presence of the pyrazine group within these complexes Unfortunately, the presence or absence of such H-bridging cannot be confirmed via X-ray crystallographic data, as this was not obtainable in the case of these complexes It is also of interest to note that, in the case of the dinuclear complexes, there are two triazoles and therefore, a two-step protonation is possible However, only one protonation step was observed in the case of both $[Ru(bpy)_2(L9)(bpy)_2Ru]^{2+}$ and $[Ru(bpy)_2(L10)(bpy)_2Ru]^{2+}$ in aqueous media in the pH value range 2 0 to 6

This indicates that in this media both protonation steps occur at effectively the same pH value and further confirms that a very weak metal-metal interaction occurs as suggested by the previous absorption data in *section 4.3.4.1.* [47] This is comparable to the data obtain for the previous dimethoxy-containing complexes and is indicative of the fact that metal-metal interaction is not substantially effected by the deprotection of the dimethoxy groups. Furthermore, the pKa values obtained for these dinuclear complexes are comparable to those of the respective mononuclear complexes. This suggests that if a hydrogen bridge is present in the mononuclear complexes then the same phenomenon also exists in the dinuclear complexes.

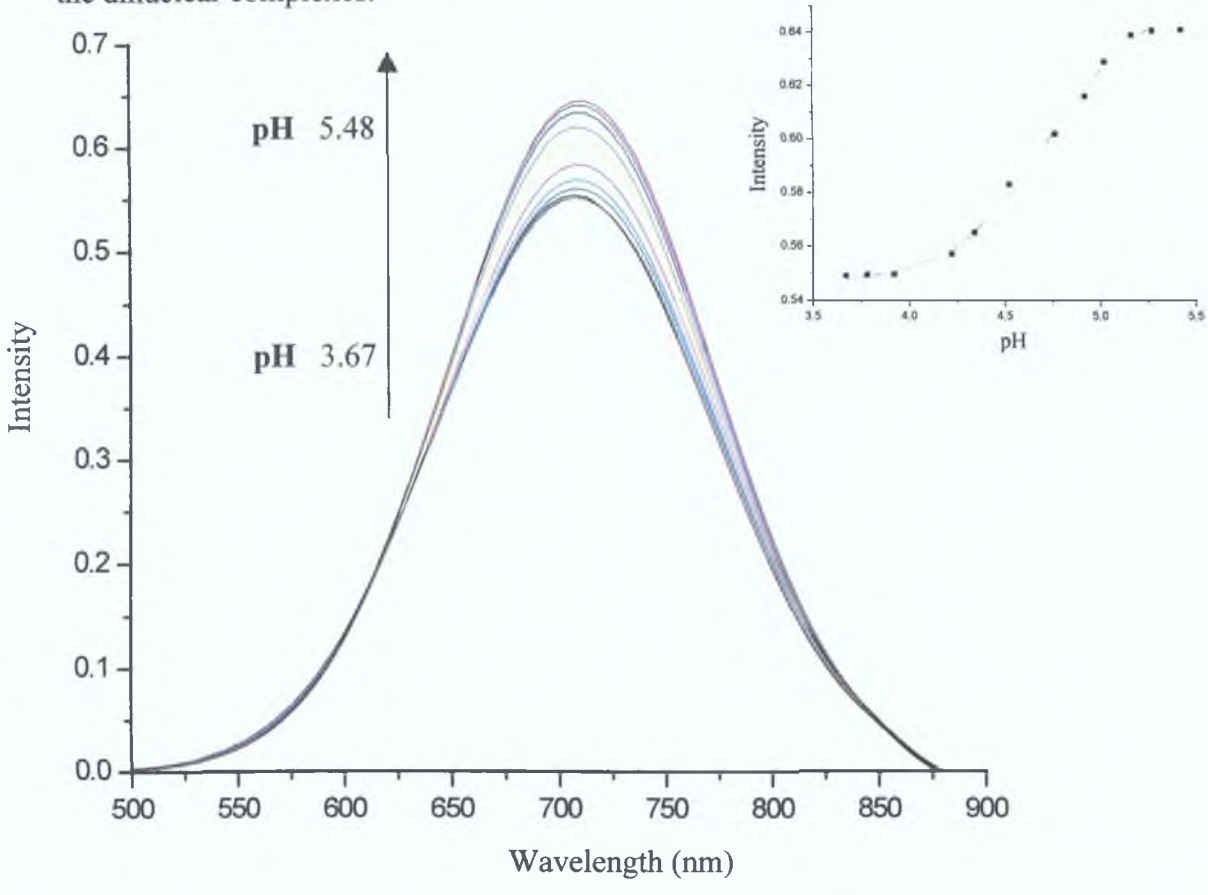

Figure 4.16 pH dependence of the Gaussian emission spectra of $[Ru(bpy)_2(L8)]^+$ in Britton-Robinson buffer. *Inset* fitted sigmoidal curve of intensity versus pH.

Excited stated (pKa*) measurements were also obtained for these complexes. These measurements for the pyridyltriazole complexes were performed as previously outlined for the protected analogues in *chapter three* (*section 3.3.3*) by monitoring changes in the emission spectra of the complexes with increasing pH value. The pKa* value was calculated from the pHi data using both the Forster method and the Ireland and Wyatt technique (*table 4.4*). [85]

In the case of the pyridyltriazole complex $[Ru(bpy)_2(L7)]^+$, a λ_{max} value of approximately 651 nm at a pH value of 2 0 gradually red-shifts to 660 nm as the acidity is decreased to a pH value of 5 0 A concomitant increase in the emission intensity is also observed as the pH value is increased *Figure 4 16* depicts the pH value dependence emission spectra of the pyrazyltriazole complex $[Ru(bpy)_2(L8)]^+$ Compared to the pyridyltriazole complexes the emissions of the pyrazyl-containing complexes in aqueous media were much weaker For example, at the pH value 2 0 emission in the latter system is almost non-existent This is similar to the situation noted for the protected complexes (*chapter three*), since, the non-coordinated N on the pyrazine ring is protonated at very low pH values (typically in the region of −1 2 [82]) [86] However, it was also noted that the changes observed in the spectra of these complexes were complicated by the weakness of the emissions, therefore, the changes in intensity proved difficult to monitor However, Gaussian curves were fitted to the emission data in order to resolve the peaks and obtain useful data These Gaussian resolved curves are shown in *figure 4 16* with a construction of the plot of pH value versus intensity (*figure 4 16* inset) from which the pKa* data could then be calculated The calculated pKa* values for these complexes are contained in table 4 4

Although, two methods were employed for the calculation of the pKa* values, it is generally accepted that the Ireland and Wyatt technique is more accurate than the Forster equation as small errors in the assessment of $E_{0\text{-}0}$ for ν_a and ν_b produce considerable errors in the pKa* value [85] If these values are considered, it can be seen that the pKa values for the pyridyltriazole complexes are higher than the pKa* values This is similar to the behaviour of the protected analogues and indicates that for these complexes the excited state is not located on the pyridyltriazole moiety but is bipyridyl based [78] This trend is also in agreement with that witnessed for previous hydroquinone-containing pyridyltriazole complexes [43][45] However, in the case of the pyrazyltriazole complexes the pKa* values are now higher than the pKa values indicating that the excited state is based on the triazolic ligand and is not bpy-based This trend was observed previously for similar ruthenium pyrazyltriazole complexes and provides further confirmation of the switching of the excited state suggested in *section 4 3 4 2* [81][47]

4.5 Electrochemical Properties

Electrochemical data for the deprotected mononuclear and dinuclear pyridyltriazole and pyrazyltriazole complexes were obtained under strict experimental conditions (*chapter two*). The optimal experimental specifications based on exhaustive electrochemical analyses (*appendix B*) were undertaken in a nitrogen-saturated environment in order to negate any environmental interference.

Complex	*Oxidation Potentials (V)*[a,b]		*Reduction Potentials (V)*[c]	
	Ru^{II}/Ru^{III}	ligand*	ligand*	bipyridyl
H3L3	-	0.54, 1.17	-0.76	-
$[Ru(bpy)_2(L7)]^+$	1.27	0.70, 1.16	0.14	-1.48, -1.75
$[Ru(bpy)_2(HL7)]^{2+}$	1.27	1.24	0.26	*d*
$[Ru(bpy)_2(L8)]^+$	1.28	0.88, 1.15	0.13	-1.43,-1.67,-1.96
$[Ru(bpy)_2(HL8)]^{2+}$	1.28	1.25	0.26	*d*
$[Ru(bpy)_2(L9)Ru(bpy)_2]^{2+}$	1.28	0.78, 0.88	0.16	-1.50, -1.76
$[Ru(bpy)_2(H_2L9)Ru(bpy)_2]^{4+}$	1.28	1.24	0.24	*d*
$[Ru(bpy)_2(L10)Ru(bpy)_2]^{2+}$	1.28	0.88, 0.99	0.11	-1.43,-1.66,-1.95
$[Ru(bpy)_2(H_2L10)Ru(bpy)_2]^{4+}$	1.28	1.25	0.25	*d*

* The anodic and cathodic peak potentials are reported

[a] Values standardised with respect to the redox potential of ferrocene (+0.38 V *vs.* SCE) under equivalent experimental conditions as a secondary electrode. [87]

[b] Protonation was achieved via addition of 1 drop of conc. $HClO_4$.

[c] All measurements were carried out under a constant flow of nitrogen. Cathodic samples also underwent deaeration by purging with argon for 15 mins.

[d] Surface effects arise in acidic solutions making reduction potentials difficult to obtain.[88]

Table 4.5 Electrochemical data for the Ru (II) complexes in acetonitrile with 0.1 M TEAP versus SCE

Furthermore, due to the presence of the hydroquinone moieties in these complexes, it was necessary to extensively pre-treat the working electrode in order to fully elucidate all peaks present within the experimental window (*chapter two*).

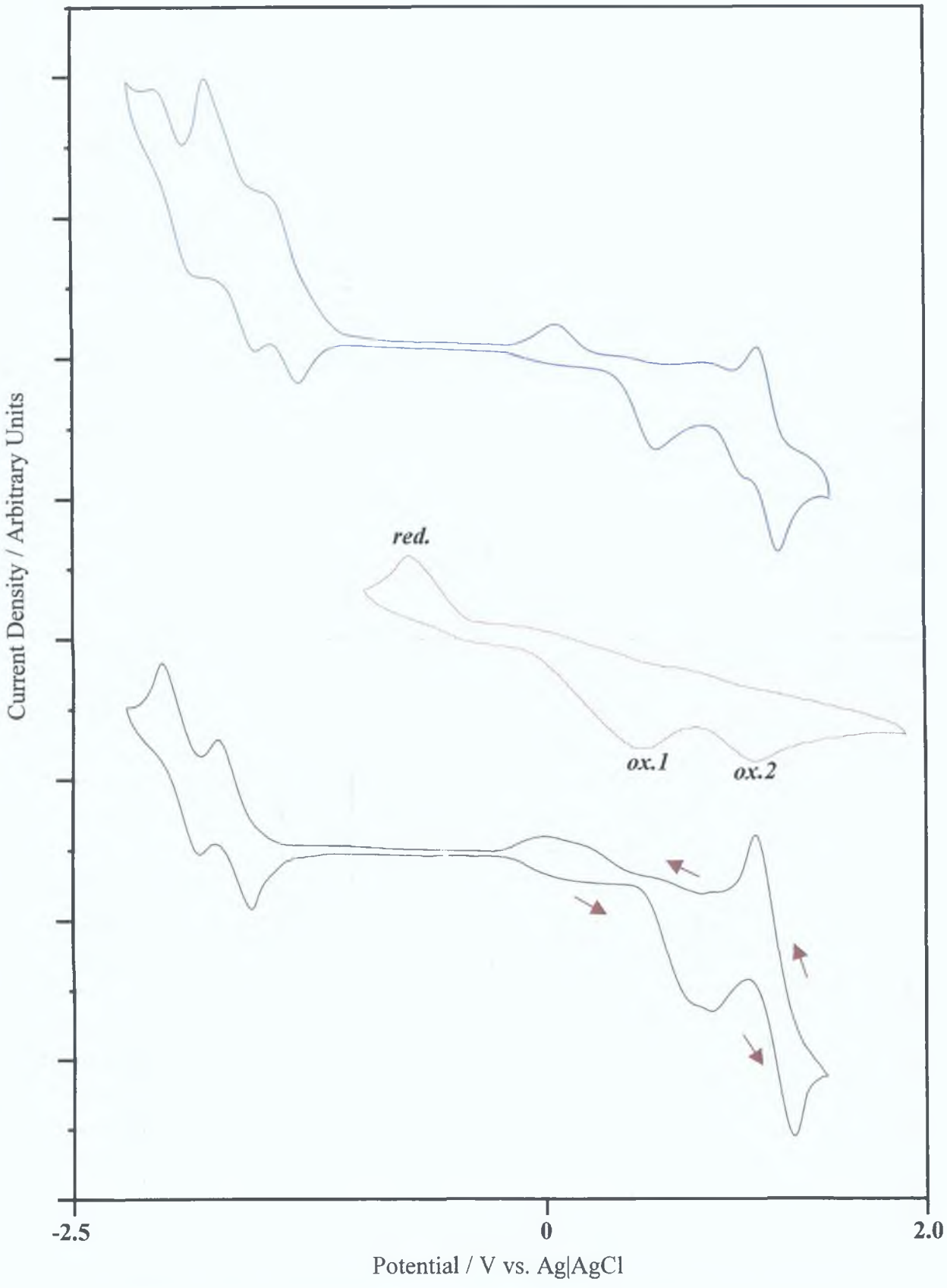

Figure 4.17 Cyclic voltammograms of $[Ru(bpy)_2(L8)]^+$ **(blue line)**, H3L3 **(red line)** $[Ru(bpy)_2(L9)Ru(bpy)_2]^{2+}$ **(black line)** in neutral MeCN with 0.1M TEAP in volts versus Ag|AgCl (*scan rate* 0.05V/s).

The oxidation and reduction potentials for the hydroquinone complexes were obtained and are recorded in the table 4 5 The cyclic voltammograms of $[Ru(bpy)_2(L8)]^+$ and $[Ru(bpy)_2(L9)Ru(bpy)_2]^{2+}$, along with that of the pyridyltriazole ligand (H_3L3) in neutral acetonitrile are shown in *figure 4 17* The electrochemistry of the dihydroxy ligand depicts the oxidation of the hydroquinone moiety to form the corresponding quinone (*figure 4 18*)

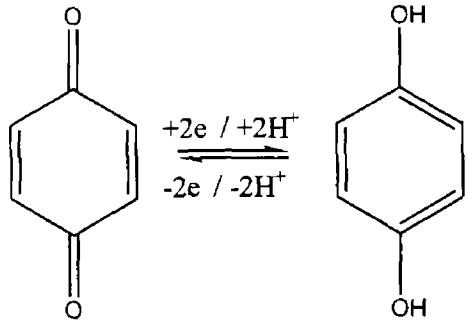

Figure 4 18 The half-reaction representing the quinone / hydroquinone couple

From an examination of the voltammogram it can be seen that the two oxidations of the hydroquinone moiety at 0 54 V and 1 17 V versus SCE are well resolved at neutral pH while the reductions occur simultaneously at – 0 76 V Such separation of the individual oxidation steps of the hydroquinone has been reported previously, using similarly treated electrodes [2] These results are also comparable to those found by both Keyes and Weldon *et al* for their hydroquinone-containing free ligands (*scheme 4 1* and *figure 4 6*) and are typical of this type of ligand [42][83] The fact the the oxidations of these ligand groups are found to be irreversible is unsurprising as the oxidation of the 1,2-dihydroxybenzene groups to the qumone involves loss of protons and are, therefore, necessarily irreversible in aprotic solvents, such as, acetonitrile [21] The assignments of these processes in the free ligand serve to aid in the elucidation of the processes observed for the ruthenium complexes, which are also depicted in *figure 4 17* These are useful observations as, from an examination of the voltammograms of the ruthenium complexes, it becomes apparent that their electrochemical behaviour is somewhat more elaborate than their precursor complexes Other workers have also reported similar complex electrochemical behaviour in the CVs of their hydroquinone-containing complexes

For example, Keyes and co-workers attributed the first two oxidation peaks at 0 74 V and 1 01 V *vs* SCE to the two one-electron oxidations of the hydroquinone ring while the third redox couple at 1 18 V was assigned to the metal-based Ru^{II}/Ru^{III} process [43] Ward and co-workers noted that in their dimethoxy complex the Ru^{II}/Ru^{III} redox couple was observed at 0 84 V and the dimethoxyphenyl oxidation then occurred at approximately 0 97 V However, in their dihydroxy complex (*figure 4 6*) the Ru^{II}/Ru^{III} couple is observed 0 88 V while an irreversible oxidation associated with the dihydroxy group was seen at 0 72 V (in MeCN vs Fc/Fc^{+}) [21] Furthermore, Keyes *et al* also noted a quasi-reversible two-electron oxidation at 0 42 V, which they assigned to the hydroquinone-quinone oxidation prior to the metal oxidation in their dihydroxy-containing complexes (*figure 4 19*) [35] Also, Ward and co-workers, who examined the electrochemical behaviour of O, N complexes bound to phenolic moieties, reported similar behaviour to that described for the hydroquinone complexes contained in this chapter For example, they reported an irreversible oxidation occurring at strongly anodic potentials (1 3 V) Furthermore, this behaviour mirrors that witnesses for a number of dioxolene complexes, such as, those examined by Lever and co-workers in which oxidation to Ru^{III} does not occur until the dioxolene ligand is oxidised to the quinone level [20]

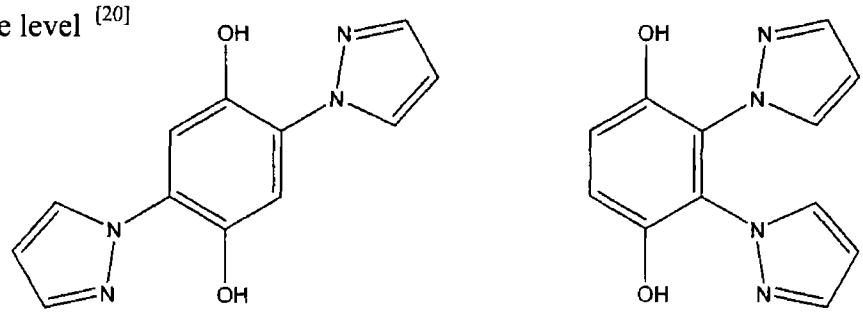

Figure 4 19 Hydroquinone-containing ligands utilised by Keyes *et al* in the synthesis of ruthenium complexes [35]

Since, both Ward *et al* and Keyes *et al* associated these processes with ligand oxidations followed by a metal-based Ru^{II}-Ru^{III} oxidation and from an examination of the processes observed for the free ligand it is, therefore, reasonable to attribute the first two anodic peaks in the CVs of the hydroquinone complexes in this chapter with hydroqumone processes while the strongly anodic processes observed in the CVs (*table 4 5, figure 4 17*) are associated with metal-based oxidation(s) These assignments are further justified by the spectroelectrochemical measurements (*section 4 6*)

For example, the compound $[Ru(bpy)_2(L3)]^+$ had a reversible metal (Ru^{II}/Ru^{III}) redox couple at 0 80 V versus SCE and the ligand oxidations then occurred at 1 20 V and 1 40 V (versus SCE) However, in the corresponding hydroquinone complex irreversible redox processes associated with the hydroquinone moiety occur at 0 70 V and 1 16 V (versus SCE) followed by the metal oxidation at 1 27 V Since, the ligand processes occur prior to the metal it means that the true oxidation potential of the metal is more difficult to determine accurately [43]

The reductions observed in the cathodic region of the mononuclear and dinuclear pyridyltriazole complexes are assigned to two one-electron reversible redox reactions of the bipyridine ligands [27] In the mononuclear and dinuclear pyrazyltriazole complexes, however, due to the electron accepting nature of the pyrazine ring the pyrazyl moiety now has a substantially lower π^* orbital than bpy and hence, the first reduction observed is assigned as pyrazine based while the second and third reduction (when present) are bipyridine centred [73][81]

It may be also be noticed that the redox potentials of the hydroquinone complexes presented in this chapter are significantly anodically shifted by comparison to other triazole complexes For example, in the complex $[Ru(bpy)_2(L3)]^+$ the metal oxidation is recorded at 0 8 V (table 3 4) compared to its deprotected analogue $[Ru(bpy)_2(L7)]^+$ which imparted a metal oxidation at 1 27 V versus SCE However, the redox potentials observed in the deprotected complexes are comparable to complexes containing a protonated triazole moiety(ies) For example, $[Ru(bpy)_2(H_2L5)Ru(bpy)_2]^{3+}$ has a metal oxidation at 1 25 V versus SCE while its dihydroxy counterpart $[Ru(bpy)_2(H_2L9)Ru(bpy)_2]^{3+}$ has an oxidation at 1 28 V It is known from the methoxylated complexes that at this pH value the triazole is protonated The previous UV-Vis data also suggests that the triazole is deprotonated at this pH value Consequently, this would imply that protonation of the triazole ring is occurring as a result of oxidation of the hydroquinone group This was noted previously by Keyes *et al* and provided as evidence of electrochemically induced proton transfer [43]

Further electrochemical investigations were, hence, undertaken to explore the behaviour of these complexes in acidic acetonitrile. The cyclic voltammograms of $[Ru(bpy)_2(L7)]^+$ in both neutral and acidic media in the potential window – 0.2 V to 1.5 V are shown in *figure 4.20*.

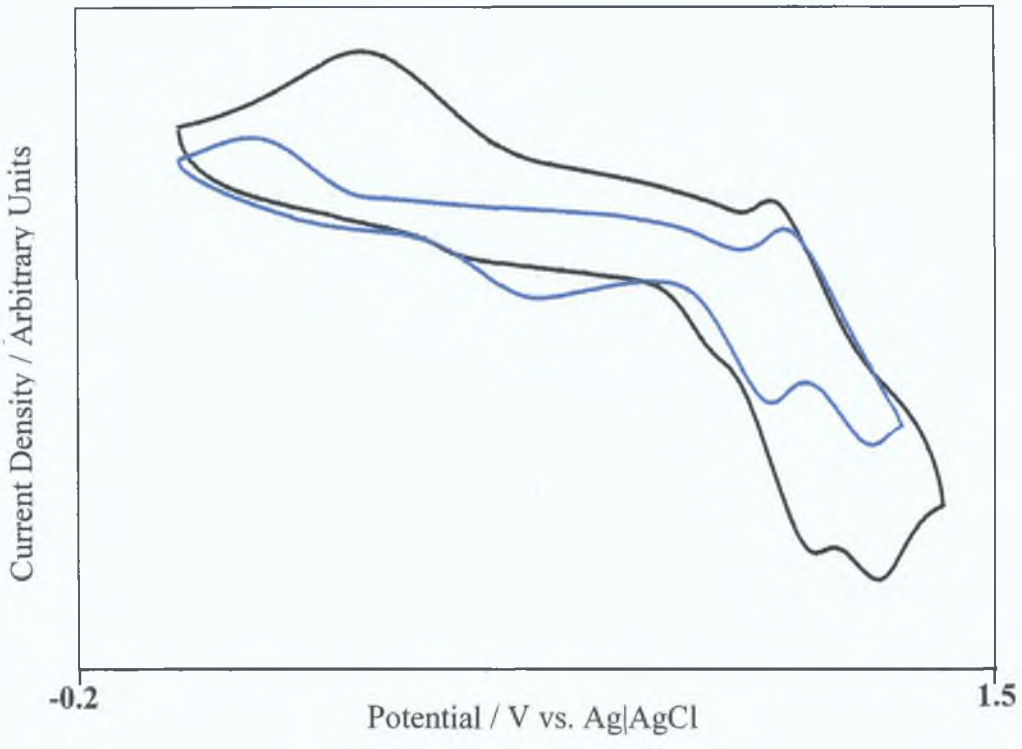

Figure 4.20 Cyclic voltammograms of $[Ru(bpy)_2(L7)]^+$ **(blue line)** in neutral MeCN, $[Ru(bpy)_2(HL7)]^{2+}$ **(black line)** in MeCN with 1 drop of $HClO_4$ with 0.1 M TEAP in volts versus Ag|AgCl (*scan rate* 0.05 V / s).

From an examination of these voltammograms it can be seen that the potential at which the metal oxidation is observed does not alter significantly upon the addition of acid (1.25 V vs SCE) compared to its value in neutral media (1.25 V in SCE). This is in stark contrast to the behaviour noted for the protected complexes in which the metal oxidation was seen to shift be between 300 mV and 400 mV. However, the oxidations of the hydroquinone groups are no longer as clearly resolved and instead occur as a single two-electron wave (confirmed by coulometric measurements), which has anodically shifted to 1.24 V. This is probably due to increased electron density on the ligand, as a result of the negative charges on the oxygen atoms after deprotonation and has been noted previously in similar complexes. [42] This further confirms that the triazole ring is protonated subsequent to oxidation of the hydroquinone.

This provides further evidence of electrochemically induced proton transfer within these complexes However, this hypothesis will be tested further in the following spectroelectrochemical analyses

Figure 4 17 also contains the cyclic voltammogram of the dinuclear complex $[Ru(bpy)_2(L9)Ru(bpy)_2]^{2+}$ From an examination of this voltammogram it can be observed that a single redox process is present, which, by comparison with the mononuclear analogue, can be associated with the metal redox process Indeed, the metal redox processes noted in the voltammograms of the dinuclear complexes are comparable to their analogous mononuclear counterpart For example, the metal oxidation potential of the dinuclear complex $[Ru(bpy)_2(L9)Ru(bpy)_2]^{2+}$ depicted in *figure 4 17* was found to be 1 28 V versus SCE while that of its complement $[Ru(bpy)_2(L7)]^{+}$ was found to be 1 27 V versus SCE Hence, the properties of the dinuclear complexes are comparable to those of their mononuclear analogues This indicates that each of the units in the dinuclear complexes behaves in quite an independent manner Furthermore, the metal peaks could not be resolved with coulometry This behaviour was also noted previously in the case of the analogous protected complexes in *chapter three* and may be attributed to the simultaneous oxidation of the two metal units Once again, it may be noted that the thermodynamic stability of a mixed-valence species relative to the reduced and oxidised isovalent ones can be evaluated through the comproportionation constant, K_c as defined by the following equation at T = 298K [89]

$$K_c = e^{\Delta E(mV) / 25\ 69}$$

Since, there is an absence of any significant difference in the two metal-based oxidations of the dinuclear complexes, this would suggest that there is weak or no electronic coupling between the two metal centres in the ground state, as previously surmised Once again, as in the methylated complexes, the value of K_c for the dinuclear complexes is, hence, less than 5 [87][88] This behaviour has been observed previously in molecules that contain a number of identical non-interacting centres

Complexes, such as, that observed in *figure 4 17* merely exhibit current-potential responses with the same shape as that of the mononuclear analogue but with a larger magnitude due to the presence of the additional electroactive centre [90] Furthermore there is also a perceivably greater peak-to-peak separation (E_p) in the metal oxidation wave of the dinuclear complexes compared to those of the mononuclear complexes This reflects the bielectronic process involved in the metal oxidation [47] If however, the interaction between the metal centres were strong, there would be a stabilisation of the mixed-valence complex and this in turn would result in the presence of discrete oxidation waves for each of the metal centres [91]

Behaviour similar to that noted for the dinuclear hydroquinone complexes in this chapter, have been witnessed in prior studies of hydroquinone-containing dinuclear complexes For example, Weldon *et al* reported the electrochemical behaviour of a dinuclear hydroquinone complex with no protonatable site on the triazole ring (*figure 4 6*), which presented a cyclic voltammogram similar to that of $[Ru(bpy)_2(L9)Ru(bpy)_2]^{2+}$ This complex too was found to have very weakly coupled metal centres with both metal oxidations occurring at 1 30 V versus SCE [42] However, in order to investigate the assignment of the order of the redox processes further, and to analyse the degree of intermetallic communication more comprehensively, spectroelectrochemical measurements were undertaken and these are presented in the following section

4.6 Spectroelectrochemistry

As in *chapter three* spectroelectrochemical techniques have proved to be a powerful tool in the verification of the assignment of the order of the redox processes explored in the previous section. This is particularly beneficial in the case of the hydroquinone complexes presented in this chapter as the electrochemical assignments and behaviours are somewhat more elusive than their counterparts due to the complex nature of the ligand moieties.

4.6.1 Absorption Spectroelectrochemistry

The specific experimental conditions utilised during the course of these analyses are defined in *chapter two*.

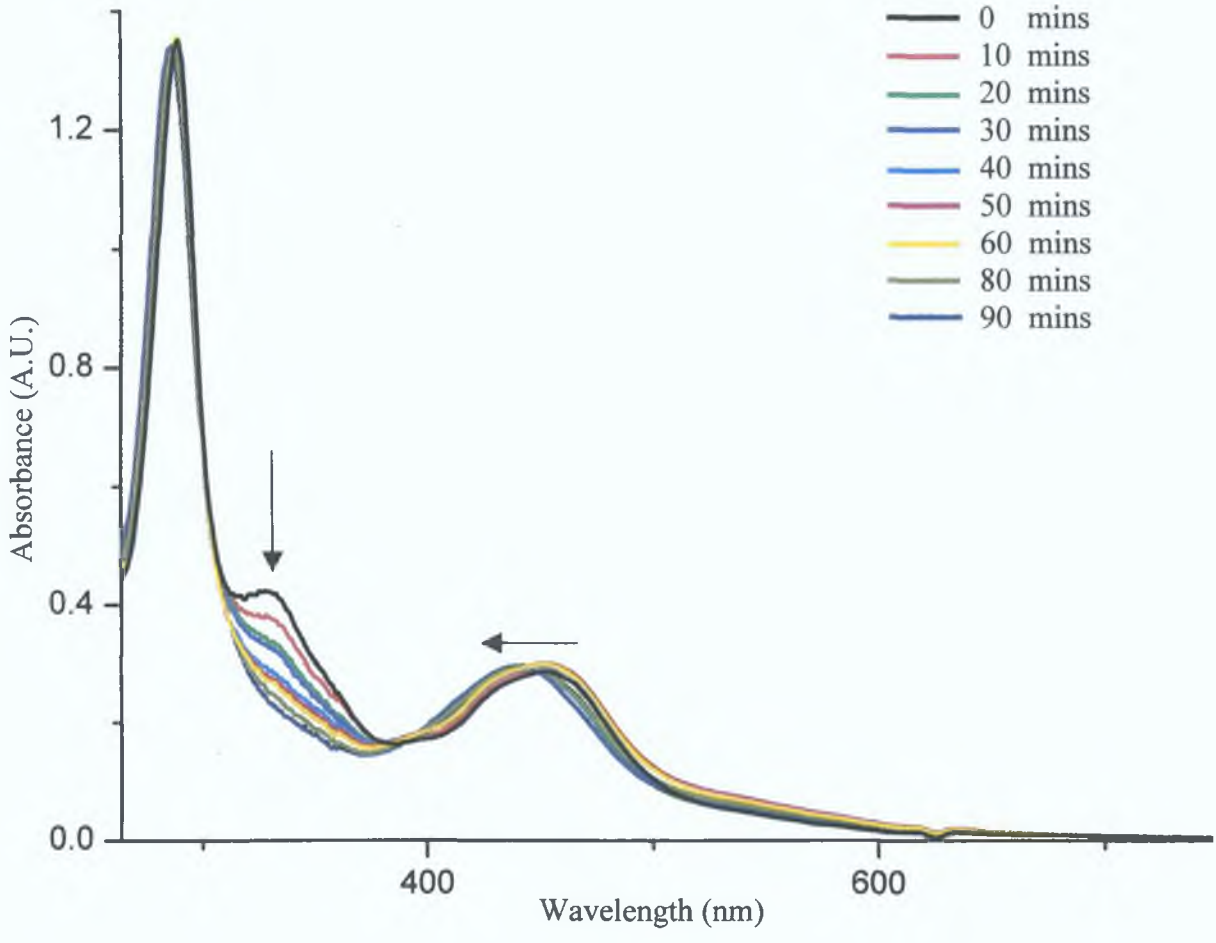

Figure 4.21 Spectroelectrochemical analysis of $[Ru(bpy)_2(L8)]^+$ at 1.00 V in neutral acetonitrile with 0.1 M TEAP vs. Ag|AgCl.

Figure 4.21 shows the spectroelectrochemical analysis of the pyrazyltriazole monomer complex $[Ru(bpy)_2(L8)]^+$ at 1.00 V versus Ag|AgCl. It was suggested in the previous electrochemical section that the two-step oxidation of the hydroquinone moiety to quinone occurred up to this potential. Indeed, from an examination of *figure 4.21* this seems to be justified. As the potential was applied there was a concomitant decrease in the band around 360 nm which is most likely associated with π-π^* transitions in hydroquinone moieties by comparison with similar complexes. [35][43] Furthermore, a broad tail prior to 600 nm also appears over time. This is indicative of the formation of semiquinone intermediates as the hydroquinone is oxidised. [42] However, the most interesting feature of these spectra are the changes noted in the MLCT band. Undoubtedly, the ruthenium unit remains unoxidised as there is no loss of this band however, the λ_{max} value is seen to increase and there is a gradual blue shift from 452 nm to 441 nm.

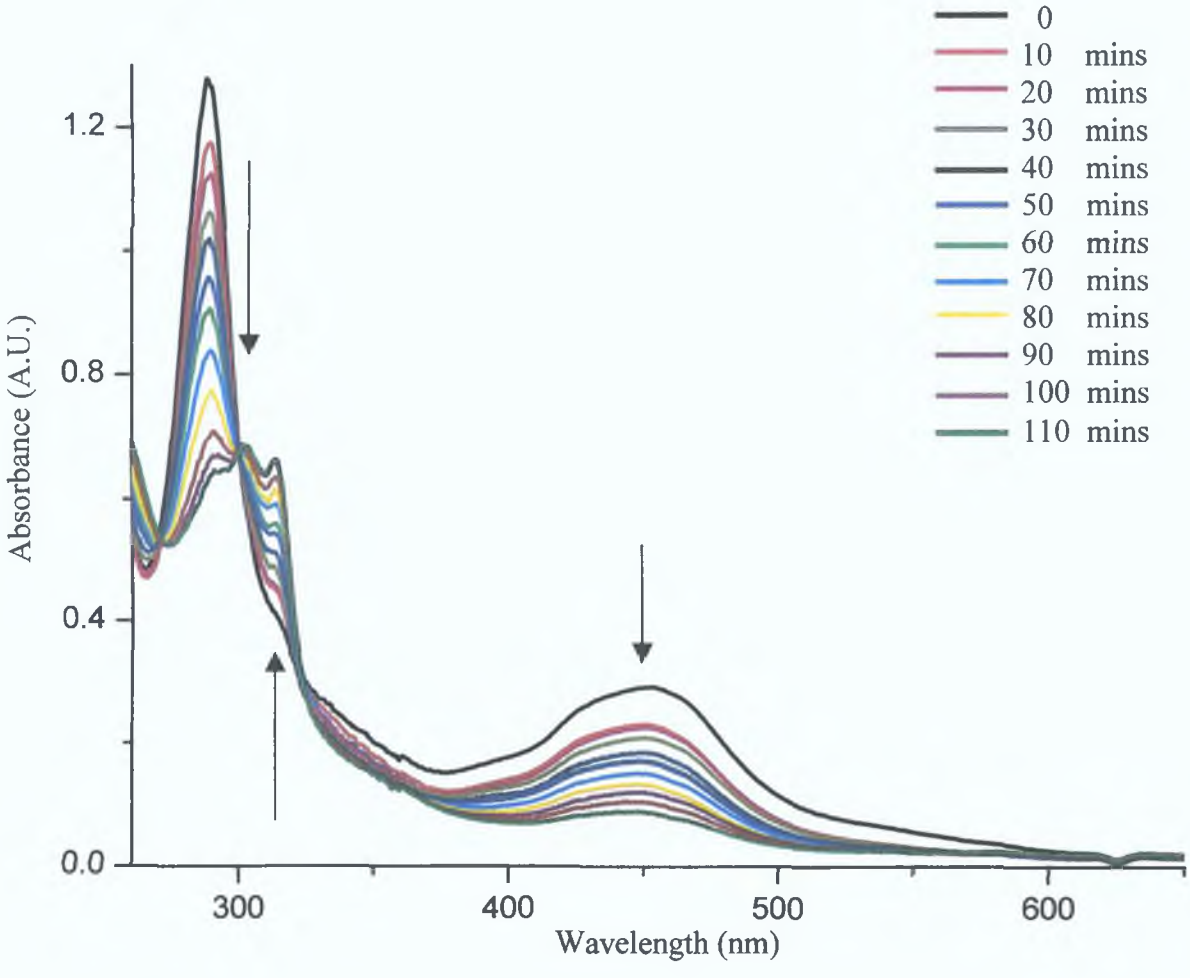

Figure 4.22 Spectroelectrochemical analysis of $[Ru(bpy)_2(L8)]^+$ at a potential of 1.60 V in neutral acetonitrile with 0.1 M TEAP vs. Ag|AgCl.

From previous UV analyses it is known that in this pH value range the hydroquinone complexes are deprotonated. The initial spectrum (red line, *figure 4.23*) at 0 V also indicates that the complex $[Ru(bpy)_2(L7)]^+$ is in a deprotonated state. However, as the oxidation proceeds and the hydroquinone moiety is oxidised, as shown in the previous electrochemical section, the complex appears to become protonated as indicated a blue shift in the λ_{max} value. This shift is comparable to the changes noted in the UV-Vis (*section 4.3.4.1*) upon protonation of the neutral complex with acid. The fact that the metal is in a protonated state subsequent to the ligand oxidation was suggested in the previous section and appears to be verified by this spectroelectrochemical data. This is in contrast to the behaviour noted for the previous methylated complexes and hence, is related to the presence of the hydroquinone moiety. The potential was then increased to 1.60 V and the changes were, once again, monitored over time. *Figure 4.22* shows the changes in the spectra of $[Ru(bpy)_2(L8)]^+$ at this potential. At this potential there is a loss of the MLCT band accompanied by the depletion of the intense π-π^* ligand-based absorbances at 290 nm. [27]

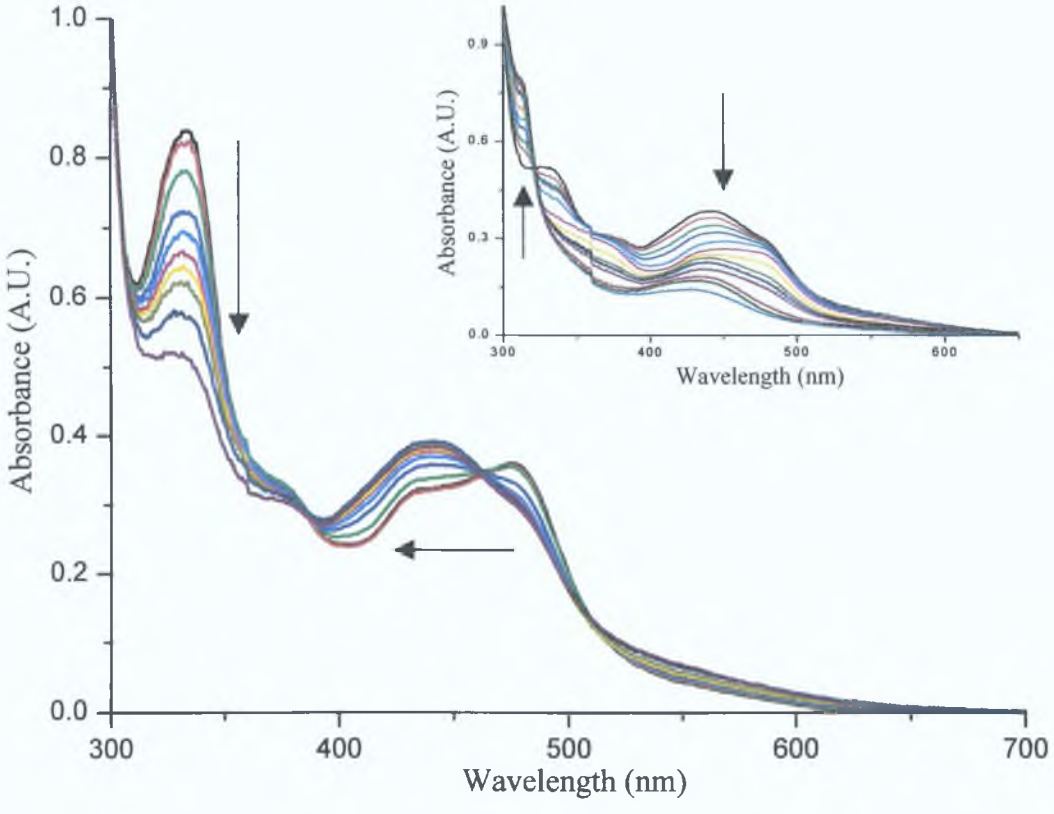

Figure 4.23 Spectroelectrochemical analysis of $[Ru(bpy)_2(L7)]^+$ at 1.00 V in neutral acetonitrile with 0.1M TEAP vs. Ag|AgCl. *Inset* changes upon oxidation at 1.60 V vs. Ag|AgCl

These changes are accompanied by the growth of a shoulder at 313 nm consistent with the formation of Ru^{III}. [92] Hence, the assignment of these processes as Ru^{II} - Ru^{III} in nature is reasonable and echoes the findings of previous investigators of analogous complexes. [43] This spectroelectrochemical behaviour, therefore, yields the most compelling evidence to support the hypothesis of an electrochemically induced proton transfer process. [43]

The changes noted in the spectra of the pyrazyltriazole monomer complexes are similar to the behaviour of the pyridyltriazole complexes (*figure 4.23*). Once again, a depletion of the hydroquinone bands occurs up the application of 1.00 V versus Ag|AgCl accompanied by a tailing prior 600 nm, which is associated with semiquinone formation. It is necessary to note that, once again, there is an apparent blue shift in the λ_{max} value of the pyridyltriazole complexes from 476 nm to 438 nm (*figure 4.23*). This further confirms that upon oxidation of the hydroquinone moieties the complex becomes protonated in line with the electrochemical findings. This, therefore, suggests that electrochemically induced proton transfer also occurs in the pyrazyltriazole complexes. [43] Further analysis of this phenomenon is contained in the following emission spectroelectrochemical data.

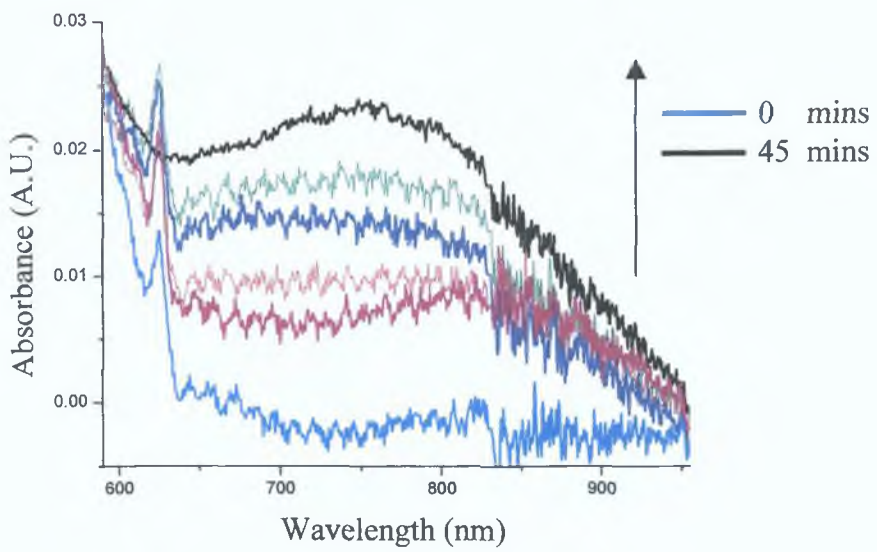

Figure 4.24 Spectroelectrochemical analysis of $[Ru(bpy)_2(L7)]^+$ in neutral acetonitrile with 0.1 M TEAP at a potential of 1.60 V vs. Ag|AgCl

Finally, in both the pyridyltriazole and pyrazyltriazole mononuclear complex spectroelectrochemical analyses from 360 nm to 2200 nm were also obtained. *Figure 4.24* shows the oxidative spectroelectrochemical analysis of $[Ru(bpy)_2(L7)]^+$ in the region 580 nm to 1000 nm at an applied potential of 1.60 V versus Ag|AgCl. The gradual formation of a weak band centred at circa. 750 nm is seen to appear as the metal is oxidised.

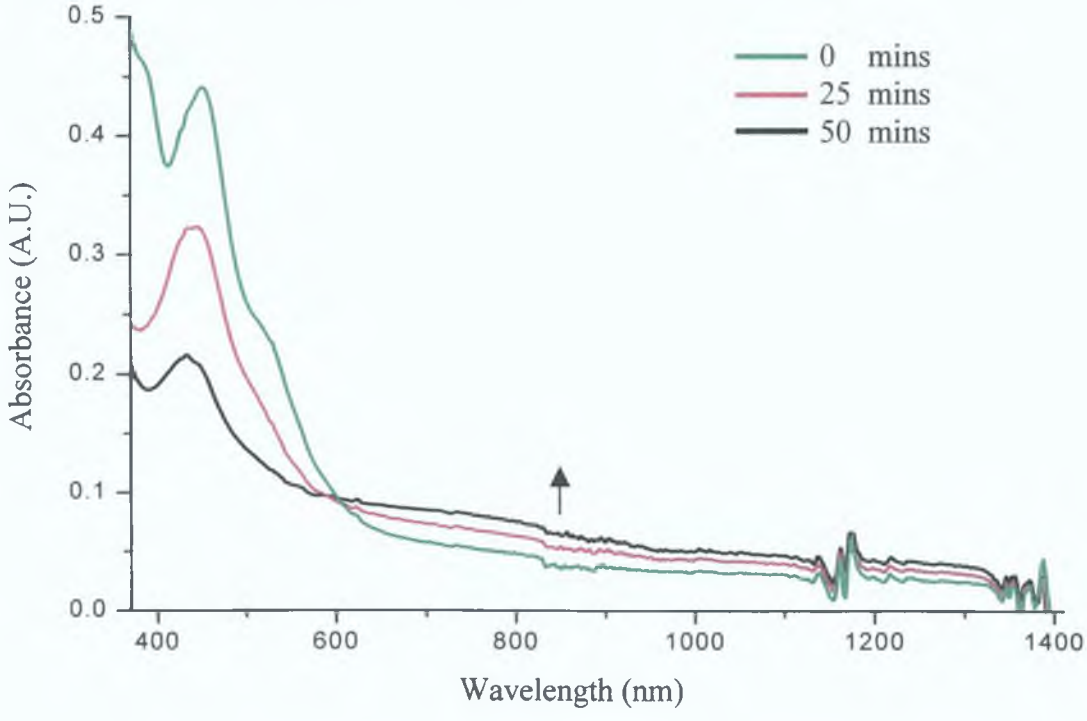

Figure 4.25 Spectroelectrochemical analysis of $[Ru(bpy)_2(L10)Ru(bpy)_2]^+$ in neutral acetonitrile with 0.1 M TEAP at 1.60 V vs. Ag|AgCl

By comparison with both the analogous methylated complexes in *chapter three* as well as similar complexes and due to its position and since, it is seen to deplete once the potential is returned to 0 V, this band is most likely associated with a new bpy(π) – Ru d(π) ligand to metal charge transfer (LMCT) arising as the metal is oxidised.[42] It is interesting to note however, that this LMCT band is considerably weakened in both the mononuclear pyridyltriazole and pyrazyltriazole complexes compared to the analogous protected complexes. Indeed, these bands are similar to those reported earlier for the LMCT bands of the protonated-methylated complexes. This is perhaps further evidence that the triazole moiety in these complexes becomes protonated following the oxidation of the hydroquinone groups.

For example, when the analogous protected mono- and dinuclear pyridyltriazole complexes (*chapter three*) were protonated the LMCT shifts from 1080 nm to circa 830 nm for $[Ru(bpy)_2(L3)]^+$ and from 1220 nm to 840 nm for $[Ru(bpy)_2(L5)Ru(bpy)_2]^{2+}$, coupled with a concomitant decrease in intensity The shifts are associated with the protonation of the triazole moiety and the subsequent decrease in the σ-donor properties of the ligand and hence, the subsequent increase in energy of both the donor and acceptor orbitals Nazeeruddin *et al* reported similar behaviour previously [93] Since, the LMCTs in these hydroquinone complexes are in a similar position to those of the protonated analogues in *chapter three*, it is further evidence that the triazole becomes protonated subsequent to the hydroquinone oxidations

Spectroelectrochemical measurements in this near-IR region are also important for the examination of the dinuclear complexes It was seen in *chapter three* that intervalence transition (IT) bands may occur in mixed valence complexes and can provide an indication of the level of communication present between two metal centres [94] Theoretically, since, these dinuclear complexes appear to have localised valences with weak metal-metal interactions, the treatment given by Hush may be applied to the properties of any prospective IT bands [95] Indeed, in the previous section the electrochemical data seemed to indicate only a very weak interaction between the metal centres in both the pyridyltriazole and pyrazyltriazole-containing dinuclear complexes Hence, oxidative spectroelectrochemical analyses in the IR / near-IR region of the dinuclear complexes were undertaken *Figure 4 25* shows the spectra of $[Ru(bpy)_2(L10)Ru(bpy)_2]^+$ in neutral acetonitrile from 380 nm to 1400 nm In this region, at an applied potential of 1 60 V versus Ag|AgCl, the growth of a broad, weak band was noted for both the pyridyltriazole and the pyrazyltriazole dinuclear complexes centred at approximately 850 nm By comparison with the mononuclear complexes these bands are most likely LMCT in nature Furthermore in the dinuclear ruthenium hydroquinone complex synthesised by Weldon *et al* (*figure 4 6*) this LMCT band was also identified and therefore, this assignment is reasonable [42]

However, unlike in the case of the methylated dinuclear pyridyltriazole complex in *chapter three*, no clearly detectable intervalence transitions were noted in the spectra of either of the dinuclear complexes although these may be present in an extremely weak form Once again, this echoes the findings of Weldon *et al* and is perhaps not surprising considering the small amount of electronic interaction indicated by the electrochemical analyses [42] Furthermore, Rocha *et al* [89] have previously shown that protonating a triazole bridging ligand can dramatically affect the intermetallic electronic coupling and hence, effect the electronic communication between metal centres If, indeed, the triazole moieties were protonated via ligand oxidation as suggested by the electrochemical, spectroelectrochemical and the following emission data it is not surprising that the dinuclear complexes show no perceivable IT band

Indeed, this band is generally very weak even in the methylated analogues and since, intermetallic communication is already weak, protonation of the triazole ring effectively 'switches' off metal-metal communication as Rocha *et al* have already shown and, therefore, the lack of IT bands is rational [89]

4 6 2 Luminescence Spectroelectrochemistry

The increased selectivity and sensitivity of emission spectroelectrochemistry relative to absorption spectroscopy should provide some informative insights into the excited states of the complexes presented in this chapter [96] Hence, emission data were obtained for each complex over a range of applied potentials in neutral acetonitrile with a Teflon shrouded Ag|AgCl reference electrode *Figure 4 26* depicts the luminescence spectroelectrochemical data obtained for $[Ru(bpy)_2(L10)Ru(bpy)_2]^{2+}$ at 1 00 V versus Ag|AgCl As reported previously, the emission of these complexes originates from the lowest excited state, which is known to be ^{3}MLCT in nature This emission is represented in *figure 4 26* by the lowest (green line) peak obtained at 1 0 V after 0 mins versus Ag|AgCl However, over time as an oxidising potential of 1 0 V was applied a change in the spectra was noted Unlike in the case of the methylated complexes this change was an increase in the emission accompanied by a concomitant shift in the λ_{max} of emission from approximately 660 nm to 670 nm

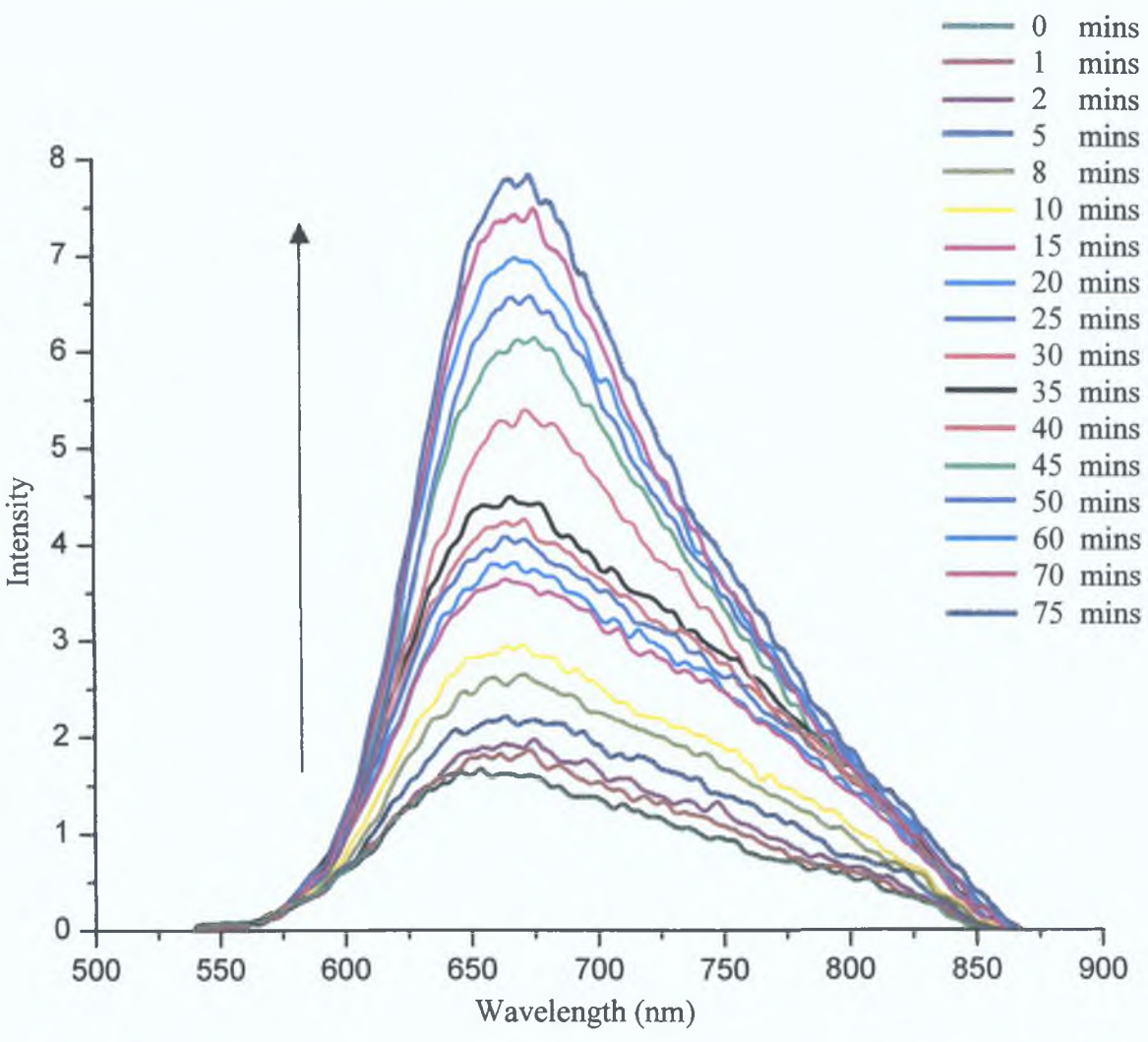

Figure 4.26 Luminescence spectroelectrochemical analysis of $[Ru(bpy)_2(L10)Ru(bpy)_2]^{2+}$ in neutral acetonitrile with 0.1 M TEAP at 1.00 V vs. Ag|AgCl

This is comparable to the behaviour noted for this complex in *section 4.3.4.2* in which a similar increase in the luminescence and concomitant increase in the λ_{max} value was noted upon protonation. This behaviour was further noted in the lifetime data of the pyrazyltriazole complexes, which also increased from 156 ns to 232 ns upon protonation (*section 4.3.4.3*). Hence, further evidence of the fact that oxidation of the hydroquinone moieties occurs at this potential prior to the metal oxidation accompanied by the concomitant protonation of the triazole ring, is provided. The potential was then increased to 1.60 V versus Ag|AgCl and *figure 4.27* depicts the oxidative luminescence spectroelectrochemical data for $[Ru(bpy)_2(L10)Ru(bpy)_2]^{2+}$.

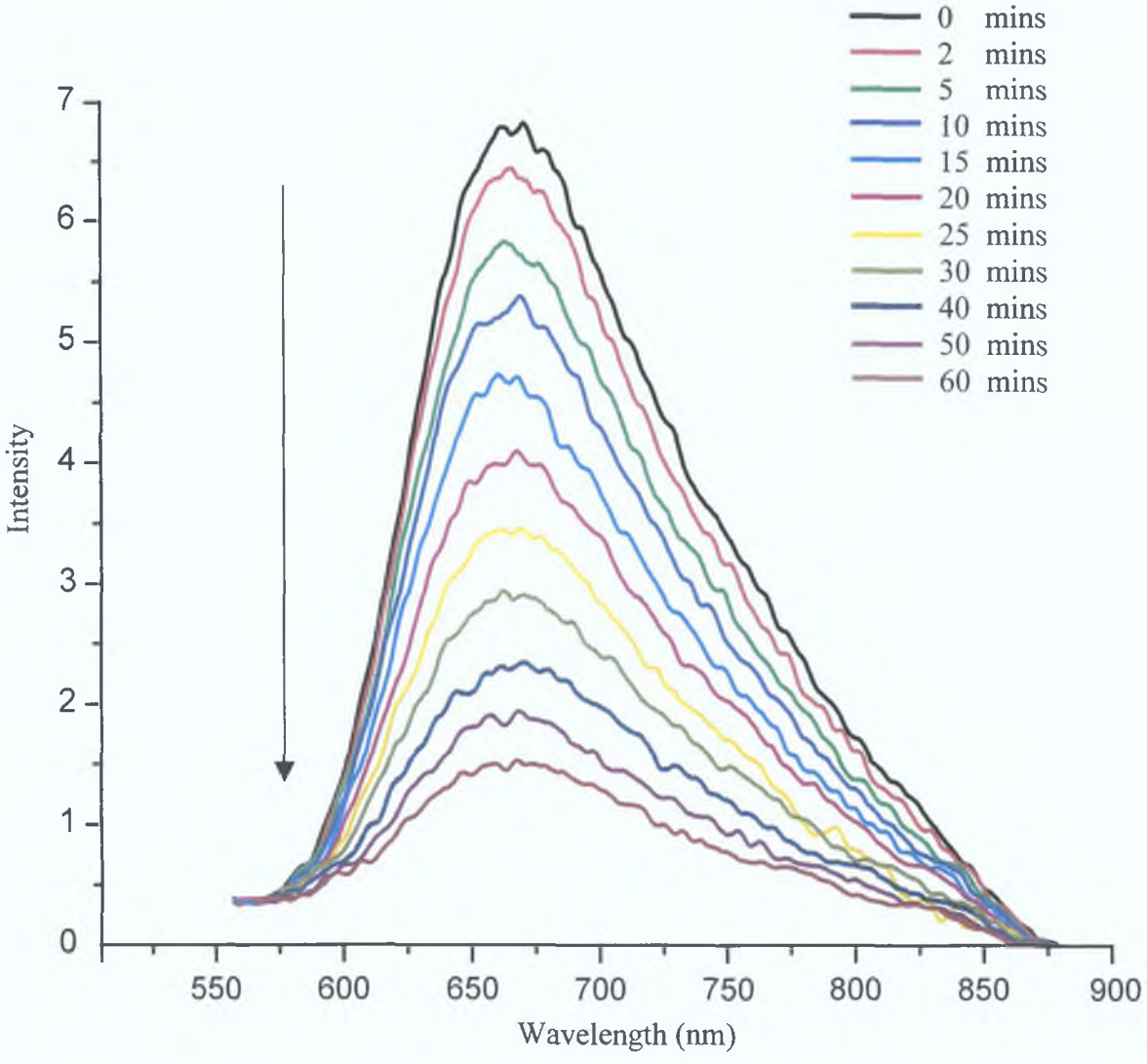

Figure 4.27 Luminescence spectroelectrochemical analysis of $[Ru(bpy)_2(L10)Ru(bpy)_2]^{2+}$ in neutral acetonitrile with 0.1 M TEAP at 1.60 V vs. Ag|AgCl

Changes in the emission spectrum at this potential were monitored over time and, as can be seen from an examination of *figure 4.27*, a loss of emission intensity is observed under these conditions. This is indicative of the oxidation of the metal from Ru^{II} to Ru^{III}. This behaviour is reminiscent of that noted in the case of the analogous methylated complex upon oxidation of the metal centre(s). Hence, it is clear that the changes occurring at this potential do, indeed, involve the metal processes.

The data obtained for the pyridyltriazole complexes are different than that noted for the pyrazyltriazole complexes. Upon the application of the initial potential of 1.00 V there is a blue shift in the λ_{max} value of about 55 nm (*figure 4.28* (*inset*)).

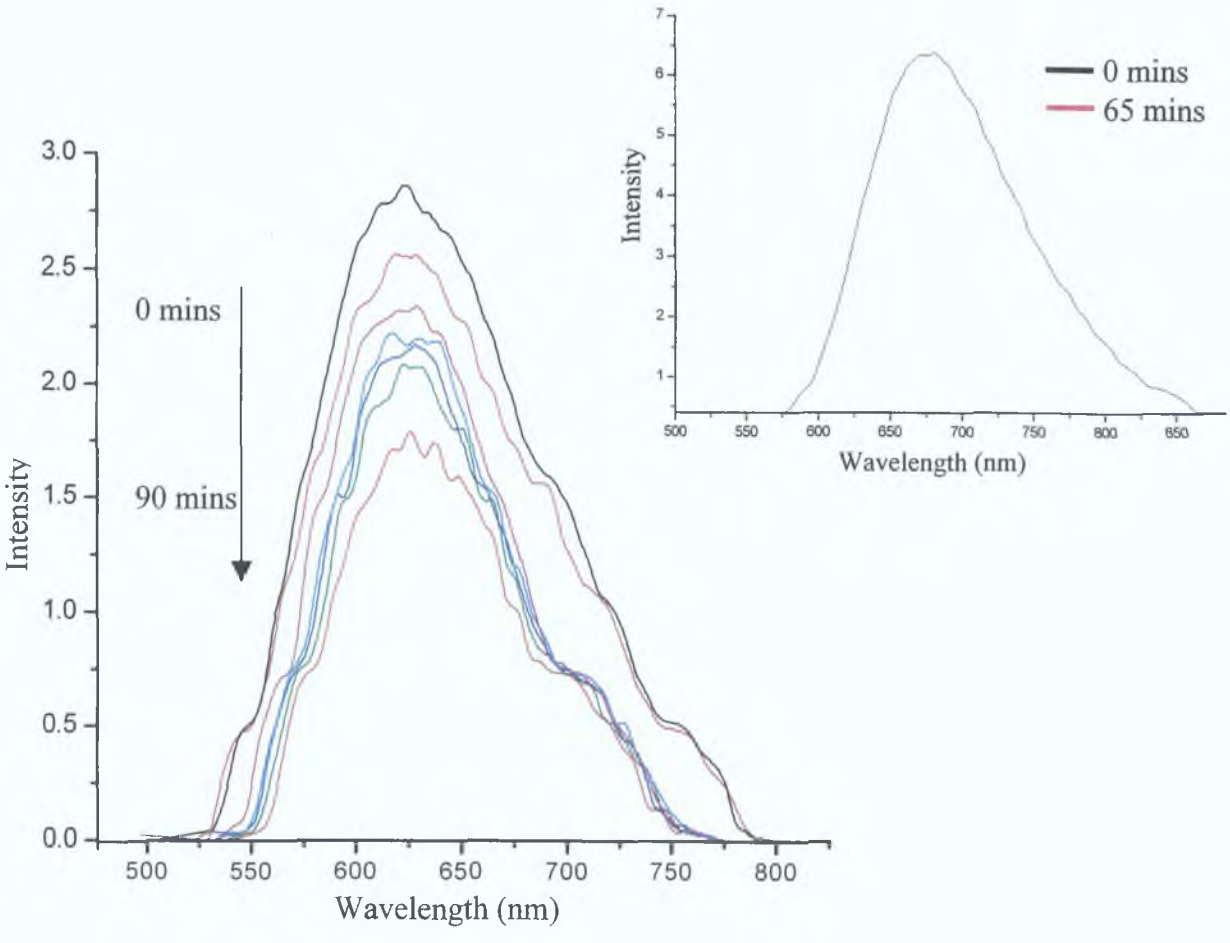

Figure 4.28 Luminescence spectroelectrochemical analysis of $[Ru(bpy)_2(L9)Ru(bpy)_2]^{2+}$ in acetonitrile with 0.1 M TEAP at 1.60 V vs. Ag|AgCl. (*Inset*) at 1.00 V vs. Ag|AgCl

These changes in the λ_{max} value are now also accompanied by a decrease in the emission at this potential. Upon increasing the potential to 1.60 V the emission is seen to deplete further as the metal is oxidised (*figure 4.28*). This behaviour is not surprising as the lifetime data in *section 4.3.4.3* and data for similar complexes indicated that protonation of the complex causes a dramatic decrease (< 20 ns) in the lifetime of the emission. [43] However, juxtaposed with the luminescence spectroelectrochemical behaviour of the pyrazyltriazole complexes, a more conclusive picture of the events occurring upon oxidation of the hydroquinone moiety(ies) emerges. This spectroelectrochemical data provides further confirmation that the hydroquinone oxidations occur prior to the metal oxidations with the concomitant protonation of the metal complex. For example, in the case of the pyridyltriazole it is clear that the initial oxidation of the hydroquinone moieties causes the changes in the spectra.

This is further evidenced by the fact the emission of the pyrazyltriazole complexes also experienced a shift in the λ_{max} value In the case of both the pyridyltriazole and the pyrazyltriazole complexes the λ_{max} value of the original complex is obtained upon returning the potential to 0 V The luminescence data hence, provides further compelling evidence of electrochemically induced proton transfer within these complexes as suggested previously by Keyes and co-workers [43]

4.7 Conclusion

The synthesis, electrochemical and spectroscopic characterisation of the ligand H3L3 and the complexes $[Ru(bpy)_2(L7)]^+$, $[Ru(bpy)_2(L8)]^+$, $[Ru(bpy)_2(L9)Ru(bpy)_2]^{2+}$ and $[Ru(bpy)_2(L10)Ru(bpy)_2]^{2+}$ which contain hydroquinone moieties are presented in this chapter These complexes are precursor molecules for the synthesis of the subsequent group of quinone-containing complexes in *chapter five* They also provide a basis for the investigation of these ensuing complexes These complexes were prepared by the demethylation of the analogous protected complex presented in *chapter three* This demethylation was achieved at low temperatures utilising an excess of boron tribromide Demethylation was verified via the loss of the –OMe peaks in the ^{1}H-NMR spectrum of the complexes accompanied by the subsequent appearance of an –OH peak above 10 50 ppm Structural and NMR data also imply the presence of a hydrogen bridge between the hydroxyl moiety and the triazolic ring

Computer generated DOS spectra provide theoretic evidence that the HOMO of these complexes is influenced by both the hydroquinone ligand and the metal while the LUMO is strongly bipyridyl in character This is in agreement with the subsequent electrochemical data Absorption spectral analyses revealed that these complexes display similar behaviour as that noted for the protected complexes However, the presence of an additional band at approximately 330 nm, and which was not present in the spectra of the protected complexes, was also noted This new band is probably associated with the presence of the hydroquinone moieties in the ligand Furthermore the possibility of generatmg semiquinone species upon the addition of base is also mooted A lack of any intermetallic interaction within $[Ru(bpy)_2(L9)Ru(bpy)_2]^{2+}$ and $[Ru(bpy)_2(L10)Ru(bpy)_2]^{2+}$ is also suggested by the absorption and electrochemical data Luminescence data was also similar to that obtained for the protected complexes Upon protonation of $[Ru(bpy)_2(L7)]^+$ and $[Ru(bpy)_2(L9)Ru(bpy)_2]^{2+}$ the emission is seen to deplete in energy due to the formation of ligands with lower σ-donation which have an increased ability to populate the ^{3}MC at room temperature This phenomenon was also supported by the lifetime data

pKa data further supported the supposition of hydrogen bridging between the hydroxyl moiety and the triazolic ring in the pyridyltriazole complexes Switching of the excited state upon protonation of the pyrazyltriazole complexes was also suggested by the luminescence analyses pKa* measurements on these complexes further supported these findings while confirming that the excited state in the pyridyltriazole complexes is bipyridyl based even upon protonation of the complex Electrochemical information gleaned with pre-treated electrodes show that the oxidation of the hydroquinone moieties within these complexes occur prior to metal oxidation while the reductions remain bipyridyl in nature as in the protected complexes These studies also suggest that the metal was protonated prior to its oxidation and that intermetallic interaction was, indeed, either very weak or non-existent Spectroelectrochemical studies supported the fact that the metal complexes were protonated prior to metal oxidation and that the processes associated with the hydroquinone moieties do occur prior to the metal oxidation Furthermore, no intermetallic communication could be established as there was either a lack of IT bands in the spectra or they were extremely weak bands

The synthesis of the quinone-containing complexes is presented in the following chapter The results of the characterisation and analysis of these complexes will further elucidate the properties observed for the complexes present within this chapter

4.8 Bibliography

1 S Patai, *The Chemistry of Quinonoid Compounds*, **1988**, Wiley-Interscience, Chichester, 2, 719

2 G E Cabaniss, A A Diamantis, W R Murphy, R W Linton, T J Meyer, *J Am Chem Soc* , **1985**, 107, 1845

3 L Hammarstrom, *Curr Op Chem Bio* , **2003**, 7, 666

4 L Sun, H Berglund, R Davydov, T Norrby, L Hammarstrom, P Korall, A Borje, C Philouze, K Berg, A Tran, M Andersson, G Stenhagen, J Mårtensson, M Almgren, S Styring, B Åkermark, *J Am Chem Soc* , **1997**, 119, 6996

5 L Sun, L Hammarstrom, B Åkermark, S Styring, *Chem Soc Rev* , **2001**, 30, 36

6 D Plancherel, J G Vos, A von Zelewsky, *J Photochem* , **1987**, 36, 257

7 J Barber, B Andersson, *Nature*, **1994**, 370, 31

8 V Balzani, F Scandola, *Comprehensive Supramolecular Chemistry*, **1996**, Pergamon Press, Oxford, 10, 688

9 G R Deviprasad, D M Eichhorn, F D'Souza, *J Chem Cryst* , **1999**, 29, 7

10 C Drexler, M W Hosseini, A De Cian, J Fischer, *Tetrahedron Letts* , **1997**, 38, 2993

11 M R Wasielewsky, *Chem Rev* , **1992**, 932, 435

12 D G Johnson, M P Niemczyk, D W Minsek, G P Wiederecht, W A Svec, G L Gaines III, M R Wasielewsky, *J Am Chem Soc* , **1993**, 115, 5692

13 M D Ryan, A Yueh, W Y Chen, *J Electrochem Soc* , **1980**, 127, 1489

14 L Papouchado, G Petrie, R N Adams, *J Electroanal Chem* , **1972**, 38, 389

15 F N Rein, R C Rocha, H E Toma, *J Electroanal Chem* , **2000**, 494, 21

16 E Laviron, *J Electroanal Chem* , **1983**, 146, 15

17 E Laviron, *J Electroanal Chem* , **1984**, 164, 213

18 E Laviron, *J Electroanal Chem* , **1986**, 208, 357

19 R A Binstead, M E McGuire, A Dovletoglou, W K Seok, L E Roecker, T J Meyer, *J Am Chem Soc* , **1992**, 114, 173

20 M Haga, E S Dodsworth, A B P Lever, *Inorg Chem* , **1986**, 25, 447

21 A D Shukla, B Whittle, H C Bajaj, A Das, M D Ward, *Inorg Chim Acta*, **1999**, 285, 89

22 M Haga, E S Dodsworth, A B P Lever, *Inorg Chem* , **1986**, 25, 447

23 A M Barthram, Z R Reeves, J C Jeffery, M D Ward, *J Chem Soc , Dalton trans* , **2000**, 3162

24 A M Barthram, R L Cleary, J C Jeffery, S M Couchman, M D Ward, *Inorg Chim Acta*, **1998**, 267, 1

25 A B P Lever, H Masui, R A Metcalfe, D J Stufkens, E S Dodsworth, P R Auburn, *Coord Chem Rev* , **1993**, 125, 317

26 C G Pierpont, R M Buchanan, *Coord Chem Rev* , **1981**, 38, 45

27 A Juris, V Balzani, F Barigelletti, S Campagna, P Belser, A von Zelewsky, *Coord Chem Rev* , **1988**, 84, 85

28 V Balzani, A Juris, M Venturi, S Campagna, S Serroni, *Chem Rev* , **1996**, 96, 759

29 H Masui, A B P Lever, P R Auburn, *Inorg Chem* , **1991**, 30, 2402

30 J C Jeffery and M D Ward, *J Chem Soc , Dalton Trans* , **1992**, 2119

31 J C Jeffery, E Schatz, M D Ward, *J Chem Soc , Dalton Trans* , **1992**, 1921

32 B M Holligan, J C Jeffery, M K Norgett, E Schatz, M D Ward, *J Chem Soc , Dalton Trans* , **1992**, 3345

33 D A Bardwell, D Black, J C Jeffery, E Schatz, M D Ward, *J Chem Soc , Dalton Trans* , **1993**, 2321

34 S Chakraborty, R H Laye, R L Paul, R G Gonnade, V G Puranik, M D Ward, G K Lahiri, *J Chem Soc , Dalton Trans* , **2002**, 1172

35 T E Keyes, P M Jayaweera, J J McGarvey, J G Vos, *J Chem Soc , Dalton Trans* , **1997**, 1627

36 T E Keyes, R Forster, P M Jayaweera, C G Coates, J J McGarvey, J G Vos, *Inorg Chem* , **1998**, 37, 5925

37 T E Keyes, D Leane, R J Forster, C G Coates, J J McGarvey, M N Nieuwenhuyzen, E Figgemeier, J G Vos, *Inorg Chem* , **2002**, 41, 5721

38 S Ernst, P Hanel, J Jordanov, W Kaim, V Kasack, E Roth, *J Am Chem Soc* , **1989**, 111, 1733

39 A K Ghosh, S M Peng, R L Paul, M D Ward, S Goswami, *J Chem Soc , Dalton Trans* , **2001**, 336

40 R S de Silva, S I Gorelsky, E S Dodsworth, E Tfouni, A B P Lever, *J Chem Soc , Dalton Trans* , **2000**, 4078

41 T E Keyes, D Leane, R J Forster, C G Coates, J J McGarvey, M N Nieuwenhuyzen, E Figgemeier, J G Vos, *Inorg Chem* , **2002**, 41, 5721

42 F M Weldon, J G Vos, *Inorg Chim Acta*, **2000**, 307, 13

43 R Wang, T E Keyes, R Hage, R H Schmehl, J G Vos, *J Chem Soc , Chem Commun* , **1993**, 1652

44 D Hughes, *Ph D Thesis*, **1999**, Dublin City University

45 L O'Brien, M Duati, S Rau, A L Guckian, T E Keyes, N M O'Boyle, A Serr, H Gorls, J G Vos, *J Chem Soc , Dalton Trans* , **2004**, 514

46 S Spyroudis, *Molecules*, **2000**, 5, 1291

47 P Passaniti, W R Browne, F C Lynch, D Hughes, M Nieuwenhuyzen, P James, M Maestri, J G Vos, *J Chem Soc , Dalton Trans* , **2002**, 1740

48 A D Shukla, B Whittle, H C Bajaj, A Das, M D Ward, *Inorg Chim Acta*, **1999**, 285, 89

49 A M W Cargill Thompson, J C Jeffery, D J Liard, M D Ward, *J Chem Soc , Dalton Trans* , **1996**, 879

50 C D Buchecker, J P Sauvage, *Tetrahedron*, **1990**, 46, 503

51 P Jacob III, P S Callery, A T Shulgin, N Castagnoli Jr , *J Org Chem* , **1976**, 41, 3627

52 O C Musgrave, *Chem Rev* , **1969**, 69, 499

53 C D Snyder, H Rapoport, *J Am Chem Soc* , **1972**, 94, 227

54 M E Jung, M A Lyster, *J Org Chem* , **1977**, 42, 3761

55 K S Schanze, K Sauer, *J Am Chem Soc* , **1988**, 110, 1180

56 L F Joulie, E Schatz, M D Ward, F, Weber, L J Yellowlees, *J Chem Soc , Dalton Trans* , **1994**, 799

57 P T Gulyas, T A Smith, M N Paddon-Row, *J Chem Soc , Dalton Trans* , **1999**, 1325

58 J L Y Kong, P A Loach, *J Heterocyc Chem* , **1980**, 17, 737

59 N Cheraiti, M E Brik, *Tetrahedron Letts* , **1999**, 40, 4327

60 V Goulle, A Harriman, J M Lehn, *J Chem Soc , Chem Comm* , **1993**, 1034

61 R Hage, J G Haasnoot, J Reedijk, R Wang, E M Ryan, J G Vos, A L Spek, A J M Duisenberg, *Inorg Chim Acta*, **1990**, 174, 77

62 M J Frisch, G W Trucks, H B Schlegel, G E Scuseria, M A Robb, J R Cheeseman, J A Montgomery, Jr , *et al* , *Gaussian 03*, **2004**, Gaussian Inc , Wallingford CT

63 Noel M O'Boyle, Johannes G Vos, *GaussSum 0 6*, **2003**, Dublin City University

64 H Rensmo, S Lunell, H Siegbahn, *J Photochem Photobiol A*, **1998**, 114, 117

65 R A Metcalfe, A B P Lever, Inorg Chem , **1997**, 4762

66 T E Keyes, C M O'Connor, U O'Dwyer, C G Coates, P Callaghan, J J McGarvey, J G Vos, *J Phys Chem A*, **1999**, 103, 8915

67 J S Killeen, *Ph D Thesis*, **2003**, Dublin City University

68 W R Browne, D Hesek, J F Gallagher, C M O'Connor, J S Killeen, F Aoki, H Ishida, Y Inoue, C Villani, J G Vos, *J Chem Soc , Dalton Trans* , **2003**, 2597

69 B E Buchanan, J G Vos, M Kaneko, W J M van der Putten, J M Kelly, R Hage, R A G de Graaff, R Prins, J G Haasnoot, J Reedijk, *J Chem Soc , Dalton Trans* , **1990**, 2425

70 R Hage, A H J Dijkhuis, J G Haasnoot, R Prins, J Reedijk, B E Buchanan, J G Vos, *Inorg Chem* , **1988**, 27, 2185

71 R Wang, J G Vos, R H Schmehl, R Hage, *J Am Chem Soc* , **1992**, 114, 1964

72 H H Thorp, J E Sumeski, G W Brudvig, R H Crabtree, *J Am Chem Soc* , **1989**, 111, 9249

73 F Barigelletti, L De Cola, V Balzani, R Hage, J G Haasnoot, J Reedijk, J G Vos, *Inorg Chem* , **1989**, 28, 4344

74 S Serroni, S Campagna, G Denti, T E Keyes, J G Vos, *Inorg Chem* , **1996**, 35, 4513

75 C Y Duan, Z L Lu, X Z You, Z Y Zhou, T C W Mak, Q Luo, J Y Zhou, *Polyhedron*, **1998**, 17, 4131

76 S Fanni, T E Keyes, S Campagna, J G Vos, *Inorg Chem* , **1998**, 37, 5933

77 Y Hou, P Xie, K Wu, J Wang, B Zhang, Y Cao, *Solar En Mat Solar Cells*, **2001**, 70, 131

78 S Fanni, T E Keyes, C M O'Connor, H Hughes, R Y Wang, J G Vos, *Coord Chem Rev* , **2000**, 208, 77

79 M Wrighton, D L Morse, *J Am Chem Soc*, **1974**, 96, 996

80 C G Coates, T E Keyes, H P Hughes, P M Jayaweera, J J McGarvey, J G Vos, *J Phys Chem A*, **1998**, 102, 5013

81 H A Nieuwenhuis, J G Haasnoot, R Hage, J Reedijk, T L Snoeck, D J Stufkens, J G Vos, *Inorg Chem*, **1991**, 30, 48

82 R Hage, J G Haasnoot, J Reedijk, R Wang, J G Vos, *Inorg Chem*, **1991**, 30, 3263

83 T E Keyes, *Ph D Thesis*, **1994**, Dublin City University

84 W R Browne, C M O'Connor, H P Hughes, R Hage, O Walter, M Doering, J F Gallagher, J G Vos, *J Chem Soc, Dalton Trans*, **2002**, 4048

85 J G Vos, *Polyhedron*, **1992**, 11, 2285

86 R J Crutchley, A B P Lever, *Inorg Chem*, **1982**, 21, 2277

87 J C Curtis, J S Bernstein, T J Meyer, *Inorg Chem*, **1985**, 24, 385

88 D E Richardson, H Taube, *Inorg Chem*, **1981**, 20, 1278

89 R C Rocha, H E Toma, *Inorg Chem Commun*, **2001**, 230

90 J B Flanagan, S Margel, A J Bard, F C Anson, *J Am Chem Soc*, **1978**, 100, 4248

91 C Creutz, H Taube, *J Am Chem Soc*, **1969**, 91, 3988

92 G A Heath, L J Yellowlees, P S Braterman, *J Chem Soc, Chem Commun*, **1981**, 287

93 M K Nazeeruddin, S M Zakeeruddin, K Kalyanasundaram, *J Phys Chem*, **1993**, 97, 9607

94 C Creutz, Prog *Inorg Chem*, **1983**, 30, 1

95 R W Callaghan, F R Keene, T J Meyer, D J Salmon, *J Am Chem Soc*, **1977**, 99, 1064

96 J R Kirchhoff, *Current Sep*, **1997**, 16, 11

Chapter Five

Mono- and Dinuclear Ruthenium(II) Complexes Containing Quinone Moieties

This chapter presents the synthesis, characterisation and photophysical properties of mononuclear and dinuclear ruthenium (II) complexes containing quinone moieties. The complexes presented in this chapter are the daughter compounds of those previously discussed in chapter three and are distinguished by the presence of either pyrazyl- or pyridyl-1,2,4-triazole unit(s) in conjunction with quinone moieties. This final group of complexes are synthesised in a novel manner from their dimethoxy analogues and the ensuing photophysical and electrochemical data examines the behaviour of ruthenium (II) compounds coupled to quinone ligands via a negatively charged bridge.

5.1 Introduction

The pivotal role performed by quinones in natural photosynthesis has been well established and the role that these electron-accepting species play in this process has been detailed previously in the introductory chapter (*section 1.1.1*) [1-3] The extraordinary characteristics of quinones may be attributed to the fact that they possess low-lying unoccupied electronic energy levels and are, therefore, ready acceptors of electrons [4] Hence, these species have been widely utilised in systems which attempt to mimic the reaction centre in natural photosynthesis Indeed, in dyad and triad systems, which attempt to mimic the photoinduced charge separation process of photosynthesis, the most widely used electron-acceptors are those of the quinone family [5] Porphyrins have taken a central role in these mimetic systems with a variety of porphyrin-quinone derivatives developed as models for photosynthetic charge separation [6-9] Zimmermann *et al* [10] and Aoyama *et al* [11] for example, have investigated photoinduced electron transfer within porphyrin-quinone dyads with the ultimate goal of constructing photosynthetic-mimetic molecular devices (PMDs) for efficient charge separation by functional qumone derivatives

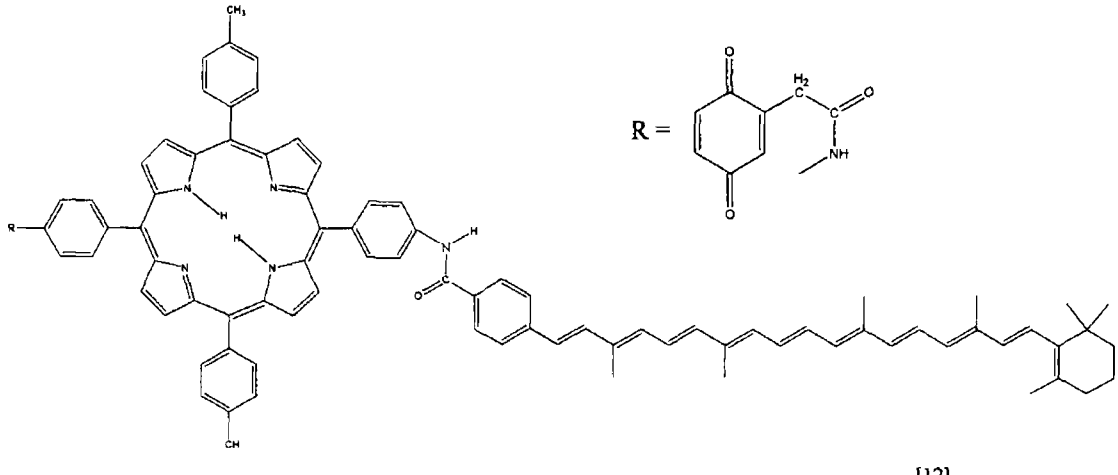

Figure 5.1 A molecular triad containing a quinone moiety [12]

Molecular triads have also been created consisting of porphyrins linked to both carotenoid polyenes and qumones The triad molecule in *figure 5.1* for example, was constructed in order to examine charge separation [12] As in porphyrin-quinone dyad molecules this molecule was found to carry out photodriven electron transfer in good yield In addition the triads produce energetic charge-separated states with lifetimes on the microsecond timescale [9][12-14]

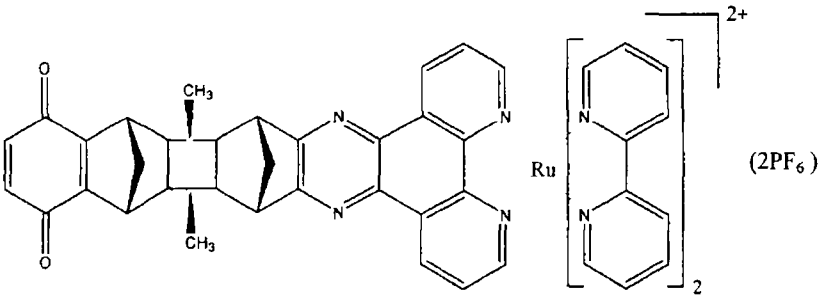

Figure 5 2 Ruthenium-quinone mononuclear complex synthesis by Guylas *et al* [15]

In the past few years there have also been a number of studies involving systems, particularly of ruthenium complexes, containing these strongly π-accepting quinonoid ligands [16-25] Some of these systems have been developed in order to examine intramolecular electron transfer within these systems which is a necessary characteristic in the design of PMDs Much attention is currently being paid to the development of such artificial PMDs [26][27] Guylas *et al* for example, synthesised mononuclear complexes in which $[Ru^{II}(bpy)_2]$ acting as an electron donor was tethered via a rigid bridge to either 1,4-naphthoquinone or 1,4-benzoquinone moieties in order to study intramolecular electron transfer (*figure 5 2*) [15]

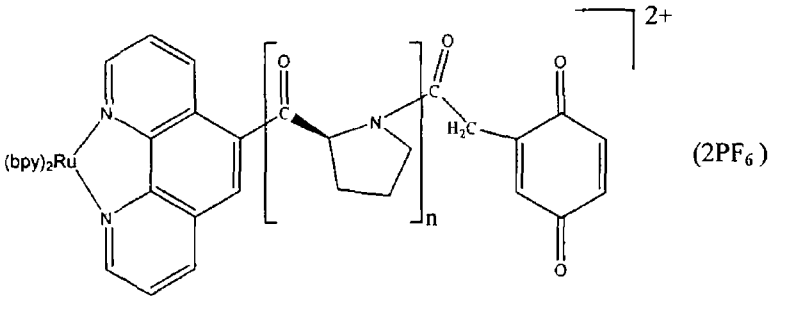

Figure 5 3 Ruthenium-quinone complex synthesised by Schanze and Sauer [28]

Schanze and Sauer also examined intramolecular electron transfer in peptide-bridged molecules (*figure 5 3*) In their complex the ruthenium(II) polypyridyl unit functioned as a photoexcited electron donor while a series of oligo(L-proline) spacers separated the *p*-benzoquinone moiety which acted as an electron acceptor [28] Within this system the rate of intramolecular electron transfer was seen to decrease as the number of bridging moieties and hence, the distance from the ruthenium centre to the quinone was increased This principle of photoinduced electron transfer can be applied to switch on/off a luminescence signal by means of a redox reaction

For instance, some species can be electrochemically converted into two different forms, one of which can, and the other cannot, quench the excited state of a connected luminescent component. For example, Lehn and co-workers synthesised the following ruthenium complex (*figure 5.4*) in which the $[Ru(bpy)_2(bpy')]^{2+}$ (P) moiety in its luminescent ^{3}MLCT excited state is a reductant strong enough to reduce the connected quinone unit (Q).

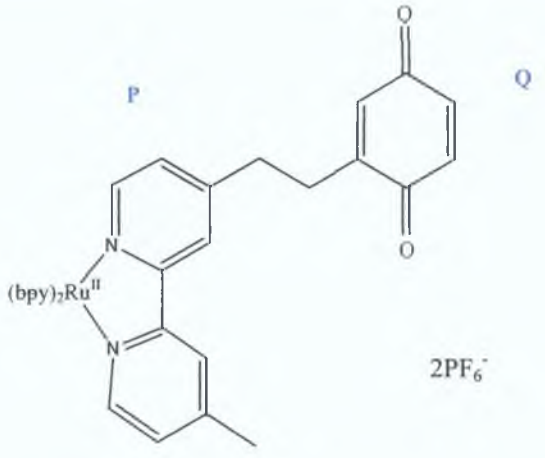

Figure 5.4 Ruthenium-quinone complex synthesised by Lehn and co-workers.[29]

Since, this electron transfer process is very fast, the luminescence of the ^{3}MLCT state is completely quenched. Quenching is followed by very fast back electron transfer, which leads to the ground state of the supramolecular compound.

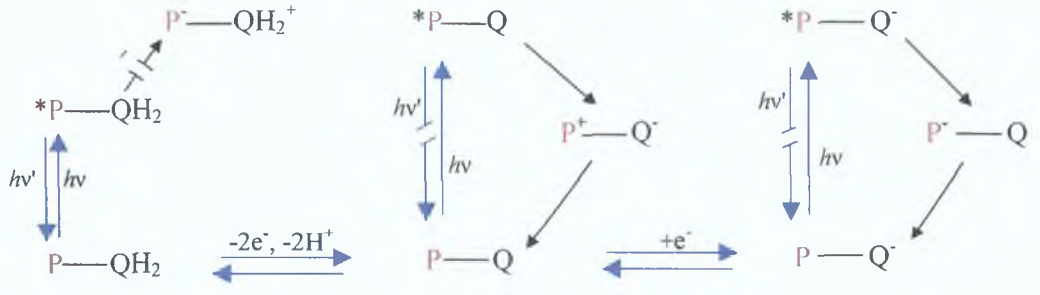

Figure 5.5 Switching of the $[Ru(bpy)_2(bpy')]^{2+}$ luminescence by reduction and protonation of a connected quinone. [29][30]

When the reduction process is performed in aqueous acetonitrile, reduction of the quinone units is followed by protonation with formation of the corresponding hydroquinone. Protonation of the reduced species promotes its stabilisation. [30] This process is illustrated in *figure 5.5* and is an excellent example of an electro-photoswitching device.

There has been also been considerable interest in the study of transition metal complexes of noninnocent, quinone-related ligands including those of dithiolenes, dioxolenes and benzoquinonediimines [31 33][20-22] The possibility of electron delocalisation between the metal and the ligand has been a major theme in the study of these systems and previous studies of ruthenium dioxolene complexes have found unusually large degrees of orbital mixing between the metal and the ligand [20 22][34][35] Indeed, a number of these ruthenium complexes containing quinoidal species have been discussed in preceding chapters

Finally, Meyer and co-workers prepared a series of chromophore-quencher complexes that incorporate the anthroquinone-based acceptor ligand and the donor bpy-PTZ ligand (*figure 5 6*)

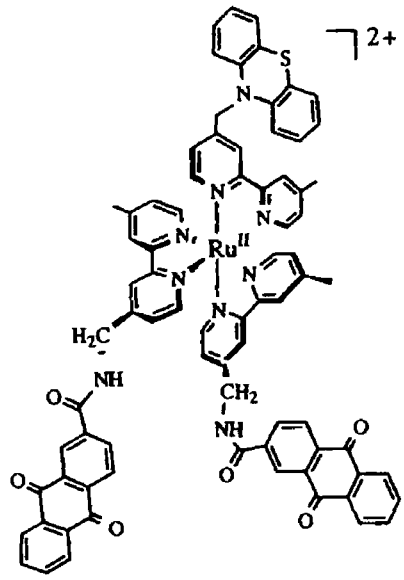

Figure 5 6 $[Ru^{II}(bpy\text{-}AQ)_2(bpy\text{-}PTZ)]^{2+}$ synthesised by Meyer and co-workers [36]

Their results provide evidence that the presence of the attached quinone group in $[Ru^{II}(bpy\text{-}AQ)_2(bpy\text{-}PTZ)]^{2+}$ (*figure 5 6*) led to a significant level of quenching of the MLCT emission Hence, this donor-chromophore-acceptor complex has the potential to mimic the photosynthetic electron processes similar to the natural photosynthetic system However, the speed of back electron transfer processes is the limiting factor within such systems and an increase in the lifetime of MLCT excited state is required [36] Vos and co-workers have provided a novel solution to this problem by synthesising complexes containing triazole moieties designed to achieve a longer-lived charge separated-state [37]

Indeed, they have provided evidence of a complex in which a reversible, electrochemically induced proton transfer reaction occurs from a hydroquinone to an attached triazole ring [38] This system has been discussed previously in detail in *chapter four* (*section 4 1, scheme 4 1*) and further evidence for the occurrence of the phenomenon of electrochemically induced proton transfer within these systems was also provided in *chapter four* Fanni *et al* have also prepared ruthenium complexes in which a donor group is attached to ruthenium via a negatively charged triazole group [39]

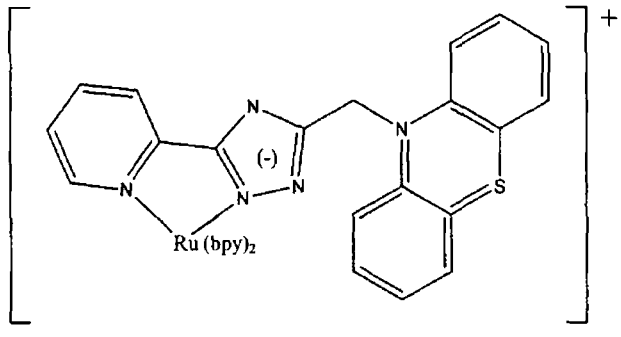

Figure 5 8 Structure of mononuclear ruthenium complex containing a phenothiazine (PTZ) group synthesised by Fanni *et al* [39]

The structure of their complex, which contains a phenothiazine (PTZ), a triazole and a pyridyl ligand, is shown in *figure 5 8* It was hoped that the inclusion of a PTZ donor linked to a bridging ligand which is *not involved* in the luminescent ^{3}MLCT state and is *negatively charged* might decrease the coupling between the donor and the excited state and hence, the rate of intramolecular charge recombination, which eventually leads to the decay of the charge separated state, might decrease Their study found that such anionic bridges could effectively mediate electron-transfer processes in covalently linked chromophore-quencher complexes [39] In this chapter the final range of complexes containing quinone groups are presented These complexes are the quinone analogues of the complexes contained in *chapter four* and provide a further basis for the understanding of the processes involved in complexes which contain quinone groups coupled to a ruthenium centre(s) via a negatively charged bridge

The structure and nomenclature of the complexes presented in this chapter are depicted in *figure 5 7* In the next section the novel synthetic procedure adopted to synthesise these complexes are presented Their purity was, hence, assessed by NMR spectroscopy, FTIR and elemental analysis and these data are also contained in the following characterisation section The complexes were then further characterised by emission and absorption spectroscopy The ground and excited state lifetimes data for each of the complexes have also been measured and are reported in the succeeding section

Since, the electrochemical behaviour of these complexes are dramatically different to the proceeding methylated and hydroquinone-containing complexes, in depth electrochemical characterisation has also been preformed Hence, the oxidations of the metal centre(s) as well as the ligand-based reductions are presented in the electrochemical section In order to investigate the nature of the lowest unoccupied molecular orbital (LUMO) acid-base measurements were also undertaken and the results of these measurements are presented along with relevant pKa and pKa* values Once again, this characteristic varied depending on whether the complex contained a pyridyltriazole or a pyrazyltriazole moiety Finally, spectroelectrochemical techniques were employed and hence, a comprehensive set of data for these quinone-containing complexes are presented in this chapter Each set of data are discussed with particular reference to their analogous hydroquinone-containing complexes outlined in *chapter four* and the ability of these quinone complexes to be quenched by the quinone moieties is investigated in light of the presence of the triazole bridge

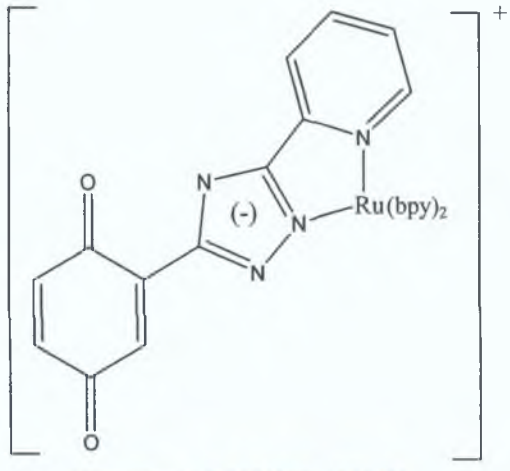

$[Ru(bpy)_2(L11)]PF_6.2H_2O$

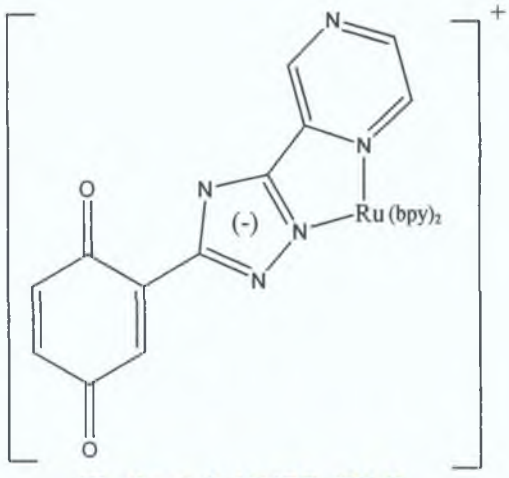

$[Ru(bpy)_2(L12)]PF_6.2H_2O$

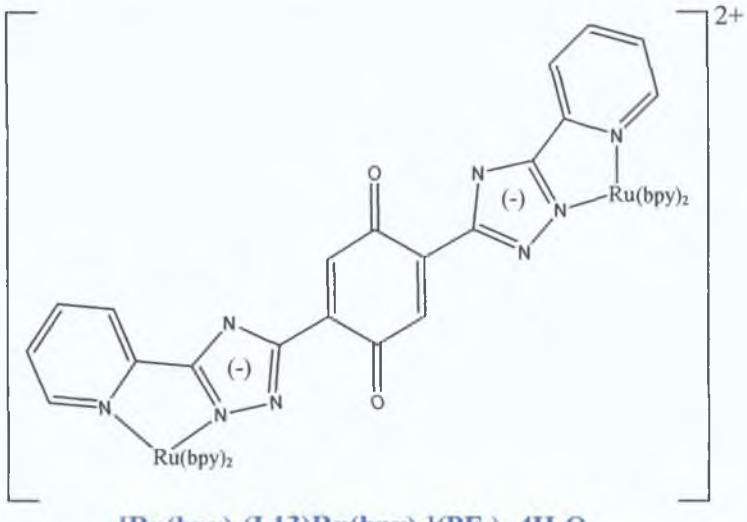

$[Ru(bpy)_2(L13)Ru(bpy)_2](PF_6)_2.4H_2O$

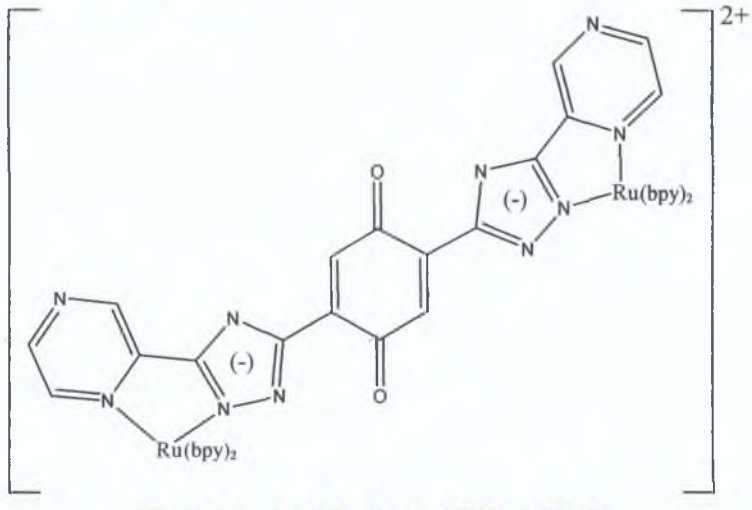

$[Ru(bpy)_2(L14)Ru(bpy)_2](PF_6)_2.4H_2O$

Figure 5.7 Structures of mononuclear and dinuclear complexes cited in this chapter.

5.2 Experimental Methodology

5.2.1 Synthesis of Quinone Complexes

The synthesis of the ruthenium(II) complexes containing pendant quinone moieties is presented in this section. The complexes were prepared directly from the protected complexes containing in *chapter three,* however, it is also possible to prepare these complexes via the hydroquinone analogues in *chapter four*. The synthesis of these complexes was achieved via modified literature methods utilised for the oxidative demethylation of *p*-dimethoxybenzene derivatives. Ceric(IV) ammonium nitrate $[Ce(NH_4)_2(NO_3)_6]$ (CAN) in aqueous acetonitrile was employed for the demethylation as this agent has been known to produce quinones often in high yield from their corresponding dimethoxy analogues.[40][41] All modifications and complications associated with this procedure are discussed in the following section (*section 5.3.1.1*).

Complex 11: $[Ru(bpy)_2(L11)]PF_6.3H_2O$

$[Ru(bpy)_2(L3)]PF_6.H_2O$ (200 mg, 0.24 mmol) was dissolved in acetonitrile (25 cm^3) and stirred at room temperature. To this solution was added, dropwise, cerium(IV) ammonium nitrate (4.0 g, 0.73 mmol) in water (20 cm^3) over a 10 min period. At this point a transient darkening to a blue / black colour was observed. The reaction mixture continued stirring for 40 min at room temperature after which time the solution was extracted with chloroform (2 x 30 cm^3). The combined organic extracts were then washed with water (3 x 30 cm^3) and dried over $MgSO_4$, filtered and concentrated under reduced pressure. The product was purified by recrystallisation from hot ethanol (3 cm^3) and the purified quinone complex was then collected on a glass frit and dried in vacuo. Purity was established by the ^{1}H-NMR spectrum and analytical HPLC. Yield = 71 mg (36 %). Calculated for $RuC_{33}N_8H_{30}O_5PF_6$: C: 45.57; H: 3.08; N: 12.80 %. Anal. Found: C: 45.56; H: 2.88; N: 12.43 %. A Carbonyl (C=O) stretching band at 1660 cm^{-1} was also noted in the IR spectrum.

Complex 12: **$[Ru(bpy)_2(L12)]PF_6.3H_2O$**

This complex was prepared in a similar manner as that described previously for **complex 11** with the exception that 200 mg (0.196 mmol) of $[Ru(bpy)_2(L4)]PF_6.H_2O$ was dissolved in acetonitrile in place of $[Ru(bpy)_2(L3)]PF_6.H_2O$. Cerium(IV) ammonium nitrate (3.3 g, 0.60 mmol) in water (20 cm^3) was then added to over a 10 min period and after stirring at room temperature for 40 min the quinone complex was collected as described previously. Purity was, once again, established by the ^{1}H-NMR spectrum and analytical HPLC. Yield = 127 mg (64 %). Calculated for $RuC_{32}N_9H_{28}O_5PF_6$: C: 44.34; H: 3.06; N: 13.55 %. Anal. Found: C: 44.32; H: 2.79; N: 13.66 %. A Carbonyl (C=O) stretching band at 1660 cm^{-1} was noted in the IR spectrum.

Complex 13: **$[Ru(bpy)_2(L13)Ru(bpy)_2](PF_6)_2.5H_2O$**

$[Ru(bpy)_2(L13)Ru(bpy)_2](PF_6)_2.4H_2O$ was, once again, prepared by an analogous method as that outlined for the above mononuclear complexes. During the preparation of this complex, however, $[Ru(bpy)_2(L5)Ru(bpy)_2](PF_6)_2.4H_2O$ (400 mg, 0.26 mmol) was used in place of the dimethoxy mononuclear complex. The complex was obtained as described above and purity was then established by the ^{1}H-NMR spectrum and analytical HPLC. Yield = 187 mg (47 %). Calculated for $Ru_2C_{60}N_{16}H_{52}O_7P_2F_{12}$: C: 43.05; H: 3.01; N: 13.09 %. Anal. Found: C: 42.90; H: 2.70; N: 12.83 %. A Carbonyl (C=O) stretching band at 1660 cm^{-1} was noted in the IR spectrum of this complex.

Complex 14: **$[Ru(bpy)_2(L14)Ru(bpy)_2](PF_6)_2.5H_2O$**

Once again, the same methodology as previously outlined for the proceeding complexes was utilised. However, 400 mg (0.26 mmol) of $[Ru(bpy)_2(L6)Ru(bpy)_2](PF_6)_2.4H_2O$ was dissolved in acetonitrile and stirred at room temperature. The solid product that precipitated was recrystallised and dried as previously outlined and the purity was established by the ^{1}H-NMR spectrum and analytical HPLC. Yield = 173 mg (43 %). Calculated for $Ru_2C_{58}N_{18}H_{50}O_7P_2F_{12}$: C: 40.26; H: 2.92; N: 14.58 %. Anal. Found: C: 40.20; H: 2.59; N: 14.53 %. A Carbonyl (C=O) stretching band at 1660 cm^{-1} was, once again, noted in the IR spectrum.

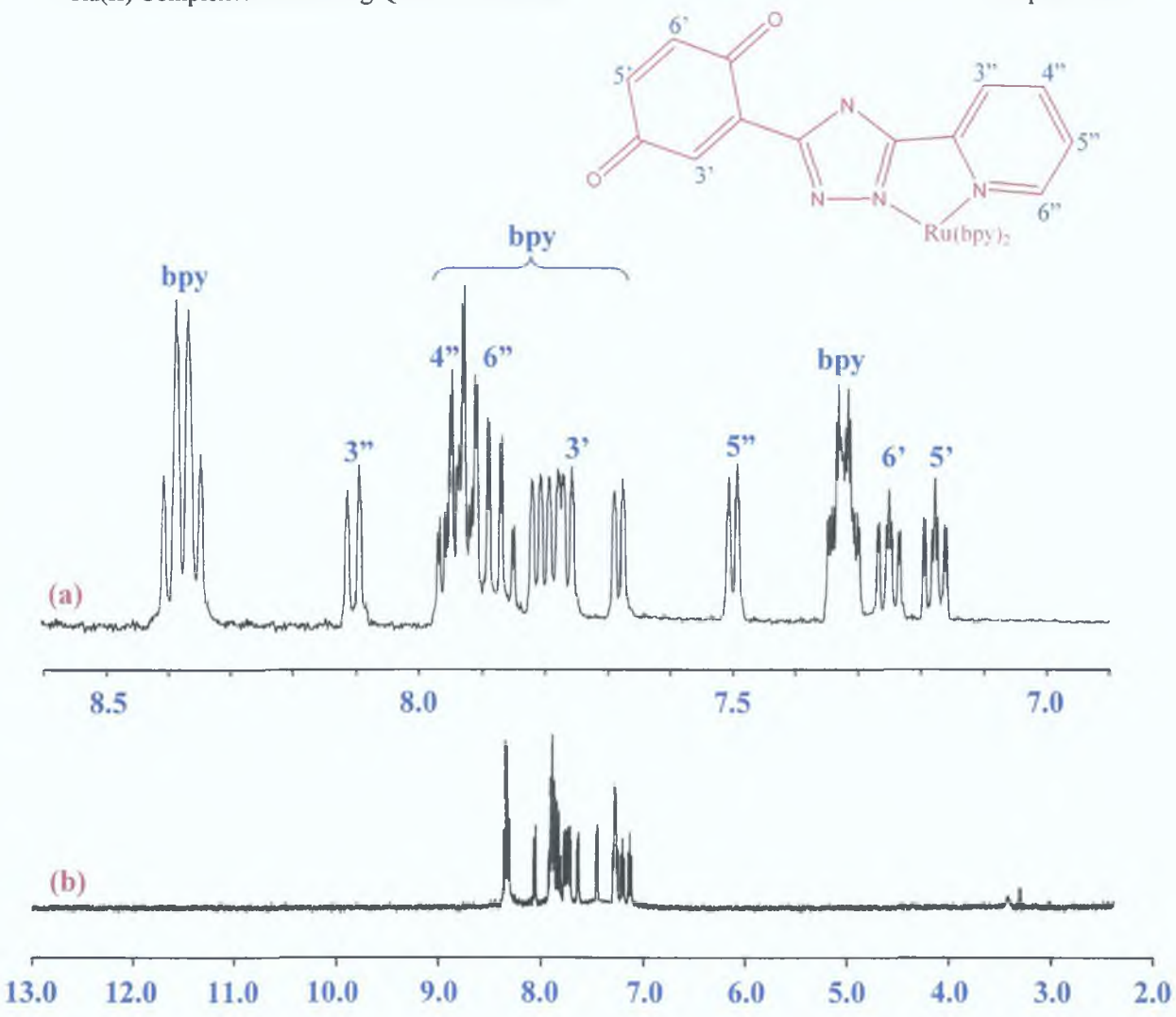

Figure 5.9 ^{1}H-NMR spectra of the complex $[Ru(bpy)_2(L11)]^+$ (a) from 7.0 – 8.5 ppm and (b) from 13.0 – 2.5 ppm in d_3-acetonitrile.

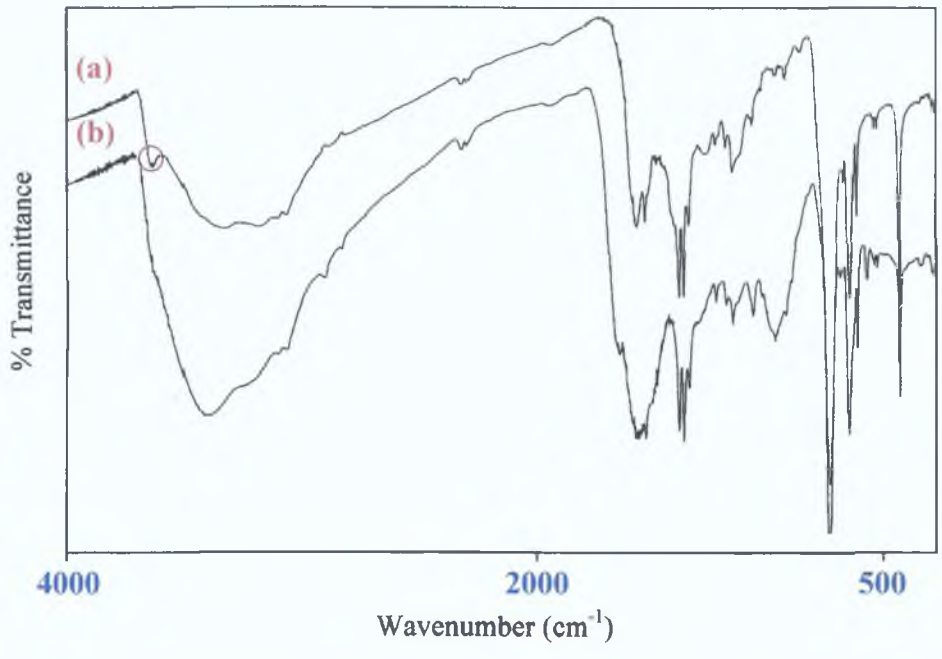

Figure 5.10 IR spectra of (a) $[Ru(bpy)_2(L7)]^+$ and (b) $[Ru(bpy)_2(L11)]^+$ in chloroform.

5 3 Results and Discussion

5 3 1 Synthetic Considerations

The synthesis of quinone containing complexes has been achieved in a variety of different manners The oxidation of ligands, such as, *p*-dimethoxybenzene to their corresponding benzoquinones has been accomplished using an assortment of oxidising agents, for example, nitric acid or argentic acid [42][43] Nitric acid has been found to work well for highly substituted 1,4-dimethoxybenezene derivatives, however, in some instances nitration of the aromatic ring occurs in addition to or instead of demethylation [40] Argentic acid has also been widely used, however, the expense of this reagent is a limiting factor for large-scale preparations Furthermore, both nitric acid and argentic acid are strongly acidic media, and acid labile functional groups may, therefore, not be tolerated [40] Therefore, a milder method for the oxidative demethylation of p-dimethoxybenzene derivatives was found by utilising ceric ammonium nitrate $[Ce(NH_4)_2(NO_3)_6]$ (CAN) in aqueous solutions Reactions involving this reactant were found to yield the qumone product in generally high yields and furthermore the reaction can be performed without strong acid in a generally fast reaction requiring only a few minutes reaction time at room temperature

Complexes similar to the qumone containing complexes presented in this chapter have been prepared via a plethora of different methodologies Schanze and Sauer, for example, synthesised similar complexes (*figure 5 3*) by first demethylating their dimethoxy ruthenium complex with BBr_3 as described in *chapter four* to yield the corresponding hydroquinone complexes These complexes were then treated further with 2,3-dichloro-5,6-dicyanoquinone (DDQ) to yield the corresponding quinone complexes [28] This procedure proved successful and no further purification was required as no impurities were formed However, the reaction conditions required that the reaction be carried out under argon coupled to the fact that a two-step procedure for the production of quinones consequently results in lower overall yields than the one step procedure adopted in this study Guylas *et al* also utilised CAN, however initially, they demethylated the methoxylated ligand to yield the quinone analogue prior to complexation with ruthenium (*figure 5 2*) [15]

This method, however, can result in purification problems, as quinones are known to degrade during column chromatography [28] An alternative approach, which was also found to successfully produce the quinone complexes described in this chapter, was also undertaken by Gulyas *et al* BBr_3 was employed as the oxidising agent to obtain the hydroquinone containing ligands that were then further treated with PbO_2 to yield the quinone complex [44] This two-step method, however, would necessarily decrease the overall yield of quinone obtainable Benzeneseleninic acid has also been reported as a viable agent for the production of qumones, however, once again, the procedure is not as mild as those mvolving CAN [45]

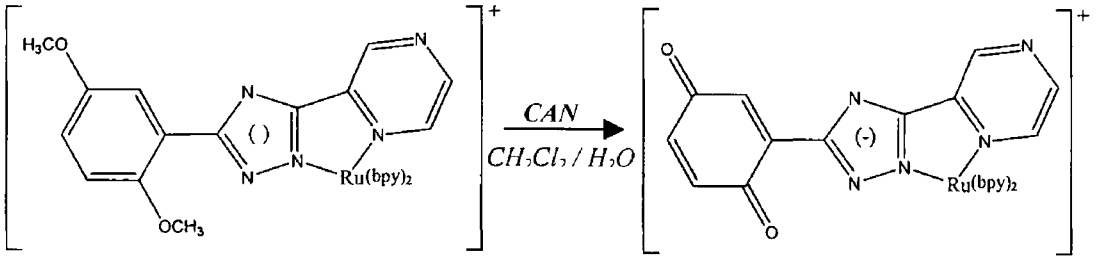

Figure 5.11 Oxidative demethylation procedure for $[Ru(bpy)_2(L4)]^{2+}$ via CAN to yield the qumone complex $[Ru(bpy)_2(L12)]^{2+}$

The quinone complexes presented in this chapter were obtained by treating the methylated complexes presented in *chapter three* with CAN in an aqueous solution (*figure 5 11*) This is similar to the synthetic approach reported by Lehn and co-workers for their quinone-containing complex (*figure 5 4*) [29] Treatment of the hydroquinone containing complexes proved just as straightforward for oxidation to their corresponding quinone analogue However, adopting a two-step procedure for the production of these complexes would decrease the overall yields of the quinone containing complexes considerably Likewise, synthesising the quinone complexes following the production of the quinone ligands would also have affected overall yields Furthermore, this would have caused purification problems as it has been observed that purification of these complexes via column chromatography results in further impurities arising due to contamination of the samples with strongly luminescent impurities as a result of reduction of the quinone [28] Finally, establishing the mode of complexation to the metal unit(s) can be quite complex and by demethylating a complex of established structure these complications are negated

5.3.2 Characterisation Considerations

^{1}H-NMR spectroscopy was utilised in the assessment of the purity and structural assignment of the complexes presented in this chapter while successful demethylation of the complexes was further confirmed via IR spectroscopy. *Table 5.1* contains NMR data for the coordinated quinone ligands in each complex and the ^{1}H-NMR spectrum of complex $[Ru(bpy)_2(L11)]^+$ in d_3-acetonitrile is shown in *figure 5.9*(b).

Reasonances for coordinated ligands L11-L14

(chemical shifts / ppm vs Me_4Si)

	11	*12*	*13*	*14*
$H^{3'}$	7.76(s)	7.32(d)	7.44(s)	7.48(s)
$H^{5'}$	7.18(m)	7.05(m)		
$H^{6'}$	7.26(m)	7.10(m)	7.44(s)	7.48(s)
$H^{3''}$	8.11(d)	9.10(s)	8.96(d)	9.34(s)
$H^{4''}$	7.94(t)		7.80(dd)	
$H^{5''}$	7.49(d)	7.57(d)	7.24(t)	7.73(d)
$H^{6''}$	7.88(d)	8.16(d)	7.48(d)	8.38(d)

* For an explanation of numbering see *figure 5.9*.

Bipyridyl reasonances were observed in the following regions for:

[1] *Pyridyltriazole complexes*: 8.30-8.55(**H^3**); 7.85-8.10(**H^4**); 7.20-7.45(**H^5**); 7.60-7.80(**H^6**).

[2] *Pyrazyltriazole complexes*: 8.20-8.60(**H^3**); 7.85-8.10(**H^4**); 7.10-7.50(**H^5** / **H^6**).

Table 5.1 ^{1}H-NMR spectral data for complexes 11 - 14 measured in d_3-acetonitrile.

These spectral tools along with the spectra obtained for the methoxy and hydroquinone analogous complexes allowed for successful elucidation of the structure of these quinone complexes. The spectrum of $[Ru(bpy)_2(L11)]^+$ is shown in *figure 5.9* and is typical of the spectra obtained for these quinone complexes. The spectra are clean and well resolved, integrate to the expected number of protons and are, therefore, consistent with the expected structure. Sharp, well-defined reasonances were observed for all complexes, confirming the presence of Ru^{II} and the absence of semiquinone radicals. [46]

In *chapter three* the ^{1}H-NMR spectra of the protected mononuclear complexes $[Ru(bpy)_2(L3)]^+$ and $[Ru(bpy)_2(L4)]^+$ contained two singlet resonances at approximately 3.70 ppm, which were associated with the methoxy moieties. [37]

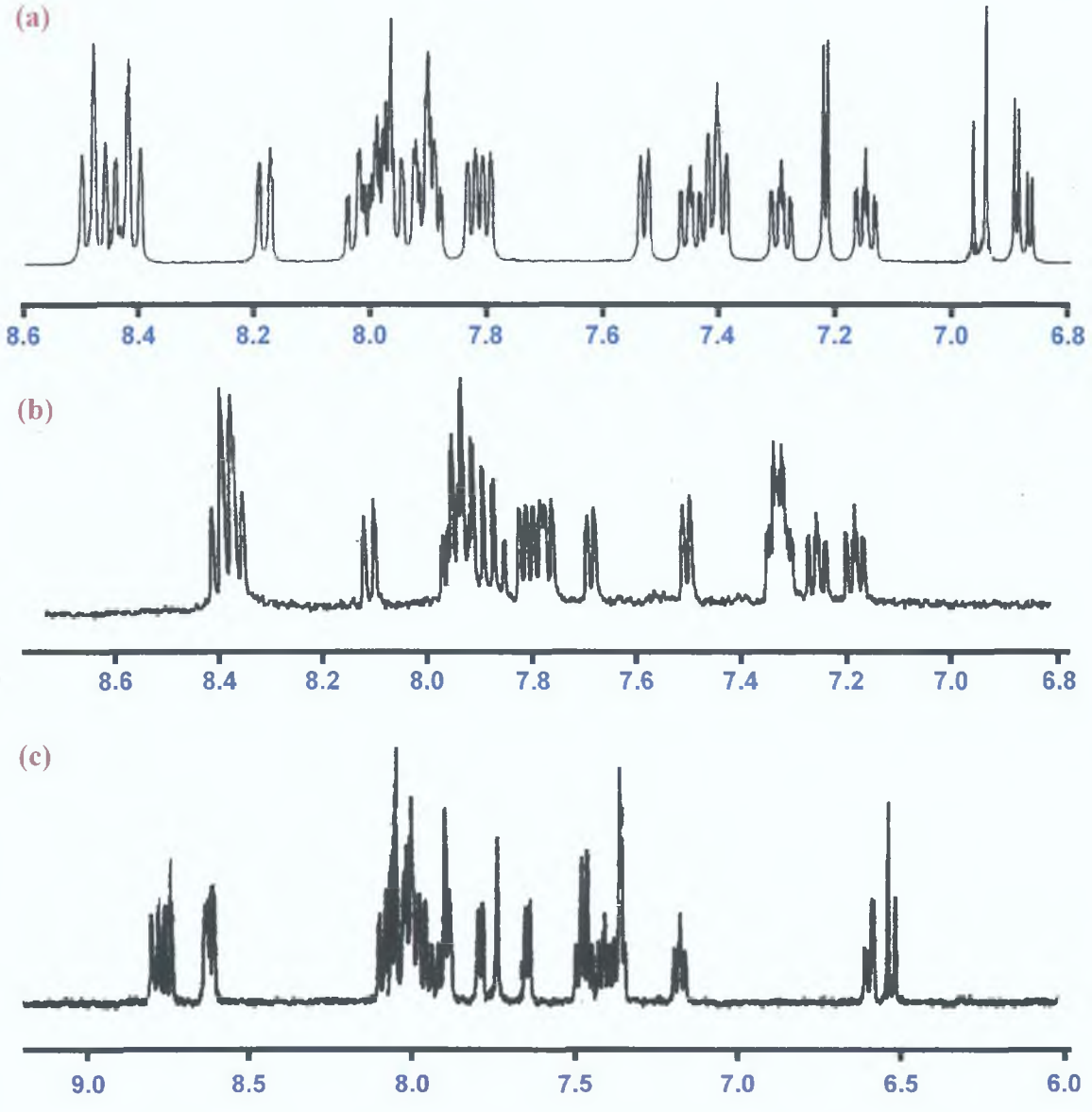

Figure 5.12 ^{1}H-NMR spectra of the complexes $[Ru(bpy)_2(L3)]^+$ (a), $[Ru(bpy)_2(L11)]^+$ (b) and $[Ru(bpy)_2(L7)]^+$ (c) in d_3-acetonitrile.

While in the case of the dinuclear complexes these signals were expressed as one large peak due to the equivalency of these moieties. Upon treatment of these complexes with CAN these peaks are seen to disappear (*figure 5.9*). In *chapter four*, the loss of these methoxy peaks is accompanied by the concomitant appearance of a broad –OH peak above 10.50 ppm.

This feature is not observed in the spectra of the quinone containing complexes further confirming the demethylation of the protected complexes to their quinone analogues and not merely to the hydroquinone analogues However, the NMR spectra obtained for these quinone complexes are similar to those of the hydroquinone species with the clear exception for the signals associated with the quinone protons This is the same situation as noted by Schanze *et al* who also observed a similar comparability of spectra of the hydroquinone and the quinone complexes [28] In the spectrum shown in *figure 5 9* the quinone protons appear as mulitplets at 7 18 and 7 26 ppm This is a considerable shift of these protons compared to either the hydroquinone or the protected analogues *Figure 5 12* contains the ^{1}H-NMR spectrum of each of the mononuclear pyridyltriazole complexes showing the shift of the protons associated with quinone moiety(ies)

The IR spectra for the complexes were also obtained *Figure 5 10* shows the spectra of $[Ru(bpy)_2(L7)]^+$ and its quinone analogue $[Ru(bpy)_2(L11)]^+$ in chloroform The presence of water in the samples is responsible for the broad band at 3420 cm^{-1}, however, the vibrational band associated with the hydroquinone moiety can be observed at 3522 cm^{1}, which is absent m the spectrum of the quinone complex [11][47] *Figure 5 10* also shows characteristic carbonyl (C=O) vibrations, which can be observed at 1660 cm^{-1} (1) [48] These peaks are clearly absent in the spectrum of both the protected and hydroquinone complexes even though bipyridyl and pyridine vibrations complicate this region [21] The vibrational peaks of the hexafluorophosphate ions occur at 558 cm^{1} and 835 cm^{1} while other peaks between 1300 – 1600 cm^{-1} are ring stretching and bending vibrations associated with the bipyridine and pyridine groups [47]

5.3.3 Computational Results

The following density functional theory (DFT) calculations were carried out on the mononuclear complex $[Ru(bpy)_2(L11)]^+$ by my colleague Dr. Noel O'Boyle using the computational chemistry program Gaussian 03.[49][50] The geometry optimised structure is shown in *Figure 5.13*.

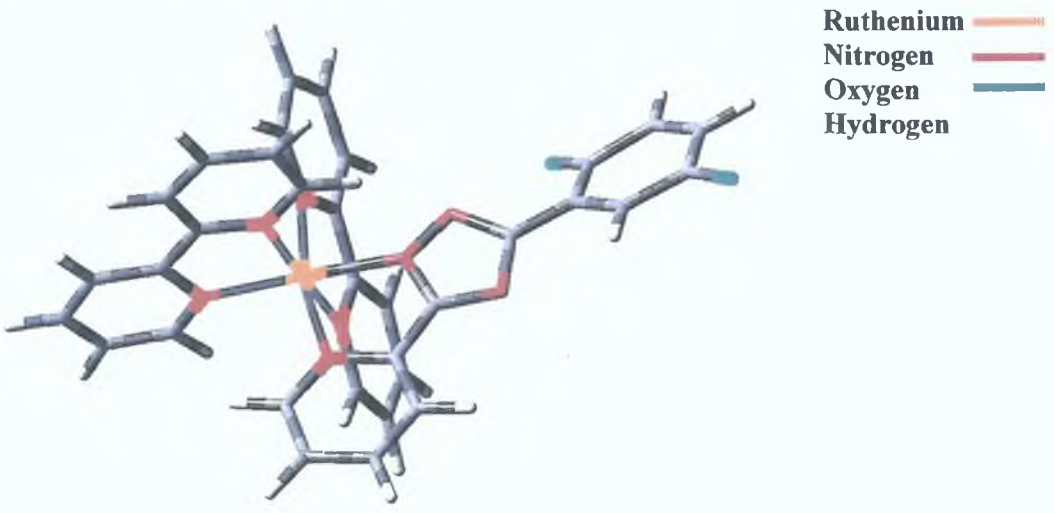

Figure 5.13 Geometry-optimised molecular structure of $[Ru(bpy)_2(L11)]^+$.

Unlike in the case of the hydroquinone complex in the previous chapter (*section 4.3.3*) there was no crystallographic data available for the calculation of the above structure. As a starting point for the geometry optimisation, the optimised geometry for the hydroquinone complex in the previous chapter was used. This calculated structure shown in *figure 5.13* is the most probable structure of the molecule based upon energy minimisation. The image is intended to provide an optical aid to the reader in the visualisation of the molecule being discussed and hence, helps in the elucidation of the following characterisation data. It, therefore, complements the following experimental data rather than replacing it.

The following *figure 5.14* was then created in which the calculated density of states (DOS) spectra of this complex are depicted. This DOS spectrum is a useful visualization method for the spatial distribution of the electronic structure of the complex. [51] Furthermore the DOS spectra give a better picture of the contributions of the various moieties to the HOMO and LUMO energy levels. [52]

The groups used are labelled in *Figure 5.14* as follows: Q, quinone moiety; Ru, the ruthenium metal atom; pyr, pyridine group; trz, the triazole ring; bpy 1 and bpy 2, the two bipyridyl rings. Along the x-axis of *figure 5.14* are a closely set series of red and green coloured lines that represent the closely spaced molecular orbitals in this complex. The 'gap' that is indicated on the graph between the orbitals, occurs between the HOMO and the LUMO states. Each line in the upper part of the graph illustrates the contribution of each moiety to the molecular orbitals in a particular energy region.

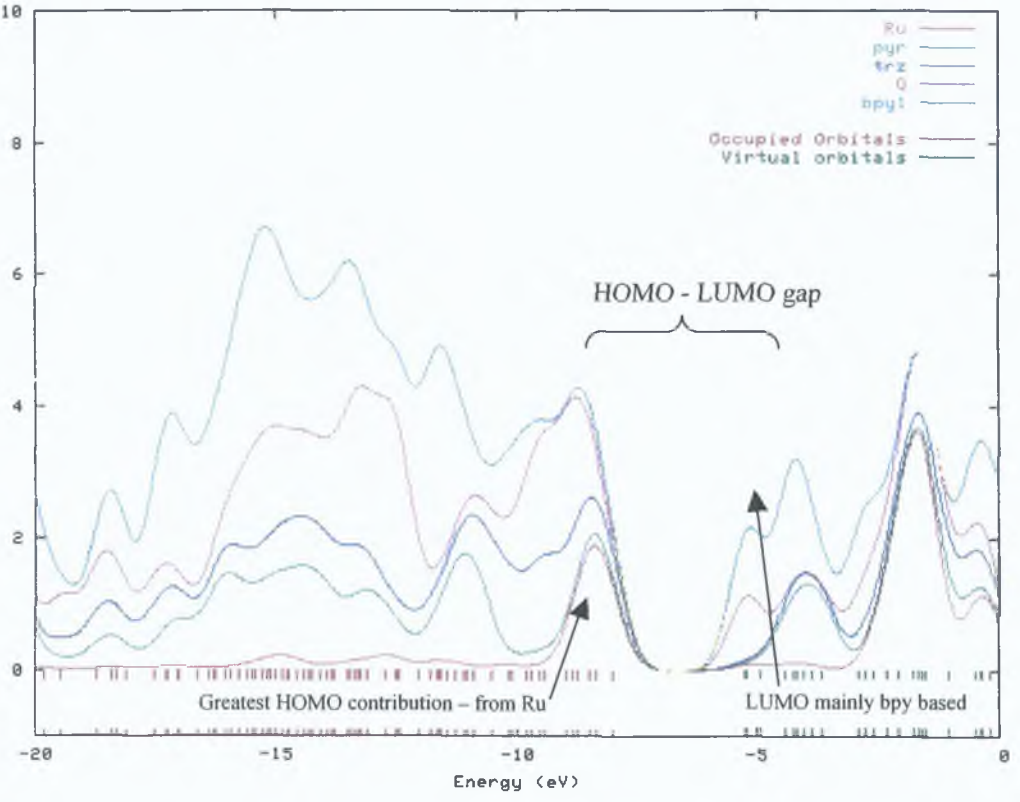

Figure 5.14 The calculated density of states (DOS) spectra of $[Ru(bpy)_2(L11)]^+$.

Upon examination of *figure 5.14*, it can then be seen that the HOMO has a large metal-based contribution from the ruthenium (**red line**). There is also a significant contribution from the quinone moiety to the HOMO. No other group, including the bipyridyl moieties, appear to contribute in any significant way to the HOMO. However, the LUMO is predominantly bipyridyl in character with some lesser contributions from the other moieties (*figure 5.14*). These results are different to those obtained for the hydroquinone analogue in the previous chapter (*section 4.3.3*).

L+3	L+2
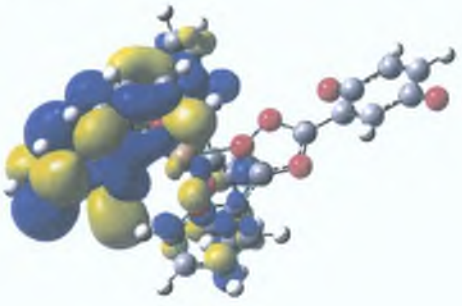	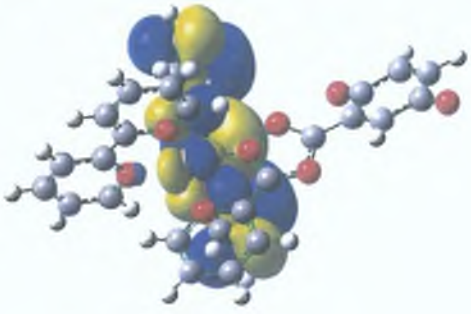
L+1	LUMO
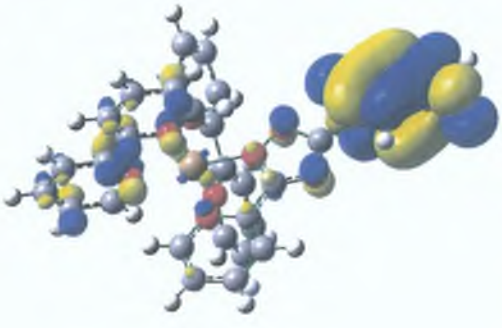	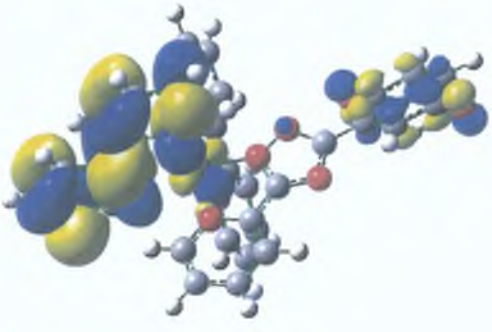
HOMO	H-1
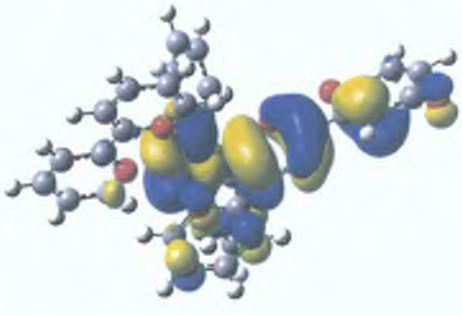	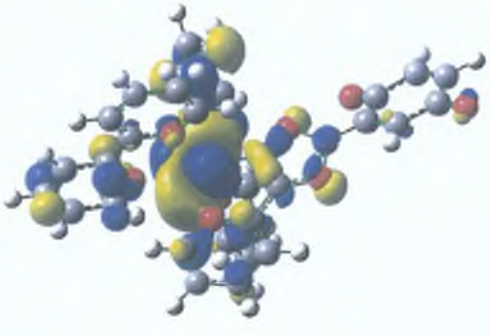
H-2	H-3
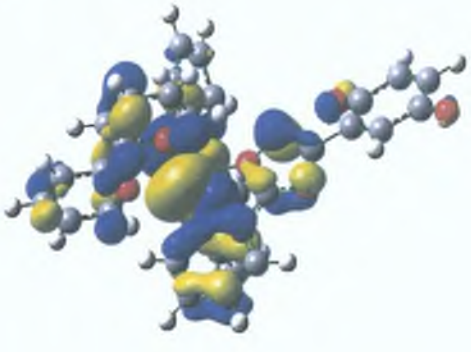	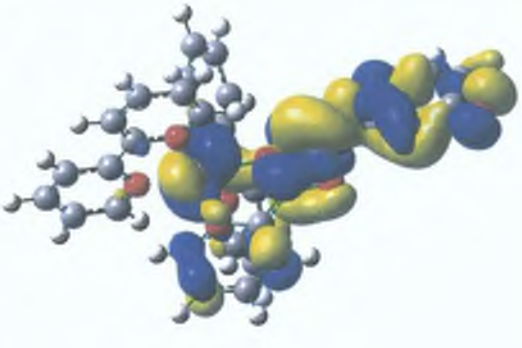

Table 5.2 Calculated isosurface images of the frontier orbitals of $[Ru(bpy)_2(L11)]^+$.

The previous DOS spectra of $[Ru(bpy)_2(L7)]^+$ seemed to show that there is a contribution to the HOMO from the hydroquinone moiety, however, in the case of this qumone complex the contribution from the qumone group (**pink line**) is not as significant (*figure 5 14*) This phenomenon is examined further in the isosurface visual representations of the graphical data in *figure 5 14*, which are contained in *table 5 2* This table shows the isosurfaces of the HOMO and LUMOs of $[Ru(bpy)_2(L11)]^+$

In *table 5 2* the nature of the ***LUMO***, ***LUMO + 1***, ***LUMO + 2*** and the ***LUMO + 3*** states are examined further For example, it can be seen that the LUMO is, indeed, strongly bipyridyl in character as suggested by the DOS spectra However, unlike in the case of the analogous hydroqumone complex in which the ***LUMO + 1*** state is mainly based on the second bipyridyl moiety, the ***LUMO + 1*** of this complex now appears to be quinone based The ***LUMO + 2*** is then based on the second bipyridyl moiety The bipyridyl moieties differ slightly in energy resulting in the fact that one bipyridyl moiety has slightly higher energy than the other while it seems that the energy of the qumone group lies in between these two energies (*table 5 2*)

The remaining diagrams illustrate the HOMO states It is now clear that the HOMO of this complex is strongly ruthenium centred with some pyridyltriazole contributions in the ***HOMO*** diagram, while the ***HOMO – 1*** is more strongly metal based Indeed, it is not until the ***HOMO - 3*** that the ligand appears to become more influential This is in contrast to the behaviour noted for $[Ru(bpy)_2(L7)]^+$ (*table 4 2*) in which the HOMO was much more strongly influenced by the pyridyltriazole moiety Hence, it can be seen that this computer-generated data provide an interesting theoretical basis for the following experimental characterisations These characteristics can be expected to be strongly influenced and hence, differ greatly from the hydroquinone analogues due to the presence of the quinone moieties

5.3.4 Electronic and Photophysical Properties

5.3.4.1 Absorption Spectra

Table 5.3 contains the absorption data for each of the quinone-containing complexes in both their protonated and deprotonated forms. The measurements for these complexes were achieved in a similar manner to the previous complexes and they were, therefore, all recorded in acetonitrile at room temperature and in ethanol / methanol at 77 K. Protonation was achieved via the addition of perchloric acid.

Table 5.3 Absorption and emission data obtained for the quinone complexes. Unless otherwise stated, all measurements were performed in acetonitrile.

Complex	λ_{max} [a] (nm) (ε x10^{-4})	E.Quantum Yield (Φ)	E_{max} 298K [b] (nm) τ (ns)	E_{max} 77K [c] (nm) τ (μs)
$[Ru(bpy)_2(L11)]^+$	470 (1.11)	0.0053	668 (201)	624 (3.0)
$[Ru(bpy)_2(HL11)]^{2+}$	440 (1.34)	-	630 (<20)	590 (5.4)
$[Ru(bpy)_2(L12)]^+$	450 (1.52)	0.0054	655 (180)	620 (3.7)
$[Ru(bpy)_2(HL12)]^{2+}$	439 (1.60)	-	666 (242)	625 (7.7)
$[Ru(bpy)_2(L13)Ru(bpy)_2]^{2+}$	468 (2.86)	0.0048	670 (188)	620 (2.8)
$[Ru(bpy)_2(H_2L13)Ru(bpy)_2]^{4+}$	440 (2.97)	-	634 (<20)	590 (5.4)
$[Ru(bpy)_2(L14)Ru(bpy)_2]^{2+}$	448 (2.33)	0.0052	658 (176)	619 (3.7)
$[Ru(bpy)_2(H_2L14)Ru(bpy)_2]^{4+}$	439 (2.67)	-	668 (232)	623 (6.9)

[a] Protonation of the complexes achieved by addition of perchloric acid.

[b] Lifetime samples at 298 K underwent freeze-pumped-thaw pre-treatment.

[c] Data at 77 K were recorded in EtOH/MeOH (4:1 v/v).

Figure 5.15 shows the absorption spectra of the mononuclear pyrazyltriazole complexes $[Ru(bpy)_2(L12)]^+$, $[Ru(bpy)_2(L8)]^+$ and $[Ru(bpy)_2(L4)]^+$ at room temperature in neutral acetonitrile. The spectra of the quinone-containing complexes are dominated in the visible region by dπ-π^* metal-to-ligand charge transfer (MLCT) transitions typical of these complexes. [53]

This is comparable to the UV data obtained by Gulyas *et al.* who also noted an MLCT for their ruthenium quinone complex (*figure 5.2*) with a λ_{max} value centred at 450 nm. [15] The intense π-π^* ligand transitions below 280 nm in the UV region are also observed in the spectra of the quinone complexes. However, from an examination of *figure 5.15*, it can be seen that the spectrum of the quinone complex differs from both the hydroquinone and the dimethoxy analogues. For example, the π-π^* transitions of the hydroquinone moiety that generally arise in the absorption spectra around 330-350 nm, are now absent. [38][54] Like the hydroquinone complex, however, the spectrum does exhibit a shift in the λ_{max} from 456 nm for the methoxy-containing pyrazyltriazole to 450 nm for the quinone complex. This shift is slightly more apparent in the spectra of the pyridyltriazole complexes and more pronounced than in the case of the hydroquinone complexes.

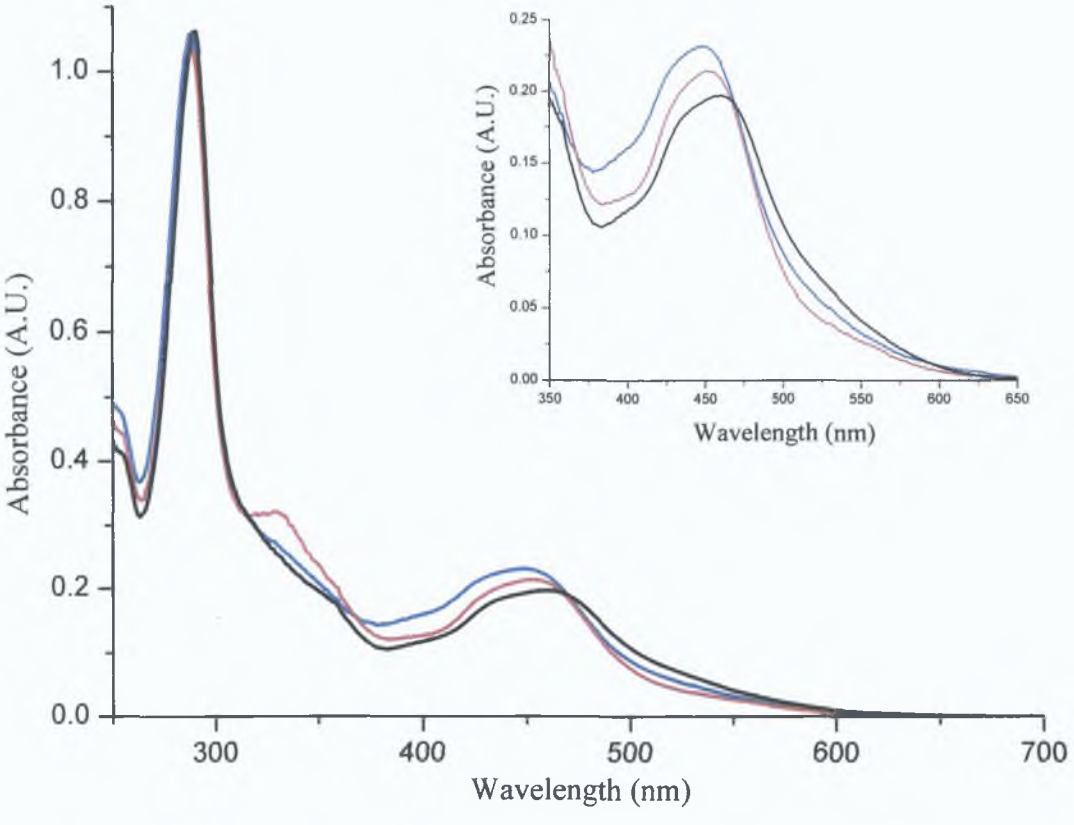

Figure 5.15 Absorption spectra of $[Ru(bpy)_2(L12)]^+$ c. 2.29 x 10^{-5}M (**blue line**) and $[Ru(bpy)_2(L8)]^+$ c. 1.90 x 10^{-5}M (**red line**) and $[Ru(bpy)_2(L4)]^+$ c. 1.47 x 10^{-5}M (**black line**) and (*inset*) MLCT region in neutral acetonitrile at room temperature.

A red-shift of the MLCT with respect to $[Ru(bpy)_3]^{2+}$ was noted in the spectra of the methylated and hydroquinone complexes and is again observed in the spectra of the quinone complexes. The shift arises due to the strong σ-donation of the deprotonated pyridyltriazole or pyrazyltriazole moiety (*table 5.3*). However, the further shift in the λ_{max} that arises in the quinone complexes may be attributed to the loss of the more strongly electron donating methoxy substituent. This shift is not as pronounced in the case of the pyrazyltriazole complexes due to the strong π-acceptor properties of the pyrazine (*table 5.3*). [23][55] The behaviour of the quinone complexes is comparable to other ruthenium quinone complexes, for example, the quinone complex prepared by Goulle *et al.* (*figure 5.4*) has a similar absorption spectrum. [29]

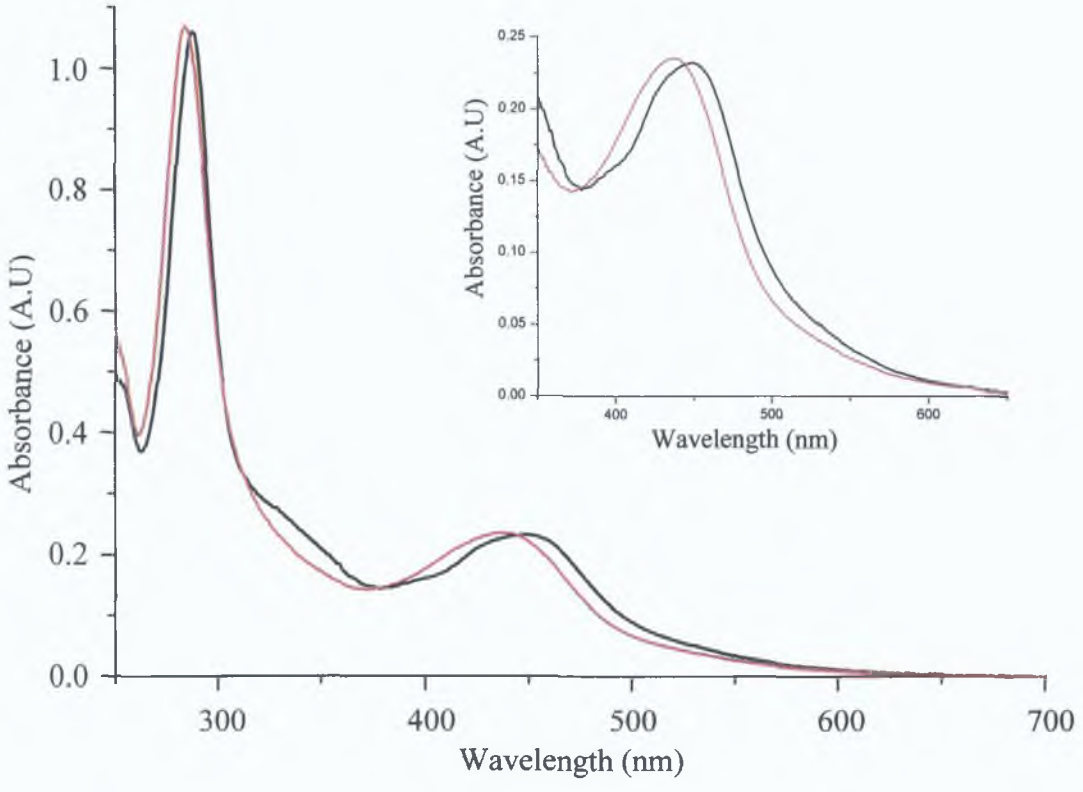

Figure 5.16 Absorption spectra of $[Ru(bpy)_2(L12)]^+$ in neutral acetonitrile (**black line**) and after the addition of 1 drop of trifluoroacetic acid (**red line**) and (*inset*) MLCT band.

Figure 5.16 depicts the absorption spectra of $[Ru(bpy)_2(L12)]^+$ in neutral acetonitrile and after the addition of 1 drop acid. The deprotonated status of the triazole ring in these quinone complexes is corroborated by the λ_{max} value of the lowest energy ^{1}MLCT transition, which is circa 450 nm for the mononuclear pyrazyltriazole complex.

Upon protonation of both the pyridyltriazole and pyrazyltriazole quinone complexes, a blue shift of the λ_{max} of the complexes occurs (*table 5 3*) An analogous shift of the λ_{max} was observed previously in the spectra of the hydroquinone and dimethoxy analogues upon protonation The protonated quinone-pyridyltriazole complexes experience a blue shift of the absorption of about 30 nm accompanied by a concomitant increase in the extinction coefficient However, in the case of the pyrazyltriazole complexes this shift is slightly less (circa 10 nm) due to the presence of the π-acceptor pyrazine moiety It must also be noted that no difference in the spectra were noted between the mononuclear quinone complexes and their dinuclear analogues As was the case for the analogous hydroquinone and dimethoxy complexes, this would seem to indicate that there is little or no interaction between the metal centres This is of interest as it suggests that the replacement of the quinone moiety perhaps does not influence the level of intermetallic communication between the ruthenium centres significantly The following sections will explore this possibility further

5 3 4 2 Luminescence Properties

The luminescence data obtained for these ruthenium quinone complexes are also presented in *table 5 3* All measurements were performed in neutral acetonitrile with the exception of the low temperature data, which were obtained in an ethanol-methanol solution, which provides a better glass Protonation was, once again, achieved via the addition of a small quantity of acid as described in the experimental chapter It was noted previously that the luminescence observed for both the hydroquinone and the dimethoxy-containing complexes was much weaker than that of the archetypal complex $[Ru(bpy)_3]^{2+}$ (Φ = 0 062) Once again however, an emission spectrum is observed for these quinone complexes that is typical of an emission from the lowest ^{3}MLCT (dπ Ru → π* bpy) excited state (*figure 5 17*) [56] These results are comparable to those obtained by a number of previous authors for their quinone-containing complexes [15][28][29][36][57] For example, Gulyas *et al* observed an emission spectrum for their quinone complex (*figure 5 2*) with a λ_{max} centred at 588 nm [15] Schanze and Sauer observed an emission with a λ_{max} of 598 nm for their ruthenium quinone complex (*figure 5 3*)

However, there is a red-shift of emission in these ruthenium quinone complexes compared to the model $[Ru(bpy)_3]^{2+}$ complexes. This shift was also reported previously for the analogous methylated and hydroquinone complexes and arises due to the effect of the triazole ring. This group contains a negative charge, which increases the electron density on the metal centre and therefore, reduces the t_2g - MLCT energy gap. [58]

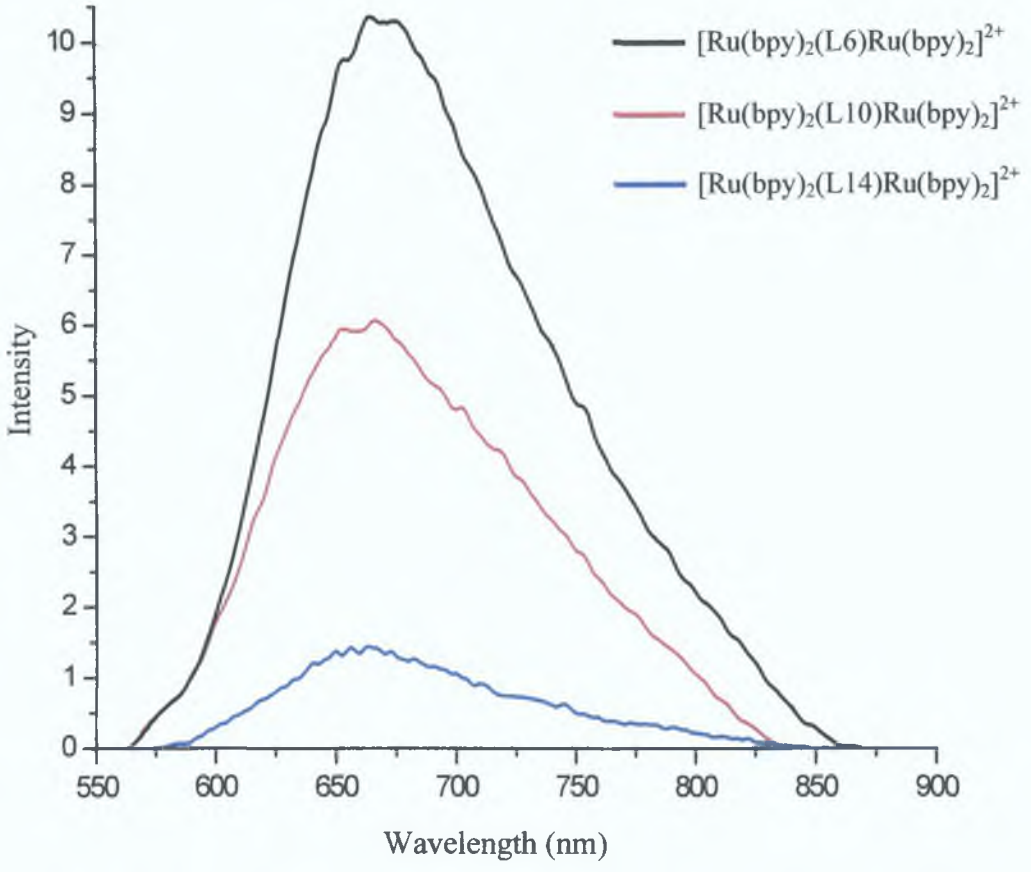

Figure 5.17 Emission spectra of $[Ru(bpy)_2(L6)Ru(bpy)_2]^{2+}$ (conc. 1.64 x 10^{-5}M), $[Ru(bpy)_2(L10)Ru(bpy)_2]^{2+}$ (conc. 1.45 x 10^{-5}M), $[Ru(bpy)_2(L14)Ru(bpy)_2]^{2+}$ (conc. 1.01 x 10^{-5}M) in acetonitrile at room temperature

The emission spectra of the each of the pyrazyltriazole dinuclear complexes in neutral acetonitrile at room temperature, which were prepared over the course of this study, are presented in *figure 5.17*. The mononuclear and dinuclear pyrazyltriazole complexes, which contain quinone moieties, have an emission λ_{max} value at approximately 656 nm.

The luminescence behaviour noted for the range of pyrazyltriazole complexes is essentially very similar with the slight changes noted in the emission λ_{max} arising due to the replacement of the dimethoxy groups by the less strongly electron donating substituents [23] Interestingly, however, no significant quenching of the emission is observable in the quinone complexes This differs for the results obtained by previous authors, such as, Lehn and co-workers who reported very efficient quenching of the excited state by the quinone moiety [29] However, in their study the quenching quinone moiety was linked via a different bridge Schanze and Sauer also reported similar quenching in their quinone complexes, however, they also found that the observed quenching is reduced depending on the number of peptide groups present within the bridging ligand [28] The lack of quenching observed within the complexes presented in this chapter may, therefore, perhaps be attributed to the insulating effect of the triazole ring This group when incorporated into the bridging ligand may weaken direct electronic coupling between the quinone group and the excited state bipyridyl [39] This would concur with the findings of Fanni *et al* who also observed a reduction in quenching in their triazole-containing bridging ligand (*figure 5 8*) [39] Further evidence for this may come from the fact that a number of previous complexes, including the complexes contained in *chapter four*, containing hydroquinone ligands bridged by triazole groups also report no quenching of the luminescence compared to complexes containing hydroquinone ligands which were not bridged by a triazole group [52][29]

These results are also reflected in the lifetime data recorded in *table 5 3* From an examination of these data it can be seen that there is no decrease in the lifetimes compared to either the hydroquinone or the protected complexes For example, a lifetime of 156 nm was obtained for $[Ru(bpy)_2(L10)Ru(bpy)_2]^{2+}$ while $[Ru(bpy)_2(L14)Ru(bpy)_2]^{2+}$ reported a lifetime of 176 nm In fact the lifetimes of these mononuclear and dinuclear complexes reveal a relatively long-lived excited states compared to the methylated analogues [59] The lifetime of $[Ru(bpy)_2(L11)]^+$, for example, was found to be 201 nm at room temperature compared to 110ns for the analogous dimethoxy complex (*chapter three*) This was also the case for the hydroquinone complex $[Ru(bpy)_2(L7)]^+$

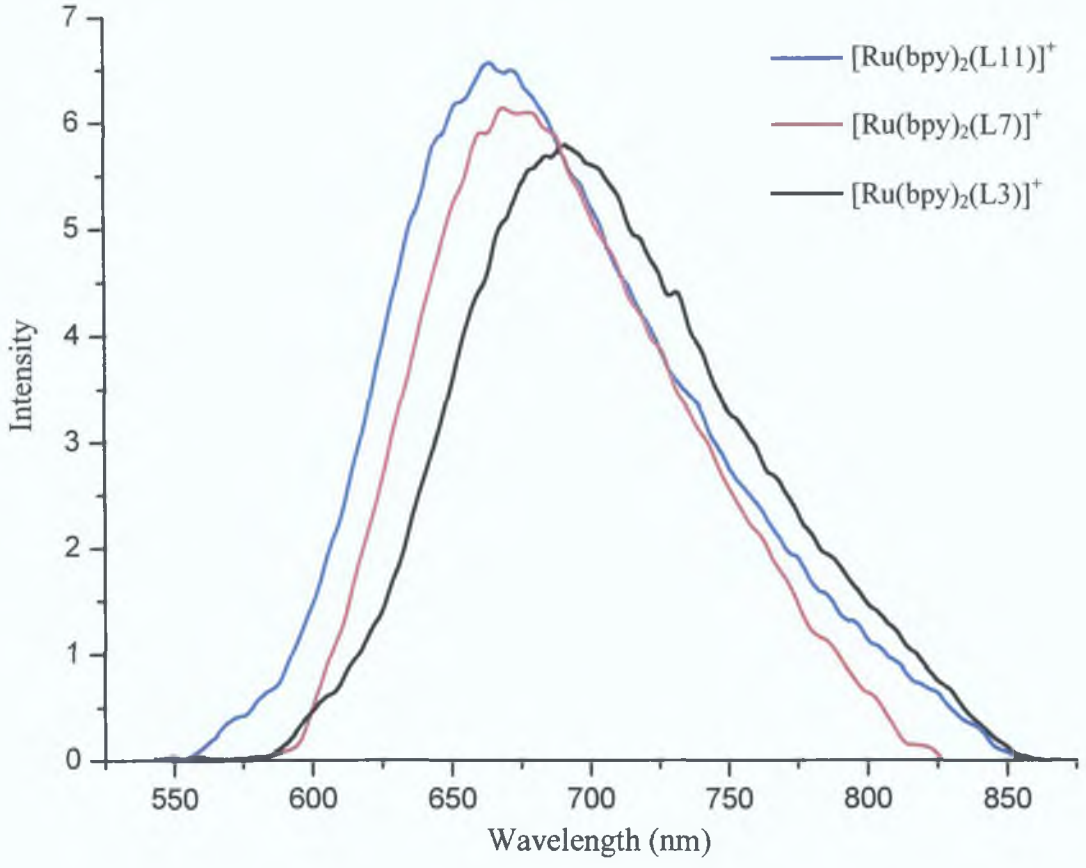

Figure 5.18 Emission spectra of $[Ru(bpy)_2(L11)]^+$ (conc. 5.10 x 10^{-5}M), $[Ru(bpy)_2(L7)]^+$ (conc.5.01 x 10^{-5}M), $[Ru(bpy)_2(L3)]^+$ (conc. 4.99 x 10^{-5}M) in acetonitrile at room temperature

The emission spectra obtained for the range of mononuclear pyridyltriazole complexes are presented in *figure 5.18*. The emission λ_{max} for the mononuclear and dinuclear quinone complexes was observed at approximately 670 nm in neutral acetonitrile at room temperature. Again the luminescence behaviour observed for the range of pyridyltriazole complexes is extraordinarily similar with the small shift of the λ_{max} arising due to the replacement of the relatively strongly electron donating methoxy moieties by electron accepting quinone moieties.[23][60][61] The emission spectra of the quinone complexes was also recorded at 77 K and once again, the spectra obtained for both the pyridyltriazole and the pyrazyltriazole complexes containing quinone moieties were analogous to those obtained previously for the hydroquinone and dimethoxy complexes.

Once more the emergence of the vibrational structure is noted along with a concomitant increase in the intensity compared to the room temperature luminescence as discussed previously for the methoxy and hydroquinone complexes [62] The quinone complexes were also protonated by the addition of a small quantity of acid and their emission spectra were recorded at room temperature and 77 K These results are recorded in *table 5 3* As expected, the lifetimes at low temperatures increase considerably

Upon protonation a shift is seen in the emission λ_{max} value of each of the complexes In the case of the pyridyltriazole complexes a shift to higher energy of approximately 35 nm occurs This shift in the emission of these complexes is accompanied by a decrease in the emission intensity This mirrors the behaviour noted for both the hydroquinone and methoxy analogues in *chapter three* and *four* The lifetime data of the pyridyltriazole complexes are also seen to decrease sharply (<20ns) and are no longer measurable on the conventional (ns) laser set-up In the case of the quinone pyrazyltriazole complexes a shift to a reduced energy upon protonation is noted Similar luminescence behaviour was observed previously for the protected and hydroquinone complexes Again this shift is quite small (circa 7 nm) and there is no comparable loss of emission intensity as seen for the pyridyltriazole complexes Once again, this shift is associated with the switching of the excited state upon protonation as noted previously for other pyrazyltriazole complexes [55][63]

The luminescence spectra of these quinone complexes upon protonation at 77 K was also recorded (*table 5 3*) Again the behaviour noted for each of the complexes is comparable to that noted previously for the protected and dihydroxy complexes A blue shift (circa 33 nm) upon protonation of the qumone pyridyltriazole complexes is again observed Whereas, at room temperature a decrease in luminescence intensity was observed, no such decrease is observed at 77 K Again this can be attributed to the decreased availability of the thermally accessible ^{3}MC In the case of the pyrazyltriazole complexes a slightly smaller shift in the emission to a reduced energy is noted (circa 5 nm) An increase in the intensity is also observed However, the behaviour of these complexes is further explored in the following sections

5 .4 Acid-Base Properties

In this section the pKa data obtained on these ruthenium quinone complexes are reported (table 5.4). A significant electronic redistribution occurs within these complexes due to the presence of the triazole moiety. This allows them to be protonated or deprotonated by altering their σ-donor and π-acceptor properties. This is particularly evident in the case of the pyrazyltriazole complexes due to the fact that protonation of these complexes leads to a switching of the excited state. [64][65][66] It was anticipated that some difficulties may be encountered in obtaining these data on the quinone-containing complexes due to the complexities in the behaviour of these complexes in aqueous media. [21] However, within the pH value range examined no such complexities were encountered and the pKa and pKa* data were obtained in Britton-Robinson buffer. The experiment conditions are outlined in *chapter two*.

Complex	pKa	pHi	pKa*
$[Ru(bpy)_2(L11)]^+$	4.1	2.5	2.8 (2.4)
$[Ru(bpy)_2(L12)]^+$	3.0	4.7	5.0 (4.6)
$[Ru(bpy)_2(L13)Ru(bpy)_2]^{2+}$	4.0	2.6	2.9 (2.3)
$[Ru(bpy)_2(L14)Ru(bpy)_2]^{2+}$	2.9	4.6	4.9 (4.3)

Table 5.4 Ground state and excited state pKa values for the mononuclear and dinuclear quinone complexes. pKa* values were obtained using both the Forster equation **(in Blue)** and the Ireland and Wyatt method. [69]

Figure 5.20 depicts the absorption spectra of $[Ru(bpy)_2(L11)]^+$ in the pH value range 1.09 to 4.88 and these are typical for the spectra obtained for the quinone complexes within this pH value range. Within this pH value range the acid-base behaviour of all of the complexes presented in this chapter were found to be reversible with clean isobestic points at approximately 455 nm, 390 nm and 305 nm (*figure 5.20*). A plot of the pH value versus the change in absorption was, hence, obtained and used to yield the pKa value of each of the complexes (inset *figure 5.20*). The isobestic point from the absorption spectra was consequently used as the excitation wavelength in order to obtain the emission data.

The pHi value or point of inflection of the emission graph (*figure 5.20*) was, hence, obtained. This value was then utilised in two equations (as *chapter four*) in order to generate pKa* values. From an examination of *figure 5.19* it may be observed that a λ_{max} of 438 nm exists at the pH value 1.09 when the complex is in the protonated state. The pH value was then increased to a pH value of 4.88 and a concomitant shifting of the λ_{max} to 462 nm is noted.

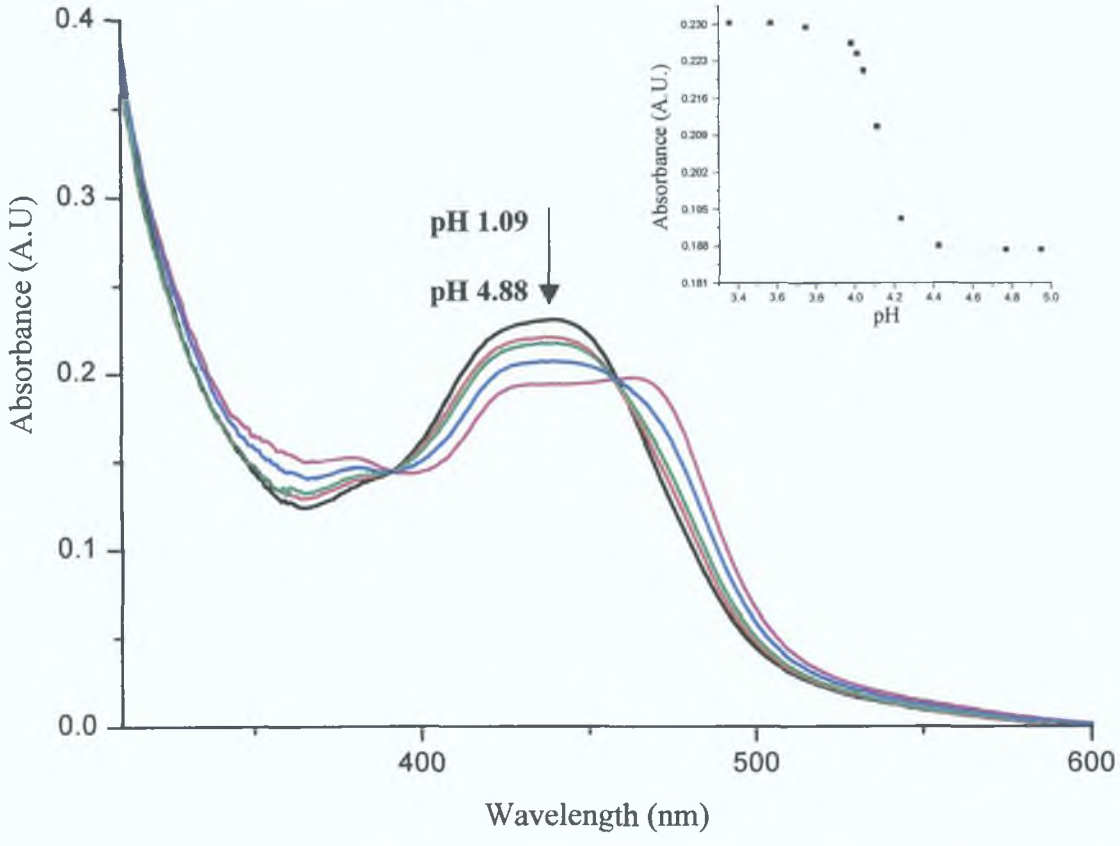

Figure 5.19 pH dependence of the absorption spectra of $[Ru(bpy)_2(L11)]^+$ in Britton-Robinson buffer. *Inset* fitted sigmoidal curve of absorbance versus increasing pH.

From an examination of the pKa values for this complex (*table 5.4*) it may be seen that the results correlate well with those obtained for the analogous protected pyridyltriazole and pyrazyltriazole complexes presented in *chapter three*. For example, the pKa value for $[Ru(bpy)_2(L3)]^+$ was found to be 4.0 which correlates well to 4.1 obtained for $[Ru(bpy)_2(L11)]^+$. This is in contrast to the decrease in the pKa values obtained for the analogous pyridyltriazole complexes containing hydroquinone complexes (*chapter four*). For example, $[Ru(bpy)_2(L7)]^+$ yielded a pKa value of 3.2, however, no such decrease is evident within these complexes.

It is of interest to note, that the pKa values obtained for these quinone-containing complexes are comparable to those obtained by O'Brien and co-workers, who examined the analogous catechol complex shown in *figure 4 8* This hydroquinone-containing complex and its protected analogue also both yielded a pKa value of 4 2 [52] It was suggested in the previous chapter that the decrease in the pKa value of the pyridyltriazole hydroquinone complexes arose as a result of the hydroquinone moieties If hydrogen bridging was occurring in the hydroquinone complexes this may explain the increased acidity of the triazolic nitrogen in these complexes This suggestion seems to be further supported by the pKa data obtained for these quinone complexes Since, these complexes differ from their hydroquinone analogues only by the presence of the quinone moieties, it is compelling evidence that the decrease in the pKa values observed for the hydroquinones is as a result of the hydroquinone moiety

Table 5 4 also contains the pKa data obtained for the mononuclear and dinuclear pyrazyltriazole complexes Once again, as was the case for the previous complexes, the data obtained in aqueous Britton-Robinson buffer were reversible over the pH value range examined Clear and well-defined isobestic points were observed at approximately 560 nm, 420 nm and 360 nm A comparable shift in the λ_{max} value is again observed although to a lesser extent than for the pyridyltriazole complexes Hence, at the pH value 1 58 the λ_{max} value is observed at 450 nm and this gradually shifts to 440 nm as the pH value is increased to 5 88 This behaviour is consistent with that observed previously in both the protected pyrazyltriazole analogues and the hydroquinone analogues (*chapter three*) [68] It is also interesting to note that the pKa data obtained for each of the pyrazyltriazole complexes are very similar For example, the pKa value of $[Ru(bpy)_2(L6)Ru(bpy)_2]^{2+}$ was found to be 2 8, $[Ru(bpy)_2(L10)Ru(bpy)_2]^{2+}$ was 2 9 and $[Ru(bpy)_2(L14)Ru(bpy)_2]^{2+}$ is 2 9 At this point, therefore, it is not possible to make any conclusions about the presence of hydrogen bridging in the pyrazyltriazole hydroquinone complexes as an increase in the acidity of the triazolic nitrogen was not noted in for these complexes It is also important to point out that the dinuclear complexes reported within this chapter have the potential to undergo a two-step protonation, as there are two triazoles present

In each of the dinuclear complexes, $[Ru(bpy)_2(L13)(bpy)_2Ru]^{2+}$ and $[Ru(bpy)_2(L14)(bpy)_2Ru]^{2+}$, however, only one protonation step is observed over the pH value range examined (circa pH 2 – 6). This would, therefore, seem to suggest that in this aqueous media both protonation steps occur simultaneously. This is, once again, indicative of either very weak or no metal-metal interaction within these complexes. [37] This was also the case for the previous protected and dihydroxy complexes and suggests that the intermetallic behaviour of these bimetallic complexes is unaffected by the altering of the quinone moiety. This phenomenon is explored further in the following spectroelectrochemical section.

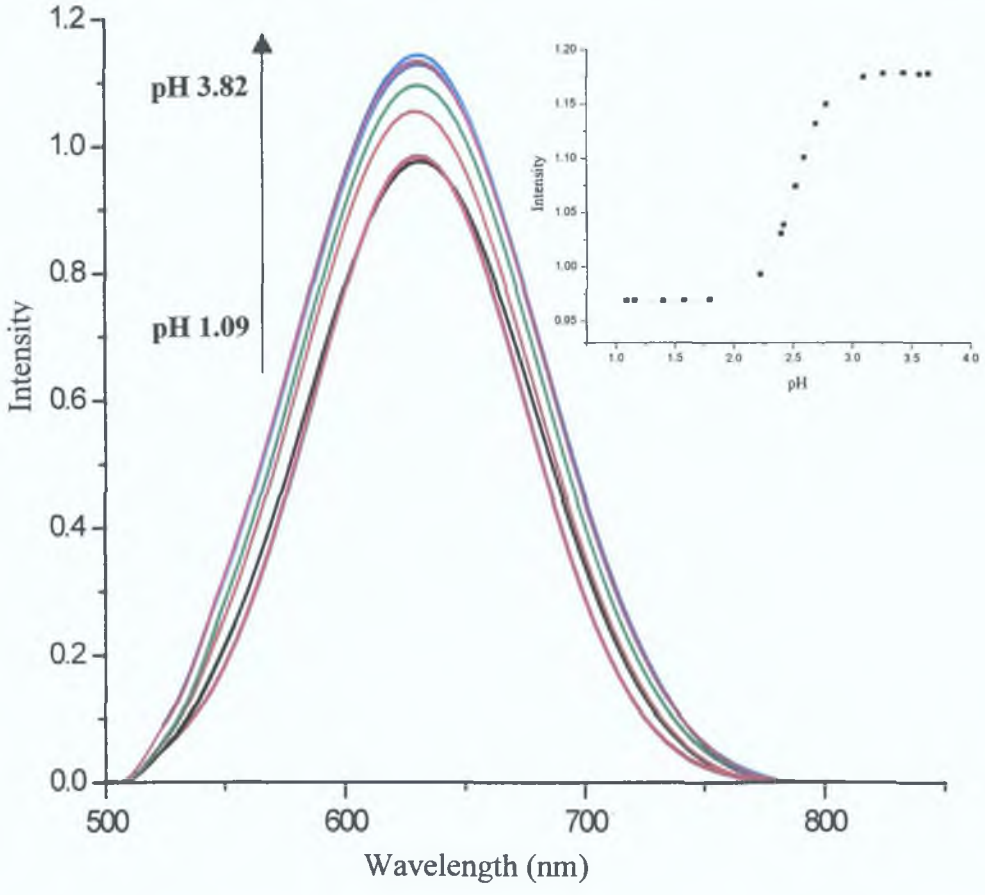

Figure 5.20 pH dependence of the emission spectra of $[Ru(bpy)_2(L11)]^+$ in Britton Robinson buffer. *Inset* fitted sigmoidal curve of intensity versus increasing pH.

Emission measurements were also performed on these complexes in aqueous buffer in a similar manner as the absorption measurements and the excited stated (pKa*) data for these complexes are also listed in *table 5.4*. The pKa* values could be calculated from pHi values both by the Forster method and by the Ireland and Wyatt technique (*chapter four*). [69] *Figure 5.20* depicts the emission spectra of the pyridyltriazole complex $[Ru(bpy)_2(L11)]^+$ as a function of pH value.

An increase of the emission intensity can be noted with increasing pH value, however, the luminescence intensity noted for theses quinone complexes is still very weak and hence, it was necessary to obtain Gaussian fittings in order to calculate the pHi value (*figure 5 20* inset) This is comparable to the behaviour noted for both the protected and hydroquinone complexes and arises for the same reasons (*chapter three*)

Of the two techniques employed in calculating the pKa* values the Ireland and Wyatt method is more dependable for reasons outlined previously (*chapter three*) [69] Hence, it can be seen from an examination of *table 5 4*, that the pKa* values of these complexes is comparable to those of the hydroquinone complexes (see *table 4 4*) For example, both $[Ru(bpy)_2(L8)]^+$ and $[Ru(bpy)_2(L12)]^+$ yielded a pKa* values of 5 0 Once again, the pKa* values obtained for the pyridyltriazole complexes were lower than their pKa values (*table 5 4*) This is comparable to the behaviour noted for the range of pyridyltriazole complexes in the previous chapters and therefore, suggests that within these complexes the excited state is bipyridyl based rather than located on the triazole ligand The quinone pyrazyltriazole complexes have pKa* values greater than their pKa values suggesting that the excited state is based on the pyrazine moiety and not on the bipyridyl moiety Again this tendency of the excited state of the pyrazyltriazole complexes to switch upon protonation was reported previously [65][37] These data are, hence, a further indicating of switching of the excited state within these complexes upon protonation as previously suggested by the luminescence data (*section 5 3 4*)

5.5 Electrochemical Properties

In this section the electrochemical data obtain for the quinone complexes are presented. The experimental conditions and methodologies utilised during the course of these measurements are contained both in *chapter two* and the electrochemical appendix (*appendix B*). *Table 5.5* contains the electrochemical data obtained during these measurements in volts versus SCE.

Complex	*Oxidation Potentials (V)*[a,b]	*Reduction Potentials (V)*[c]	
	Ru^{II}/Ru^{III}	ligand*	bipyridyl
$[Ru(bpy)_2(L11)]^+$	1.00	-1.29	-1.49, -1.76
$[Ru(bpy)_2(HL11)]^{2+}$	1.28		*d*
$[Ru(bpy)_2(L12)]^+$	1.13	-1.22	-1.45,-1.68,-1.95
$[Ru(bpy)_2(HL12)]^{2+}$	1.28		*d*
$[Ru(bpy)_2(L13)Ru(bpy)_2]^{2+}$	1.00	-1.31	-1.47, -1.75
$[Ru(bpy)_2(H_2L13)Ru(bpy)_2]^{4+}$	1.28		*d*
$[Ru(bpy)_2(L14)Ru(bpy)_2]^{2+}$	1.12	-1.23	-1.48,-1.67,-1.99
$[Ru(bpy)_2(H_2L14)Ru(bpy)_2]^{4+}$	1.28		*d*

*The values shown are the cathodic peak potentials

[a] Values standardised with respect to the redox potential of ferrocene (+0.38 V *vs.* SCE) under equivalent experimental conditions as a secondary electrode. [70]

[b] Protonation was achieved via addition of 1 drop of conc. $HClO_4$

[c] All measurements were carried out under a constant flow of nitrogen.

[d] Surface effects arise in acidic solutions making reduction potentials difficult to obtain.[71]

Table 5.5 Electrochemical data for the Ru (II) complexes in acetonitrile with 0.1 M TEAP versus SCE

Unlike in the case of the hydroquinone-containing complexes, contained in the previous chapter, no pre-treatment of the electrodes was deemed necessary. Indeed, any such pre-treatments complicated the measurements further. However, extensive electrode cleaning and polishing was undertaken prior to all scans.

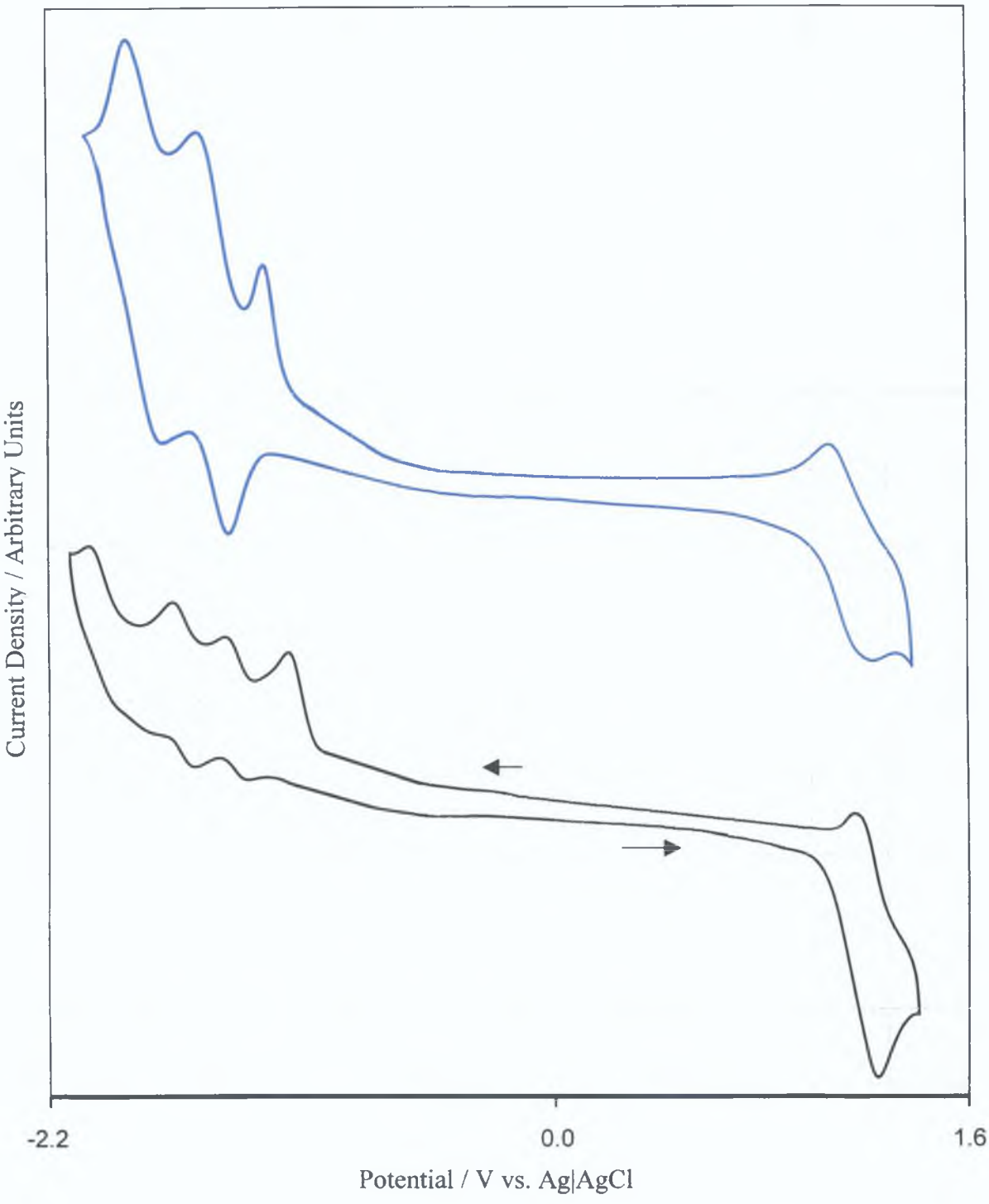

Figure 5.21 Cyclic voltammograms of $[Ru(bpy)_2(L11)]^+$ **(blue line)** and $[Ru(bpy)_2(L14)Ru(bpy)_2]^{2+}$ **(black line)** in neutral MeCN with 0.1 M TEAP in volts versus Ag|AgCl (*scan rate* 0.10 V / s).

The electrochemical reduction of quinones and quinone species particularly in aprotic solvents has been scrupulously studied. [72][73][74] In aprotic solvents the reduction of these complexes takes place in two $1e^-$ stages (*figure 5.22*).

The most oxidised form is known as benzoquinone, the next one-electron reduced form is called the semiquinonate radical anion and the fully reduced form is the catecholate dianion (*figure 5.22*). [75] However, this process can be affected by the electrolyte and this will be examined further in the coming section. [72][76]

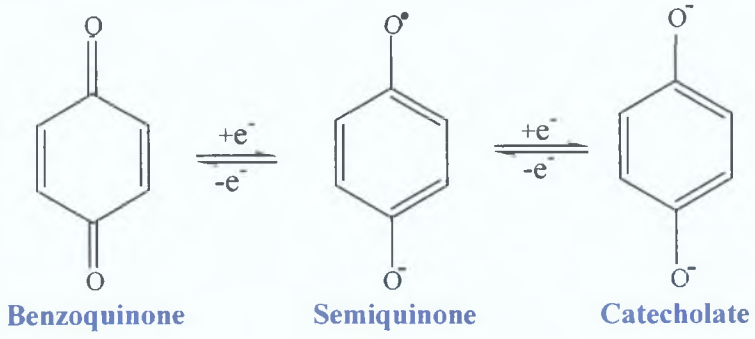

Figure 5.22 The two 1e⁻ reduction steps of quinones in aprotic solvents. [72]

The cyclic voltammograms of the pyridyltriazole mononuclear complex $[Ru(bpy)_2(L11)]^+$ and the dinuclear pyrazyltriazole $[Ru(bpy)_2(L14)Ru(bpy)_2]^{2+}$ in neutral acetonitrile are shown in *figure 5.21*. From an examination of the CV of these complexes it becomes evident that they are quite similar to the protected analogues presented in *chapter three* and are lacking the complications encountered in the CVs of the hydroquinone complexes (*chapter four*). There are no hydroquinone processes occurring prior to the metal oxidation in the anodic region of the CV. However, unlike the dimethoxy analogues, there is an additional process observable in the cathodic region of the CV prior to the bipyridyl reduction processes (*figure 5.21*). For example, in the CV of the pyridyltriazole complex, a reversible metal (Ru^{II}/Ru^{III}) redox couple is clearly observable at 1.00 V vs SCE at a neutral pH value while three reduction processes are present at – 1.29 V, - 1.49 V, and - 1.76 V versus SCE (*table 5.5*). Similarly, the pyrazyltriazole dinuclear complex exhibits well-resolved, uninhibited metal processes at 1.12 V versus SCE and four reduction processes at - 1.23 V, - 1.48 V, - 1.67 V and – 1.99 V versus SCE (*table 5.5*). Furthermore, the values obtained for the metal redox processes differ from those reported previously for the analogous methoxy complexes. For example, the metal redox potential for $[Ru(bpy)_2(L3)]^+$ was found to be 0.80 V while $[Ru(bpy)_2(L11)]^+$ reported a metal redox process at 1.00 V. The slight shift noted in the potentials is unsurprising considering the loss of the strongly electron donating methoxy groups. [61]

Also, these oxidations are not anodically shifted to the high potentials noted for the hydroquinone complexes For example, the metal oxidation occurred at 1 27 V versus SCE subsequent to the ligand processes in the hydroquinone complex $[Ru(bpy)_2(L7)]^+$ This is an important observation as it was suggested in the previous chapter that the metal oxidations were shifted to higher potentials as a result of a proton transfer related to the previous oxidation of the hydroquinone moiety The fact that the metal processes in the quinone complexes are not as anodically shifted as in the hydroquinone complexes is further evidence of the occurrence of intermolecular proton transfer in the hydroquinone complexes

The reductions are perhaps the most intriguing processes observed in the CVs of the complexes The most negative reductions, that is the final two reductions observed in the pyridyltriazole complexes and the final three in the case of the pyrazyltriazole complexes, may be assigned based on comparisons with similar ruthenium bipyridyl complexes and the previous protected and deprotected complexes For example, in the case of the pyridyltriazole complexes these final two reductions in the cathodic region may be assigned as the two one-electron reversible redox reactions of the bipyridine ligands [53] This is also the case for the mononuclear and dinuclear pyrazyltriazole complexes, however once again, due to the electron accepting nature of the pyrazine ring, the pyrazyl moiety now has a substantially lower π^* orbital than bpy and hence, the second reduction observed can be said to be pyrazine based while the last two reductions are bipyridine centred [56][65] However, there is now a new irreversible cathodic wave present prior to these reductions that was not present in the previous CVs of either the protected or the hydroquinone complexes It is there suggested that this process is as a result of the quinoid moiety This is a reasonable assumption not only due to its absence in the voltammograms of the previous analogous complexes but also based on comparisons with other quinone-containing complexes The quinone complex reported by Lehn and co-workers, for example, shown in *figure 5 4* has a quinone reduction at - 0 44 V [29] The ruthenium-quinone complex reported by Schanze and Sauer (*figure 5 3*) also has an usual ruthenium processes (1 25 V versus SCE in neutral acetonitrile) and the first bipyridyl reduction at – 1 35 V but in addition an irreversible cathodic wave was also observed at – 0 45 V

They too associated this wave with the reduction of the quinone *functional* group [28] Other authors also reported E½ (Q/Q^{-}) ≈ - 0 50 V measurements on very similar quinones [77] While, the reduction of the free quinone was observed at – 0 57 V versus SCE [78] Namazian also reported the density functional theory (DFT) calculations of electrode potentials of quinones in acetonitrile He reported a reduction process for benzoquinone at approximately - 1 23 V [73][79] Oppermann *et al* examined another ruthenium complex containing quinone moieties (*figure 5 6*) The electrochemistry of this complex included a Ru^{II}/Ru^{III} process at + 1 26 V versus SCE while the quinone had a reduction at – 0 79 V followed by the bipyridyl reduction at – 1 38 V [36] Gulyas *et al* also prepared and studied a ruthenium complex containing a quinone moiety (*figure 5 2*) Once again, the metal centred couple of this complex bearing coordinated ruthenium was observed at 0 90 V (in MeCN vs $Fc^{+/0}$) and a first reduction a – 0 90 V Once again, they point out that this is at a significantly more positive potential than for metal complexes without quinone functionalities and hence, is likely to correspond to the reduction of the benzoquinone moiety [15]

The status of the quinone wave is also noteworthy For example, quinone ligands generally report a two-step $1e^{-}$ reduction process in aprotic solvents [72] However, this process is affected by the nature of the electrolyte Pletcher *et al* [72] studied a number of ruthenium quinone complexes and reported that for all of the quinones and electrolytes that they examined there was significant interactions between the cations of the electrolytes and the semiquinones (Q^{-}) (*figure 5 22*) For example, this process can occur in two steps (- 1 21 V and – 1 19 V) in some electrolytes, however, sometimes two separate waves are not observed for each reaction [41][78] This has been proposed to be attributable to wave broadening which could arise from the overlapping of the two waves for the two reactions (*figure 5 22*) However, it is also possible that the wave could be concealed under the first bipyridyl process (i e the second reduction wave) However, in some of the electrolytes that Pletcher *et al* studied the quinones only showed a single reduction wave corresponding to the Q/Q^{-} couple [72] For example, Schanze *et al* reported an irreversible quinone reduction and noted that this irreversibility was due to the fact that the chemical reactions of the quinone radical anion are significant on the timescale of the electrochemical experiment [28]

Beer *et al.* also mooted that the irreversibility of the quinone wave could be due to the formation of insoluble hydroquinone species in solution. [80]

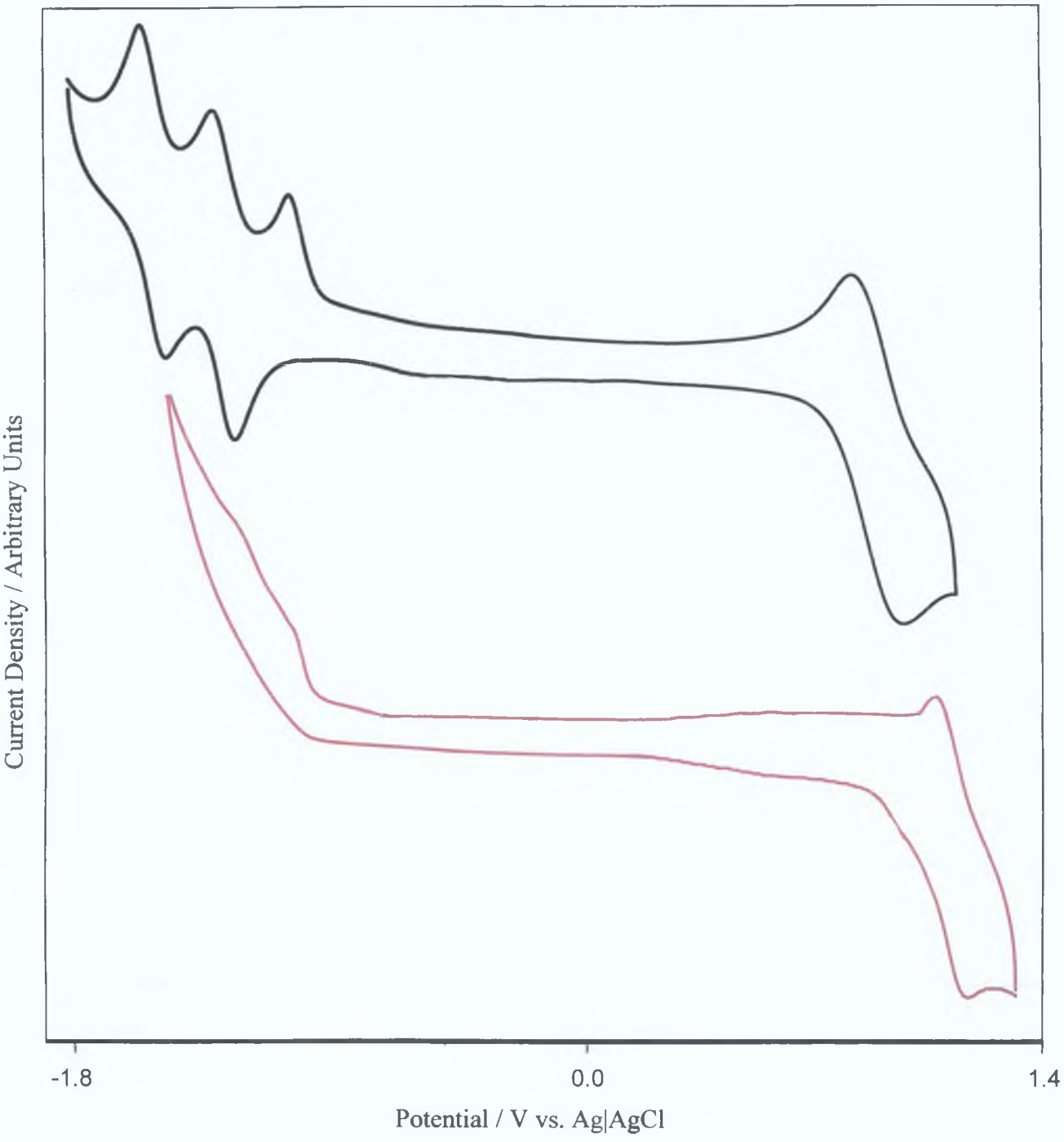

Figure 5.23 Cyclic voltammograms of $[Ru(bpy)_2(L13)Ru(bpy)_2]^{2+}$ (**black line**) in neutral MeCN, $[Ru(bpy)_2(HL13)Ru(bpy)_2]^{4+}$ (**red line**) in MeCN with 1 drop of $HClO_4$ with 0.1 M TEAP in volts versus Ag|AgCl (*scan rate* 0.10 V / s).

Since, the electrochemistries of these complexes are also strongly affected by the pH value of the system, electrochemical investigations in acidic acetonitrile were undertaken. [54]

Hence, the cyclic voltammograms of $[Ru(bpy)_2(L13)Ru(bpy)_2]^{2+}$ in both neutral and acidic media are shown in *figure 5 23* The addition of acid to these systems leads to numerous complications in obtaining the CVs due to surface effects on the electrode This is particularly evident in the cathodic region of the CVs in which the reduction potentials are all but obliterated (*figure 5 23*) However, the metal processes are still observable and an anodic shift in the metal redox potential of each of the complexes is clearly evident For example, the metal redox potential of $[Ru(bpy)_2(L13)Ru(bpy)_2]^{2+}$ clearly shifts from 1 00 V versus SCE to 1 28 V versus SCE (*figure 5 23, table 5 5*) upon acidification This is comparable to the shift noted in the voltammograms of the protected complexes in which the metal oxidation was seen to shift to between 300 mV and 400 mV upon protonation of the triazole moiety(ies) However, no such anodic shift was noted in the voltammograms of the hydroquinone complexes in which the metal oxidation in each of the complexes does not alter significantly (circa 1 28 V versus SCE for each of the hydroquinone complexes) upon the addition of acid (*chapter four*) As the hydroquinone complexes differ only from these quinone complexes by the presence of the hydroquinone moieties this is an important observation It is perhaps further compelling evidence that the hydroquinone complexes are protonated subsequent to the hydroquinone oxidations and therefore, via an intermolecular proton transfer arising from these oxidations as suggested previously by Keyes and co-workers [63]

Finally, the cyclic voltammograms of the dinuclear complexes must also be scrutinised further *Figure 5 21* and *figure 5 23* contain the cyclic voltammograms of the dinuclear complexes From an examination of these figures it may be seen that the voltammograms of these dinuclear complexes differ little from their mononuclear counterparts For example, in these CVs only a single $2e^-$ redox process is present in the anodic region of the voltammograms By comparison with the mononuclear analogues this process can be associated with the metal redox process For example, *figure 5 23* depicts the CV of the dinuclear complex $[Ru(bpy)_2(L13)Ru(bpy)_2]^{2+}$ The metal process in this complex can be observed at 1 00 V versus SCE Its complement $[Ru(bpy)_2(L11)]^+$ is also shown in *figure 5 21* and the metal process is clearly observable at 1 00 V

Therefore, it appears that the properties of the dinuclear complexes are very similar to those of their mononuclear counterparts This was also the behaviour noted for the analogous dimethoxy and dihydroxy-containing complexes reported in previous chapters and may indicate that each of the metal units in the dinuclear complexes behaves in an independent manner

The dinuclear complexes depicted in *figure 5 21* and *5 23* are like the mononuclear complexes in that the current-potential responses are the same shape However, in the dinuclear they have a larger magnitude due to the presence of the additional electroactive centre [81] This fact that the metal processes appear as one 2e redox process that was not resolvable by coulometric methods, suggests that there is weak intermetallic communication in these dinuclear complexes However, spectroelectrochemical measurements are presented in the following section with the aim of investigating the assignment of the redox processes further and also to analyse the degree of intermetallic communication further

5.6 Spectroelectrochemistry

In this section the spectroelectrochemical characteristics of the ruthenium-quinone complexes are examined. This technique was utilised, as it is known to be an excellent tool for the verification of the assignment of the order of the redox processes explored in the previous section.

5.6.1 Absorption Spectroelectrochemistry

Chapter two contains the experimental methodologies employed during this technique. In each case the measurements were preformed in neutral acetonitrile with an Ag|AgCl reference electrode and the changes in the absorption spectra of the complexes were hence, monitored as they underwent electrochemical oxidation (*figure 5.24* and *5.25*).

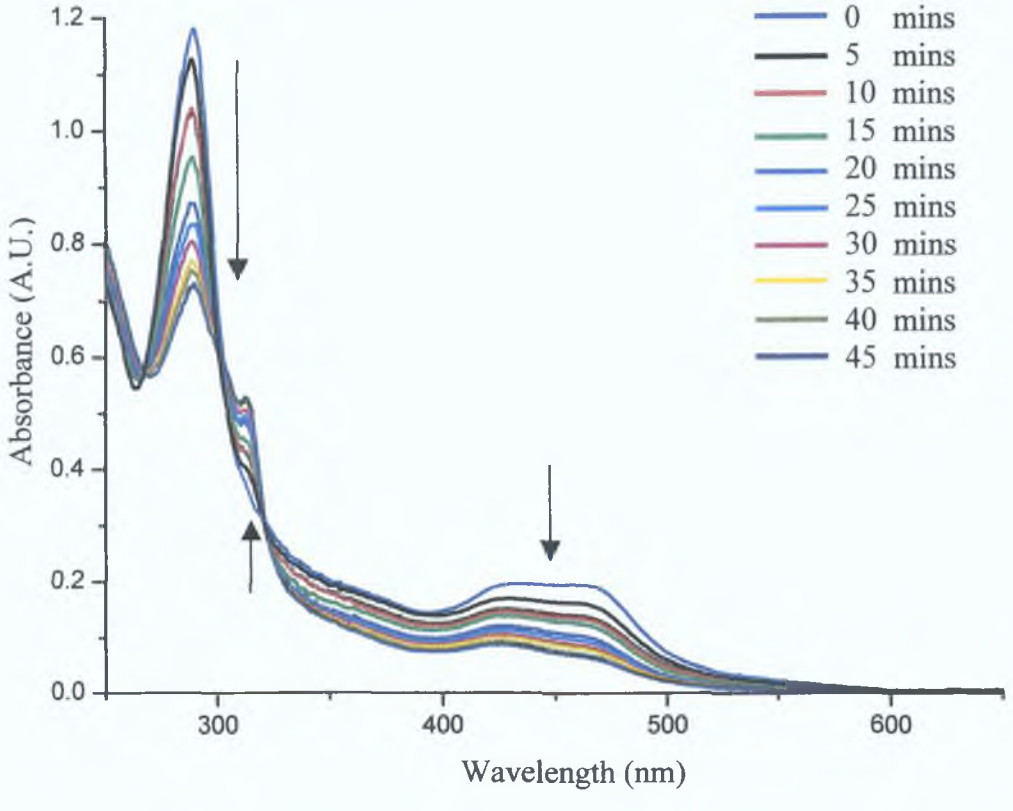

Figure 5.24 Spectroelectrochemical analysis of $[Ru(bpy)_2(L11)]^+$ at 1.20 V in neutral acetonitrile with 0.1 M TEAP vs. Ag|AgCl.

Figure 5.24 depicts the spectroelectrochemical analysis of the mononuclear pyridyltriazole complex $[Ru(bpy)_2(L11)]^+$ at 1.20 V versus Ag|AgCl while *figure 5.25* depicts the changes in the spectra of the mono- and dinuclear complexes $[Ru(bpy)_2(L12)]^+$ and $[Ru(bpy)_2(L14)Ru(bpy)_2]^{2+}$ at 1.30 V versus Ag|AgCl.

Electrochemical data in the previous section suggested that only the oxidation of the metal centre(s) (Ru^{II} to Ru^{III}) occurred in the anodic region of the cyclic voltammograms. This analysis seems reasonable from an examination of the spectroelectrochemical data obtained. For example, *figure 5.24* shows that as a potential of 1.20 V versus Ag|AgCl is applied to this system there is a concomitant loss of the MLCT accompanied by the appearance of a shoulder at circa 318 nm due to the formation of the Ru(III) species.[82] These changes are also accompanied by a depletion of the intense π-π* ligand-based absorbances at circa 290 nm (*figure 5.24*). [53]

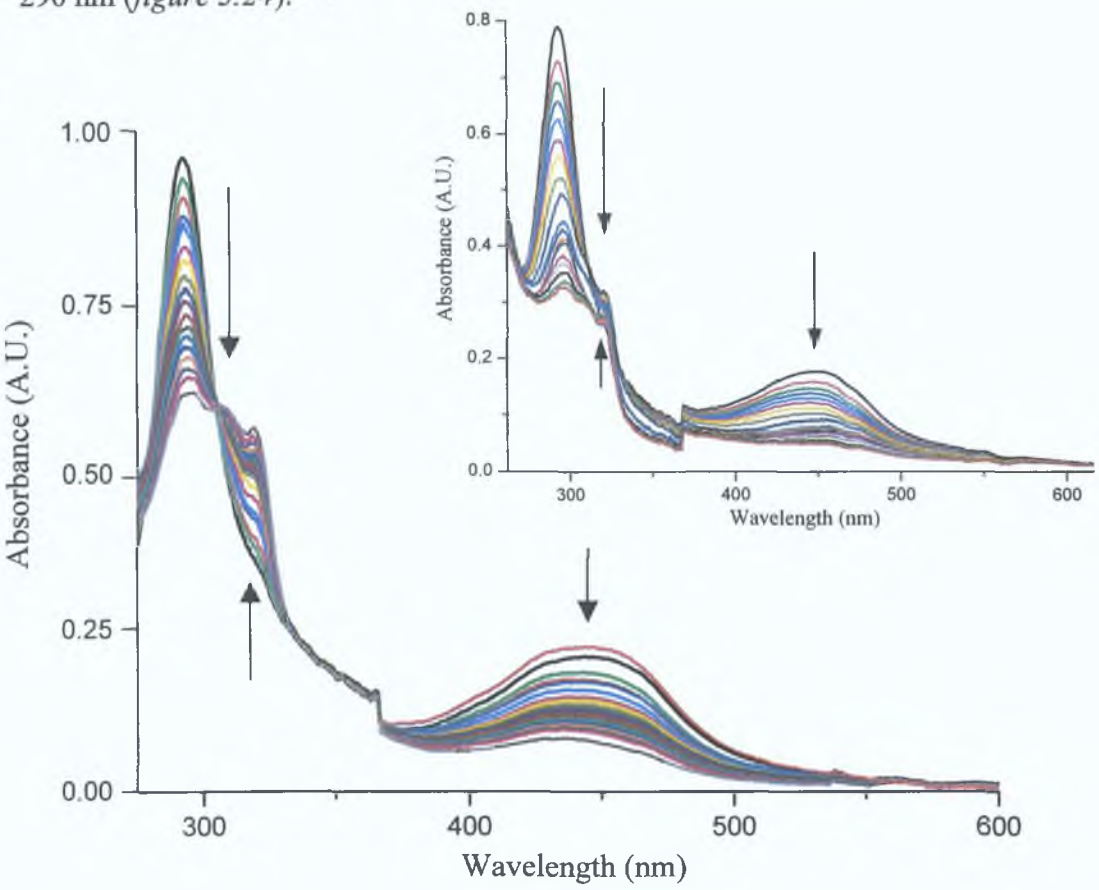

Figure 5.25 Spectroelectrochemical analysis of $[Ru(bpy)_2(L14)Ru(bpy)_2]^{2+}$ and (inset) $[Ru(bpy)_2(L12)]^{+}$ at 1.30 V in neutral acetonitrile with 0.1 M TEAP vs. Ag|AgCl.

This behaviour is reminiscent of the data obtained for the analogous methylated complexes (*section 3.3.5*) and contrasts starkly with that obtained for the hydroquinone-containing complexes (*section 4.6*). In the methylated analogues the same loss of bands was noted upon application of an oxidising potential, however, unlike in the case of these complexes there are no further ligand processes occurring beyond the metal oxidations.

There are also no complications in these quinone complexes arising from ligand processes occurring prior to the metal processes as was the case for the hydroquinone complexes (*section 4.6*) and hence, the changes in the spectra of these complexes are associated only with metal oxidation processes. The changes noted in the spectra of the mononuclear and dinuclear quinone complexes are also comparable to those observed for the protected pyridyltriazole complex. Therefore, it is clear that the oxidation of Ru(II) to Ru(III) is also occurring within this anodic potential window. Furthermore, the changes noted in the spectra of these complexes are clean and clear isobestic points are observable in all spectra indicating that only one process is occurring (*figure 5.24* and *figure 5.25*). Once again, this is reminiscent of the behaviour noted in the case of the methylated analogues although without the added complications of the subsequent ligand processes (*section 3.3.5*).

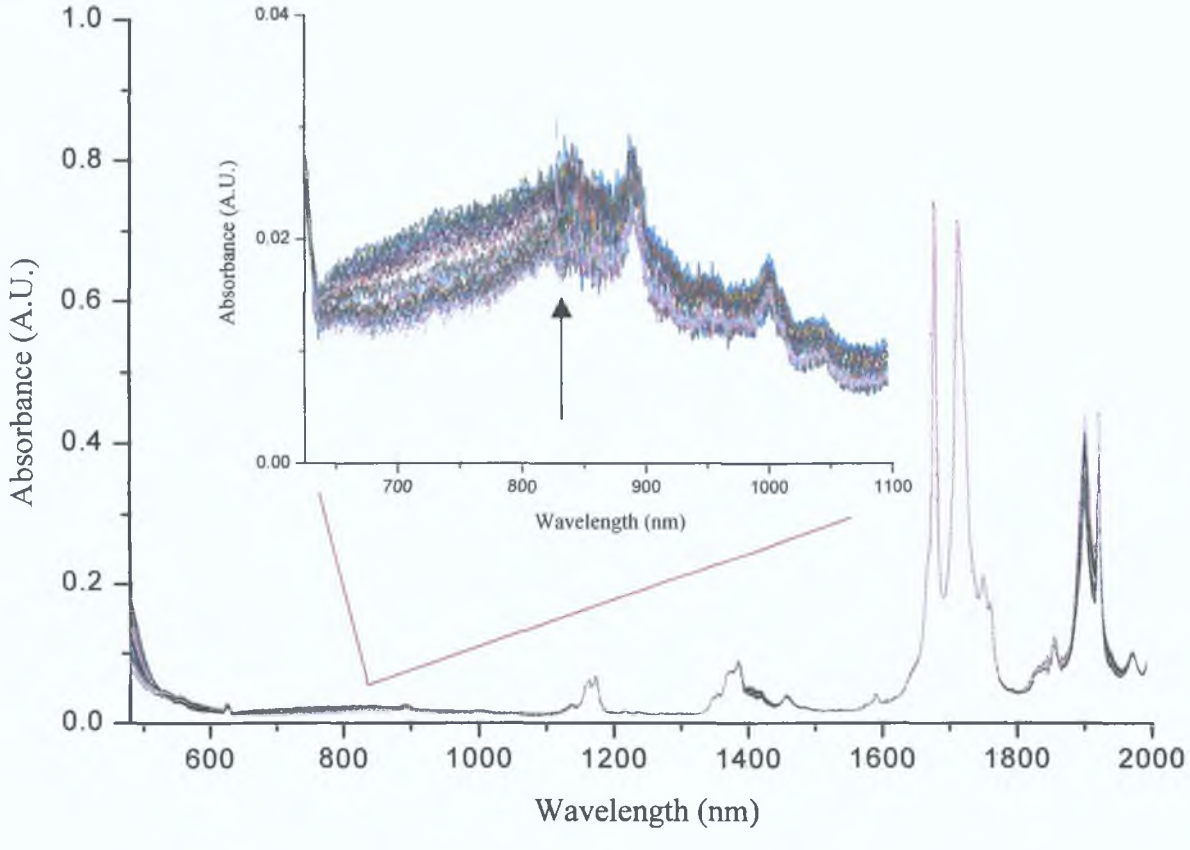

Figure 5.26 Spectroelectrochemical analysis of $[Ru(bpy)_2(L13)Ru(bpy)_2]^{2+}$ from 480 nm to 2000 nm and (*inset*) LMCT in the 625 nm to 1100 nm region at 1.20 V in acetonitrile with 0.1 M TEAP vs. Ag|AgCl.

Spectroelectrochemical measurements in region 300 nm to 2200 nm were also performed As potentials of 1 20 V for the pyridyltriazole complexes and 1 30 V versus Ag|AgCl for the pyrazyltriazole were applied to the mononuclear complexes the growth of an additional band is noted This band is centred at approximately 850 nm and appears as the metal is oxidised This band is similar to a band observed in the spectra of the dimethoxy and dihydroxy-containing complexes By comparison with these complexes and due to its position and also, since, it depletes once the potential is returned to 0 V this band may be associated with the formation of a bpy(π) – Ru d(π), ligand-to-metal-charge-transfer (LMCT) which arises due to the oxidation of the metal [54]

The position and intensity of this LMCT transition is also worth examining further in light of the LMCT transitions obtained in the case of the analogous dimethoxy and dihydroxy complexes For example, Nazeeruddin *et al* [83] examined the effects of the ligand on the LMCT Their findings indicated that the nature of these moieties has a significant effect on this transition and they found that replacement of a donor ligand by a weaker donor or acceptor ligand caused a red shift m the observed LMCT band In the case of the complexes presented in this chapter a shift in the LMCT compared to the methylated analogues is noted For example, the LMCT in the methylated complexes is centred at approximately 1200 nm in the spectrum while these quinone complexes have and LMCT in the region of 850 nm When considered in the light of the findings of Nazeeruddin *et al* [83] it is understandable as these quinone complexes are now acceptor ligands while the methylated ligands contained in the complexes m *chapter three* are relatively strong donor ligands They also found that the larger the σ-donor capacity of the ligand the more intense is the observed band and indeed, the methylated complexes yielded a more intense LMCT transition (*figure 3 29*) than the quinone complexes (*figure 5 26*) [83][84]

The dinuclear complexes were also analysed in this region of the spectrum and *figure 5 26* contains the spectroelectrochemical analysis of $[Ru(bpy)_2(L13)Ru(bpy)_2]^{2+}$ at 1 20 V versus Ag|AgCl in neutral acetonitrile

The spectroelectrochemical analyses of the dinuclear complexes is particularly relevant as it is in this region that intervalence transition bands (IT) can occur in mixed valence species and hence, provide an indication of the level of metal-metal inter-communication [85] From an examination of *figure 5 26* it can be seen that there is, indeed, the gradual appearance of a broad, weak band This band was also noted in the spectra of the pyrazyltriazole dinuclear complex However, by comparison with the mononuclear analogues this band, centred at approximately 850 nm, can be deemed to be LMCT in nature However, only solvent peaks are present in the rest of the spectrum as the oxidation proceeds and no other identifiable transitions were observed to appear in the 350 nm to 2200 nm region of the spectra (*figure 5 26*) Hence, no IT bands or at least no detectable IT bands were seen to form during the course of the oxidation This is perhaps unsurprising as it was suggested in the electrochemical data that there was a relatively small if any electronic interaction present between the metal centres (*section 5 5*)

5 6 2 Luminescence Spectroelectrochemistry

Luminescence spectroelectrochemical analyses were also performed on these quinone complexes and the data obtained from these measurements are presented in this section The experimental techniques utilised during these measurements are outlined in depth in *chapter two* The changes in the emission spectra with applied potentials versus Ag|AgCl in acetonitrile were monitored *Figure 5 27* was obtained for the mononuclear pyrazyltriazole complex $[Ru(bpy)_2(L12)]^+$ at 1 30 V versus Ag|AgCl This figure is typical of the emission spectra obtained for each of the quinone complexes presented within this chapter From the previous luminescence section it was seen that the emission emanates from the lowest excited state, which was deemed to be ^{3}MLCT in nature (*section 5 3 4*) The initial emission obtained at 0 V versus Ag|AgCl is represented in *figure 5 27* by a black line

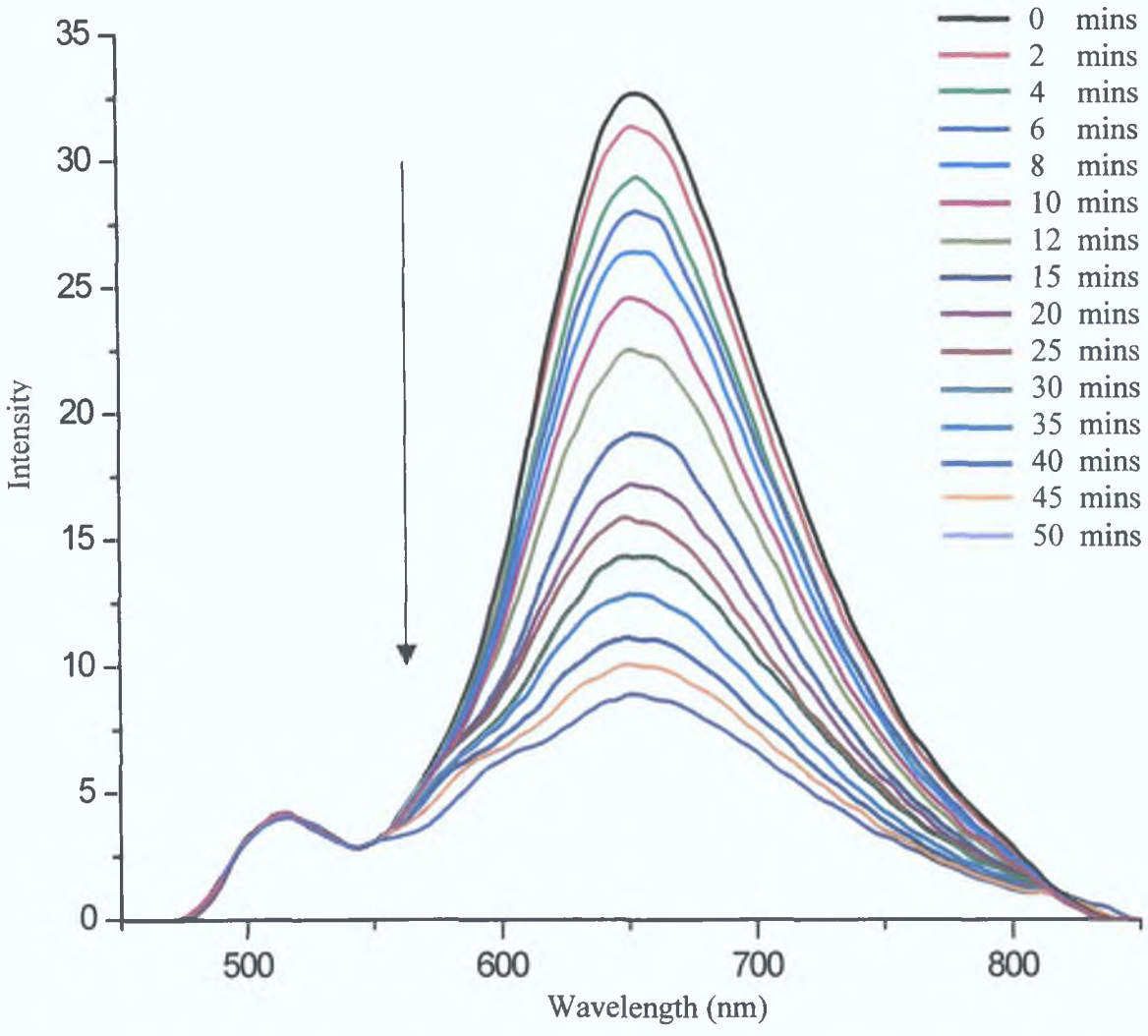

Figure 5.27 Luminescence spectroelectrochemical analysis of $[Ru(bpy)_2(L12)]^+$ in neutral acetonitrile with 0.1 M TEAP at 1.30 V vs. Ag|AgCl

The emission is observed to decrease upon the application of an oxidising potential (*figure 5.27*). This is, once again, indicative of the fact that at the potential applied the oxidation of the metal from Ru^{II} to Ru^{III} occurs and mirrors the behaviour noted for the emission measurements obtained for the methylated counterparts (*section 3.3.5*). This process was found to be reversible and upon returning the potential to 0 V versus Ag|AgCl the initial emission curve was returned. This is also suggestive of the fact that there was only one process occurring during the course of the application of an oxidising potential of 1.30 V versus Ag|AgCl. Analogous data were also obtained for the pyridyltriazole complexes in which an oxidising potential of 1.20 V versus Ag|AgCl also resulted in the depletion of the emission associated with the oxidation of the metal centre(s).

It must also finally be noted that the data obtained for the dinuclear complexes, once again, mirror the behaviour observed for their analogous mononuclear counterparts Hence, it is, once again, suggestive of the fact that the metal centres behave independently of each other

5.7 Conclusion

The synthesis, electrochemical and spectroscopic characterisation of the complexes $[Ru(bpy)_2(L11)]^+$, $[Ru(bpy)_2(L12)]^+$, $[Ru(bpy)_2(L13)Ru(bpy)_2]^{2+}$ and $[Ru(bpy)_2(L14)Ru(bpy)_2]^{2+}$ which contain quinone moieties are presented in this chapter These complexes represent the final group of compounds in the series of complexes presented in this thesis They provide a basis for the understanding of the processes occurring in the proceeding hydroquinone complexes in *chapter four* The quinone complexes were synthesised utilising the analogous protected complex presented in *chapter three* although their synthesis via the analogous hydroquinone-containing complexes is just as viable The synthesis of these quinone complexes was achieved utilising an aqueous solution of ceric ammonium nitrate (CAN) under mild reaction conditions Formation of the desired complex was verified via the loss of the –OMe peaks in the NMR spectrum of the complexes accompanied by a concomitant shift in the protons associated with the quinone moiety IR analyses were also used in order to ensure that the desired complexes were obtained

Computer generated DOS spectra provided theoretical evidence that the HOMO of these complexes is strongly influenced by the metal centre while the quinone ligand also contributes to a significant degree The LUMO, however, is strongly bipyridyl in nature This is an interesting observation as it is contrary to what was observed for the hydroquinone complexes and reflects the subsequent electrochemical measurements Absorption data were obtained which show that the quinone complexes display similar behaviour to their methylated counterparts However, there is a significant shift in the energies of the MLCT of these complexes compared to the protected analogues and a slight shift compared to the dihydroxy analogues This shift is associated with the replacement of one of the ligand moieties with an acceptor quinone ligand

Furthermore there was also an indication in the absorption measurements that there was little if any intermetallic communication in the dinuclear complexes $[Ru(bpy)_2(L13)Ru(bpy)_2]^{2+}$ and $[Ru(bpy)_2(L14)Ru(bpy)_2]^{2+}$ The luminescence measurements obtained for the dinuclear complexes also supported this supposition and the emission data for these complexes was also reminiscent of the protected and hydroquinone analogues Protonation of these complexes also displayed behaviour analogous to their protected analogues A decrease in the emission of the pyridyltriazole complexes is noted upon protonation This was also mirrored in the lifetimes of these complexes, which also depleted sharply upon the addition of acid due to the increased ability of the protonated complexes to populate the ^3MC This phenomenon is not noted in the low temperature luminescence or lifetime data, since, this is a thermally accessible level The addition of acid to the pyridyltriazole complexes also suggested that, once again, switching of the excited state of these complexes occurs upon protonation

The pKa data further confirmed the suggestion of switching of the excited state of the pyrazyltriazole complexes upon protonation pKa* measurements also confirmed that the excited state in the pyridyltriazole complexes is bipyridyl based upon protonation of the complex The acid-base properties of the quinone complexes were comparable to those of the protected complexes and the drop in the pKa value noted for the hydroquinone complexes was not observed for the quinone compounds This pKa data, therefore, may provide further evidence of hydrogen bridging in the hydroquinone complexes Electrochemical studies yielded cyclic voltammograms, which were unhindered by ligand processes in the anodic region This is quite unlike the situation noted for the protected or hydroquinone complexes, which do exhibit ligand redox processes in this region The metal processes observed in this region of the CV, however, are comparable to those witnessed in the CV of the methoxy complexes The cathodic region of the spectrum was also similar to that of the protected and dihydroxy-containing complexes in that similar pyrazine and bipyridyl processes were noted The electrochemical data also provided further compelling evidence of intermolecular proton transfer in the hydroquinone complexes

The cathodic regions of the CVs of the quinone complexes were found to contain an additional process associated with the reduction of the quinone moiety

Spectroelectrochemical analyses further supported the supposition that the oxidation of the metal(s) occurs upon the application of an oxidising potential These measurements also indicated, once again, that little or no intermetallic communication existed within the dinuclear complexes as no observable IT bands could be detected in the spectra of these complexes although there is a possibility that these transitions are extremely weak for these complexes Finally the luminescence spectroelectrochemical analyses also indicated that metal oxidation occurs upon the application of an oxidising potential and the independent nature of the metal centres in the dinuclear complexes is also re-established from the electrochemical measurements

The following chapter (*chapter six*) contain some final remarks and conclusions based on the observations made in the chapters three to five Some suggestions for future work are also contained in this final chapter

5.8 Bibliography

1 J P Deisenhofer, O Epp, K Miki, R Huber, H Michel, *J Mol Biol*, **1984**, 180, 385

2 J P Deisenhofer, O Epp, K Miki, R Huber, H Michel, *Nature*, **1985**, 318, 618

3 M R Gunner, P L Dutton, *J Am Chem Soc*, **1989**, 111, 3400

4 S Patai, *The Chemistry of Quinonoid Compounds*, **1988**, Wiley-Interscience, Chichester, 2, 719

5 J P Sauvage, J P Collin, J C Chambron, S Guillerez, C Coudret, *Chem Rev*, **1994**, 94, 993

6 G Dirks, A L Moore, T A Moore, D Gust, *Photochem Photobiol*, **1980**, 32, 277

7 R V Bensasson, E J Land, A L Moore, R L Crouch, G Dirks, T A Moore, D Gust, *Nature*, **1981**, 290, 329

8 D Gust, T A Moore, R V Bensasson, P Mathis, E J Land, C Chachaty, A L Moore, P A Liddell, G A Nemeth, *J Am Chem Soc*, **1985**, 107, 3631

9 D Gust, T A Moore, *J Photochem*, **1985**, 29, 173

10 J Zimmermann, J von Gersdorff, H Kurreck, B Roder, *J Photochem Photobio B*, **1997**, 40, 209

11 Y Aoyama, M Asakawa, Y Matsui, H Ogoshi, *J Am Chem Soc*, **1991**, 113, 6233

12 D Gust, T A Moore, P A Liddell, G A Nemeth, L R Makings, A L Moore, D Barrett, P J Pessiki, R V Bensasson, M Rougee, C Chachaty, F C De Schryver, M Van der Auweraer, A R Holzwarth, J S Connolly, *J Am Chem Soc*, **1987**, 109, 846

13 D Gust, P Mathis, A L Moore, P A Liddell, G A Nemeth, W R Lehman, T A Moore, R V Bensasson, E J Land, C Chachaty, Photochem Photobiol, **1983**, 37, 46

14 P Seta, E Bienvenue, A L Moore, P Mathis, R V Bensasson, P A Liddell, P J Pessiki, A Joy, T A Moore, D Gust, *Nature*, **1985**, 316, 653

15 P T Gulyas, T A Smith, M N Paddon-Row, *J Chem Soc, Dalton Trans*, **1999**, 1325

16 S I Gorelsky, E S Dodsworth, A B P Lever, A A Vlcek, *Coord Chem Rev*, **1998**, 174, 469

17 H Masui, P R Auburn, A B P Lever, *Inorg Chem*, **1991**, 30, 2402

18 H Masui, A B P Lever, E S Dodsworth, *Inorg Chem*, **1993**, 32, 258

19 A B P Lever, H Masui, R A Metcalfe, D J Stufkens, E S Dodsworth, P R Auburn, *Coord Chem Rev*, **1993**, 125, 317

20 D J Stufkens, T L Snoeck, A B P Lever, *Inorg Chem*, **1988**, 27, 953

21 M Haga, E S Dodsworth, A B P Lever, *Inorg Chem*, **1986**, 25, 447

22 A B P Lever, P Auburn, E S Dodsworth, M Haga, M Melnik, W A Nevin, *J Am Chem Soc*, **1988**, 110, 8076

23 R A Metcalfe, A B P Lever, *Inorg Chem*, **1997**, 36, 4762

24 P R Auburn, E S Dodsworth, M Haga, W Liu, W A Nevin, A B P Lever, *Inorg Chem*, **1991**, 31, 3502

25 C J da Cunha, S S Fielder, D V Stynes, H Masui, P R Auburn, A B P Lever, *Inorg Chim Acta*, **1996**, 242, 293

26 V Balzani, F Scandola, *Supramolecular Photochemistry*, **1991**, Ellis Horwood, Chichester

27 V Balzani, A Juris, M Venturi, S Campagna, S Serroni, *Chem Rev*, **1996**, 96, 759

28 K S Schanze, K Sauer, *J Am Chem Soc*, **1988**, 110, 1180

29 V Goulle, A Harriman, J M Lehn, *J Chem Soc, Chem Commun*, **1993**, 1034

30 V Balzani, F Scandola, *Comprehensive Supramolecular Chemistry, Supramolecular Technology*, **1996**, Pergamon Press, Oxford, 10, 687

31 R Eisenberg, *Prog Inorg Chem*, **1970**, 12, 295

32 J A McCleverty, *Prog Inorg Chem*, **1968**, 10, 49

33 R M Buchanan, J Claflin, C G Pierpont, *Inorg Chem*, **1983**, 22, 2552

34 E Mehrdad, *Inorg Chem*, **1999**, 38, 467

35 C G Pierpont, C W Lange, *Prog Inorg Chem*, **1994**, 41, 331

36 K A Oppermann, S L Mecklenburg, T J Meyer, *Inorg Chem*, **1994**, 33, 5295

37 P Passaniti, W R Browne, F C Lynch, D Hughes, M Nieuwenhuyzen, P James, M Maestri, J G Vos, *J Chem Soc, Dalton Trans*, **2002**, 1740

38 R Wang, T E Keyes, J G Vos, R H Schmehl, R Haga, *J Chem Soc, Chem Commun*, **1993**, 1652

39 S Fanni, T E Keyes, S Campagna, J G Vos, *Inorg Chem*, **1998**, 37, 5933

40 P Jacob III, P S Callery, A T Shulgin, N Castagnoli Jr, *J Org Chem*, **1976**, 41, 22

41 B Halton, A J Kay, Z Zha-mei, R Boses, T Haumann, *J Chem Soc, Perkin Trans*, **1996**, 1445

42 O C Musgrave, *Chem Rev*, **1969**, 69, 499

43 C D Snyder, H Rapoport, *J Am Chem Soc*, **1972**, 94, 227

44 K N Ganesh, J K M Sanders, *J Chem Soc, Perkins Trans*, **1982**, 1611

45 L Henriksen, *Tetrahedron Letts*, **1994**, 35, 7057

46 T E Keyes, P M Jayaweera, J J McGarvey, J G Vos, *J Chem Soc, Dalton Trans*, **1997**, 1627

47 H E Toma, P S Santos, A B P Lever, *Inorg Chem*, **1988**, 27, 3850

48 S D Pell, R B Salmonsen, A Abelleira, M J Clarke, *Inorg Chem Comm*, **1984**, 385

49 M J Frisch, G W Trucks, H B Schlegel, G E Scuseria, M A Robb, J R Cheeseman, J A Montgomery, Jr, *et al*, *Gaussian 03*, **2004**, Gaussian Inc, Wallingford CT

50 N M O'Boyle, J G Vos, *GaussSum 0 6*, **2003**, Dublin City University

51 H Rensmo, S Lunell, H Siegbahn, *J Photochem Photobiol A*, **1998**, 114, 117

52 L O'Brien, M Duati, S Rau, A L Guckian, T E Keyes, N M O'Boyle, A Serr, H Gorls, J G Vos, *J Chem Soc, Dalton Trans*, **2004**, 514

53 A Juris, V Balzani, F Barigelletti, S Campagna, P Belser, A von Zelewsky, *Coord Chem Rev*, **1988**, 84, 85

54 F M Weldon, J G Vos, *Inorg Chim Acta*, **2000**, 307, 13

55 T E Keyes, C M O'Connor, U O'Dwyer, C G Coates, P Callaghan, J J McGarvey, J G Vos, *J Phys Chem A*, **1999**, 103, 8915

56 F Barigelletti, L De Cola, V Balzani, R Hage, J G Haasnoot, J Reedijk, J G Vos, *Inorg Chem*, **1989**, 28, 4344

57 D G Whitten, *J Chem Ed*, **1983**, 60, 867

58 S Serroni, S Campagna, G Denti, T E Keyes, J G Vos, *Inorg Chem*, **1996**, 35, 4513

59 R Wang, J G Vos, R H Schmehl, R Hage, *J Am Chem Soc*, **1992**, 114, 1964

60 A D Shukla, B Whittle, H C Bajaj, A Das, M D Ward, *Inorg Chim Acta*, **1999**, 285, 89

61 Y Hou, P Xie, K Wu, J Wang, B Zhang, Y Cao, *Solar En Mat Solar Cells*, **2001**, 70, 131

62 M Wrighton, D L Morse, *J Am Chem Soc*, **1974**, 96, 996

63 S Fanni, T E Keyes, C M O'Connor, H Hughes, R Y Wang, J G Vos, *Coord Chem Rev*, **2000**, 208, 77

64 C G Coates, T E Keyes, H P Hughes, P M Jayaweera, J J McGarvey, J G Vos, *J Phys Chem A*, **1998**, 102, 5013

65 H A Nieuwenhuis, J G Haasnoot, R Hage, J Reedijk, T L Snoeck, D J Stufkens, J G Vos, *Inorg Chem*, **1991**, 30, 48

66 R Hage, J G Haasnoot, J Reedijk, R Wang, J G Vos, *Inorg Chem*, **1991**, 30, 3263

67 G A Heath, L J Yellowlees, P S Braterman, *J Chem Soc, Chem Commun*, **1981**, 287

68 W R Browne, C M O'Connor, H P Hughes, R Hage, O Walter, M Doering, J F Gallagher, J G Vos, *J Chem Soc, Dalton Trans*, **2002**, 4048

69 J G Vos, *Polyhedron*, **1992**, 11, 2285

70 J C Curtis, J S Bernstein, T J Meyer, *Inorg Chem*, **1985**, 24, 385

71 D E Richardson, H Taube, *Inorg Chem*, **1981**, 20, 1278

72 D Pletcher, H Thompson, *J Chem Soc, Faraday Trans*, **1998**, 3445

73 M Namazian, *J Mol Structure*, **2003**, 664, 273

74 M W Lehmann, D H Evans, *J Electroanal Chem*, **2001**, 500, 12

75 C G Pierpont, R M Buchanan, *Coord Chem Rev*, **1981**, 38, 45

76 S Bhattacharya, *Polyhedron*, **1994**, 13, 451

77 J H Wilford, M D Archer, J R Bolton, T F Ho, J A Schmidt, A C Weedon, *J Phys Chem*, **1985**, 89, 5395

78 M E Bodini, V Arancibia, *Trans Met Chem*, **1997**, 22, 150

79 M Namazian, P Norouzi, R Ranjbar, *J Mol Struct*, **2003**, 625, 235

80 P D Beer, P A Gale, Z Chen, M G B Drew, J A Heath, M I Ogden, H R Powell, *Inorg Chem*, **1997**, 36, 5880

81 J B Flanagan, S Margel, A J Bard, F C Anson, *J Am Chem Soc*, **1978**, 100, 4248

82 J R Kirchhoff, *Current Sep*, **1997**, 16, 11

83 Nazeeruddin M K, Zakeeruddin S M, Kalyanasundaram K, *J Phys Chem*, **1993**, 97, 9607

84 Thummel R P, Lefoulon F, Chirayil S, *Inorg Chem*, **1987**, 26, 3072

85 C Creutz, Prog *Inorg Chem*, **1983**, 30, 1

Chapter Six

Final Conclusions and Future Work

In this chapter the data obtained in the previous chapters are considered as a whole Some final remarks and conclusions based upon these amalgamated considerations are also reported along with some suggestions for future work

6 1 Final Conclusions

In this thesis, the synthesis and characterisation of a number of mononuclear and dinuclear ruthenium (II) bipyridyl complexes containing various triazole ligands is described In light of the experimental observations described in the previous three chapters a number of conclusions can be addressed which take into account the preceding observations as a whole These conclusions will be discussed under the following headings

1 General observations
2 Electrochemically induced proton transfer
3 Intramolecular communication
4 Quenching of the excited state
5 Intramolecular hydrogen bonding

1 *General observations*

In *chapter three* the synthesis of a group of ligands containing pyrazyltriazole and pyridyltriazole ligands with dimethoxyphenyl groups is described These ligands were then utilised in the preparation of mononuclear and dinuclear complexes and the photophysical and electrochemical properties of these complexes was investigated These complexes are characterised by the presence of strong $-OCH_3$ peaks in the ^{1}H-NMR spectra In the case of the mononuclear complexes two peaks are present, however, due to the highly symmetric nature of the dinuclear complexes, these methoxy peaks appear as one entity [1] The photophysical data obtained for these complexes shows that generally the complexes behave like $[Ru(bpy)_3]^{2+}$, however, the difference between the pyridyltriazole and the pyrazyltriazole complexes also becomes apparent Most notable of these differences is the ability of the pyrazyltriazole complexes to "switch" excited states from bipyridyl based to pyrazine based upon protonation [2] This is further substantiated by both the lifetime and pH data These dimethoxy containing complexes were then used as precursor complexes in the synthesis of the subsequent hydroquinone complexes

These complexes are analogous to the dimethoxy complexes, however, dihydroxy groups are now present in place of the dimethoxy moieties The methoxy complexes were demethylated using BBr_3 to yield the subsequent hydroquinone complexes [3] The ^{1}H-NMR spectra of these complexes are characterised by the lack of $-OCH_3$ peaks and the appearance of broad –OH peaks The photophysical data obtained for these complexes are comparable to that of the protected analogues with the exception that an extra band is present in the absorption spectra and it was suggested that this is associated with the hydroqumone moieties [4-6] A similar "switching" of the excited state is, once again, noted for the pyrazyltriazole complexes [2] This phenomenon is also substantiated by the pH data

A final group of complexes were also synthesised from the protected analogues These complexes are similar to the dimethoxy analogues with the exception that the dimethoxy phenyl group has been replaced by a benzoquinone moiety The synthesis of these complexes was achieved under mild conditions using CAN These complexes are characterised by the absence of either $-OCH_3$ or –OH peaks and a shifting of the protons associated with the phenyl moiety in the ^{1}H-NMR spectra [7] A band associated with the C=O moiety was also observed in the IR spectra of these complexes The photophysical data obtained for these complexes are comparable to that of the protected complexes, however, the MLCT of these complexes were observed to shift to lower energies due to the presence of the quinone moieties The pyrazyltriazole complexes also display a "switching" of the excited state upon protonation, a fact substantiated by both the lifetime and pH measurements [2]

2 *Electrochemically induced proton transfer*

It has been suggested previously that these hydroqumone-containing complexes display a reversible, electrochemically induced proton transfer reaction, which occurs from the hydroquinone group to the attached triazole ring (*scheme 4 1*) [4] The possibility that this proton transfer process is occurring in the hydroquinone complexes presented in this thesis, is also suggested by the experimental data For example, the electrochemical data for each group of complexes provides strong evidence of this phenomenon

In *chapter three* it was noted that the Ru^{II}/Ru^{III} oxidation processes occurred prior to those of the ligand moieties Conversely, the metal oxidations in the hydroquinone complexes are observed to occur subsequent to the ligand oxidations The computational calculations had already suggested that this would be observed for these complexes Furthermore, these metal processes are anodically shifted compared to the dimethoxy complexes The metal processes in the hydroquinone complexes are now observed to occur at approximately the same potential as the protonated dimethoxy complexes Upon addition of acid to the hydroquinone complexes, no shift was observed in the redox potential of the metal processes In the electrochemistry of the quinone complexes, the metal oxidations, which are not complicated by ligand processes as these are now observed in the cathodic region of the CV, are also observed to shift anodically compared to the protected analogues However, these processes are not shifted to potentials as high as those noted for the hydroquinone complexes Also, addition of acid to these complexes yields a shift in the redox potential of the metal(s) These data, therefore, seem to indicate that proton transfer *is* occurring in the hydroquinone complexes [4]

The most compelling evidence for the occurrence of this proton transfer comes from an examination of the spectroelectrochemical data obtained for the complexes In the case of the dimethoxy complexes the spectroelectrochemical data confirms that the metal oxidation(s) occur prior to the ligand processes Similarly, the spectroelectrochemical data obtained for the hydroquinone complexes shows that the ligand-based oxidations are occurring prior to those of the metals However, the triazole ring(s) are also observed to become "protonated" as the oxidation of the ligand moieties progresses Spectroelectrochemical analysis of the quinone complexes also confirmed that, at anodic potentials, oxidation of the metal(s) occurs During the course of the quinone investigations no such protonation was observed to occur Furthermore, the emission spectroelectrochemical data obtained for the hydroquinone complexes also confirms that, as the ligand groups are oxidised, protonation of the complexes occurs This is not observed for the dimethoxy or quinone complexes

These data, when considered as a whole, therefore, provide compelling evidence for the occurrence of electrochemically induced proton transfer from the hydroquinone group to the triazole moiety in both the pyridyltriazole and pyrazyltriazole mononuclear and dinuclear hydroquinone complexes

3 *Intramolecular communication*

In *chapter three* dinuclear pyridyltriazole and pyrazyltriazole complexes containing dimethoxyphenyl moieties were prepared The photophysical data obtained for these complexes shows that these dinuclear complexes have centres that behave independently of each other and the data obtained for these complexes are, therefore, similar to those obtained for their mononuclear counterparts The electrochemical measurements performed on these complexes also show a single bielectronic wave, associated with the simultaneous oxidation of the metal centres [1][5] This, therefore, suggests that intramolecular communication in these dinuclear complexes is weak [1][5] In the case of the pyridyltriazole dinuclear complex, spectroelectrochemical measurements yielded an IT band which aided in classifying this complex as class II with a weak metal-metal interaction [8][9] Unfortunately, no such data are obtainable for the pyrazyltriazole complex and therefore, the status of the intramolecular communication cannot be confirmed further at this point However, on the basis of the electrochemical measurements, it may be suggested that these complexes are either class II complexes with weak intramolecular communication or perhaps class I, with no metal-metal communication [8][9] A more comprehensive indication of the degree of intramolecular communication could be facilitated via the synthesis of the mixed-metal analogues and this possibility is explored further in the following section (*section 6 2*)

Replacement of the dimethoxy groups by hydroquinone moieties did not alter the intramolecular communication greatly In the case of the hydroquinone dinuclear complexes, a single bielectronic wave is observed in the cathodic region of the CVs The metal centres in these complexes also appear to behave independently of one another and the photophysical data obtained for the dinuclear complexes are comparable to that obtained for their mononuclear counterparts

Spectroelectrochemical measurements yielded no observable IT bands in the spectra of either the pyridyltriazole or pyrazyltriazole dinuclear complexes and therefore, the degree in intramolecular communication present in these complexes cannot be further classified at present However, it is possible that these complexes are either class II with weak metal-metal interactions or class I with no intramolecular communication [8][9] It would, therefore, be of interest to demethylate the mixed metal dinuclear protected analogues, as suggested previously These complexes may then aid in the elucidation of the degree of intramolecular communication in the hydroquinone complexes

The quinone dmuclear complexes also displayed photophysical characteristics similar to those of their mononuclear analogues The CVs of these complexes depicted a single bielectronic wave associated with the $2e^-$ oxidation of the metal centres On the basis of these data the degree of metal-metal communication m these quinone complexes is also deemed to be, at best, weak However, a lack of observable IT bands for the pyridyltriazole and pyrazyltriazole dmuclear complexes means that the degree of communication cannot be classified further On the basis of these data, therefore, it appears as if these quinone complexes are also either class I or class II in nature However, if the mixed metal analogues of these complexes were to be synthesised intramolecular communication could be examined further (*section 6 2*)

Overall, therefore, the pyridyltriazole dimethoxy dinuclear complex is a class II complex while it appears that metal-metal interaction in the rest of the dinuclear complexes is at best weak or possible not present at all Changing the nature of the phenyl group appears to invoke little change in the degree of intramolecular communication in these complexes

4 ***Quenching of the excited state***

It was hoped that the presence of the anionic triazole-bridging group in these complexes would evoke interesting characteristic due to the fact that the donor group is linked to a bridging ligand, which is not involved in the luminescent ^{3}MLCT state and is also negatively charged This *could*, therefore, facilitate a longer-lived charge separated state In previous studies, in which an anionic linker was not included, it was found that quinones are excellent quenchers of the excited state [7][10] Hydroquinones were also found to effect the lifetime of the excited state in previous studies [11] The hydroquinone complexes contained in this thesis, however, are not observed to quench the excited state when the lifetimes of these complexes were compared to those obtained for the dimethoxy analogues This is also the case for previously reported catechol complexes containing triazole bridges [3]

Furthermore, there is no observable quenching of the excited state noted for the quinone-containing complexes compared to the dimethoxy analogues Single photon counting techniques verified this observation This is an interesting observation as it suggests that the negatively charge triazole bridge can stop quenching of the excited state by the quinone moieties Fanni *et al* made a similar observation previously They prepared a ruthenium complex in which a phenothiazine group was attached to ruthenium via a negatively charged triazole group (*figure 5 8*) These workers found that the presence of the triazole ring in the bridging ligand could effectively mediate electron-transfer processes, as the excited state was not as efficiently quenched, as was the case for the analogous complexes, which did not contain a triazole moiety [12]

It is, therefore, possible to conclude that the presence of the negatively charged triazole ring in the bridging ligand of the complexes presented in this thesis plays a significant role in controlling the interaction between the excited state and the quenching moiety

5 ***Intramolecular Hydrogen Bonding***

Although the presence of intramolecular hydrogen bonding in these complexes cannot be verified without X-ray crystallographic data, which was unfortunately not obtained for the hydroquinone or quinone-containing complexes, some of the data obtained for these complexes does justify the suggestion that intramolecular hydrogen bonding may be present in the hydroquinone complexes The pH data provides the most compelling evidence for this phenomenon The ground-state data obtained for the hydroquinone complexes suggested that they were considerably more acidic than their dimethoxy analogues One of the reasons for this is the presence of hydrogen bridging between the hydroquinone and the triazole Furthermore, the pH data obtained for the quinone complexes were not more acidic than their protected analogues This, therefore, suggests that the cause of the increased acidity in the hydroquinone complexes is associated with the hydroquinone moieties Also, it is not just the presence of the hydroquinone moieties that results in this increase in the ground state pKa value as the analogous catecholate complex does not display a similar increase in the acidity of the ground state [3] It is, therefore, justified to suggest that this occurs as a result of hydrogen bridging between the hydroquinone and the adjacent triazole ring

6.2 Future Work

The series of complexes containing dimethoxy, hydroquinone and quinone moieties have been examined in this thesis and a number of interesting conclusions have been reached as a result of the analysis of their photophysical and electrochemical properties However, additional work could now be conducted on these complexes to support the conclusions made in *section 6 1* For instance, it would be helpful to obtain the X-ray crystal structure for both the quinone and the hydroquinone complexes This could confirm the presence of hydrogen bonding in the hydroquinone complexes Transient absorption studies could also be undertaken in order to further examine the process of photoinduced proton transfer that occurs within the hydroquinone complexes

Furthermore, as the mononuclear and dinuclear complexes described within this thesis have proved to have interesting characteristics, these could be further utilised For example, it may be of interest to synthesis the osmium analogues of the complexes discussed in this thesis in order investigate the effect that this metal evokes within these complexes prior to the preparation of the heterodinuclear analogues The ligands, utilised in the preparation of the dinuclear complexes discussed in this thesis, could then be used to produce a vast quantity of mixed metal complexes These complexes could aid in elucidating the degree of metal-metal communication present in these complexes, since, the ruthenium-osmium complexes display two separate oxidation waves for the metal centres

A number of authors have prepared the hetrodinuclear ruthenium-osmium analogues of homonuclear ruthemum-ruthenium complexes in order to elucidate the degree of intramolecular communication Weldon *et al* prepared both homo- and heteronuclear ruthenium and osmium polypyridyl complexes containing the following bridging ligands (*figure 6 1*)

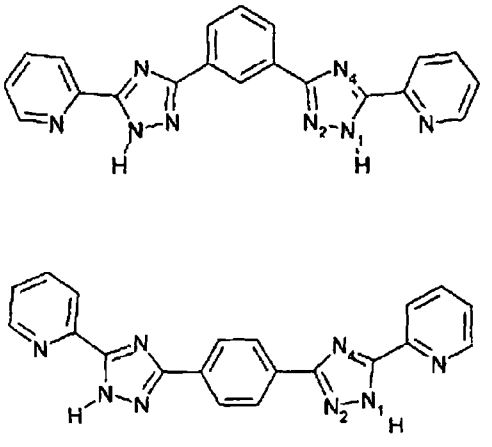

Figure 6 1 Bridging ligands utilised by *Weldon et al* in the synthesis of mixed-metal ruthenium-osmium complexes [13]

The homodinuclear ruthenium complexes were also prepared and these complexes show a single two-electron redox wave without any evidence of splitting [14] This is indicative of, at best, a weak interaction between the two metal centers in the ground state This suggestion was substantiated by spectroelectrochemical measurements [14]

The fact that the oxidation potentials of the Os(II) and Ru(II) centers in their respective mononuclear and dinuclear complexes are identical, within experimental uncertainty, is in agreement with their observation [13] These heterodmuclear complexes, therefore, showed excited state interactions and confirmed that intramolecular communication across this triazole bridging ligand is weak A similar approach could be taken for the dinuclear complexes contained in this thesis *Appendix C* contains the synthesis of the ruthenium mononuclear complexes that could act as precursor complexes for mixed-metal synthesis

The possibility of introducing bipyridyl moieties within these metal units containing groups, which bind to surfaces, is also a further possibility Once again, both the hydroquinone and quinone versions could also be obtained For example, Vos and co-workers prepared mononuclear, homodinuclear and heterodinuclear ruthenium and osmium complexes in which the bipyridyl moieties contained pendant dicarboxylate groups [14][15] These groups facilitated in the adsorption of the dyes complexes onto nanostructured TiO_2 and ZnO surfaces These dye-sensitized nanostructured film electrodes were then investigated for their potential use in solar cells [14][15]

6.3 Bibliography

1 P Passaniti, W R Browne, F C Lynch, D Hughes, M Nieuwenhuyzen, P James, M Maestri, J G Vos, *J Chem Soc , Dalton Trans* , **2002**, 1740

2 S Fanni, T E Keyes, C M O'Connor, H Hughes, R Wang, J G Vos, *Coord Chem Rev* , **2000**, 208, 77

3 L O'Brien, M Duati, S Rau, A L Guckian, T E Keyes, N M O'Boyle, A Serr, H Gorls, J G Vos, *J Chem Soc , Dalton Trans* , **2004**, 514

4 R Wang, T E Keyes, R Hage, R H Schmehl, J G Vos, *J Chem Soc , Chem Commun* , **1993**, 1652

5 F M Weldon, J G Vos, *Inorg Chim Acta*, **2000**, 307, 13

6 T E Keyes, P M Jayaweera, J J McGarvey, J G Vos, *J Chem Soc , Dalton Trans* , **1997**, 1627

7 V Goulle, A Harriman, J M Lehn, *J Chem Soc , Chem Commun* , **1993**, 1034

8 A C Ribou, J P Launay, M L Sachtleben, H Li, C W Spangler, *Inorg Chem* , **1996**, 35, 3735

9 A C Ribou, J P Launay, K Takahashi, T Nihira, S Tarutani, C W Spangler, *Inorg Chem* , **1994**, 33, 1325

10 K S Schanze, K Sauer, *J Am Chem Soc* , **1988**, 110, 1180

11 C Y Duan, Z L Lu, X Z You, Z Y Zhou, T C W Mak, Q Luo, J Y Zhou, *Polyhedron*, **1998**, 17, *23*, 4131

12 S Fanni, T E Keyes, S Campagna, J G Vos, *Inorg Chem* , **1998**, 37, 5933

13 F Weldon, L Hammarstrom, E Mukhtar, R Hage, E Gunneweg, J G Haasnoot, J Reedijk, W R Browne, A L Guckian, J G Vos, *Inorg Chem* **2004**, 43, 4471

14 W R Browne, F Weldon, A Guckian, J G Vos, *Collect Czech Chem Commun* , **2003**, 1467

15 K Westermark, H Rensmo, A C Lees, J G Vos, H Siegbahn, *J Phys Chem B*, **2002**, 106, 10108

Appendix A

Additional NMR Data

This appendix contains additional NMR data pertaining to the mono- and dinuclear ruthenium (II) complexes with pyridyl- or pyrazyl-1,2,4-triazole and dimethoxy-, dihydroxy- or quinone moieties that were not already presented in the main body of this thesis

A.1 Introduction

In the following sections the NMR data for the complexes contained in this thesis, which are not included in any of the preceding chapters, have been provided. The experimental details for this NMR data can be found in chapter two. In the case of each of the ligands the NMR data was obtained in d_6-dimethyl sulphoxide while the complexes were run in d_8-acetonitrile.

A.2 NMR Spectra

A.2.1 NMR Spectra of Ligands

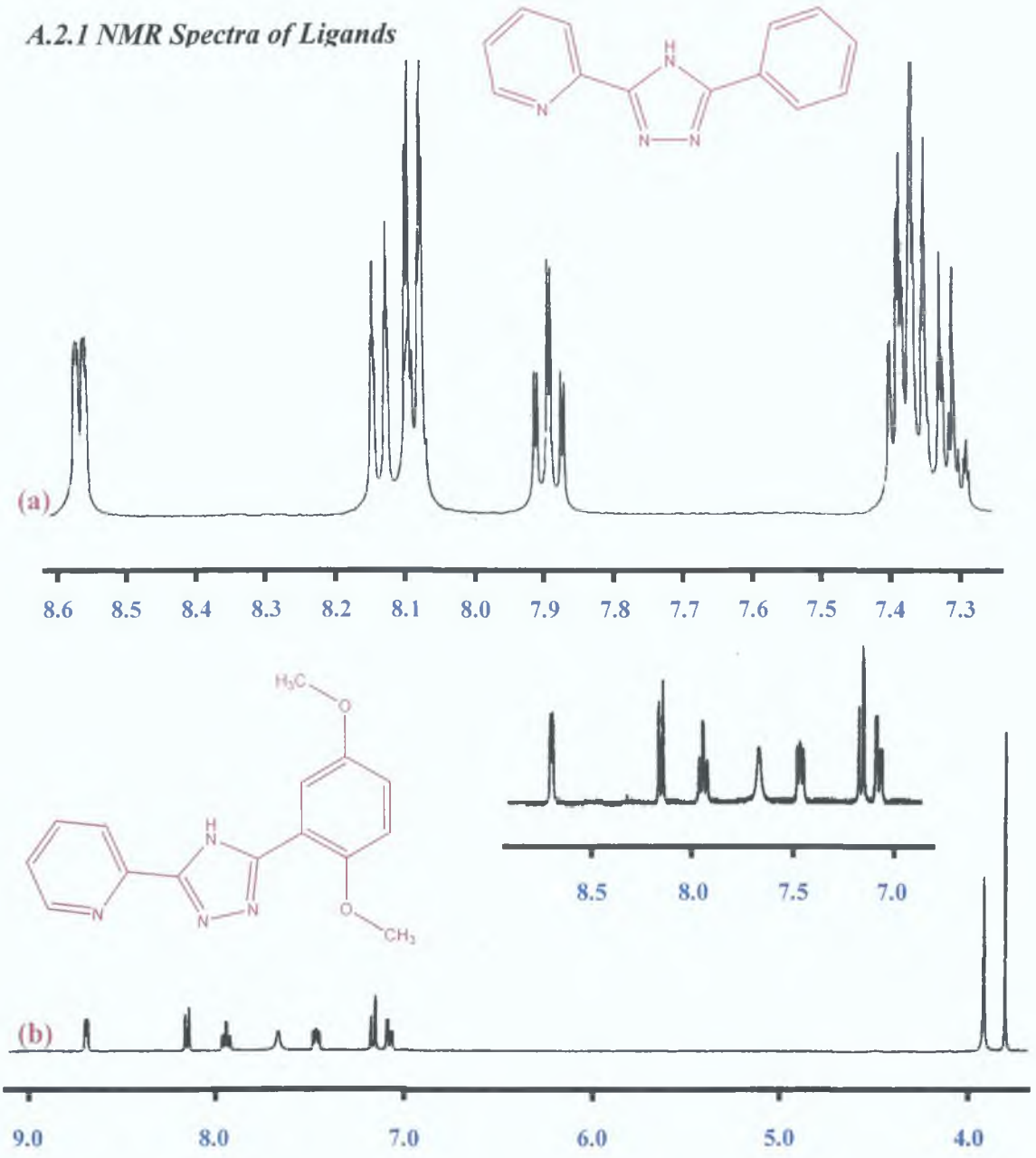

Figure A.1 ^{1}H-NMR spectra of the ligands **(a)** HL1 and **(b)** HL3 measured in d_6-dimethyl sulphoxide (chemical shifts / ppm vs Me_4Si)

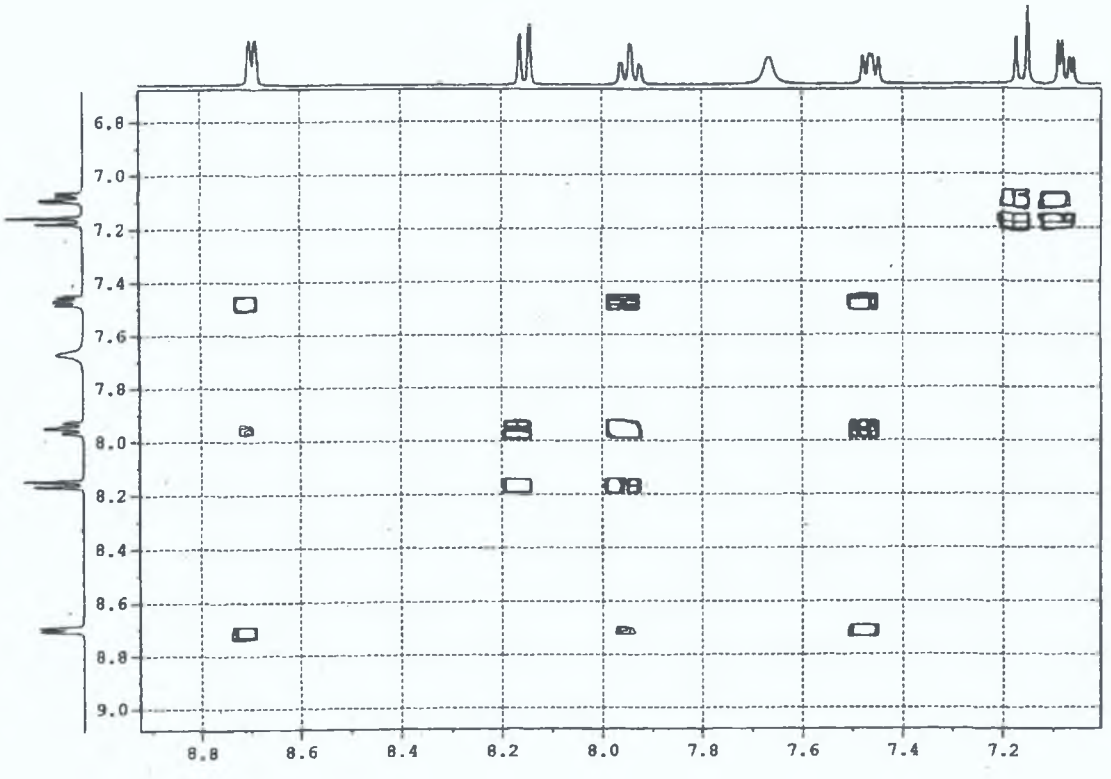

Figure A.2 COSY spectrum of the ligand HL3 measured in d_6-dimethyl sulphoxide (chemical shifts / ppm vs Me_4Si)

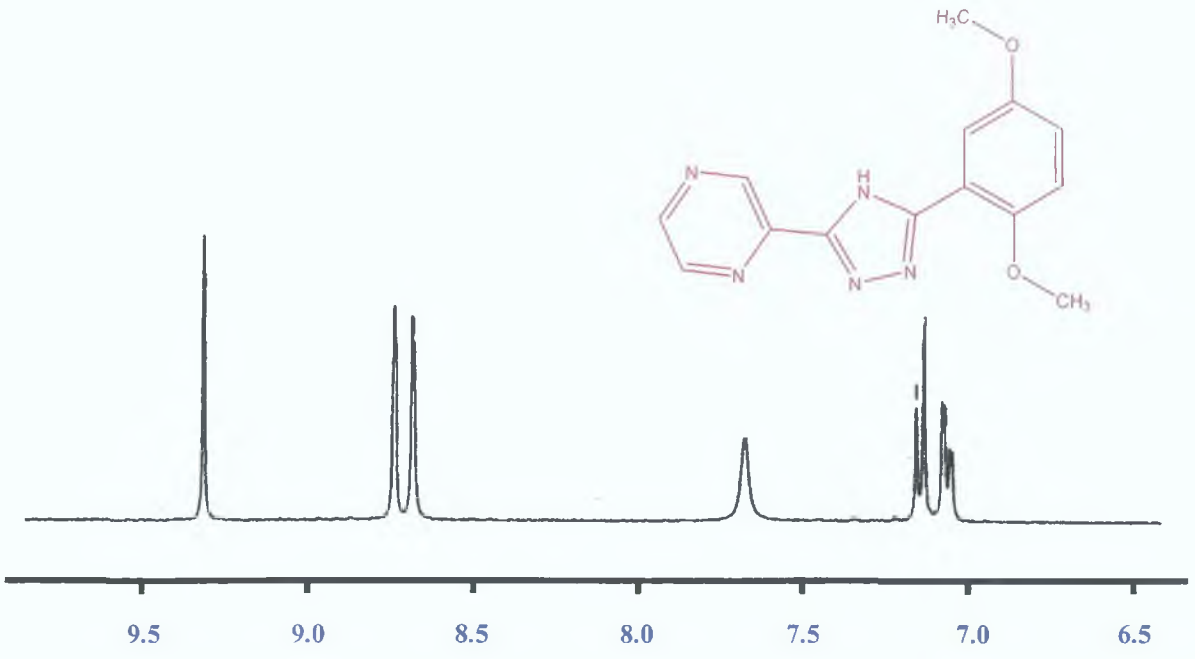

Figure A.3 ^{1}H-NMR spectrum of the ligand HL4 measured in d_6-dimethyl sulphoxide (chemical shifts / ppm vs Me_4Si)

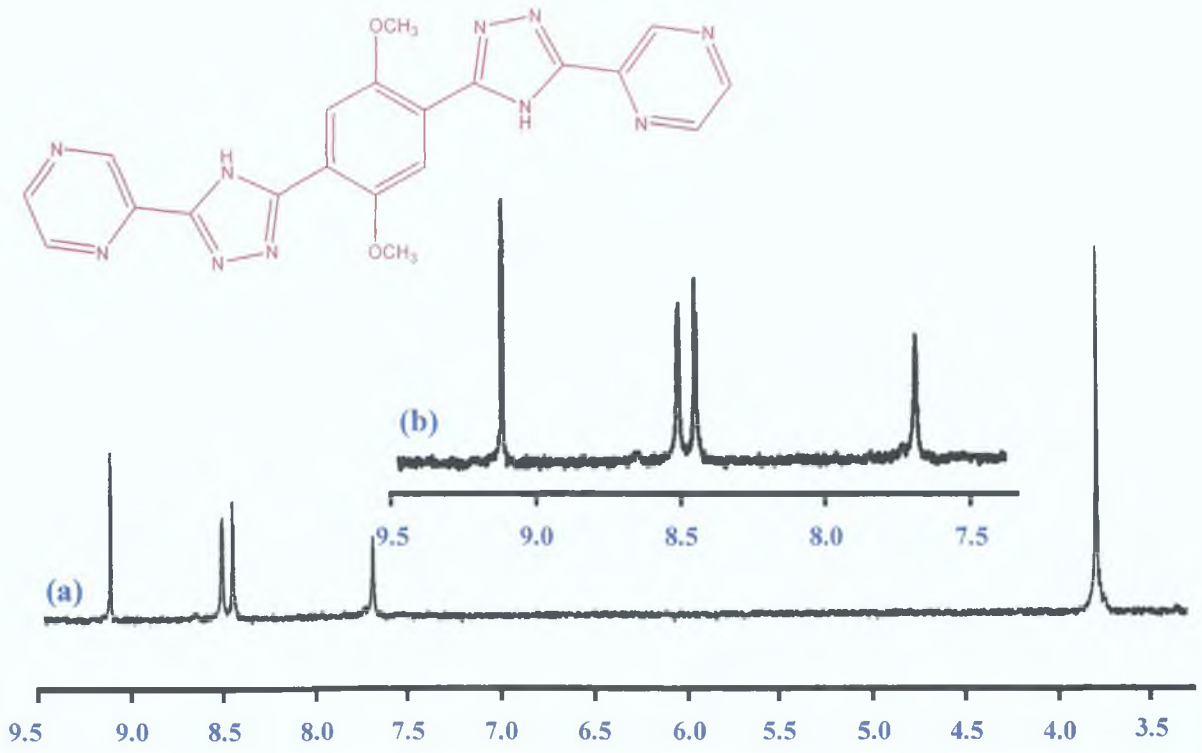

Figure A.4 ^{1}H-NMR spectrum of the ligand H_2L4 measured in d_6-dimethyl sulphoxide (chemical shifts / ppm vs Me_4Si)

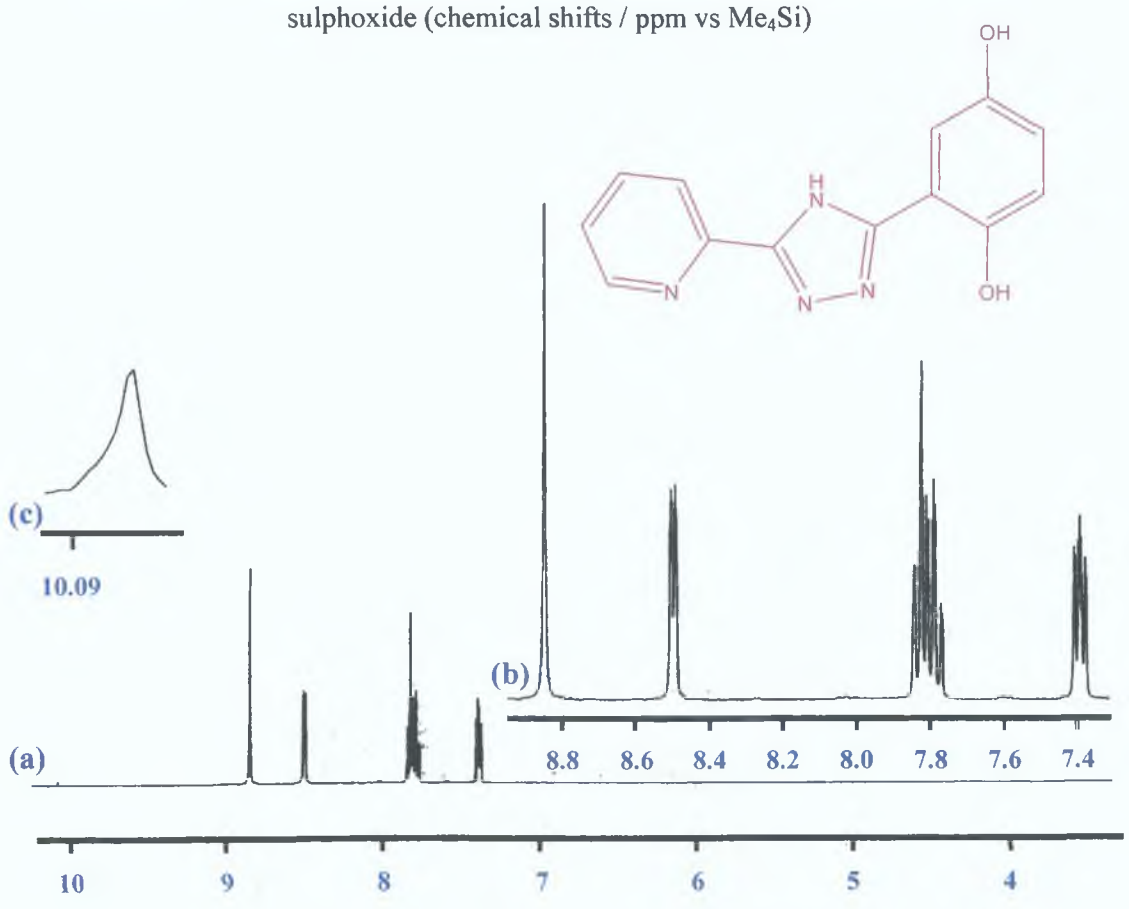

Figure A.5 ^{1}H-NMR spectrum of the ligand H_2L4 measured in d_6-dimethyl sulphoxide (chemical shifts / ppm vs Me_4Si)

A.2.2 NMR Spectra of Complexes

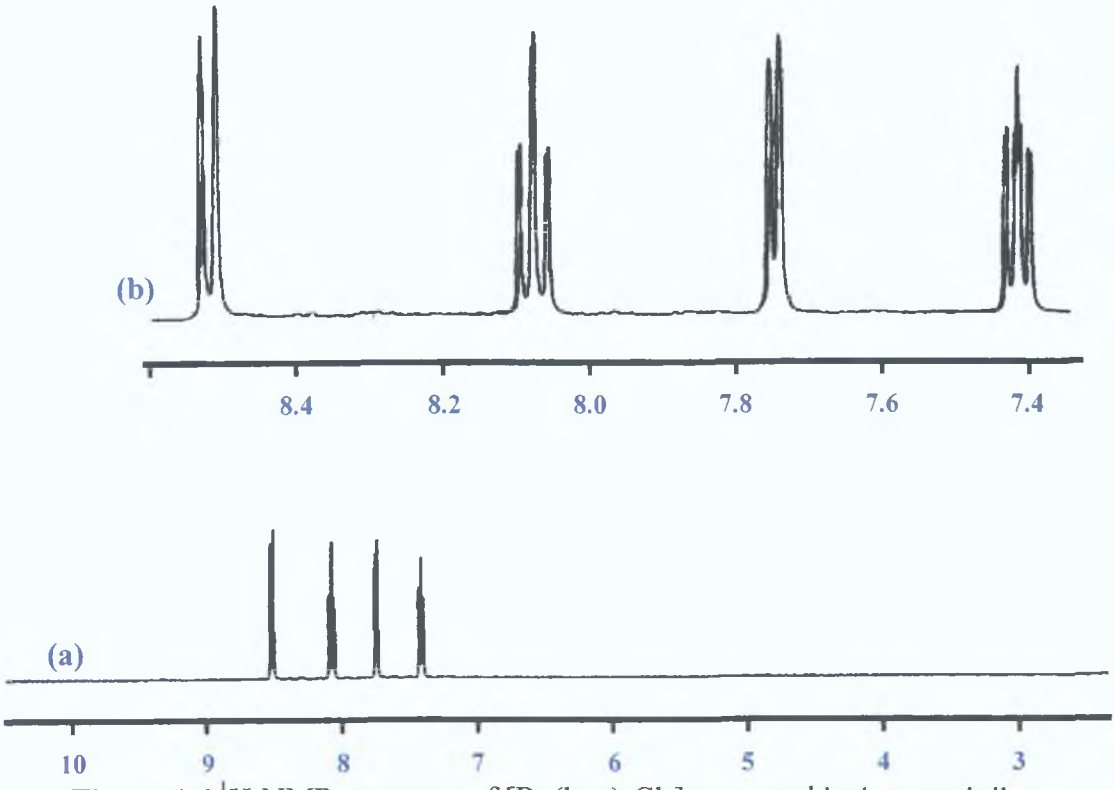

Figure A.6 ^{1}H-NMR spectrum of $[Ru(bpy)_2Cl_2]$ measured in d_8-acetonitrile (chemical shifts / ppm vs Me_4Si)

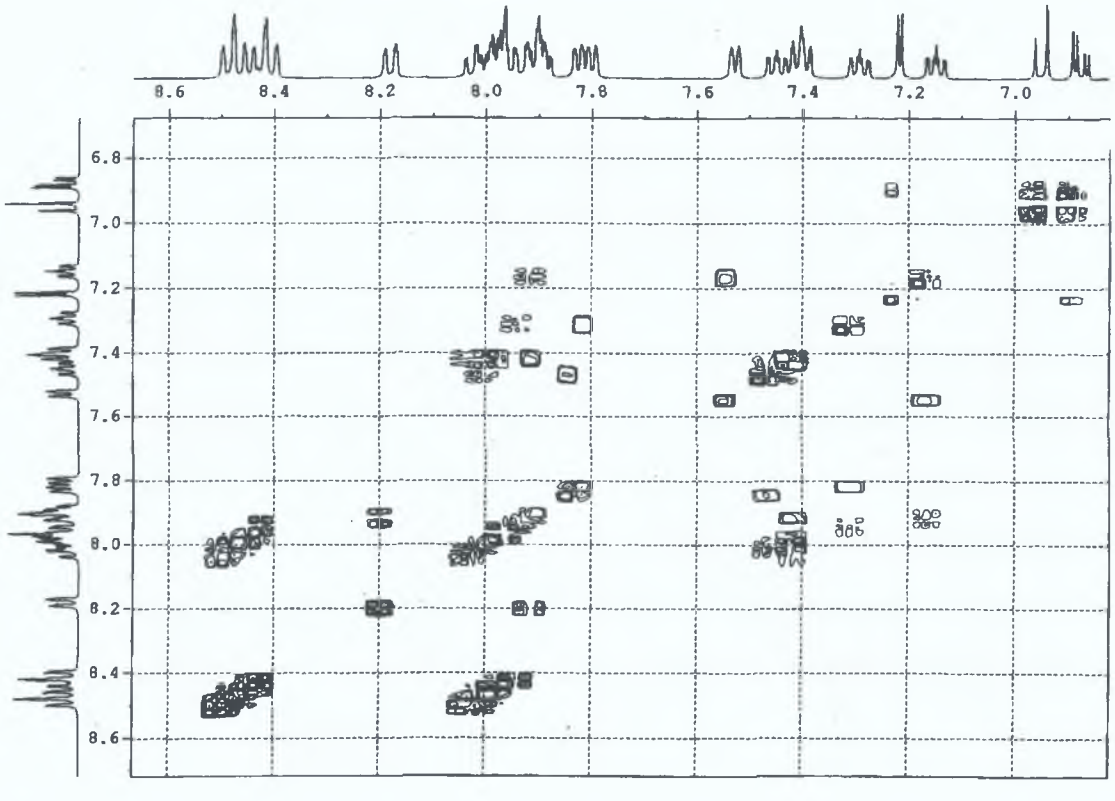

Figure A.7 COSY Spectrum of $[Ru(bpy)_2(L3)]^+$ measured in d_8-acetonitrile (chemical shifts / ppm vs Me_4Si)

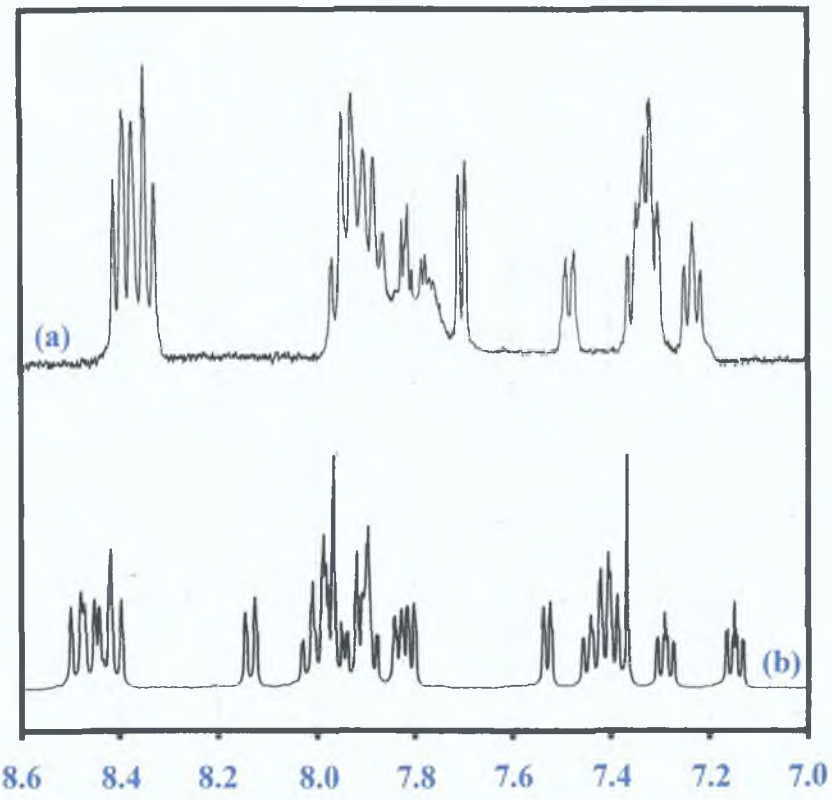

Figure A.8 ^{1}H-NMR spectra of **(a)** $[Ru(bpy)_2(L13)\ Ru(bpy)_2]^{2+}$ and **(b)** $[Ru(bpy)_2(L5)Ru(bpy)_2]^{2+}$ in d_3-acetonitrile

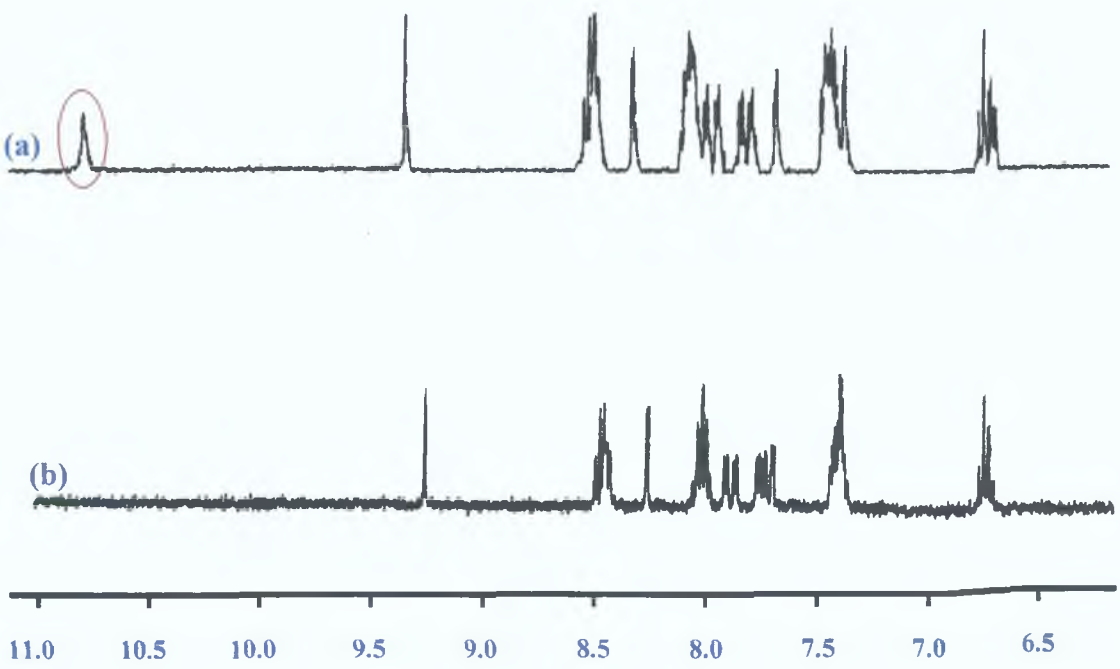

Figure A.9 ^{1}H-NMR spectra of **(a)** $[Ru(bpy)_2(L8)]^+$ and **(b)** $[Ru(bpy)_2(L8)]^+$ with 1 drop of D_2O in d_3-acetonitrile

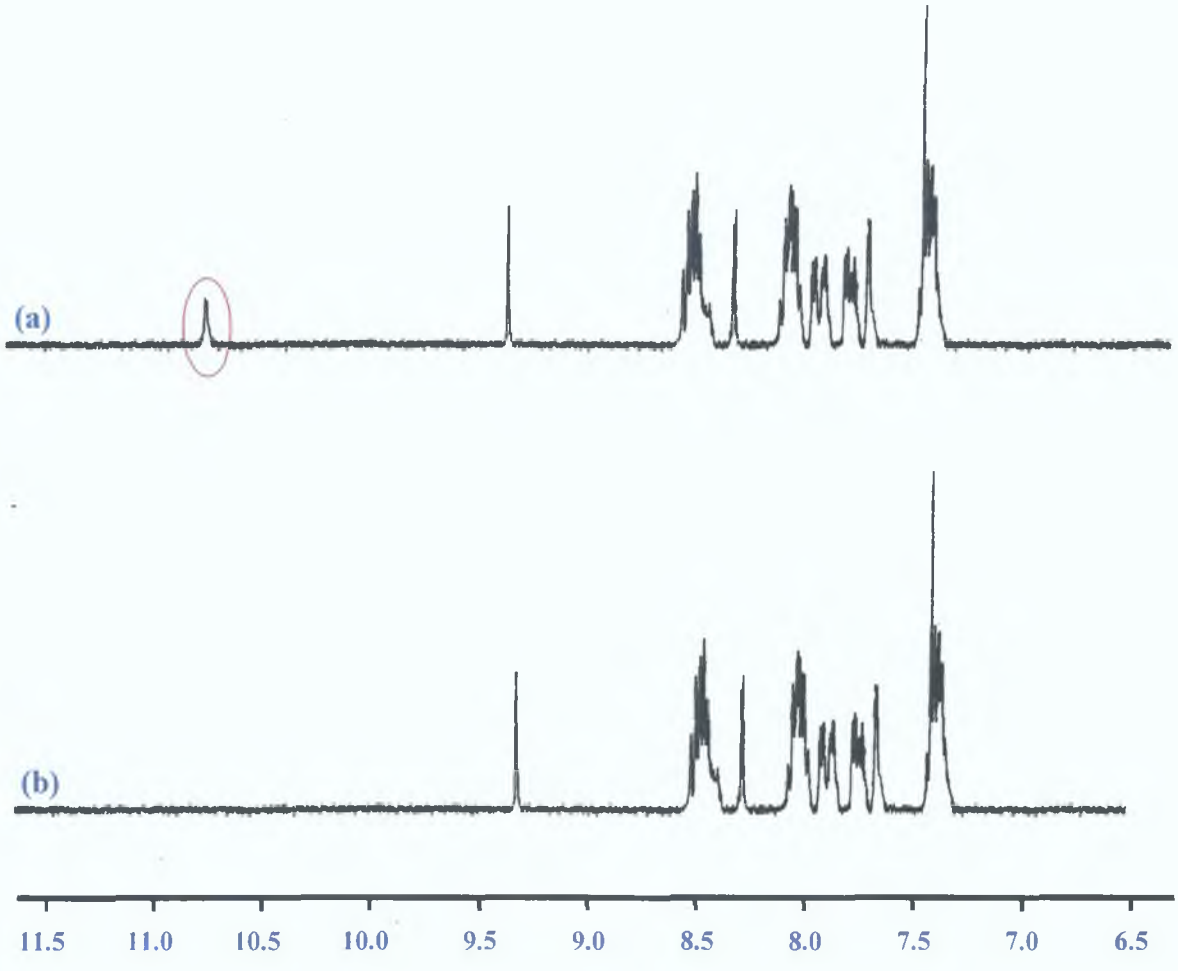

Figure A.10 ^{1}H-NMR spectra of **(a)** $[Ru(bpy)_2(L10)Ru(bpy)_2]^{2+}$ and **(b)** $[Ru(bpy)_2(L10)Ru(bpy)_2]^{2+}$ with 1 drop of D_2O in d_3-acetonitrile

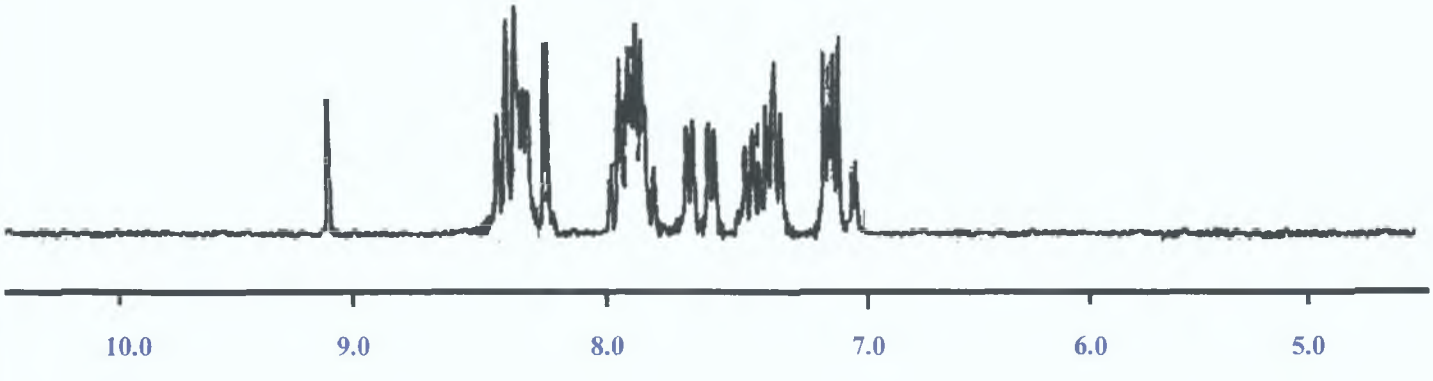

Figure A.11 ^{1}H-NMR spectrum of the complex $[Ru(bpy)_2(L12)]^{+}$ in d_3-acetonitrile

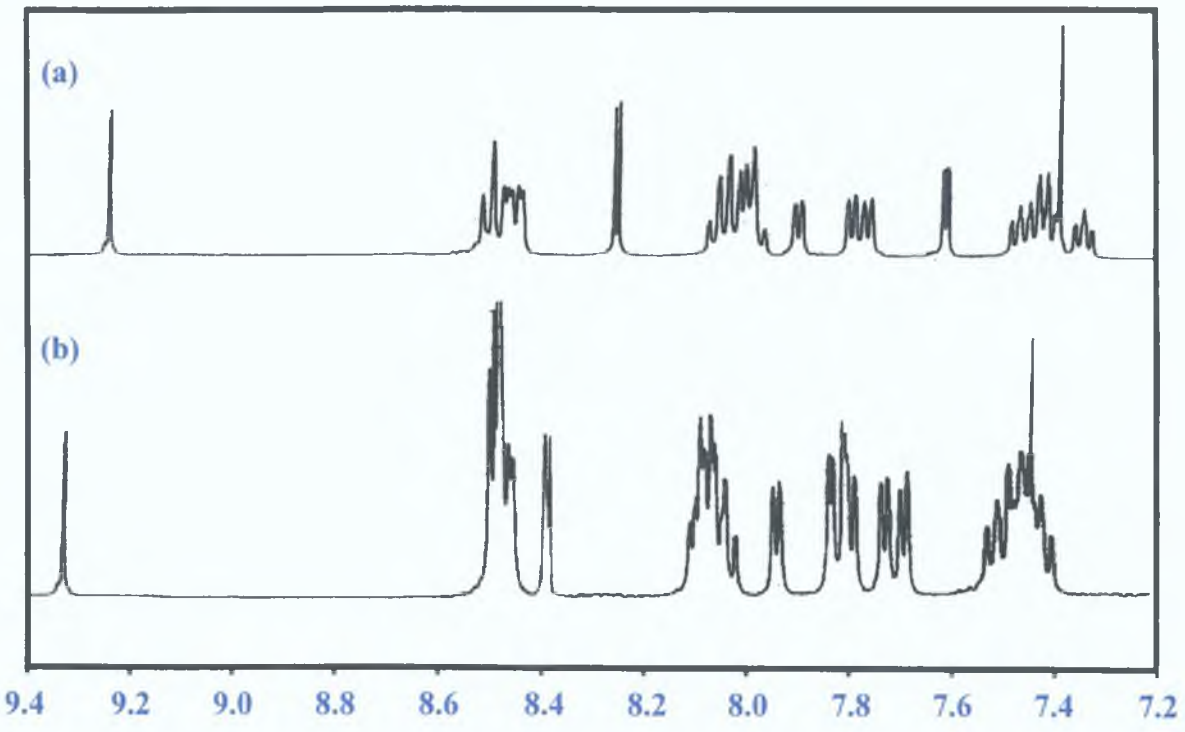

Figure A.12 ^{1}H-NMR spectra of **(a)** $[Ru(bpy)_2(L6)Ru(bpy)_2]^{2+}$ and **(b)** $[Ru(bpy)_2(L14)Ru(bpy)_2]^{2+}$ in d_8-acetonitrile (chemical shifts / ppm vs Me_4Si)

A.2.3 NMR Spectra of Deuterated Complexes

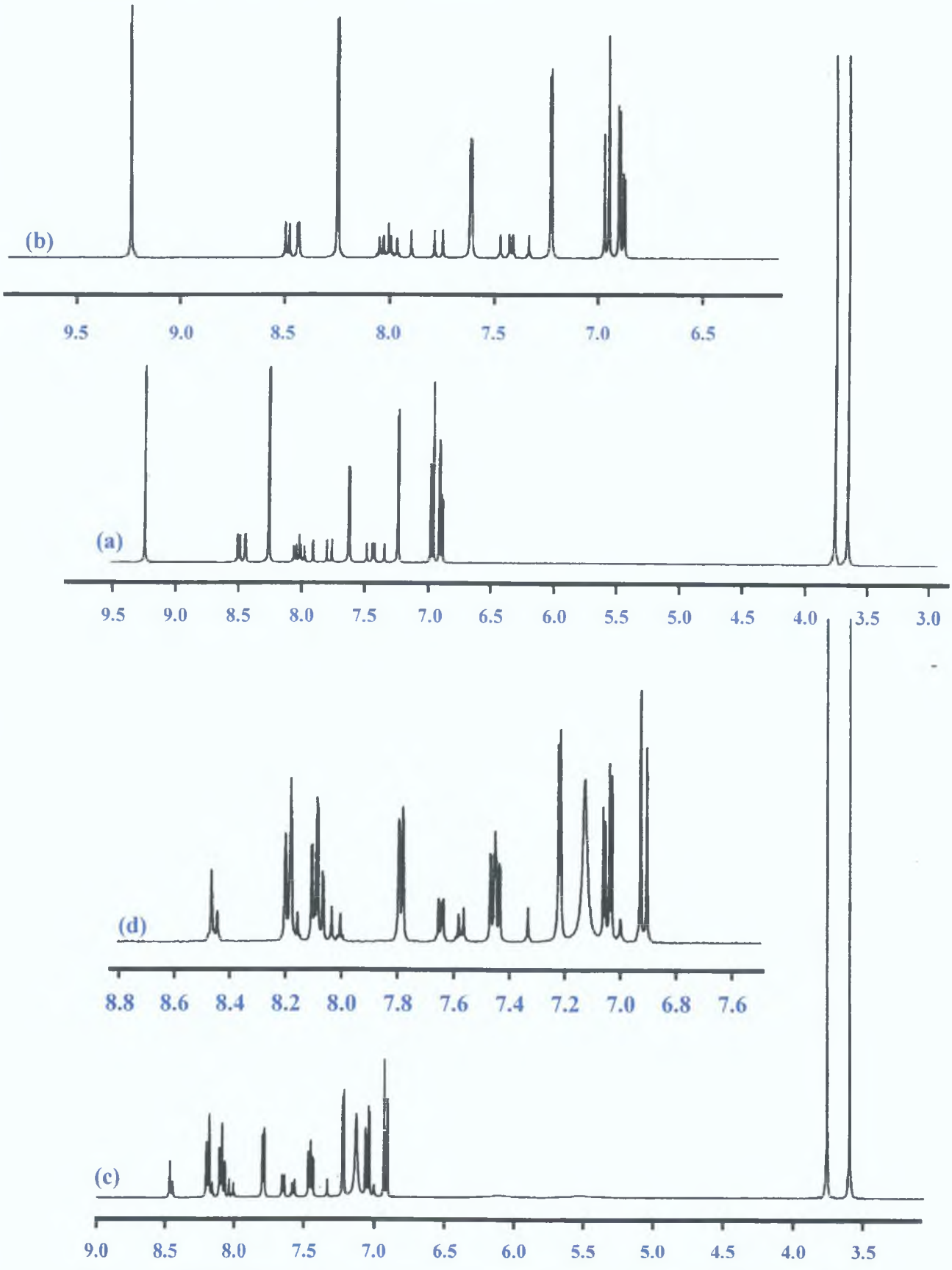

Figure A.13 ^{1}H-NMR spectra of **(a)** $[Ru(bpy)_2(L18)]^+$ and **(c)** $[Ru(bpy)_2(L17)]^+$ in d_3-acetonitrile

A.2.4 NMR Data of Mononuclear Complexes from appendix C

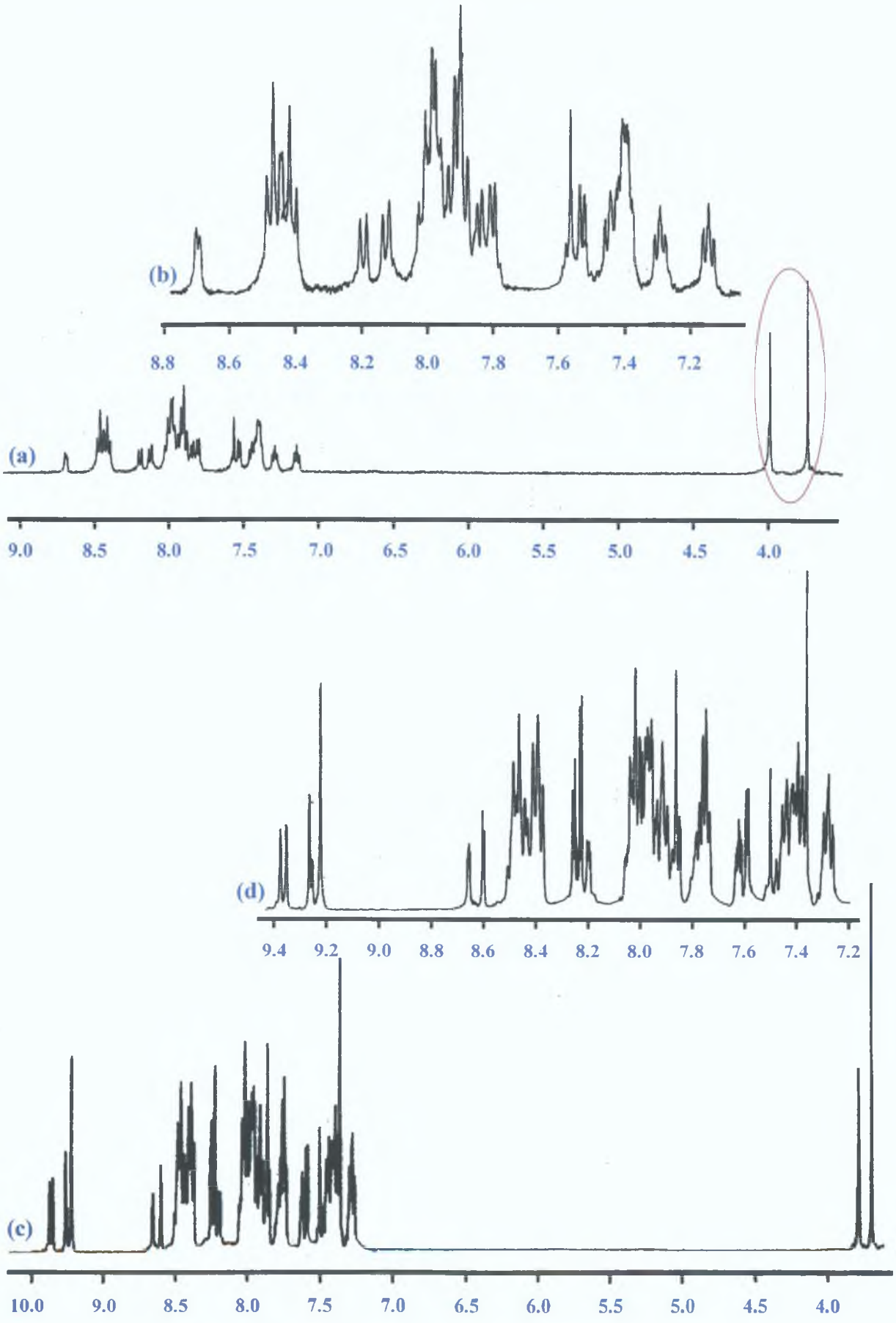

Figure A.14 ^{1}H-NMR spectra of **(a)** $[Ru(bpy)_2(L15)]^+$ and **(c)** $[Ru(bpy)_2(L16)]^+$ in d_3-acetonitrile

Appendix B

Additional Electrochemical Data

This appendix contains additional electrochemical measurements that were preformed on each genre of complex presented in this thesis These studies were undertaken in order to ascertain the optimum experimental conditions achievable for these measurements by exploring the roles of the solvent environment and the working electrode on the cyclic voltammograms of the ruthenium (II) complexes presented in this thesis

B.1 Introduction

In order to identify the optimal solvent environs and working electrode and to ensure the accuracy and reproducibility of the electrochemical measurements provided in this thesis, detailed electrochemical studies were undertaken A variety of solvents were investigated in conjunction with different working electrodes over the entire range of complexes presented in this thesis Hence, the most favourable solvent conditions and the most versatile working electrode were identified

The choice of solvent in an electrochemical investigation is usually dictated by circumstances For example, the electrochemical technique used to study a solvent-solute system is generally one that has been studied already [1] Therefore, in order for results to be comparable, a particular experimental regime is generally adhered to This is important for a number of reasons the most important of which is the ability to compare one system with that of another previously reported For example, generally the ruthenium bipyridyl systems studied to date reported electrochemical measurements in acetonitrile with a glassy carbon electrode [2-6] However, it is useful to examine other experimental environs in order to establish with confidence that the processes being reported do not arise merely as a result of solvent interactions or reactions which take place at the surface of a particular electrode

The choice of solvent is particularly system dependent For example, mutual solubility of the solvent and solute, availability, cost of solvent, ease of purification, toxicity and general ease of handling are all-important factors when choosing a solvent system The voltage limits of a solvent, which define the "window" of accessible electronic energy levels available for electron-transfer processes, must also be considered [7] Although solvents may have intrinsic limits on the basis of their oxidation-reduction properties, the practical working limits depend also on the nature of the working electrode material and the composition of the supporting electrolyte In practical terms the voltage limits are a system property [1] For example, DMF and acetonitrile have high dielectric constants (ε = 36 7 and 30, respectively)

When possible a solvent with a substantial dielectric constant should be used in electrochemical work to minimise the solution resistance. This will minimise ohmic losses and diminish the problem of potential-control errors. Acetonitrile is resistant also to both oxidation and reduction and is, therefore, considered to be an excellent solvent for many compounds. In general the voltage range for DMF attained in reductions is comparable to acetonitrile but DMF is less suitable for the study of oxidations. [1][2]

The choice of working electrode in these solvents is also system dependent. However, generally for an electrode to be useful well into the negative potential region, it must have a low exchange current density and high overpotential for the reduction of hydronium ions. On the positive side, the potential range will be limited by oxidation of supporting electrolyte or solvent, by oxidation of the electrode material to form soluble metal ions or metal oxides, or by formation of molecular and chemiabsorbed oxygen in water or other oxygen-containing solvents. [1][2][8] Absolute values of the electrode potential for different solvent systems cannot be directly compared, however, because they are often referred to different reference electrodes and because of the uncertainty of junction potentials between different solvent systems. Traditionally platinum electrodes have been the electrodes of choice for the electrochemist. [1]

Both platinum and gold are the most commonly used metallic solid electrodes as these metals are readily obtained in high purity and they are resistant, but not totally inert, to oxidation. [1][2] Platinum also has an extremely small overpotential for hydrogen evolution, however, it adsorbs hydrogen readily and it is, therefore, not the most useful material for the study of cathodic processes. Gold on the other hand, has a significantly larger overpotential than platinum for hydrogen evolution and it does not appreciably adsorb hydrogen. It is, therefore, the metal of choice for the study of cathodic processes. Furthermore, in aprotic solvents platinum shows a positive limit that is larger than any of the other commonly used electrode materials although gold is almost as good. [2] The voltage limits for platinum in acetonitrile with TEAP is + 2.2 to – 1.5 V and in DMF and TEAP are from + 2 to – 1.5 V.

The used of vitreous or glassy carbon as an electrode material was first suggested in 1962 [9][10] It has numerous advantages over the traditionally favoured platinum It has a lower cost, it can be pre-treatment by polishing, and it has a larger overpotential for production of hydrogen and dissolved oxygen with increased reversibility for several redox couples Furthermore, surfaces that were examined by techniques, such as, infrared spectroscopy and scanning electron microscopy indicate that the glassy carbon electrode has a negligible concentration of surface acid-base groups and comes closest to an ideal inert redox electrode However, it has the tendency for surface roughening as a result of recrystallisation at high current densities, which does not occur in platinum [1][2]

Effects arising from the nature of the electrode surface frequently complicate electrochemical investigations using solid electrodes [11] An electrode surface that is not clean will usually manifest itself in a voltage-sweep experiment to give a decrease in the peak current and a shift in the peak potential [1] Therefore, prior to these measurements and exhaustive pre-treatment regime was adopted Various pre-treatment methods have been employed to clean or "activate" the surface of electrodes with the intention of enhancing the reversibility of the reaction [12] Generally this procedure begins with polishing which removes adsorbed materials that inhibit electron transfer The surface of a platinum or gold electrode may also be cleaned with nitric acid in order to remove surface detritus Pre-treatment may also involve altering the microstructure of the electrode surface [11] For example, a number of studies have shown how pre-treatment of a glassy carbon electrode can have dramatic effects on the CVs obtained [13-15] Cabaniss et al for example, have developed a pre-treatment method to create surface chemical sites at carbon electrode surfaces, which would have the characteristics needed to provide a basis for proton-coupled electron transfer pathways [11] This technique has been particularly useful for the measurement of the hydroquinone complexes contained in *chapter four* of this thesis Finally, since, atmospheric oxygen can create artefacts in the cathodic region of the spectra a purging of the solution and cell with a flow of inert gas proved entirely satisfactory, as it is capable of reducing the oxygen concentration in the cell atmosphere by between 20 and 200 ppm [1]

The following sections, therefore, contain the results obtained for the range of complexes contained in this thesis under a variety of experimental conditions Numerous solvents were examined in conjunction with a platinum, glassy carbon and a gold electrode and hence, the optimal bespoke experimental method applicable for these systems, based on an overall consideration of these findings, were chosen

B.2 Experimental Methodology

The cyclic voltammograms of the dimethoxyphenyl, dihydroxyphenyl and quinone-containing complexes are presented in this section in various solvents and with different working electrodes The experimental parameters employed during these measurements are contained in *chapter two* Prior to each of these measurements the electrodes were submitted to an extensive polishing regime and three varying grades of alumina were used followed by sonication to remove the grains of polish Each of the electrodes was also cychsed in 0 2 M H_2SO_4 between – 0 2 V and 1 8 V, washed in water and allowed to air dry In the case of the hydroquinone-containing complexes, the electrodes were held at a potential of 1 8 V in 0 2 M H_2SO_4 for two minutes, m order to anodise the electrodes This step was not preformed on either the dimethoxyphenyl or quinone-containing complexes, as it did not enhance the quality of the cyclic voltammograms obtained For each measurement only dry spectrochemical grade solvents were used and all measurements were carried out under a blanket of nitrogen in order to negate interferences from atmospheric oxygen

B.3 Results and Discussion

Electrochemical analyses of this protected group of complexes were carried out in acetone, acetomtrile, dichloromethane, THF and ethanol Three different working electrodes were also used during these studies – glassy carbon, gold and platinum In this section the electrochemical behaviour of these dimethoxy complexes under different experimental conditions are presented As stated in the introduction the mutual solubility of the solvent and solute are of paramount importance when considering which solvent to use to obtain a measurement

Table B.1, therefore, contains the data relating to the degree of solubility exhibited by each type of complex contained in this thesis.

Table B.1 Solubility data obtained for the complexes in a range of solvents at room temperature.

Solvent	Dimethoxy	Dihydroxy	Quinone
Acetone	Quite Soluble	*Soluble*	Slight Solubility
Acetonitrile	*Soluble*	*Soluble*	*Soluble*
Ethanol	Not Soluble	Slight Solubility	Slight Solubility
Dichloromethane	*Soluble*	*Soluble*	Slight Solubility
THF	Not Soluble	Not Soluble	Not Soluble

From an examination of the above table it can be seen that in the range of solvents examined there were various degrees of solubility observed. For example, THF is clearly not a viable solvent for these systems and the following data for each genre of complex do not contain CVs generated in this solvent. The following sections, however, contain data generated in most of the other solvents when a sufficient degree of solubility could be achieved in order to generate a CV.

B.3.1 Dimethoxyphenyl Complexes

From an examination of the above table (*table B.1*) it can be seen that these complexes were not soluble in a number of the solvents examined. It was therefore, not possible to obtain the cyclic voltammograms of these complexes in these solvents. However, the following figures contain the cyclic voltammograms that were obtainable in acetone with a glassy carbon, a gold and a platinum electrode. *Figure B.1* shows the cyclic voltammogram of the protected dinuclear ruthenium complex containing a dimethoxyphenyl moiety. From an examination of this CV, which was obtained, using a glassy carbon-working electrode in acetone it is apparent that the cathodic region of the CV is sufficiently well resolved while the anodic region is less clear. The use of acetone in these measurements had a number of limitations. For example, acetone readily absorbs water and this resulted in a broadening of the spectra and may account for the loss of clear processes in the anodic region.

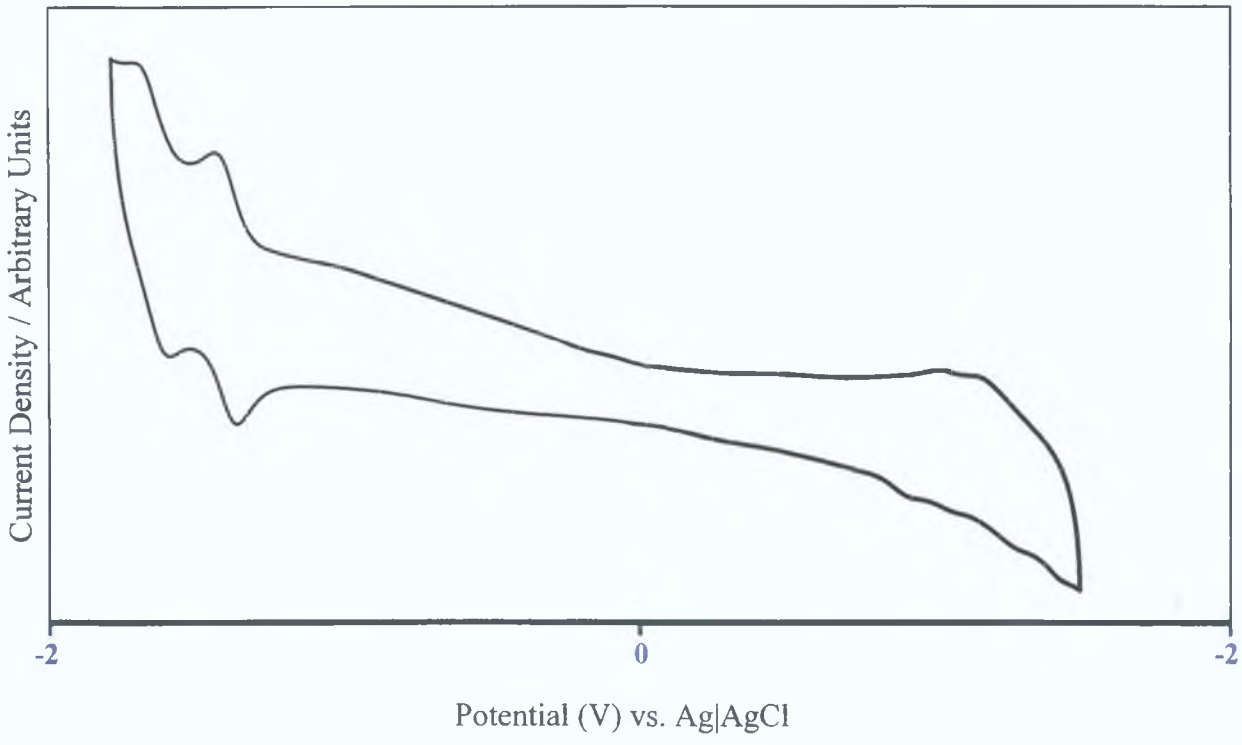

Figure B.1 Cyclic voltammogram of $[Ru(bpy)_2(L5)Ru(bpy)_2]^{2+}$ with a glassy carbon working electrode in acetone and 0.1 M TEAP in Volt versus Ag|AgCl (scan rate 0.10 V / s)

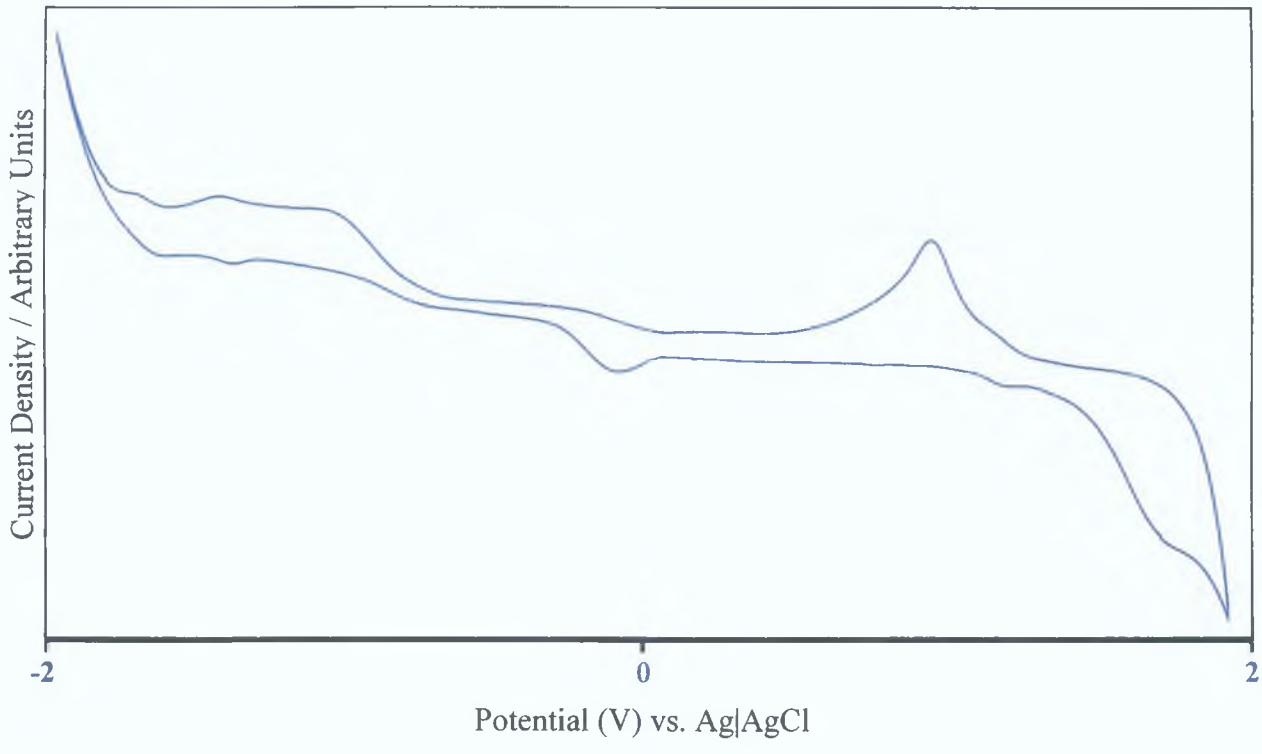

Figure B.2 Cyclic voltammogram of $[Ru(bpy)_2(L5)Ru(bpy)_2]^{2+}$ with a gold working electrode in acetone and 0.1 M TEAP in Volt versus Ag|AgCl (scan rate 0.10 V / s)

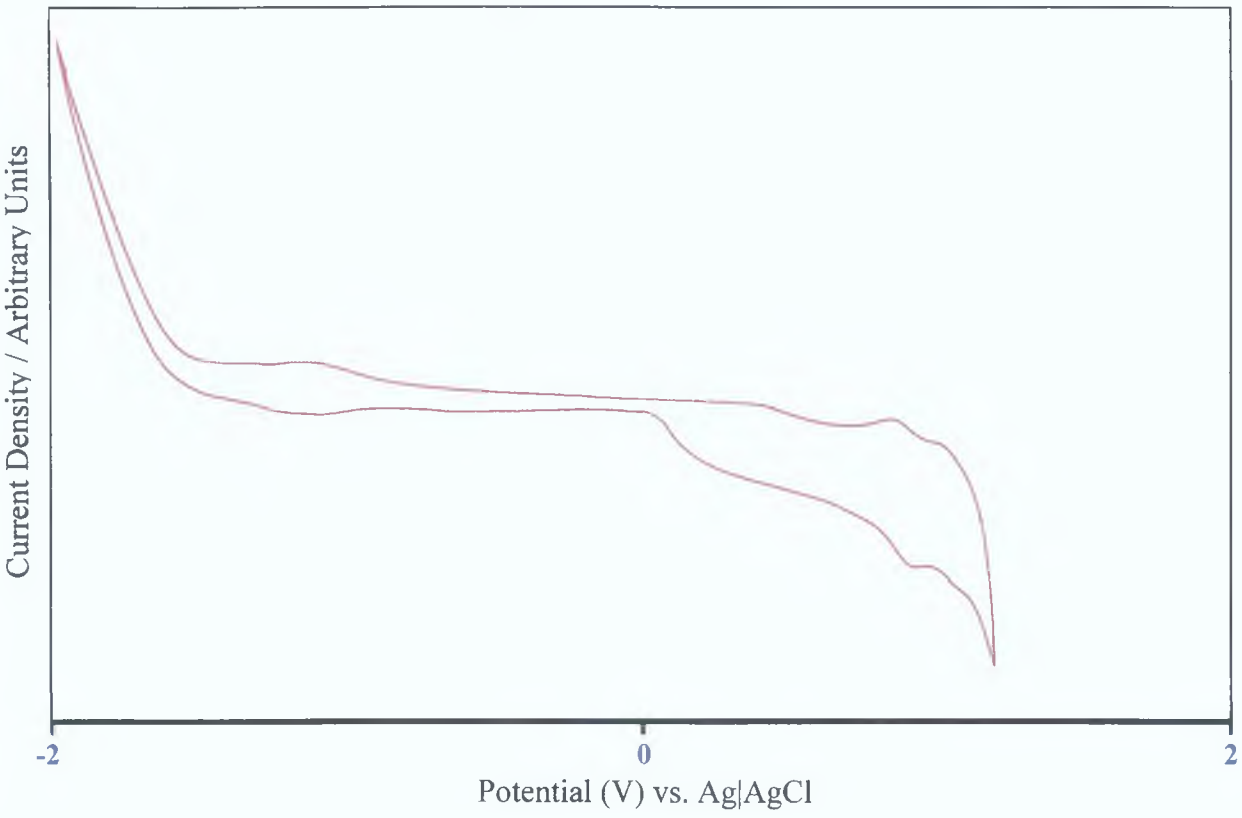

Figure B.3 Cyclic voltammogram of $[Ru(bpy)_2(L5)Ru(bpy)_2]^{2+}$ with a platinum working electrode in acetone and 0.1 M TEAP in Volt vs Ag|AgCl (scan rate 0.10 V / s)

The measurements were repeated in a similar manner with a gold electrode. *Figure B.2* contains the CV of this complex and once again, it can be seen that the in this solvent utilising a gold electrode the redox processes are not clearly resolved. This may be related to the tendency for gold to interact very well with each component in solution as well. Furthermore, as the complex examined was not completely soluble in this solvent this would exasperate the problem. Finally *figure B.3* was obtained with a platinum electrode in acetone. Again this data are not well resolved and both the cathodic and anodic redox processes are unclear. Overall, therefore, the solubility in acetone for these complexes proved to be of an insufficient degree to allow the production of clear cyclic voltammograms. Furthermore, since, acetone has a low boiling point it proved difficult to maintain the samples under a flow of nitrogen or to degas the samples for long periods prior to reduction analyses, as this simply evaporated the solvent. The following set of electrochemical data was, hence, obtained in acetonitrile in which these dimethoxy complexes were found to display excellent solubility.

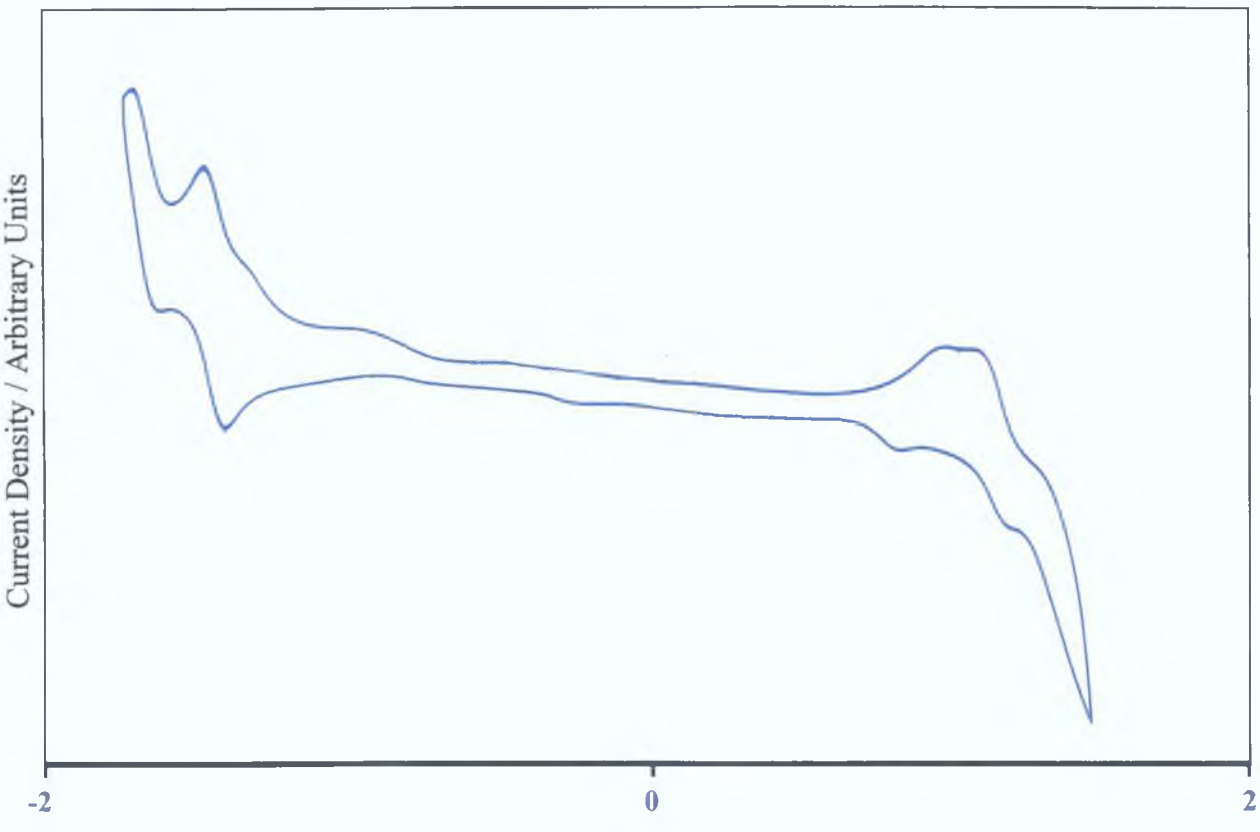

Figure B.4 Cyclic voltammogram of $[Ru(bpy)_2(L5)Ru(bpy)_2]^{2+}$ with a gold working electrode in acetonitrile and 0.1 M TEAP in Volt versus Ag|AgCl (scan rate 0.10 V / s)

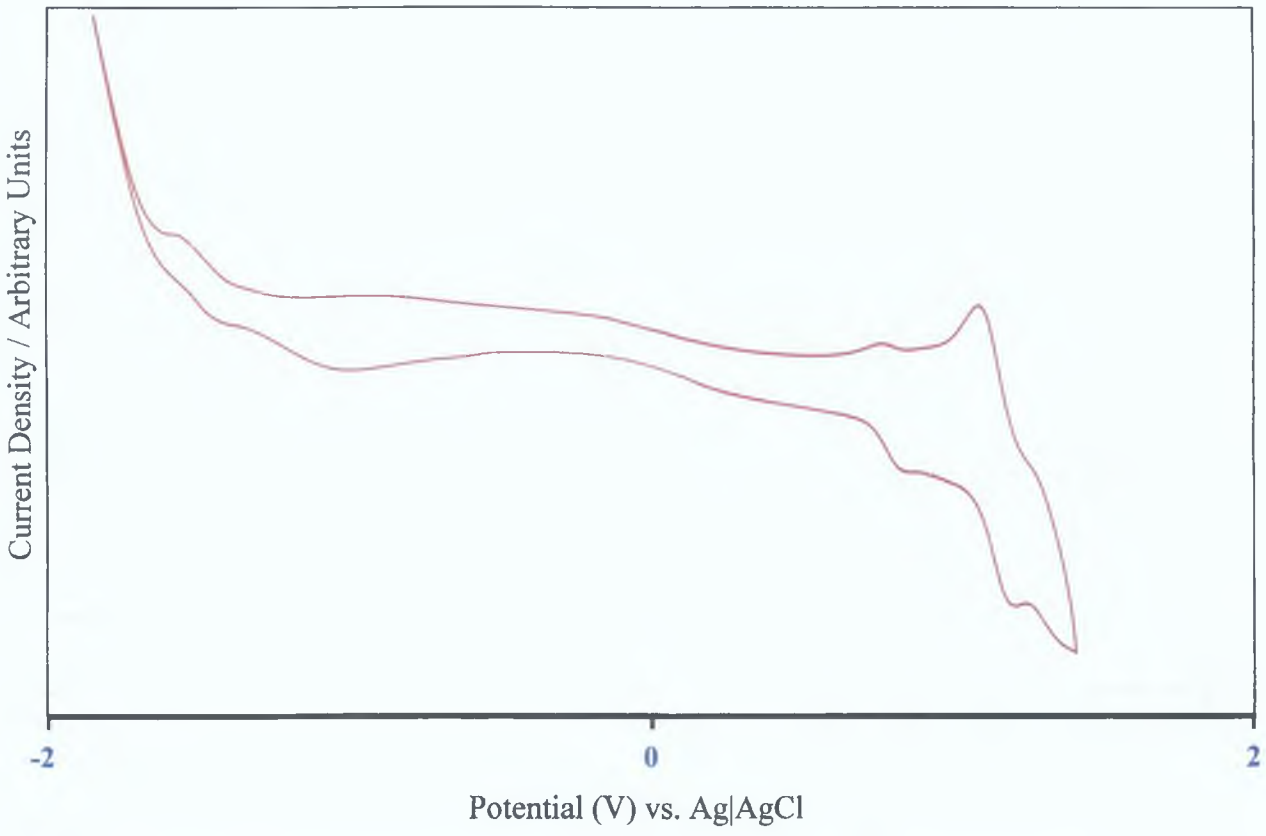

Figure B.5 Cyclic voltammogram of $[Ru(bpy)_2(L5)Ru(bpy)_2]^{2+}$ with a Pt working electrode in acetonitrile and 0.1 M TEAP in Volt vs Ag|AgCl (scan rate 0.10 V / s)

The cyclic voltammograms of these complexes, which were obtained with a glassy carbon electrode in acetonitrile, are depicted in *figure 3 26* in *chapter three* In the above measurements acetonitrile proved to be a viable solvent and did not hinder attainment of the CVs with any of the working electrodes From an examination of *figure B 4*, that was obtained using a gold electrode, it can be seen that the CV of the dinuclear dimethoxyphenyl complex is of satisfactory quality in both anodic and cathodic regions However, the cathodic region of the CV is somewhat better resolved than that of the anodic region in which the ligand process, which occur subsequent to the metal oxidation (Ru^{II}/Ru^{III}), are not clearly evident

This is not surprising as pointed out in the introductory section this electrode is not traditionally the electrode of choice for the anodic region but demonstrates excellent behaviour in the cathodic region [2] The reverse is generally true for platinum and this is demonstrated well in *figure B 5* In this CV the anodic region depicts clear, well defined redox processes while the cathodic region contains indistinct processes In contrast the CV of this complex, which was obtained with a glassy carbon electrode, (*figure 3 26*) has clear and well-defined redox process in both the anodic and cathodic regions of the voltammogram in this solvent Furthermore, this solvent proved to be a more practical choice than that of acetone as its increased boiling point (81 - 82° C) allowed for purging prior to reduction measurements without appreciable loss of the solution Further CVs were then obtained in dichloromethane with the various working electrodes and the following CVs depict the measurements obtained for the dimethoxy-containing mononuclear ruthenium complex $[Ru(bpy)_2(L3)]^+$ These methoxylated complexes were found to be of sufficient solubility in DCM to enable the electrochemical data to be generated *Figure B 6* contains the CV of $[Ru(bpy)_2(L3)]^+$ in dichloromethane with a glassy carbon electrode The CV of this complex shows clear and well-resolved oxidations of the metal prior to the ligand oxidations in the anodic region, however, in the cathodic region, the reduction processes are not so unambiguous and indeed, the separate bipyridyl reductions, which are expected in this region, now appear as a single process In fact a similar behaviour was noted in the cathodic region of each of the CVs obtained in DCM and hence, can be associated with processes occurring due to the presence of this solvent

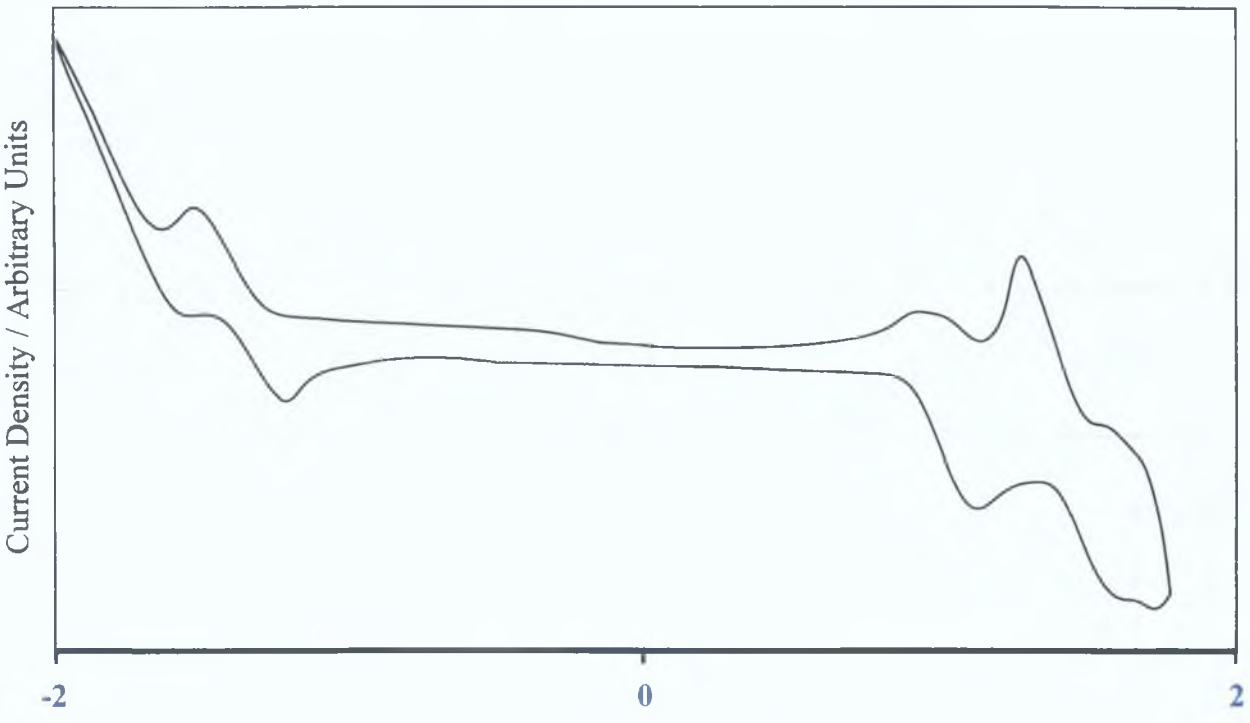

Figure B.6 Cyclic voltammogram of $[Ru(bpy)_2(L3)]^+$ with a glassy carbon working electrode in dichloromethane and 0.1 M TEAP in Volt vs Ag|AgCl (scan rate 0.10 V / s)

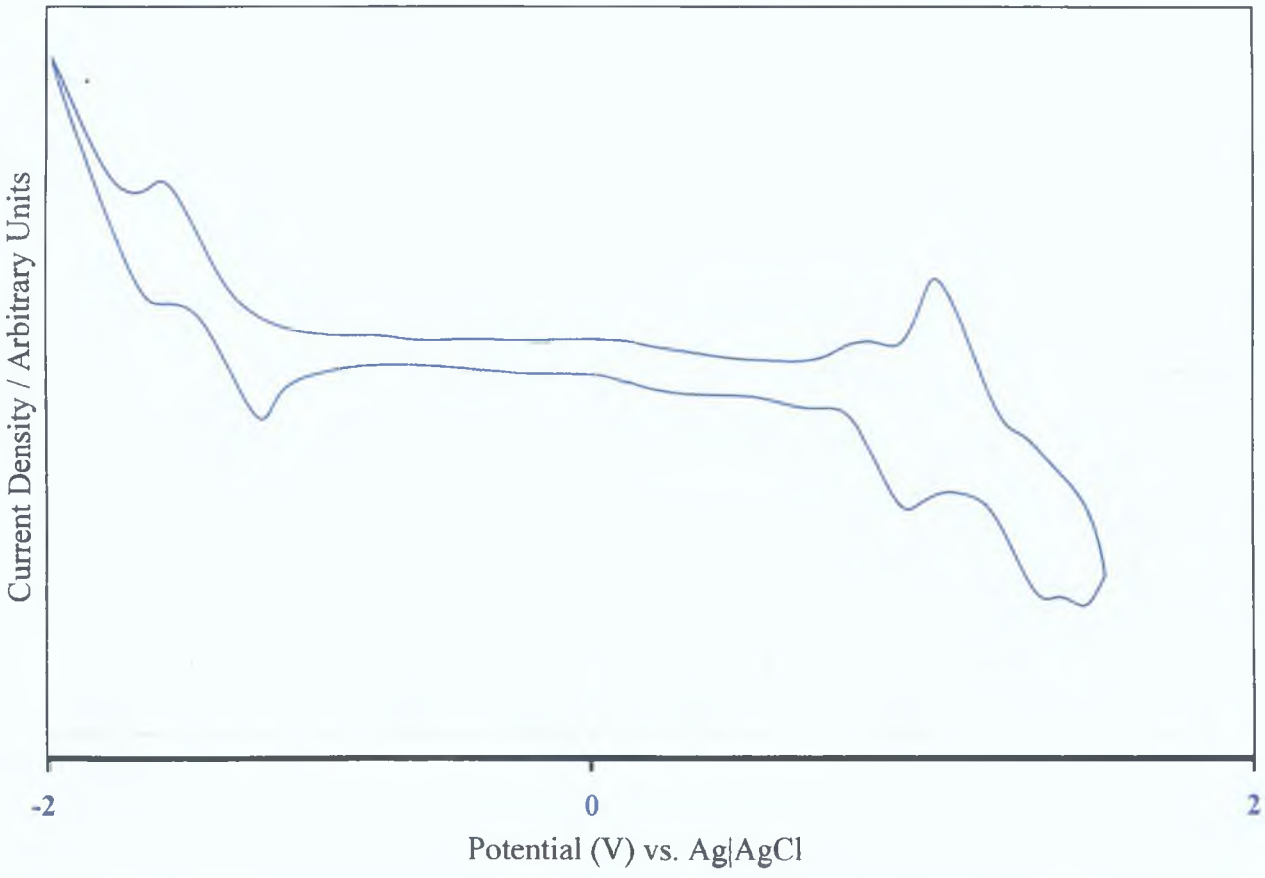

Figure B.7 Cyclic voltammogram of $[Ru(bpy)_2(L3)]^+$ with a gold working electrode in dichloromethane and 0.1 M TEAP in Volt vs Ag|AgCl (scan rate 0.10 V / s)

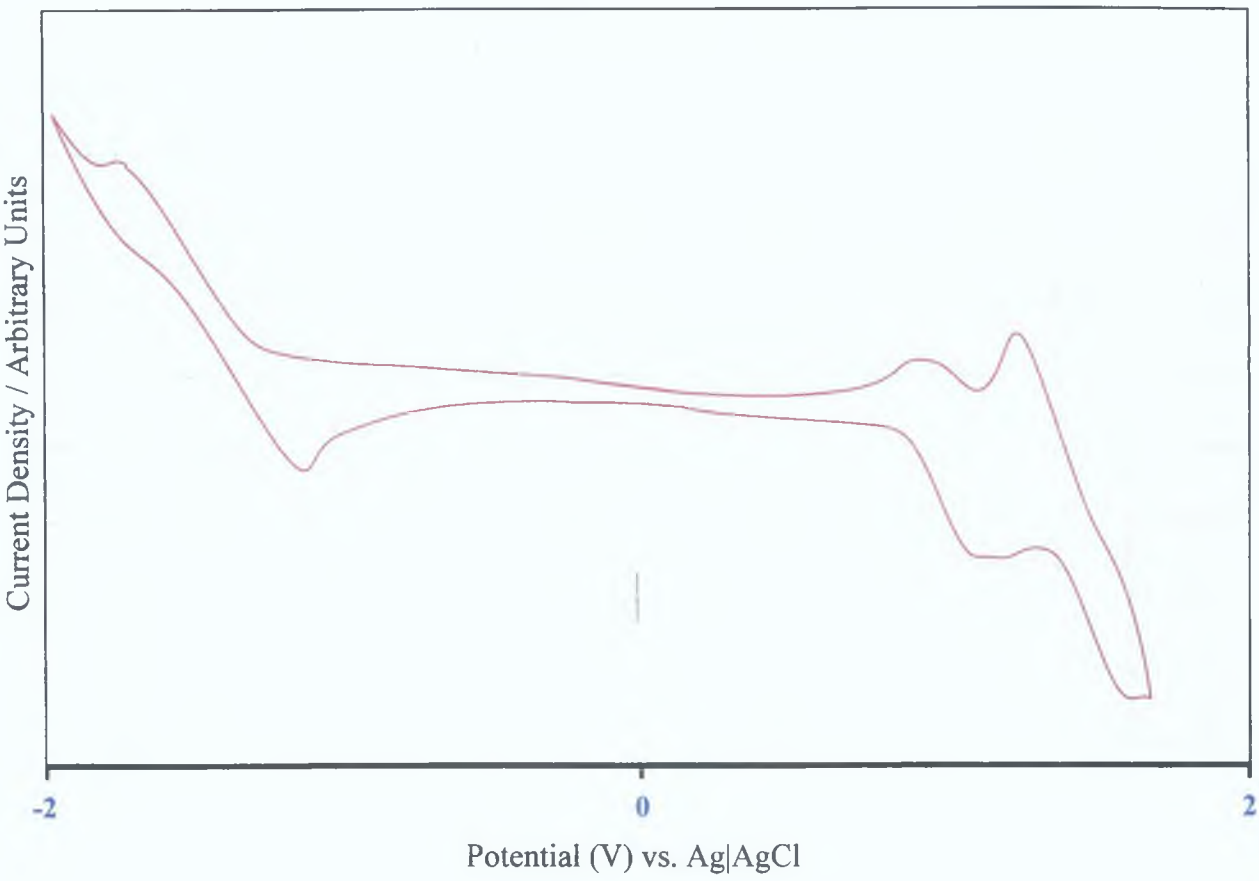

Figure B.8 Cyclic voltammogram of $[Ru(bpy)_2(L3)]^+$ with a platinum working electrode in dichloromethane and 0.1 M TEAP in Volt vs Ag|AgCl (scan rate 0.10 V / s)

In *figure B.7* the CV of this complexes was, once again, obtained in dichloromethane in which a gold electrode has now replaced the glassy carbon-working electrode. Again there is clear resolution of the oxidation processes in the anodic region while the cathodic region again depicts the reductions of the bipyridyl moieties as one single entity. A similar situation was noted in the case of the CVs obtained with a platinum-working electrode (*figure B.8*) while the anodic region is satisfactory; the cathodic region is not sufficiently resolved. Again this can be attributed to the use of dichloromethane within these systems and it appears as if this is not a viable solvent overall for use in the measurement of these complexes. No other solvents proved adequate for the measurement of this group of compounds and hence, no further CVs could be generated for these complexes (*table B.1*). The following section contains the cyclic voltammogram measurements obtained for the hydroquinone complexes.

B.3.2 Dihydroxyphenyl Complexes

Electrochemical analyses of the dihydroxy-containing complexes were also performed in a range of solvents and a variety of working electrodes. Once again, these complexes were found to either be poorly soluble or not soluble in a number of the solvents chosen (*table B.1*). However, the following section contains the cyclic voltammograms that were obtainable in a number of different solvent environs.

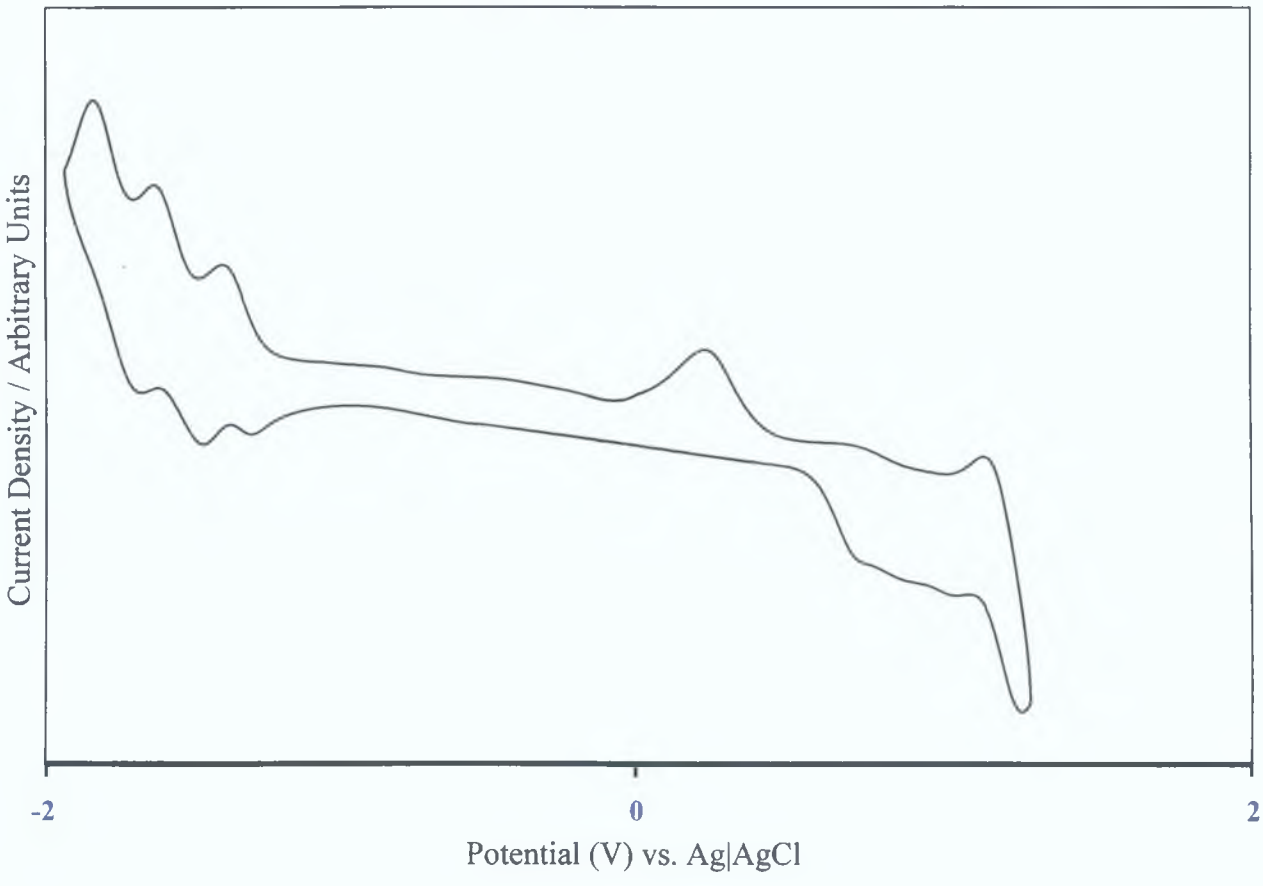

Figure B.9 Cyclic voltammogram of $[Ru(bpy)_2(L8)]^+$ with a glassy carbon working electrode in acetone and 0.1 M TEAP in Volt vs Ag|AgCl (scan rate 0.10 V / s).

Figure B.9 contains the CV of the pyrazyltriazole complex $[Ru(bpy)_2(L8)]^+$ in acetone with a glassy carbon electrode. It can be seen that compared to the methoxylated analogues, these hydroquinone-containing complexes have an increased solubility in this solvent and this is apparent in the CVs obtained (*figure B.9* compared to *figure B.1*). There is, therefore, an increased resolution of both the anodic and cathodic process in the CV obtained for these complexes with a glassy carbon electrode (*figure B.9*).

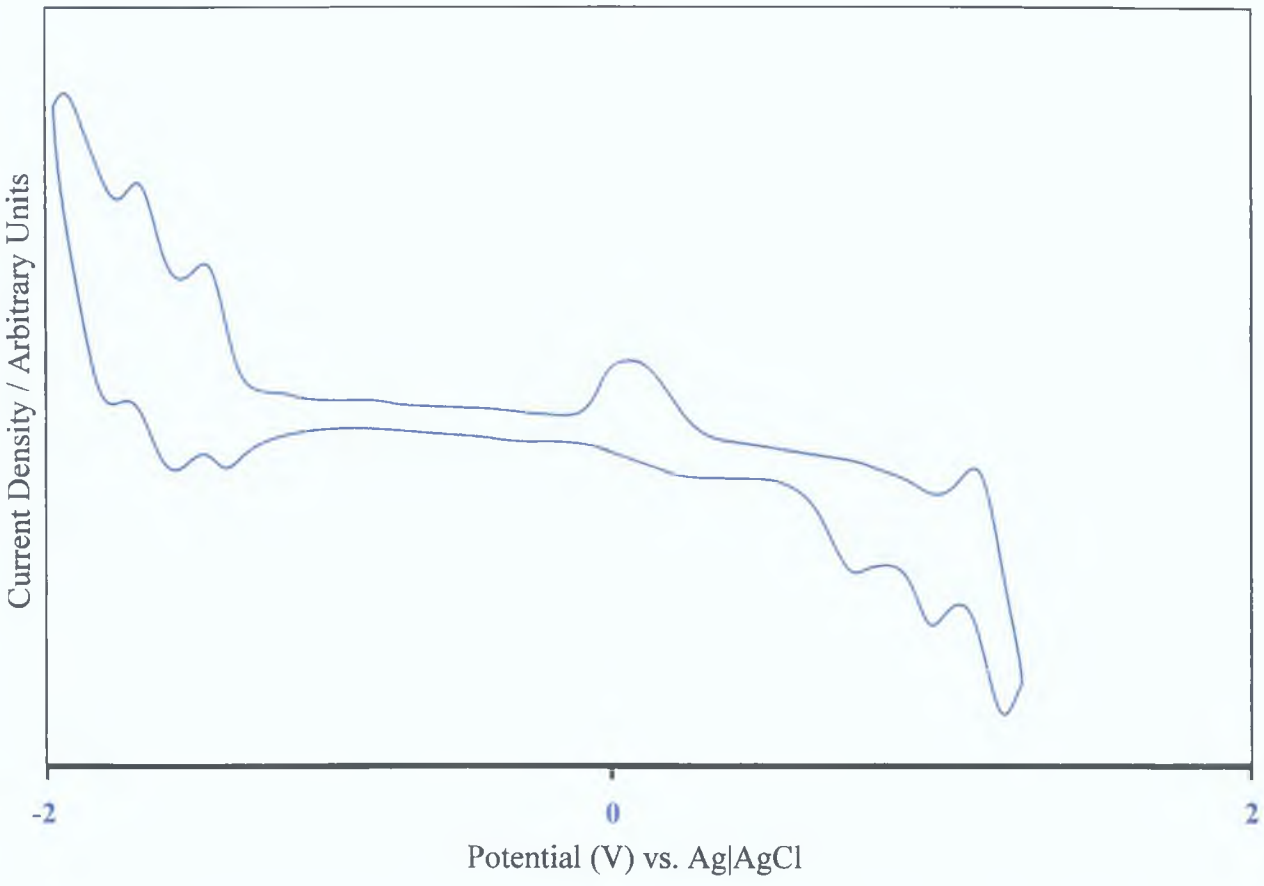

Figure B.10 Cyclic voltammogram of $[Ru(bpy)_2(L8)]^+$ with a gold working electrode in acetone and 0.1 M TEAP in Volt vs Ag|AgCl (scan rate 0.10 V / s).

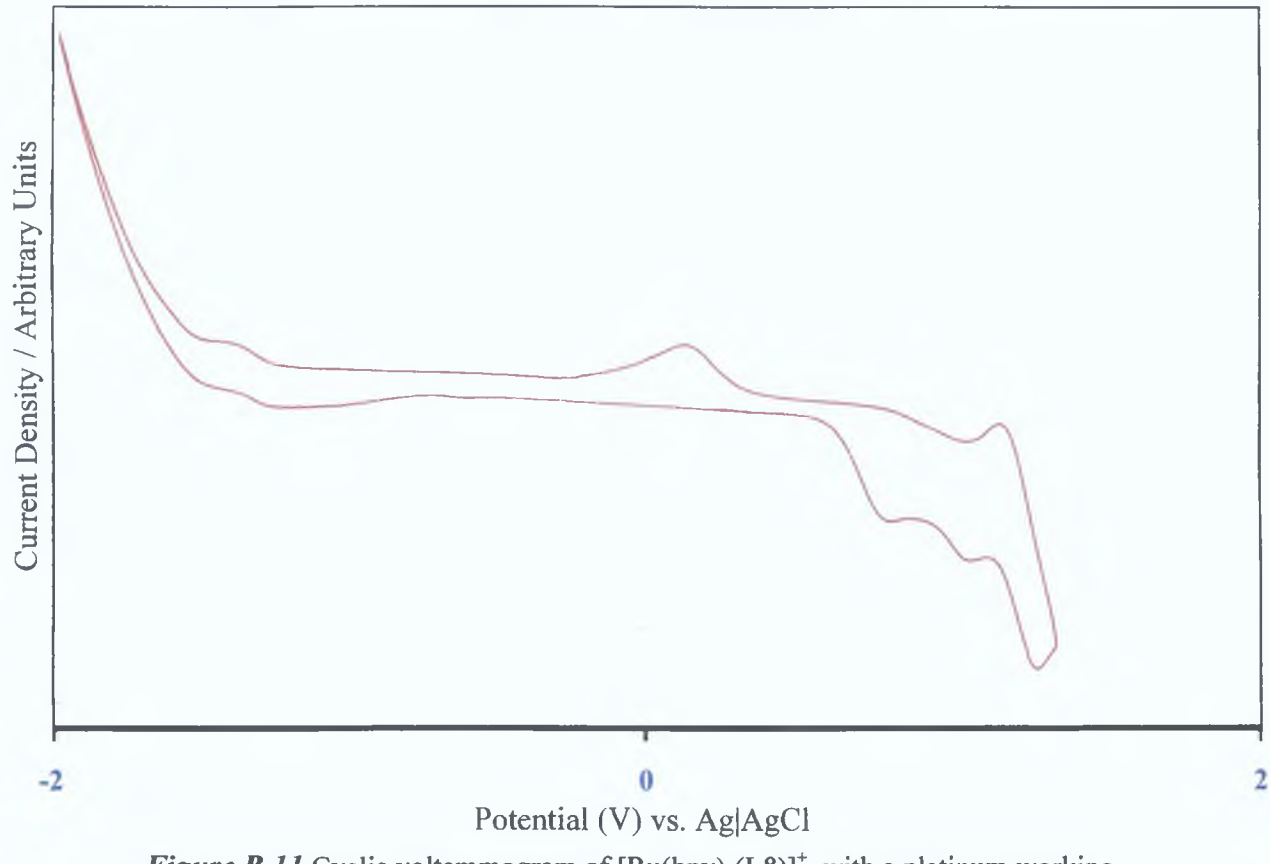

Figure B.11 Cyclic voltammogram of $[Ru(bpy)_2(L8)]^+$ with a platinum working electrode in acetone and 0.1 M TEAP in Volt vs Ag|AgCl (scan rate 0.10 V / s)

The CVs obtained with the gold working electrode also depict clear reduction and oxidation processes (*figure B 10*), however, the CV obtained with the platinum-working electrode is again badly resolved in the cathodic region This result is not surprising, however, as this electrode is known to generate poor results in the cathodic region [1][2] Furthermore, it again proved difficult to purge the acetone solutions with nitrogen prior to the reduction measurements without the causing solvent evaporation The following CVs were, therefore, generated in DCM

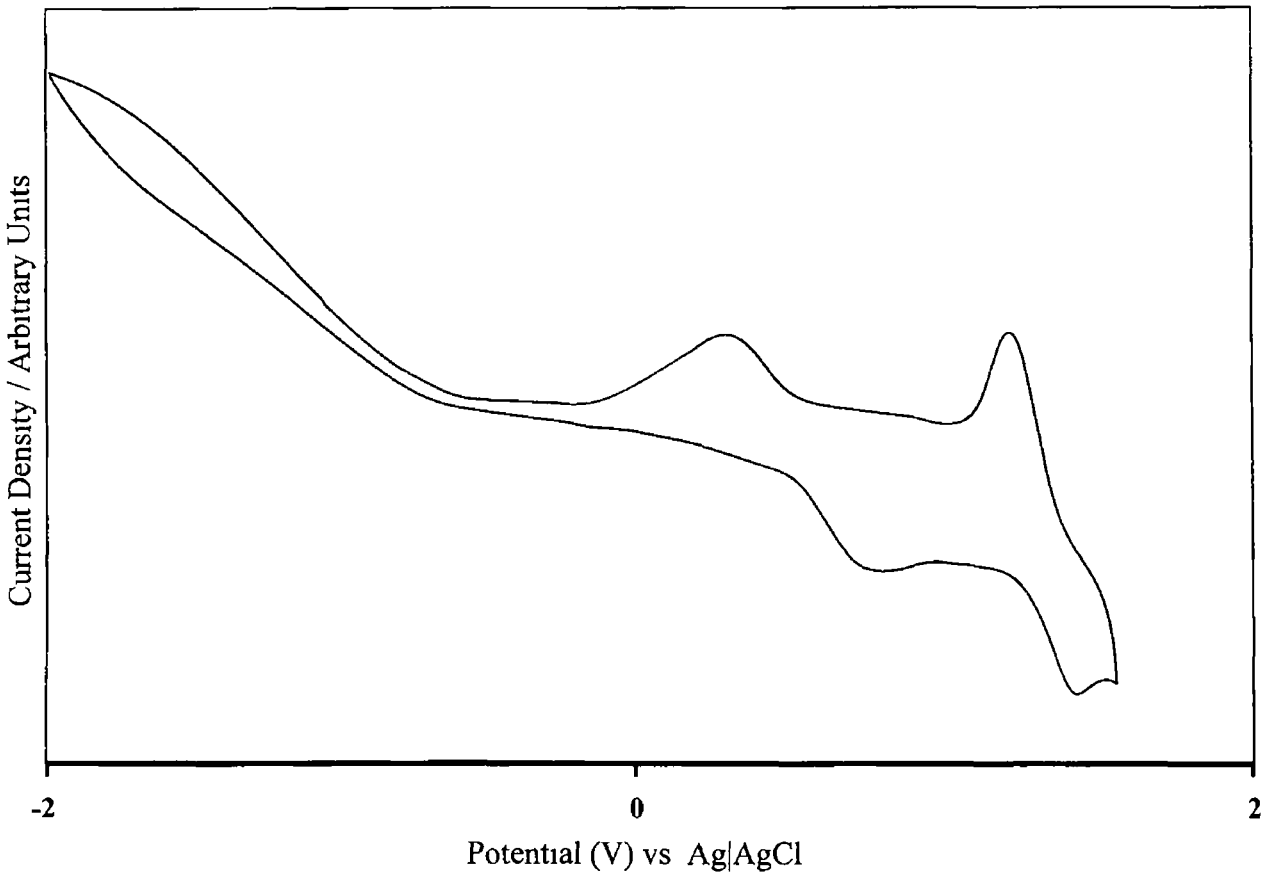

Figure B.12 Cyclic voltammogram of $[Ru(bpy)_2(L8)]^+$ with a glassy carbon working electrode in dichloromethane and 0 1 M TEAP in Volt vs Ag|AgCl (scan rate 0 10 V / s)

Figure B 12 contains the CV of $[Ru(bpy)_2(L8)]^+$ in dichloromethane with a glassy carbon working electrode It was noted in the previous section that the CVs obtained for the dimethoxy-containing complexes in DCM had an obscured cathodic region It can be seen from the above spectra (*figure B 12*) that this is also the case for the hydroquinone-containing complexes The CVs obtained with each of the working electrodes in this solvent yielded similar CV as that shown above and this, therefore, provides further evidence that the cause is solvent related

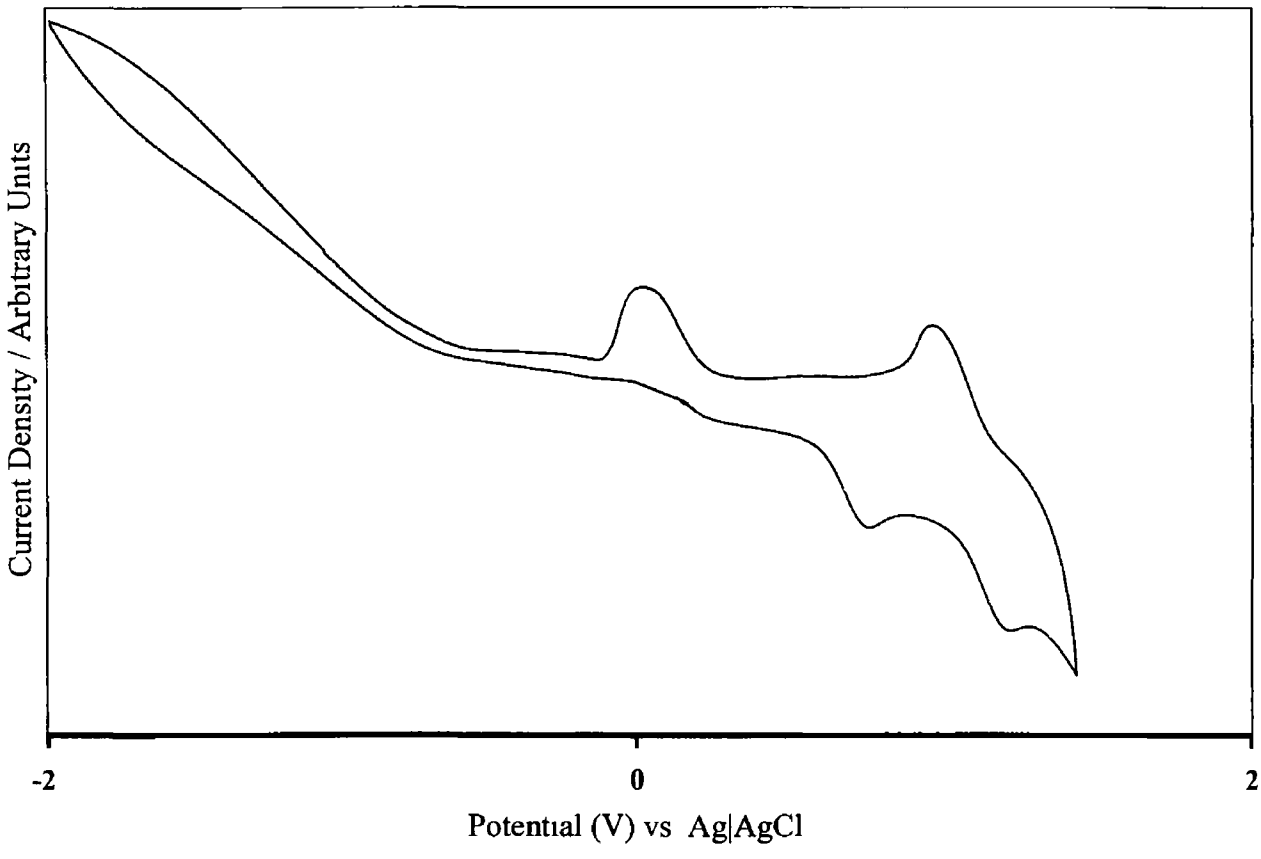

Figure B 13 Cyclic voltammogram of $[Ru(bpy)_2(L8)]^+$ with a glassy carbon working electrode in ethanol and 0 1 M TEAP in Volt vs Ag|AgCl (scan rate 0 10 V / s)

Figure B 13 contains the CV of $[Ru(bpy)_2(L8)]^+$ in ethanol with a glassy carbon working electrode Each of the CVs obtained in this solvent appear quite similar regardless of the working electrode used The anodic region of each of the CVs show clear processes while the cathodic region is obscured As in the case of the CVs obtained in DCM, the processes occurring in the reductive region of the CVs may be associated with the solvent This is particularly likely as it was noted in each of the CVs regardless of working electrode and therefore, is unlike to have arisen because of the electrode It was, therefore, decided to analyse the CVs of these complexes in acetomtrile and the following figures depict the CVs obtained A CV obtained in acetomtrile with a glassy carbon electrode for this group of complexes is contained in *figure 4 18* From an examination of *figure 4 18* it can be seen that both the cathodic and anodic process obtained in this solvent for this group of hydroquinone complexes are clear and well resolved However, in the following *figure B 14* obtained with a gold electrode the anodic region is not as sufficiently resolved

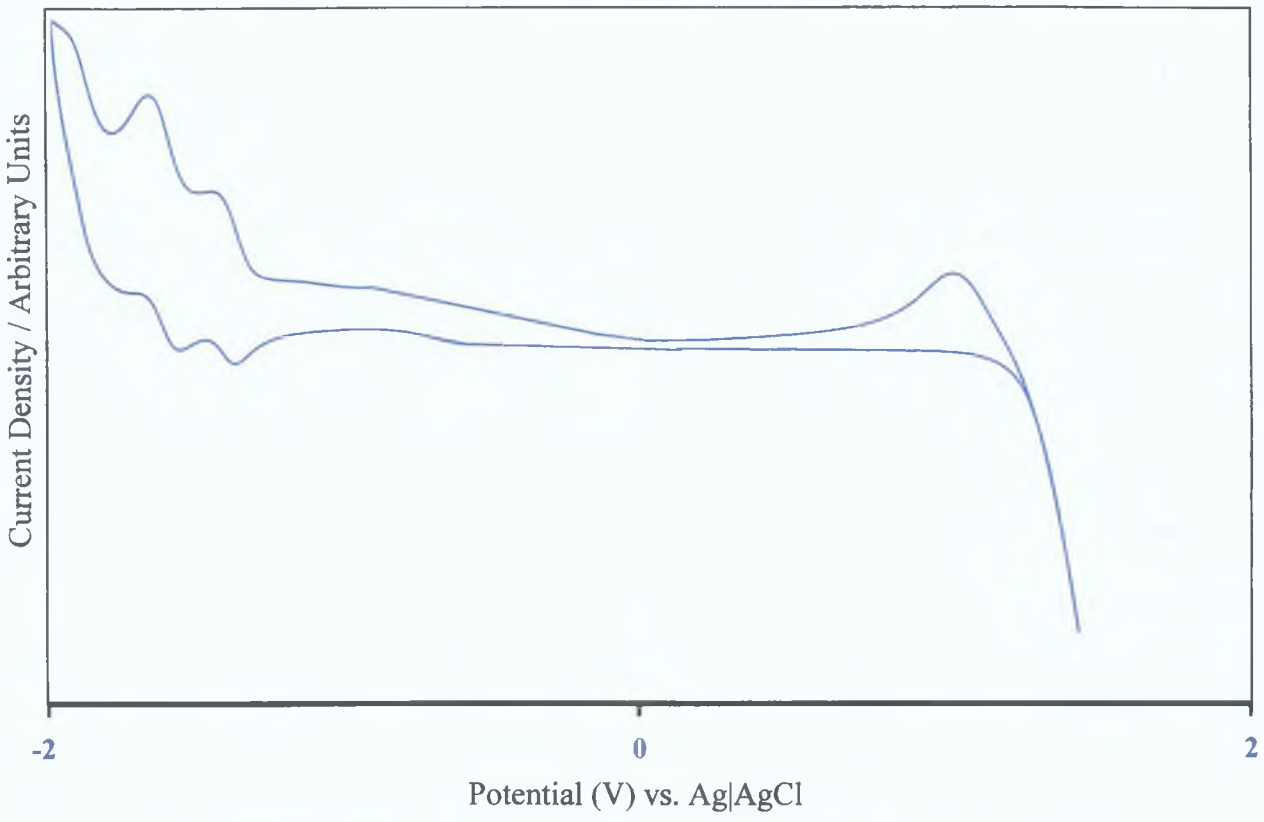

Figure B.14 Cyclic voltammogram of $[Ru(bpy)_2(L8)]^+$ with a gold working electrode in acetonitrile and 0.1 M TEAP in Volt vs Ag|AgCl (scan rate 0.10 V / s)

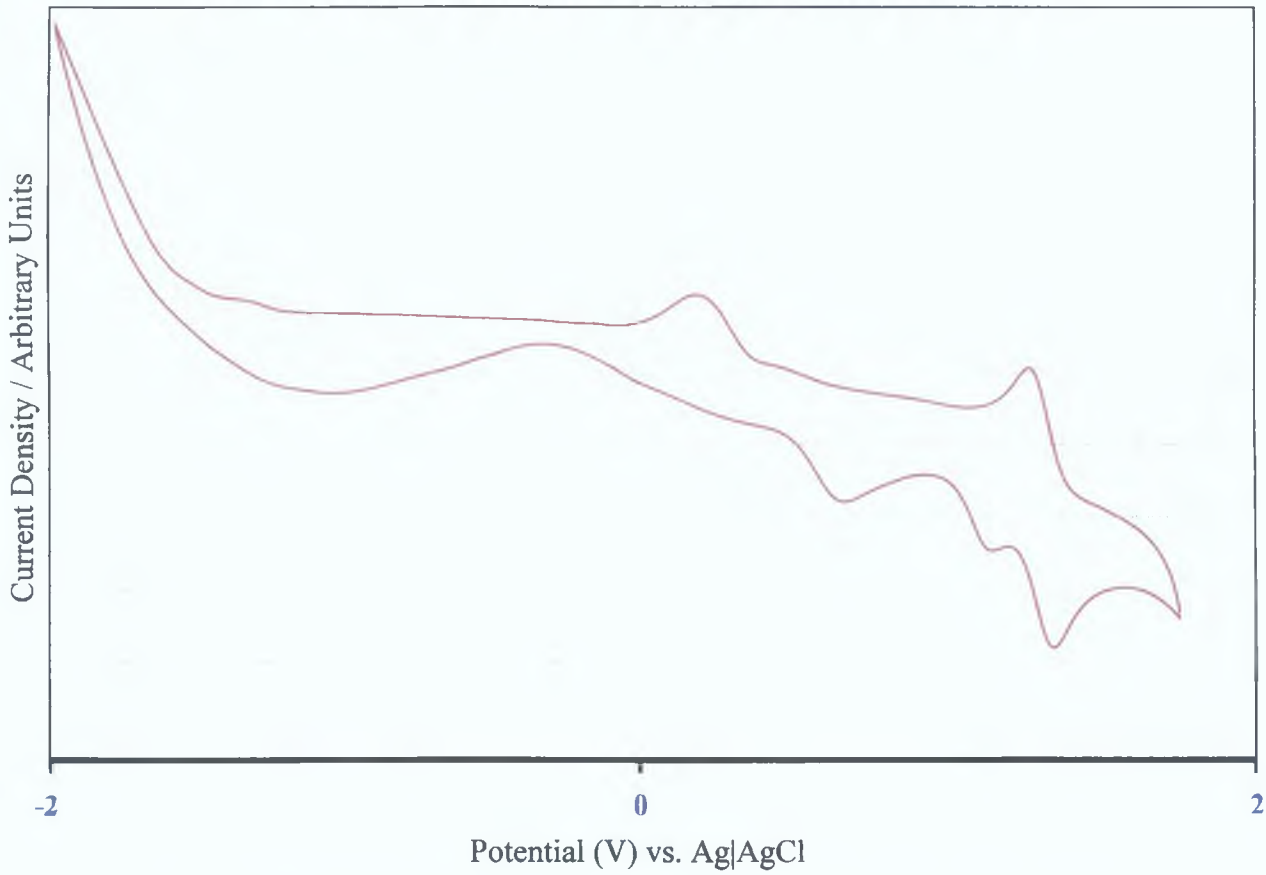

Figure B.15 Cyclic Voltammogram of $[Ru(bpy)_2(L8)]^+$ with a platinum working electrode in acetonitrile and 0.1M TEAP in Volt vs Ag|AgCl (scan rate 0.10V/s)

This is comparable to the result obtained previously with a gold electrode and again emphasises that this electrode not the electrode of choice for this system in the anodic region although it demonstrates excellent behaviour in the cathodic region. The reverse situation is generally true for CVs obtained with a platinum-working electrode and this is demonstrated well in *figure B.15*. In this CV the anodic region depicts clear, well defined redox processes while the cathodic region contains indistinct processes.

B.3.3 Quinone Complexes

Electrochemical analyses of the quinone complexes were also performed in a range of solvents and a variety of working electrodes. These complexes were found be particularly poorly soluble in a number of organic solvents (*table B.1*) however, the following section contains the cyclic voltammograms that were obtainable under a number of different experimental conditions.

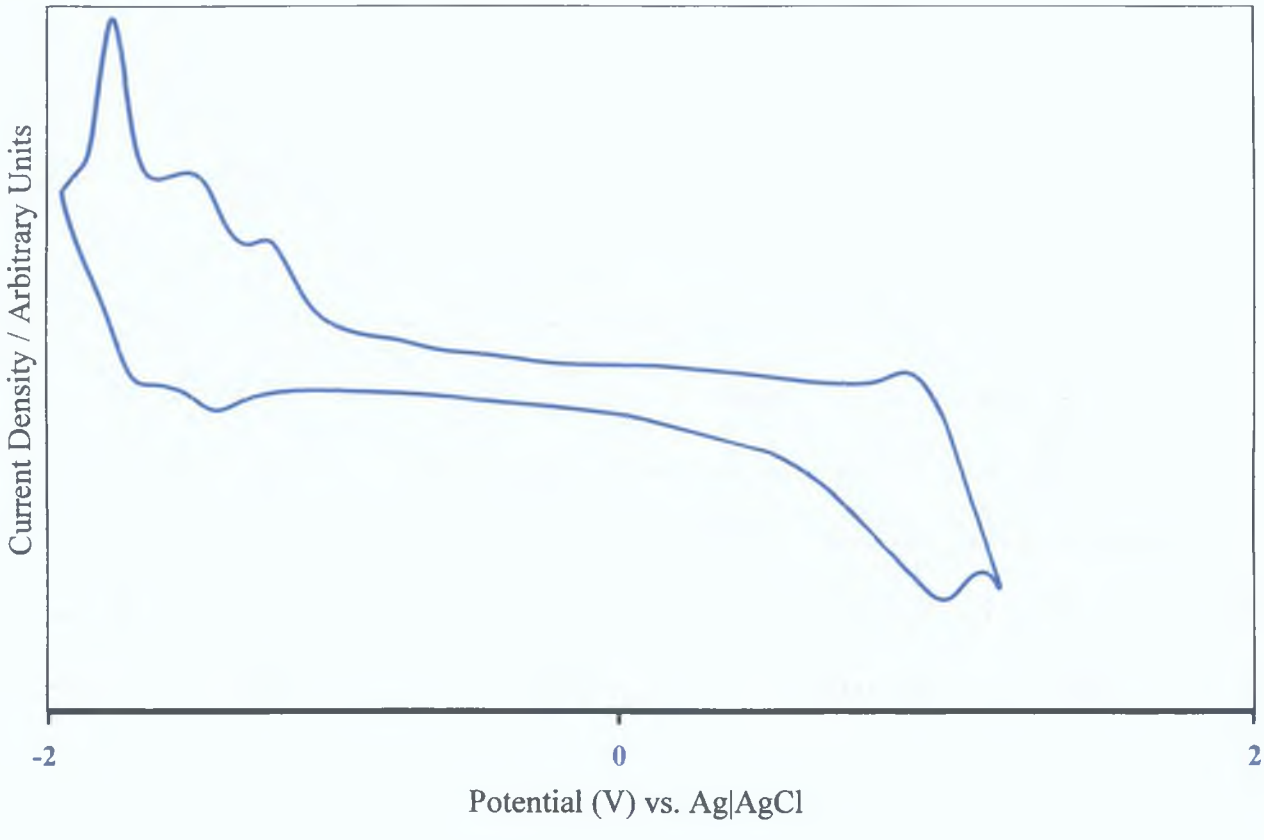

Figure B.16 Cyclic voltammogram of $[Ru(bpy)_2(L11)]^+$ with a gold working electrode in acetonitrile and 0.1 M TEAP in Volt vs Ag|AgCl (scan rate 0.10 V / s)

Figure B.16 and *B.17* depict the cyclic voltammograms of $[Ru(bpy)_2(L11)]^+$ in acetonitrile with a gold and a platinum electrode respectively. The CV of this complex in acetonitrile obtained with a glassy carbon electrode is contained in the electrochemical section of *chapter five* (*figure 5.20*). From *table B.1* it can be seen that these quinone complexes are only slightly soluble or not at all soluble in most of the solvents examined. Acetonitrile is the obvious exception and hence, the CVs obtained in this solvent with differing working electrodes were generated (*figure B.16, B.17* and *5.20*). From an examination of *figure B.16* it can be seen that the CV of this quinone complex obtained with a gold working electrode is very similar to that obtained with a glassy carbon electrode (*figure 5.20*). The anodic region of the voltammogram depicts the Ru^{II}/Ru^{III} metal oxidation process while the cathodic region contains the bipyridyl processes prior to the quinone oxidation.

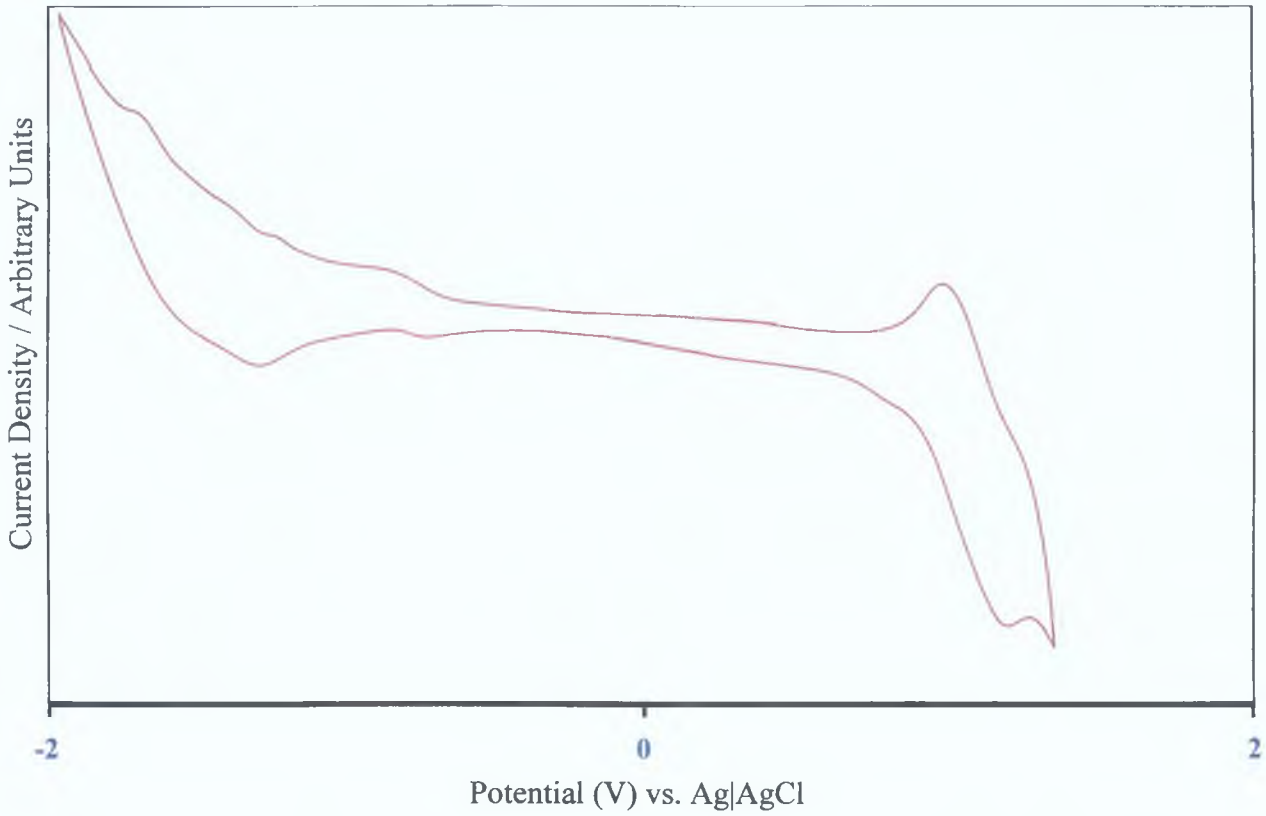

Figure B.17 Cyclic Voltammogram of $[Ru(bpy)_2(L11)]^+$ with a platinum working electrode in acetonitrile and 0.1M TEAP in Volt vs Ag|AgCl (scan rate 0.10V/s)

Figure B.17 depicts the spectra of $[Ru(bpy)_2(L11)]^+$ in acetonitrile with a platinum electrode.

The anodic region of this CV depict clearly resolved metal redox processes (Ru^{II}/Ru^{III}), however, the cathodic region of the CV is less well resolved than those observed for the glassy carbon and gold electrode As discussed previously (section B 1) this is due to the limitations of the platinum working electrode in this region of the CV [1][2]

B.4 Conclusion

The electrochemical behaviour of the dimethoxy, hydroquinone and quinone-containing complexes contained in this thesis were examined in a range of solvents and the CVs of these complexes were generated with a range of working electrodes In the case of the dimethoxy complexes it was found that these complexes were sufficiently soluble in acetone, acetonitrile and dichloromethane and that the CVs of these complexes in these solvents were achievable While the CVs obtained in acetomtrile and acetone were both satisfactory, acetone proved to be a difficult solvent to work with due to its low boiling point The CVs obtained in dichloromethane contained clear anodic processes, however, clear processes were not observed in the cathodic region Overall the CVs generated for these complexes with a glassy carbon electrode produced good CVs in the + 2 V to – 2 V potential window Overall the gold and platinum electrodes produced badly resolved CVs for these complexes

In the case of the dihydroxy complexes a similar trend was noted for the gold and platinum electrodes with disappointing resolution of the process in the positive and negation regions respectively The CVs generated with a glassy carbon electrode were of a sufficient quality over the range of potentials examined These complexes were found to be soluble in acetone, dichloromethane, ethanol and acetonitrile and the CVs of these complexes were generated m each of these solvents Acetone proved to be a difficult solvent to work with due to is low boiling point although the CVs of these complexes obtained in this solvent proved to be of a good quality DCM produced clear anodic processes, however, the cathodic processes were unclear in this solvent This was also the case for the CVs obtained in ethanol Overall acetonitrile produced clear CVs in the – 2 V to + 2 V potential window

The quinone complexes exhibited weak solubility in most of the solvents with the exception of acetonitrile The CVs generated in this solvent with a platinum electrode depict unclear cathodic processes while the CVs obtained with a glassy carbon or gold electrode were both of a good quality in both the anodic and cathodic region

Overall, therefore, acetonitrile proved to be the most successful solvent as the CV of each of the complexes can be obtained in this solvent while glassy carbon is the clear choice for the working electrode However, it is important to note that the processes observed for each of the working electrodes (where processes were sufficiently resolved) were similar Therefore, the processes reported in the CVs of the complexes contained in this thesis that were generated with a glassy carbon electrode, are 'real' That is the processes are not generated due to the interaction of the complex with glassy carbon electrode surface For example, this confirms that the hydroquinone process noted in the anodic region of the CVs of these complexes and the additional quinone processes noted in the spectra of the quinone complexes are 'real' and are not merely artefacts caused on the surface of the glassy carbon electrode

These electrochemical studies, therefore, rationalise the experimental conditions chosen for the range of complexes contained in this thesis As the experimental conditions are system dependent these are very important observations Hence, the choice of acetomtrile as solvent and glassy carbon as working electrode is justified

B.5 Bibliography

1 D J Sawyer, A Sobkowiak, J L Roberts Jr , *Electrochemistry for Chemists*, **1995**, 2nd Edition, Wiley-Interscience, New York

2 R Hage, A H J Dijkhuis,J G Haasnoot, R Prim, J Reedijk, B E Buchanan, J G Vos, *Inorg Chem* , **1988**, 27, 2185

3 R Hage, J G Haasnoot, D J Stufkens, T L Snoeck, J G Vos, J Reedijk, *Inorg Chem* , **1989**, 28, 1413

4 R Wang, T E Keyes, R Hage, R H Schmehl, J G Vos, *J Chem Soc , Chem Commun* , **1993**, 1652

5 F M Weldon, J G Vos, *Inorg Chim Acta*, **2000**, 307, 13

6 P Passaniti, W R Browne, F C Lynch, D Hughes, M Nieuwenhuyzen, P James, M Maestri, J G Vos, *J Chem Soc , Dalton Trans* , **2002**, 1740

7 A J Bard, L R Faulkner, *Electrochemical Methods, Fundamentals and Applications*, **2001**, 2nd Edition, Wiley, New York

8 A J Bard, *Pure Appl Chem* , **1992**, 2, 185

9 S Yamada, H Sato, *Nature*, **1962**, 193, 261

10 C E Plock, *J Electroanal Chem* , **1968**, 18, 289

11 G E Cabaniss, A A Diamantis, W R Murphy Jnr , R W Linton, T J Meyer, *J Am Chem Soc* , **1985**, 107, 1845

12 W G French, T Kuwana, *J Phys Chem* , **1964**, 68, 1279

13 L J Bjelica, L S Jovanovic, *Electrochim Acta* , **1992**, 37, 371

14 L J Bjelica, L S Jovanovic, N L Rehak, *Electroanal* , **1995**, 7, 990

15 M Brezina, A Hofmanova, *Collect Czech Chem Commun* , **1973**, 985

Appendix C

Synthesis of Mononuclear and Deuteriated Ruthenium Complexes

This appendix contains additional synthetic information including the synthesis of two mononuclear ruthenium (II) complexes with pyrazyl-1,2,4-triazole or pyrazyl-1,2,4-triazole and dimethoxy moieties as precursors for the preparation of hetero-dinuclear complexes The preparation of various deuteriated mononuclear complexes are also described

C.1 Introduction

In chapters two, three and four, a range of complexes containing differing moieties on the bridging ligands was presented By differing the nature of one on the moieties, variations in the characteristics of each of the groups of complexes were noted These variations resulted in the formation of a covey of compounds with novel and interesting characteristics In future work the bidentate ligands H_2L5 and H_2L6 (*figure 3 6*) have the potential to be utilised further

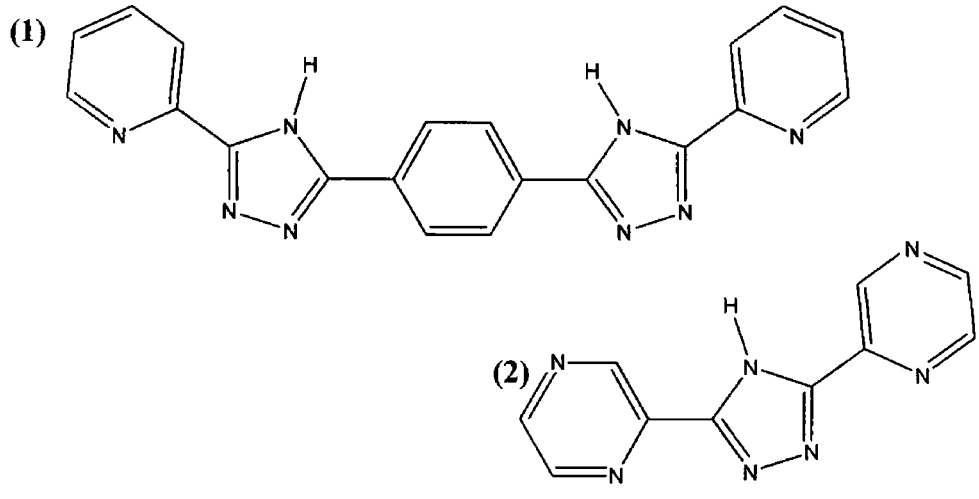

Figure C.1 Ligands utilised in the preparation of ruthenium-osmium bipyridyl heterodinuclear complexes [1][2]

For example, the possibility of synthesising heterodinulcear complexes containing both a ruthenium and, for example, an osmium unit is a viable and interesting possibility The design and synthesis of such polynuclear metal complexes has been a topic of great interest over the past number of years Authors, such as, Balzani et al have investigated such systems due to their potential as building blocks for supramolecular assemblies and photomolecular devices [3-6] In the previous chapters the importance of dinuclear complexes was discussed in depth and their potential to create mixed-valence species of the type M^{II}-M^{III} was examined This degree of metal-metal interaction separates mere polynuclear compounds from their supramolecular counterparts and the degree of metal-metal interaction can be gauged via the Hush technique from an examination of IT bands

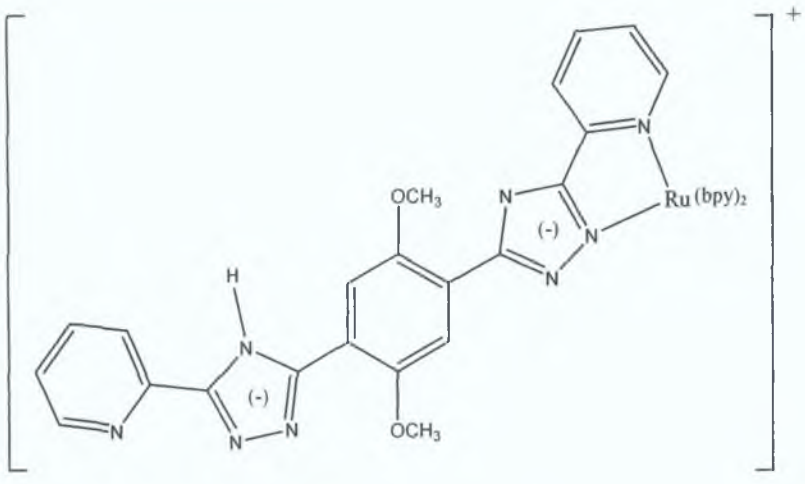

[Ru(bpy)$_2$(L15)](PF$_6$)

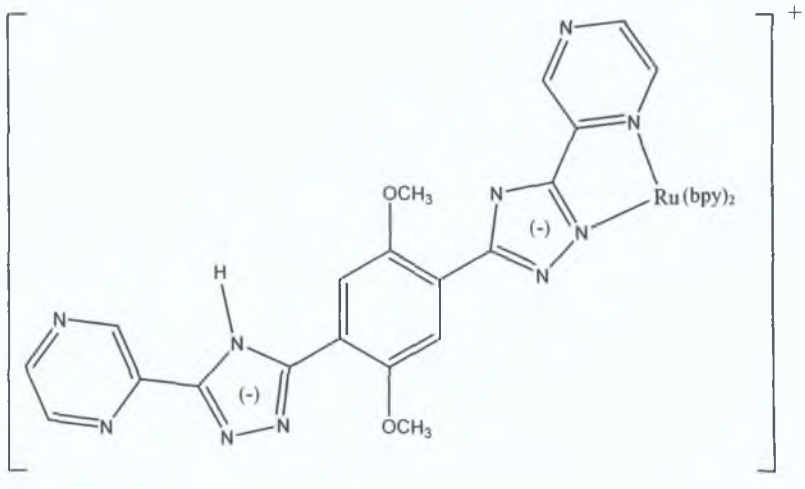

[Ru(bpy)$_2$(L16)](PF$_6$)

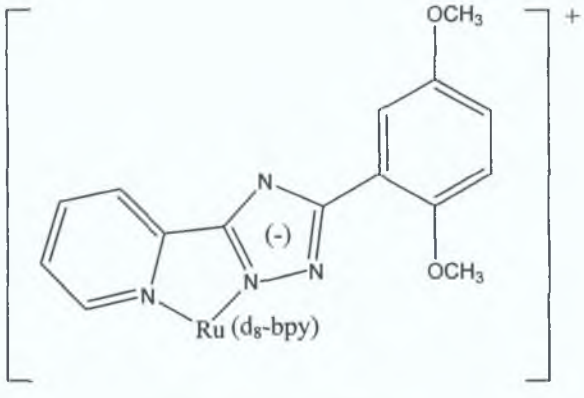

[Ru(bpy)$_2$(L17)] PF$_6$

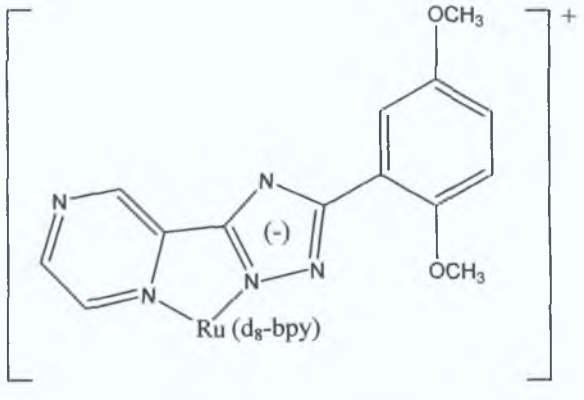

[Ru(bpy)$_2$(L18)] PF$_6$

Figure C.2 Structures of the complexes cited in this chapter.

Within these systems the nature of the bridging ligand has been of paramount importance (*figure C.1*). Triazole bridging systems have been found to be very promising bridging groups within these systems and Hage and co-workers have found that such dinuclear compounds have a significant degree of metal-metal interaction. [7] Hence, the synthesis of heteronuclear complexes containing the triazole based ligands H_2L5 and H_2L6 is an exciting prospect. Furthermore, there is also the potential to synthesise such complexes containing moieties, such as, dicarboxy groups, which allow for the attachment of the complexes directly onto a surface. With these aims in mind the mononuclear complexes $[Ru(bpy)_2(L15)]^{2+}$ and $[Ru(bpy)_2(L16)]^{2+}$ (*figure C.2*) were prepared. In the following section the synthesis and H^1-NMR spectral characterisation of these complexes is discussed and investigated. The deuteriated analogues of $[Ru(bpy)_2(L3)]^+$ and $[Ru(bpy)_2(L4)]^+$ were also synthesised and hence, the preparation of complexes 17 and 18 (*figure C.2*) is also presented in the following experimental section. Deuteriated complexes, such as these, aid in protons assignment and are, hence, a useful tool for the further elucidation of the NMR data.

C.2 Experimental Methodology

C.2.1 Synthesis of Mononuclear Complexes

The syntheses of the mononuclear complexes $[Ru(bpy)_2(L15)]^{2+}$, $[Ru(bpy)_2(L16)]^{2+}$,which contain the ligands H_2L5 and H_2L6 and $[Ru(d_8\text{-}bpy)_2(L17)]^+$ and $[Ru(d_8\text{-}bpy)_2(L18)]^+$, which contain deuteriated bipyridyl moieties are presented in this section. The synthesis of the ligands H_2L5 and H_2L6 has already been described previously in chapter three. The synthetic methodologies, upon which the following complexes were prepared, are based upon modified literature methods. [7][8]

Complex 15: $[Ru(bpy)_2(L15)]^{2+}$

cis-$[Ru(bpy)_2Cl_2].2H_2O$ (0.47 g, 0.90 mmol) and 0.76 g (1.80 mmol) of H_2L5 were heated at reflux at reflux for 8 h in 50 cm^3 $EtOH/H_2O$ (2:1 v/v). The hot solution was then filtered and evaporated to dryness. To this was added 10 cm^3 of water was added to the red-brown product. The product was precipitated with an excess aqueous solution of NH_4PF_6.

The resulting solid was collected by filteration and recrystallised from hot ethanol/H_2O. The crude product contained traces of the dinuclear ruthenium complex and was, hence, purified by column chromatography on neutral alumina. The dinuclear complex was eluted with acetonitrile and then the mononuclear complex was eluted using a mixture of acetonitrile and methanol (6:1 v/v) as eluent. The desired product was then isolated as the hexafluorophosphate salt and recrystallised from hot ethanol/H_2O (with 1 drop of conc. ammonia). Yield = 0.35 g (41 %). **^{1}H-NMR (d_8-ACN): δ 8.65 (d, 1H, pyridyl $H^{6''}$), 8.19 (d, 1H, pyridyl $H^{3''}$), 8.10 (d, 1H, pyridyl $H^{3''}$), 7.94 (d, 1H, pyridyl $H^{5''}$), 7.85 (d, 1H, pyridyl $H^{4''}$), 7.81 (d, 1H, pyridyl $H^{4''}$), 7.57 (s, 1H, phenyl $H^{6'}$), 7.52 (d, 1H, pyridyl $H^{6''}$), 7.42 (s, 1H, phenyl $H^{3'}$), 7.10 (dd, 1H, pyridyl $H^{5''}$), 3.88 (s, 3H, -OCH_3), 3.70 (s, 3H, -OCH_3).**

Complex 16: $[Ru(bpy)_2(L16)]^{2+}$

This complex was prepared in a similar to that described for *complex 15* with the exception that H_2L6 was used in place of H_2L5. Yield = 0.40 g (40 %).**^{1}H-NMR (d_8-ACN): δ 9.25 (s, 1H, phenyl $H^{3''}$), 9.21 (s, 1H, phenyl $H^{3''}$), 8.62 (d, 1H, pyridyl $H^{6''}$), 8.40 (dd, 1H, pyridyl $H^{5''}$), 8.20 (d, 1H, pyridyl $H^{6''}$), 7.62 (dd, 1H, pyridyl $H^{5''}$), 7.51 (s, 1H, phenyl $H^{6'}$), 7.38 (s, 1H, phenyl $H^{3'}$), 3.52 (s, 3H, -OCH_3), 3.40 (s, 3H, -OCH_3).**

C.2.2 Synthesis of Deuteriated Complexes

The follow synthesis describe the preparation of the deuteriated analogues of complexes $[Ru(bpy)_2(L3)]^+$ and $[Ru(bpy)_2(L4)]^+$. The preparation of the ligands HL3 and HL4 has already been discussed in chapter three.

Complex 17: $[Ru(d_8\text{-}bpy)_2(L17)]PF_6.H_20$

The synthesis of this complex is the same as that described for the non-deuteriated analogue in chapter three (*section 3.2.2*) with the exception that $[Ru(d_8\text{-}bpy)_2Cl_2]$ was used in place of $[Ru(bpy)_2Cl_2]$. Yield = 0.20 g (86 %). **^{1}H-NMR (d_8-ACN): δ 8.18 (d, 1H, pyridyl $H^{3''}$), 7.80 (dd, 1H, pyridyl $H^{4''}$), 7.48 (d, 1H, pyridyl $H^{6''}$), 7.20 (s, 1H, phenyl $H^{3'}$), 7.13 (dd, 1H, pyridyl $H^{5''}$), 7.01 (dd, 1H, phenyl $H^{6'}$), 6.89 (d, 1H, phenyl $H^{5'}$), 3.55 (s, 3H, -OCH_3), 3.70 (s, 3H, -OCH_3).** Calculated for $C_{32}N_8H_{15}O_3PF_6Ru$: C: 41.27; H: 1.39; N: 11.00 %. Anal. Found: C: 41.28; H: 3.16; N: 10.66 %.

Complex 18: **$[Ru(d_8\text{-bpy})_2(L18)]PF_6.H_2O$**

Again, the synthesis of this complex is the same as that described for the non-deuteriated analogue in chapter three (*section 3.2.2*) with the exception that $[Ru(d_8\text{-bpy})_2Cl_2]$ was used in place of $[Ru(bpy)_2Cl_2]$. Yield = 0.28 g (81 %). **^{1}H-NMR (d_8-ACN): δ 9.26 (s, 1H, pyrazyl $H^{3''}$), 8.26 (d, 1H, pyrazyl $H^{6''}$), 7.63 (d, 1H, pyrazyl $H^{5''}$), 7.23 (s, 1H, phenyl $H^{3'}$), 6.98 (d, 1H, phenyl $H^{5'}$), 6.90 (d, 1H, phenyl $H^{6'}$), 3.60 (s, 3H, -OCH_3), 3.65 (s, 3H, -OCH_3).** Calculated for $C_{32}N_9H_{14}O_3PF_6Ru$: C: 40.43; H: 1.08; N: 12.51 %. Anal. Found: C: 39.93; H: 2.79; N: 12.19 %.

C.3 Results and Discussion

C.3.1 Synthetic and Characteristic Considerations

C.3.3.1.1 Mononuclear Complexes

The mononuclear ruthenium complexes were synthesised using an excess of ligand starting product in order to ensure the production of the desired end product. Furthermore, the ligand was fully dissolved prior to addition to $[Ru(bpy)_2Cl_2]$ in order to decrease the amount of unwanted dinuclear complex being formed. However, subsequent to refluxing there was a small quantity of dinuclear complex formed, which was removed by column chromatography. During this procedure the dinuclear complex was removed by elution with acetonitrile while the remaining mononuclear complex was then eluted with a small percentage of methanol. The ^{1}H-NMR spectrum was then utilised to identify the mononuclear complexes. From an examination of the data contained in *appendix A* it can clearly be seen that there are great differences between the NMR spectrum of the mononuclear complex described here and its dinuclear counterpart contained in chapter three. For example, in the NMR spectrum of both of the mononuclear complexes the dimethoxy peaks now appear as separate entities compared to the NMR spectrum of the dinuclear complex in which these peaks formed a strong singlet based on the fact that in the dinuclear complex these components are equivalent. [9] Also the phenyl protons no longer appear as a singlet as in the dinuclear complexes as they are also no longer equivalent. Furthermore, as explained in chapter three there is an upfield shift of the $H^{6''}$ proton upon coordination due to its interaction with adjacent bipyridyl rings.

This shift is evident for only one H^6 proton in these mononuclear complexes which further verifies their mononuclear status [2][10-12]

C 3 3 1 2 Deuteriated Complexes

Partial deuteriation of a complex simplifies the analysis of the NMR spectra of a complex, since, it allows the ligand based signals to be identified with more clarity Hence, the deuteriated analogues of $[Ru(bpy)_2(L3)]^+$ and $[Ru(bpy)_2(L4)]^+$ were prepared and the NMR spectra of these complexes are contained in *appendix A* The synthesis of these complexes was straightforward and analogous to that of the undeuteriated analogues with the exception that $[Ru(d_8\text{-}bpy)_2Cl_2]$ is used in place of $[Ru(bpy)_2Cl_2]$ Purification of these complexes is also similar to that utilised for the undeuterated counterparts The ^{1}H-NMR spectra of these complexes, therefore, clearly show the location of the ligand protons in the coordinated complex with only small quantities of the bipyridyl moieties visible

C.4 Conclusions

The synthesis of the mononuclear ruthenium complexes $[Ru(bpy)_2(L15)]^{2+}$ and $[Ru(bpy)_2(L16)]^{2+}$ was described in this appendix and hence, these complexes are now potentially available as starting materials for the production of a wide variety of heterodinuclear complexes The synthesis and purification of these mononuclear complexes proved uncomplicated and the subsequent NMR data is contained in *appendix A* The synthesis of the deuteriated complexes $[Ru(d_8\text{-}bpy)_2(L17)]^+$ and $[Ru(d_8\text{-}bpy)_2(L17)]^+$ which are deuteriated analogues of $[Ru(bpy)_2(L3)]^+$ and $[Ru(bpy)_2(L4)]^+$ was also described The complexes were prepared in an analogous manner to that of their undeuteriated counterparts (chapter three) and the NMR data for these complexes is contained in *appendix A* These complexes were utilised in the assignment of the protons in the NMR spectrum of the mononuclear contained in chapter three

C.6 Bibliography

1 F M Weldon, J G Vos, *Inorg Chim Acta*, **2000**, 307, 13

2 R Hage, R Prins, J G Haasnoot, J Reedijk, J G Vos, *J Chem Soc, Dalton Trans*, **1987**, 1389

3 V Balzani, *Tetrahedron*, **1992**, 48, 10443

4 V Balzani, S Campagna, G Denti, A Juris, S Serroni, M Venturi, *Acc Chem Res*, **1998**, 31, 26

5 H E B Lempers, J G Haasnoot, J Reedjik, R Hage, F M Weldon, J G Vos, *Inorg Chim Acta*, **1994**, 225, 67

6 V Balzani, A Juris, M Venturi, S Campagna, S Serroni, *Chem Rev*, **1996**, 96, 759

7 R Hage, H E B Lempers, J G Haasnoot, J Reedjik, F M Weldon, J G Vos, *Inorg Chem*, **1997**, 36, 3139

8 T E Keyes, F Weldon, E Muller, P Pechy, M Gratzel, J G Vos, *J Chem Soc, Dalton Trans*, **1995**, 2705

9 P Passanti, W R Browne, F C Lynch, D Hughes, M Nieuwenhuyzen, P James, M Maestri, J G Vos, *J Chem Soc, Dalton Trans*, **2002**, 1740

10 H A Nieuwenhuis, J G Haasnoot, R Hage, J Reedijk, T L Snoeck, D J Stufkins, J G Vos, *Inorg Chem*, **1990**, 30, 48

11 B E Buchanan, R Wang, J G Vos, R Hage, J G Haasnoot, J Reedijk, *Inorg Chem*, **1990**, 29, 3263

12 S Fanni, T E Keyes, C M O'Connor, H Hughes, R Wang, J G Vos, *Coord Chem Rev*, **2000**, 208, 77